ISSN 2458-973X

JSCMT

Journal of Sustainable Construction Materials and Technologies

Volume 9
Number 2
Year 2024

YTU PRESS

www.jscmt.yildiz.edu.tr

ISSN 2458-973X

Journal of Sustainable Construction Materials and Technologies

Volume 9 Number 2 Year 2024

ISSN 2458-973X

JSCMT

Journal of Sustainable Construction Materials and Technologies

Volume 9 Number 2 Year 2024

CONTENTS

J Sustain Const Mater Technol, Vol. 9, Issue. 2, pp. 93–105, June 2024

Journal of Sustainable Construction Materials and Technologies
Web page info: https://jscmt.yildiz.edu.tr
DOI: 10.47481/jscmt.1501001

Journal of Sustainable Construction Materials and Technologies

Research Article

Synergistic effects of GGBFS addition and oven drying on the physical and mechanical properties of fly ash-based geopolymer aggregates

Chereddy SONALI SRI DURGA[1], Chava VENKATESH*[1], Mukkala PRIYANKA[2], Bypaneni KRISHNA CHAITANYA[3], B. Naga Malleswara RAO[1], T. Muralidhara RAO[1]

[1]Department of Civil Engineering, CVR College of Engineering, Vastunagar, Telangana, India
[2]Department of Civil Engineering, Malla Reddy Engineering College and Management Sciences, Telangana, India
[3]Department of Civil Engineering, R.V.R. & J.C. College of Engineering (A), Andhra Pradesh, India

ARTICLE INFO

Article history
Received: 20 April 2024
Revised: 07 June 2024
Accepted: 10 June 2024

Key words:
Alkali activator solution, compressive strength, environmental impacts, geopolymer aggregates, water absorption

ABSTRACT

Conventional coarse aggregates, extracted from natural sources, pose environmental challenges such as habitat destruction, resource depletion, and high energy consumption. To mitigate these effects, this study prepared geopolymer aggregates (G.A.) using fly ash–GGBFS and an alkali activator solution through pelletization. Furthermore, two aggregate drying methods, oven drying, and ambient air drying, are adopted to evaluate their optimal performance through physical and mechanical tests. The results Indicated that oven-dried geopolymer aggregates exhibited optimal behavior in all experimental aspects compared to ambient air-dried aggregates. Specifically, the 80% fly ash–20% GGBFS mixed aggregates demonstrated lower crushing value (20.80%), impact value (24.7%), water absorption (13.67%), and abrasion values (7.01%) than other mixes. No considerable difference was observed in the density and specific gravity of aggregates between the two drying methods. Subsequently, these aggregates were used as a 100% replacement for conventional coarse aggregates in concrete, and the concrete's mechanical properties, such as compressive, split tensile, and flexural strengths, were investigated. Please update the following sentence in place of the highlighted sentence. The mix M3 (i.e., 80% fly ash–20% GGBFS mixed aggregates incorporated concrete) showed superior performance and are considered the optimum mix. Specifically, in the compressive strength results, the mix M3 showed a 26.31% and 14.28% strength increase compared to the 100% fly ash aggregates incorporated concrete mix in oven-dried aggregates and ambient-dried aggregates incorporated concrete, respectively. The linear regression equation derived from the experimental results was used to predict the split tensile and flexural strength, showing a good correlation between the experimental and expected results.

Cite this article as: Sonali Sri Durga, C., Venkatesh, C., Priyanka, M., Krishna Chaitanya, B., Rao, B. N. M., & Rao, T. M. (2024). Synergistic effects of GGBFS addition and oven drying on the physical and mechanical properties of fly ash-based geopolymer aggregates. *J Sustain Const Mater Technol*, 9(2), 93–105.

1. INTRODUCTION

Concrete, the most commonly used construction material, comprises aggregates and a cementitious matrix [1, 2]. The increasing demand for natural aggregates (N.A.) due to the rapid growth of the construction industry in the twenty-first century has significantly strained the environment [3]. To address this issue, researchers have been working on developing sustainable alternatives to natural aggregates for concrete production. These alternative aggregates can help conserve natural resourc-

***Corresponding author.**
*E-mail address: chvenky288@gmail.com

es, reduce the need for landfills by utilizing industrial and urban waste products, and contribute to a more sustainable built environment. A variety of grain-like solid wastes, such as recycled aggregates [4], waste glass [5], and steel slag [6], have been successfully used as alternative aggregates in concrete. As research on these grain-like solid wastes has advanced, there has been a growing interest in transforming powder-like solid wastes into grain-like artificial aggregates [7, 8].

Artificial aggregate technology offers a promising solution to two major problems: the excessive excavation of natural rock sources and the accumulation of waste materials [9]. This technology involves binding powder-like materials together and allowing them to harden, resulting in the formation of grain-like materials with desired aggregate sizes [10]. Among the various types of lightweight aggregates, sintered fly ash aggregates and cold-bonded cement-based aggregates have shown superior performance. However, the sintering method requires high temperatures ranging from 1000 °C to 1200 °C, which results in significant energy consumption and CO_2 emissions during the production of solid and lightweight aggregates [11, 12]. In contrast, the cold-bonding technique requires temperatures below 100 °C, consuming minimal energy and producing no CO_2 emissions in the creation of aggregates [13].

The characteristics of artificial aggregates, including bulk density and specific gravity, are influenced by various factors such as the curing regime, binder content, sintering temperature, and grain size [14]. Typically, artificial aggregates exhibit a compacted bulk density below 2.0 g/cm^3 and a loose bulk density below 1.2 g/cm^3. Their oven-dry and saturated surface-dried specific gravity range from 1.10 to 2.0 and 1.51 to 2.25, respectively. These properties classify them as lightweight aggregates (L.W.A.) according to UNE-EN-13055-1 (2003) [15, 16]. Higher binder content and grain size increase specific gravity and bulk density, while sintering at higher temperatures (950 °C–1100 °C) decreases bulk density due to bloating, moisture removal, and combustion of organic materials [17]. Water absorption of artificial aggregates ranges from 0.7 to 32.8% for 24 hours of immersion, influencing concrete workability [18]. Increased binder content, sintering temperature and duration, NaOH molarity, and Na_2SiO_3 content reduce water absorption by creating a denser microstructure [19, 20]. Two-step pelletization also decreases porosity compared to single-step pelletization [17].

The crushing strength of aggregates depends on pelletization factors, curing regime and age, binder content, density, size, and shape. Higher binder content, curing age, pelletization duration, and accelerated curing improve crushing strength [21]. Smaller aggregates (4–12 mm) exhibit greater crushing strength than coarser ones due to lower porosity [17, 22]. Surface treatment with soluble glass or water glass enhances strength by promoting hydration and repairing surface cracks [23, 24]. Sintering temperature, raw material composition, and alkali activator addition also influence strength. Geopolymer aggregates demonstrate enhanced strength through heat and solution curing, with improvements observed in Na_2O content, Na_2SiO_3-NaOH ratio, fluid-binder ratio, and molarity [25]. The pelletized artificial aggregates exhibit sufficient impact and crushing strength to meet the standards for structural applications as outlined in I.S.: 2386 (Part IV)-1963 [26].

Lightweight concrete (L.W.C.) made with sintered or alkali-activated artificial aggregates can achieve performance comparable to normal-weight concrete (N.W.C.) [27]. The compressive strength of L.W.C. is significantly influenced by the properties of lightweight aggregates (L.W.A.), such as porosity, specific gravity, crushing strength, water absorption, particle size distribution [28], as well as mix design parameters and curing conditions [29, 30]. Mineral admixtures can enhance concrete's compressive strength through pozzolanic and densification effects [31, 32]. However, concrete with artificial aggregates may have lower compressive strength than N.W.C. due to the inferior properties of the aggregates [33]. Concrete with sintered aggregates exhibits higher strength than concrete with cold-bonded aggregates due to the latter's higher porosity and lower strength [34]. Surface treatment of aggregates can improve concrete's compressive strength by up to 30% [35].

Concrete's tensile strength is contingent upon various factors, including the paste matrix, interfacial transition zone (I.T.Z.), and the tensile properties of aggregates [36]. Longer curing durations and higher strengths of mortar and aggregates typically result in increased tensile strength [37]. However, augmenting the volume of artificial aggregates may lead to a decrease in tensile strength due to failures originating within the aggregates themselves. It's worth noting that concrete's tensile properties rely more on mortar properties than aggregates, as diametric tension tends to cause splitting [38]. Comparatively, lightweight aggregates (L.W.A.) possess smaller surface areas, less angular shapes, and lower surface roughness, potentially leading to weaker aggregate transition zones when compared to normal-weight aggregates (N.W.A.) [39]. The flexural properties of concrete mirror split tensile strength, with matrix densification and reduced volumes of artificial aggregates, improving flexural performance. In lightweight concrete (L.W.C.), flexural properties primarily hinge on mortar characteristics, with artificial aggregates contributing minimally to flexural bending resistance. For instance, an increased volume of mortar can compensate for decreased aggregate volume, resulting in a higher flexural elastic modulus during bending [40, 41].

In the context of the current research, geopolymer aggregates (G.P.A.s) have emerged as a notable choice among various artificial aggregate options, including sintered aggregates and cold-bonded cement-based aggregates. G.P.A.s are favored for their lack of cement, minimal energy requirements during production, and exceptional capability to immobilize heavy metals. The development of geopolymer aggregates offers several advantages over traditional artificial aggregates. Firstly, the output of G.P.A.s does not require the use of cement, which significantly contributes to greenhouse gas emissions. By eliminating the need for cement, G.P.A.s can help reduce the carbon footprint of the construction industry. Secondly, the production of G.P.A.s consumes less energy compared to other artificial aggregate types, such as sintered aggregates, which require high-temperature processing. This lower energy consumption further enhances the environmental sus-

Table 1. Chemical characteristics (weight (%)) and physical characteristics of binders

Material	Fe_2O_3*	CaO*	SiO_2*	Al_2O_3*	MgO*	Na_2O*	SO_3*	K_2O*	LOI*	Specific gravity	Specific surface (m^2/g)
Cement	3.12	65.15	21.47	4.16	1.97	0.63	1.96	1.01	0.53	3.10	1.2
Fly ash	4.56	3.87	58.23	26.05	1.21	0.41	1.16	0.87	3.64	2.39	5.12
GGBS	2.06	44.7	32.25	12.14	4.23	0.87	0.84	–	2.91	2.86	6

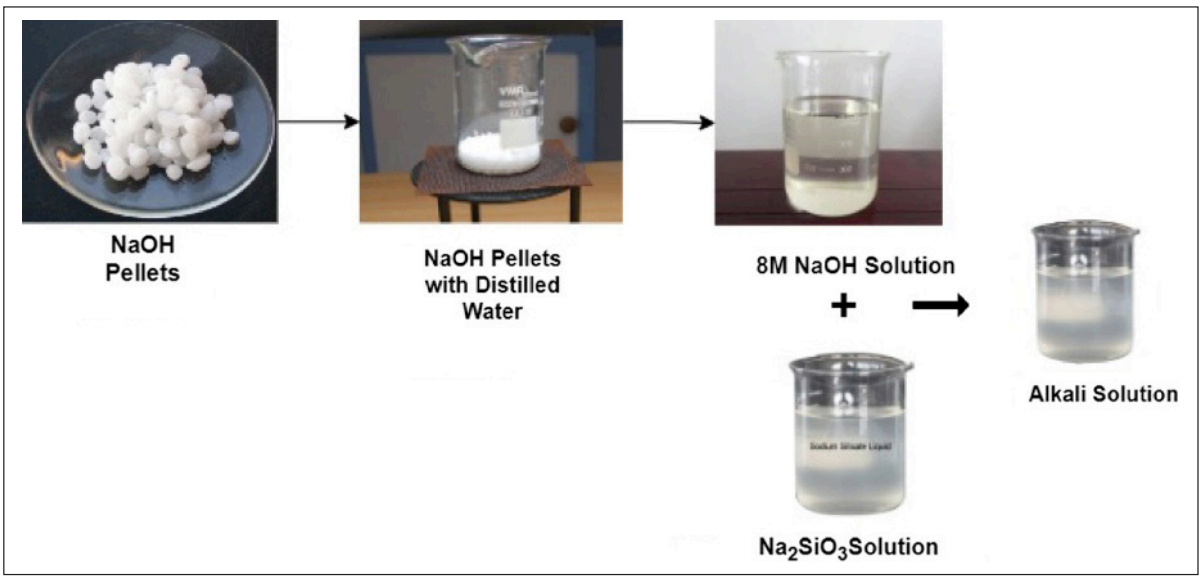

Figure 1. Preparation of Geopolymer/Alkali solution.

tainability of G.P.A.s. The drying method of the geopolymer aggregates plays a vital role in their physical and mechanical performance. Unfortunately, limited literature is available on the effect of drying methods on the mechanical and physical performance of G.P.A.s. Considering the research significance mentioned above, G.P.A.s were used as 100% replacement for the normal coarse aggregates in concrete, and their mechanical characteristics were evaluated. Furthermore, linear regression was performed using the experimental results, and prediction analysis was carried out using this equation.

2. MATERIALS AND METHODS

2.1. Materials

The cement used in this study was Type I Ordinary Portland cement conforming to ASTM C150 [42]. It was procured from a local supplier, Mahashakthi Cement Dealers, in 50 kg bags. The chemical and physical properties of the cement, provided by the manufacturer, are presented in Table 1. Similarly, two Supplementary Cementitious Materials (S.C.M.s) were used as raw materials for geopolymer aggregates preparation - Class F fly ash, confirming to ASTM C618-22 [43], and ground granulated blast furnace slag (GGBFS), conforming to ASTM C989 [44]. The fly ash was procured from Vijayawada Thermal Power Plant, and the GGBFS was obtained from Visakhapatnam Steel Plant, both in 50 kg bags. Their chemical and physical compositions are provided in Table 1. The alkali activator solution was prepared in the laboratory by mixing analytical-grade sodium silicate (Na_2SiO_3) and 8M sodium hydroxide (NaOH) solutions in a 1:1.5 ratio, as shown in Figure 1, and was used as an adhesive. Moreover, the molar ratio of SiO_2/Na_2O in the sodium silicate solution is maintained at 2 (i.e., SiO_2/Na_2O=2). Locally available river sand and crushed granite stones were used as fine and coarse aggregates, respectively. The specific gravity, water absorption, gradation, and silt content were determined as per IS 383-2016 [45] and were within permissible limits. The sand had a specific gravity of 2.65, water absorption of 1%, and fineness modulus of 2.7. The coarse aggregate had a specific gravity of 2.8, water absorption of 0.5%, and sizes ranging between 4.75 mm and 20 mm. Figure 2 depicts the grading curve for aggregates.

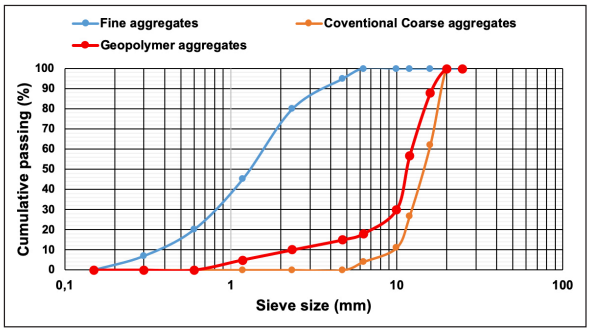

Figure 2. Grading curves of aggregates.

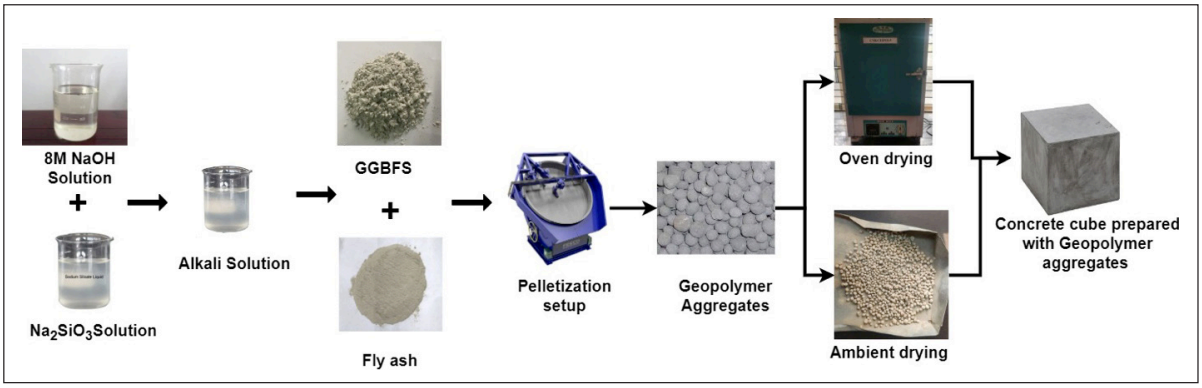

Figure 3. Preparation of Geopolymer aggregates

Table 2. Mix calculations for aggregates preparation (kg/m^3)

Aggregate mixes	Fly ash	GGBFS	NaOH	Na_2SiO_3	Geopolymer solution	The solution to binder ratio	Alkaline ratio ($NaOH/Na_2SiO_3$)	Molarity of geopolymer solution
100% FA	962	–	115.44	173.16	288.6	0.3	1:1.5	8
90% FA+10% GGBFS	865.8	96.2	115.44	173.16	288.6	0.3	1:1.5	8
80% FA+20 GGBFS	769.6	192.4	115.44	173.16	288.6	0.3	1:1.5	8

2.2. Experimental Methods

2.2.1. Pelletization

Geopolymer aggregates were manufactured utilizing a disc pelletizer set at a speed of 40 rotations per minute and an angle of tilt of 45°. A mixture of fly ash and GGBS was introduced into the pelletizer (Table 2), and the disc was rotated for 3 to 5 minutes before adding half of the solution to the binder. Rotation persisted for an additional 3 to 5 minutes. Throughout the pellet formation process, an alkaline solution was continuously sprayed onto the binder materials, facilitating accumulation [17]. Once the fresh pellets were formed, they underwent drying. Ambient-dried aggregates were exposed to standard atmospheric conditions at 25±2 °C.

In comparison, oven-dried aggregates were placed in an oven chamber set at 60 °C for 12 hours, then allowed to cool to ambient temperature. A schematic representation of the geopolymer aggregate production process is depicted in Figure 3. The resulting geopolymer aggregates exhibited a rounded shape, as shown in Figure 4. The efficiency of geopolymer aggregates is measured in terms of the weight percentage of aggregates retained on the 4.75 mm sieve [46]. In the present study, approximately 80% of the prepared geopolymer aggregates were retained on the 4.75 mm sieve. Hence, the efficiency of aggregate production is 80%. The following Eq.1 is used to calculate the efficiency of geopolymer aggregates.

Efficiency (η)=(weight of aggregates retained on the 4.75 mm sieve/total weight of aggregates produced)×100. (Eq.1)

2.2.2. Physical Tests on Aggregates

Aggregate Impact Value (A.I.V.), Aggregate Crushing Value (A.C.V.), and Aggregate Abrasion Value (AAV) are

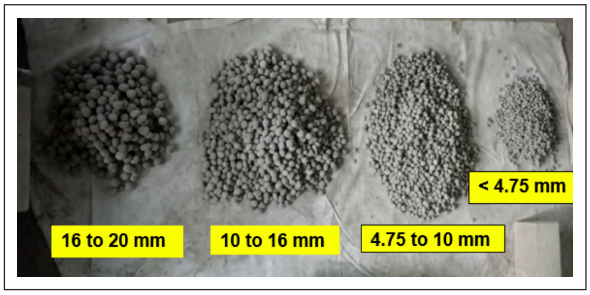

Figure 4. Geopolymer aggregates with rounded size.

measures of the resistance of an aggregate to crushing, impact, and abrasion, respectively, and are conducted as per I.S.: 2386 Part IV [47]. In the A.C.V. test, the aggregate sample is filled in a cylindrical steel mold and subjected to a compressive load of 40 tonnes for 10 minutes, and the percentage of crushed aggregate passing a 2.36 mm sieve is reported. In the A.I.V. test, the aggregate sample is subjected to blows from a hammer falling from a height of 380 mm, and the percentage of fine particles passing a 2.36 mm sieve is reported. In the AAV test, the aggregate sample is placed in an abrasion testing machine with steel balls and subjected to spinning, and the percentage of wear due to friction is reported. Specific Gravity, Bulk Density, and Water Absorption are measures of the density, weight per unit volume, and amount of water that an aggregate can absorb, respectively. They are conducted as per I.S.: 2386 Part III [48]. In the Specific Gravity test, the aggregate sample is dried, weighed, immersed in water, and weighed again. The ratio of the weight of a volume of aggregate to the weight of an equal volume of water is calculated. In the Bulk Density test, a cylindrical container is filled with an aggregate sample in three layers. Each layer is subjected to 25 strokes

Table 3. Mix calculations for concrete (kg/m³)

Drying condition	Mix ID	Mix ID	Cement	Fine aggregate	Coarse aggregates	Geopolymer aggregate	Water	Water cement ratio
C.C.A.	Conventional coarse aggregates	CCA	425.32	596	835.64	–	191.39	0.45
Oven-dried	100% F.A.	M1	425.32	596	–	835.64	191.39	0.45
	90% FA+10% GGBFS	M2	425.32	596	–	835.64	191.39	0.45
	80% FA+20 GGBFS	M1	425.32	596	–	835.64	191.39	0.45
Ambient dried	100% F.A.	M1	425.32	596	–	835.64	191.39	0.45
	90% FA+10% GGBFS	M2	425.32	596	–	835.64	191.39	0.45
	80% FA+20 GGBFS	M3	425.32	596	–	835.64	191.39	0.45

from a tamping rod, and the mass of aggregates divided by the bulk volume is calculated. In the Water Absorption test, the oven-dried sample is immersed in water for 24 hours, removed, wiped, and weighed, and the increase in weight over dry weight divided by dry weight is expressed as water absorption.

2.2.3. Mix Calculations and Sample Preparation

Concrete cubes measuring 150 mm x 150 mm x 150 mm were prepared with a target 28-day compressive strength of 40 MPa as per mix design requirements, as shown in Table 3. The mix proportions and mixing methods followed IS 10262-2019 [49]. Cube specimens were demoulded after 24 hours and subjected to standard moist curing as per IS 516-1959 [50] in curing tanks at 27±2 °C for 7 and 28 days. For the experimental studies, a total of 210 samples were tested.

2.2.4. Compressive Strength

Compressive strength testing was conducted according to the specifications outlined in IS 516-1959 [50–52], utilizing a compression testing machine with a capacity of 2000 kN. The cubes underwent a cleaning process to remove any loose sand or particles, ensuring accuracy in the test results. Subsequently, they were positioned in the testing machine in a manner where the load was applied to the opposite sides of the 150 mm edge, and the axis of the specimen was meticulously aligned with the center of thrust. The load was then gradually applied at a steady rate of approximately 140 kg/cm2/min until failure occurred. Figure 5 provides a visual representation of the compressive strength test setup.

2.2.5. Split Tensile Strength

Concrete cylinders of 150mm diameter and 300mm height were prepared as per the mix proportions and curing method outlined in IS 516-1959 [50]. After 28 days of standard moist curing, the cylinders were tested for split tensile strength as per IS 5816 [53]. The cylinder specimen was placed horizontally between the loading surfaces of a 2000 kN capacity compression testing machine, and the load was applied without shock at a steady rate of 1.4 MPa/min. The alignment was adjusted so that the line of fracture was vertical and centered. The test was carried out until failure, and the maximum load at failure was recorded. Figure 6 illustrates the experimental photograph of the split tensile strength test.

Figure 5. Experimental photograph of compressive strength test.

2.2.6. Flexural Strength

For testing flexural strength, five beam specimens of 500 mm x 100 mm x 100 mm dimensions were prepared and moist cured for 28 days as per IS 516 [50–54]. The test procedure followed IS 516 specifications using a 200 kN capacity flexural testing machine. The beam was placed horizontally on rollers spaced 300 mm apart. Two point loads were applied at 180 mm center-to-center distance until failure occurred. Figure 7 illustrates the experimental photograph of the Flexural Strength Test—eq. 1 used to calculate the flexural strength of concrete.

Flexural strength (F_s)= PL/bd^2 Eq.1

P=Load applied to the beam at the two points (in Newtons, N)

Figure 6. Experimental photograph of Split tensile strength test.

L=Span length (distance between the supports) (in millimeters, mm)

b=Width of the specimen (in millimeters, mm)

d=Depth of the specimen (in millimeters, mm)

2.2.7. Linear Regression Analysis

In this study, linear regression analysis was used to determine the relationships between compressive strength, split tensile strength, and flexural strength [55, 56]. Using the derived equations, the split tensile and flexural strength values were predicted from the compressive strength data. These predicted values were then validated against the experimental results.

3. RESULTS AND DISCUSSION

3.1. Effect of GGBFS Addition and Drying Methods on Aggregate Properties

The aggregate crushing value was reduced from 25.84% to 20.8% for oven-dried and 29.5% to 26.04% for ambient air-dried mixes with 20% fly ash replacement by GGBFS (Table 4). The lowered fragmentation under compressive loads indicates improved aggregate strength and resistance capacity due to GGBFS incorporation [57–59]. This enhancement can be attributed to the higher reactivity of Ca-rich GGBFS, which promotes the formation of a dense and well-polymerized aluminosilicate gel network (as shown in Figure 8a), resulting in superior mechanical performance [17]. Similarly, the impact values decreased from 26.8% to 24.7% for oven-dried and 30.73% to 27.49% for ambient dried aggregates with 20% GGBFS addition. The drop in fine formation during sudden impact demonstrates better bonding of the aggregate matrix particles [60]. The abrasion values also followed a declining trend with GGBFS replacement due to improved cohesion. The water absorption substantially reduced from 10.39% to 7.01% for oven-dried and 14.52% to 10.61% for ambient dried aggregates as GGBFS was increased to 20%. The refined pores and discontinuities with the Ca-rich gel formation lead to lowered permeability and sorptivity [17]. The bulk density showed marginal improvements with denser aggregates. Overall, the addition of 20% GGBFS resulted in significant enhancements in strength, resistance to attrition, and durability properties of the fly ash-based geopolymer aggregates, meeting the I.S. code limits. This establishes the positive influence of GGBFS addition through the synergistic effects of Ca-rich gel formation.

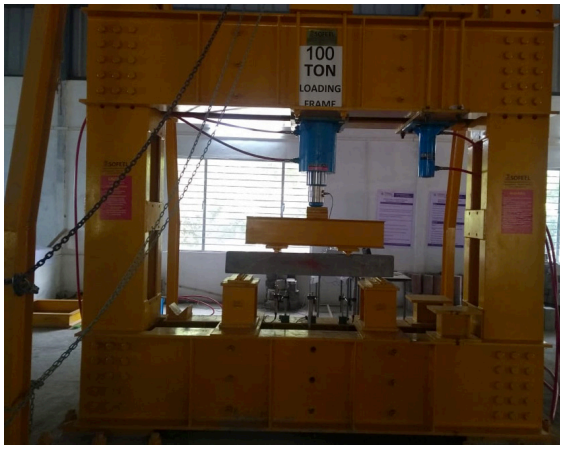

Figure 7. Experimental photograph of Flexural strength test.

Ambient air-dried aggregates showed inferior properties across all mix variations compared to oven-dried aggregates. The crushing, impact, and abrasion values were considerably higher for ambient dried aggregates. For example, the 80% fly ash - 20% GGBFS ambient dried mix exhibited 26.04% crushing compared to 20.8% for the oven-dried mix. This indicates additional microcrack formation from relatively slower moisture removal in ambient drying. Similarly, the water absorption of ambient-dried aggregates was higher, signifying increased porosity. The abrupt water evaporation in oven drying enables efficient moisture removal without damage to the aggregate structure.

On the contrary, ambient drying leads to weaker bonds by promoting shrinkage cracks. The specific gravity and density did not show any significant differences between oven-dried and ambient air-dried aggregates. However, the slower drying rate in ambient conditions ultimately affects the strength characteristics and resistance to fragmentation through microcrack development. In summary, oven drying

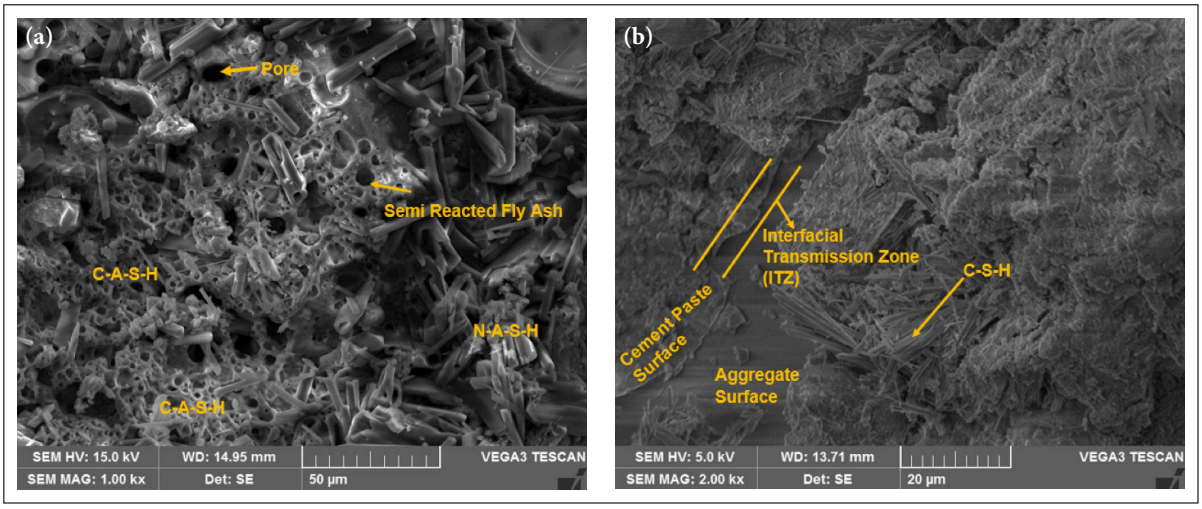

Figure 8. **(a)** S.E.M. of 80% F.A. + 20% oven-dried GGBFS geopolymer aggregates. **(b)** SEM of M3 concrete mix.

Table 4. Properties of aggregates

Test	CCA	IS 2386 limits	Oven dry			Ambient dry		
			M1	M2	M3	M1	M2	M3
Aggregate crushing value (%)	19.37	<30%	25.84	24.73	20.8	29.5	27.32	26.04
Aggregate impact value (%)	21.64	<30%	26.8	25.4	24.7	30.73	28.25	27.49
Abrasion value (%)	11.34	<3 0%	15.34	14.02	13.67	22.76	18.64	16.52
Water absorption (%)	5.34	<30%	10.39	8.46	7.01	14.52	13.05	10.61
Specific gravity	2.62	2.1–3.2	1.89	1.91	1.97	1.85	1.85	1.87
Bulk density (kg/m^3)	1556	1200–1750	962.30	969.36	969.52	961.42	964.31	958.27

enables rapid and uniform moisture removal without cracking, thereby showing consistently better properties over ambient air-drying for all aggregate mixes. The 80% fly ash - 20% GGBFS geopolymer aggregate mix with oven-drying methodology showed the most optimal performance.

3.2. Effect of GGBFS Addition and Drying Method on Compressive Strength

As evident from Figure 9, the compressive strength increased with higher GGBFS content in the geopolymer aggregate (G.A.) mixes for both oven-dried and ambient air-dried aggregates. The 80% fly ash - 20% GGBFS oven-dried Geopolymer aggregates incorporated concrete mix exhibited the maximum compressive strength of 44.64 MPa, showing 26.31% and 14.28% strength enhancements over the 100% fly ash G.A.s concrete for oven-dried and ambient dried samples respectively. The strength improvement is attributed to the higher reactivity of Ca-rich GGBFS, which promotes the formation of additional strength-contributing C-A-S-H gels along with the N-A-S-H gels from fly ash [61, 62]. The increased production of cementitious gel binds the aggregates strongly, contributing to superior load-bearing capacity. Moreover, The oven-dried G.A. incorporated concrete mixes have showed consistently higher compressive strengths over ambient air-dried G.A. concrete across all aggregate mixes. For instance, the concrete mix with 80%

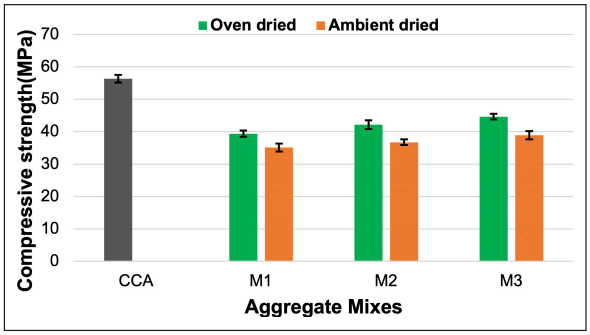

Figure 9. Compressive strength results.

fly ash and 20% GGBFS mixed aggregates had 13.3% greater strength in the oven-dried GA concrete mix compared to the ambient-dried GA concrete mix. This correlates to the denser aggregate structure from uniform, rapid oven drying, which translated to stronger interfacial transition zones (as shown in Figure 8b) and enhanced stress transfer efficiency in concrete [63].

In contrast, improper moisture removal during ambient air-drying could have led to weaker I.T.Z.s due to drying shrinkage. Slower drying also enables efflorescence formation, which increases porosity. Hence, as observed from the results, oven-dried G.A.s showed substantially better strength performance than ambient-dried G.A.s. In summary, GGBFS

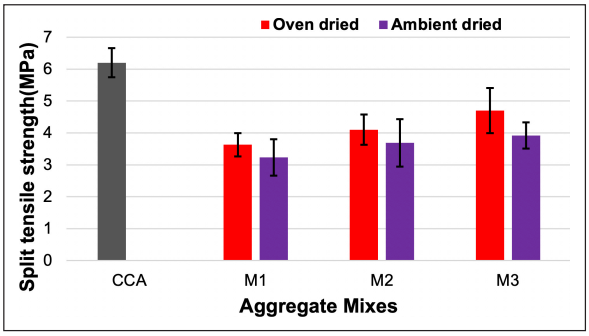

Figure 10. Split tensile strength result.

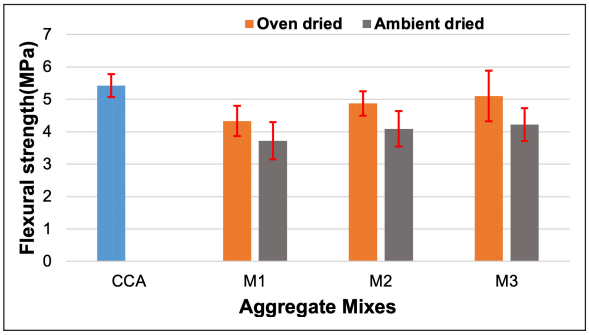

Figure 11. Flexural strength result.

addition enhances the compressive strength of G.A. concrete by promoting additional gel formation. At the same time, the oven drying method enables superior strength through a denser aggregate structure devoid of shrinkage cracks (as shown in Figure 8b). The 80% fly ash - 20% oven-dried GGBFS GA incorporated concrete mix showed the optimum results.

3.3. Effect of GGBFS Addition and Drying Method on Split Tensile Strength

As observed in Figure 10, the split tensile strength increased with higher GGBFS replacement in the geopolymer aggregate (G.A.) mixes, similar to the compressive strength trends. The concrete with 80% fly ash and 20% GGBFS mixed oven-dried aggregates exhibited a maximum split tensile strength of 4.7 MPa, showing enhancements of 29.46% and 21.67% over the 100% fly ash Geopolymer aggregates for the oven-dried and ambient air-dried aggregates, respectively. The greater production of cementitious C-A-S-H and N-A-S-H gels owing to GGBFS supplementation results in superior binding efficiency, which enables the concrete to resist better tensile cracking and opening of voids under the applied loads [61, 62]. This manifests as improved tensile strength. Moreover, the accelerator role of calcium facilitates geopolymerization, leading to refined microstructure and enhanced performance.

Additionally, oven-dried G.A. concrete showed consistently higher split tensile strengths over ambient air-dried G.A. concrete for all mixes. The 13–16% greater strength of oven-dried aggregates indicates the positive effects of controlled drying in facilitating stronger I.T.Z.s, allowing efficient transfer of stresses without crack propagation through

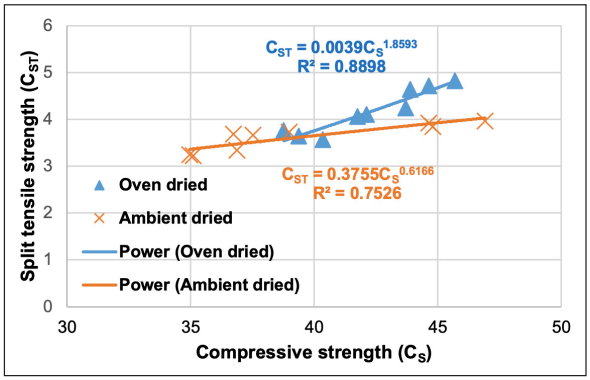

Figure 12. Regression analysis of compressive strength with split tensile strength.

the cross-section under tension [63]. In contrast, ambient drying leads to drying shrinkage cracks and poor bonding between aggregate and paste, lowering the tensile resistance [64]. The split tensile strength trends thus complement the compressive strength patterns, affirming the synergistic benefits of GGBFS incorporation and oven drying methodology in improving the strength attributes. The 80% fly ash - 20% GGBFS oven-dried G.A. demonstrated the optimal results meeting the target mean strength.

3.4. Effect of GGBFS Addition and Drying Method on Flexural Strength

The flexural strength increased from 4.33 MPa (Mix M1) to 5.1 MPa (Mix M3) for the oven-dried aggregates incorporated concrete mix and from 3.72 MPa to 4.22 MPa for the ambient air-dried geopolymer aggregate (GA) incorporated concrete mixes, as shown in Figure 11. The increment aligns with the formation of additional C-S-H gels (as shown in Figure 8b) owing to the higher reactivity of Ca-rich GGBFS, which enhances the load-bearing capacity [64]. As elucidated by Sitarz et al. [65], calcium modification disrupts aluminosilicate networks, facilitating increased dissolution and polycondensation, yielding semi-crystalline reaction products. This accelerated geopolymerization process aided by GGBFS produces a refined microstructure with superior inter-particle bonding strength, enabling enhanced resistance to bending stresses and cracks. Moreover, the release of Ca^{2+} ions further promotes the clay solubility and decomposition of mullite phases in fly ash, aiding better geopolymeric gel formation [66]. These synergistic effects facilitate notable improvements in flexural performance with GGBFS addition, as reflected in Figure 11.

The oven-dried G.A. concrete showed 12–15% higher flexural strength relative to ambient air-dried concrete across the different aggregate mixes (Fig. 11). The substantial enhancement highlights the significant impact of controlled drying in achieving consistent moisture removal without microcracking. This produces stronger transition zones between the aggregate and binder matrix (as shown in Figure 8b). Meanwhile, variable drying rates can induce stresses in ambient drying, causing shrinkage cracks that weaken the I.T.Z.s [63, 64]. Barbarey et al. [67] also reported a 10% drop in strength for ambient dried geopolymer

concrete compared to oven drying, which was attributed to cracking effects that influence flexural capacity.

3.5. Compressive Strength-Split Tensile Strength Correlation

A strong positive correlation (R^2=0.906) was obtained between the compressive and split tensile strength of geopolymer aggregates-based concrete prepared with varying GGBFS content and drying methods (Fig. 12). The split tensile strength increased concurrently from 3.63 MPa to 4.7 MPa as the compressive strength improved from 39.37 MPa to 44.64 MPa for oven-dried aggregates. The proportional enhancements are related to the comparable influences of GGBFS addition and controlled oven drying in refining the microstructure and paste-aggregate interfacial bonding [63]. The Ca-rich GGBFS promotes the dissolution of fly ash particles, aiding geopolymerization, which, along with the rapid, uniform drying, results in stronger transition zones between the two phases. This manifests as enhanced efficiency in transferring stresses under both compression and tension without crack initiation and propagation through the matrix [66]. Moreover, factors like the reduction in flaws and unreacted fly ash particles, which improve the compressive resistance by minimizing stress concentration sites, also raise the tensile strength by impeding crack propagation [68].

3.6. Compressive Strength-Flexural Strength Correlation

The compressive strength variations were also strongly correlated (R^2=0.898) with the flexural strength improvements between 3.72 MPa and 4.87 MPa for the geopolymer aggregates-based concrete (Fig. 13). The analogous effects of Ca-rich gel production from GGBFS and controlled oven drying in strengthening the paste matrix and aggregate interaction enhanced both capacities. The reduction in porosity refined the microstructure and improved inter-particle bonding while mitigating stress concentration sites. This mechanism simultaneously elevated the compressive and flexural strengths by delaying fracture under the respective loading scenarios. Additionally, the factors enhancing compressive resistance, like the decline in unreacted fly ash content and densification, aided superior flexural resistance by impeding crack initiation and propagation through the depth. Thus, the excellent correlation verifies that the strengthening mechanisms influencing both properties are interrelated.

3.7. Prediction of Split Tensile Strength

The experimental compressive strengths exhibited a strong linear correlation (R^2=0.906) with split tensile strengths for geopolymer aggregates incorporated concrete containing varying fly ash-GGBFS aggregate mixes and drying methods (Fig. 12). Leveraging this relationship, the regression equation derived was utilized to predict the split tensile strength values, which showed good agreement with experimental results, with variations within 1–3% (Table 5). For instance, the 100% fly ash based oven-dried geopolymer aggregates incorporated concrete showed only a 3.31% deviation between the experimental (3.63 MPa) and predicted (3.61 MPa) split tensile strengths. This concurrence verifies that the microstructural enhancements increasing the compressive strength, such as gel enrichment and reduced porosity, boost the tensile resistance by delaying crack initiation and propagation under tension loads. Additionally, factors like a refinement of flaws elevate the compressive capacity by minimizing stress concentration effects, and they raise the tensile strength simultaneously by impeding failure through the cross-section. Hence, a proportional increase in both strengths is obtained via similar strengthening mechanisms, as confirmed by the accurate prediction. The minor variations between experimental and predicted split tensile strengths for all oven-dried and ambient air-dried mixes substantiate the precision of the developed regression model for reliable forecasting based solely on the compressive strength data.

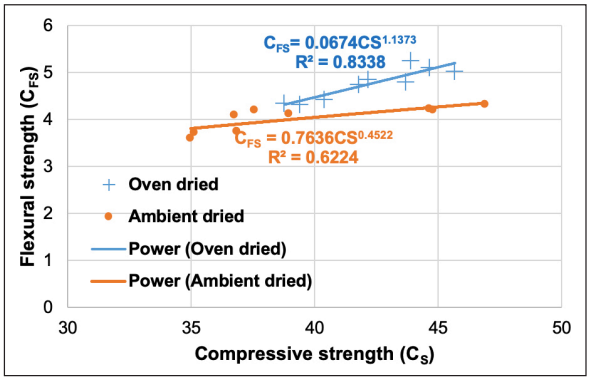

Figure 13. Regression analysis of compressive strength with flexural strength.

3.8. Prediction of Flexural Strength

The experimental relationship between compressive strength and flexural strength for the geopolymer aggregates incorporated concrete mixes (Fig. 13), represented by the linear regression equation, was utilized for anticipating flexural performance. As noted in Table 5, a good agreement was achieved between the experimental and predicted flexur-

Table 5. Predication of split tensile strength and flexural strength

Mixes	Experimental values						Predicted values			
	Oven-dried			Ambient dried			Oven-dried		Ambient dried	
	CS	ST	FS	CS	ST	FS	ST	FS	ST	FS
M1	39.37	3.63	5.42	35.11	3.23	3.72	3.61	4.39	3.37	3.82
M2	42.13	4.1	4.33	36.73	3.69	4.09	4.09	4.75	3.46	3.90
M3	44.64	4.7	4.87	38.94	3.92	4.22	4.55	5.07	3.59	4.00

al strengths with slight variations within 2–4%. This further verifies that the improvements in compressive strength from GGBFS-induced matrix densification and controlled oven drying can be correlated with concurrent flexural strength enhancements. The reduced porosity and enhanced paste-aggregate bonding enabled elevated resistance to bending stresses and fracture. Hence, the accurate prediction confirms that analogous mechanisms simultaneously elevate both capacities. Moreover, the precision substantiates the capability of the developed regression model for reliable flexural strength forecasting in geopolymer aggregate-based concretes using the easier-to-obtain compressive test data. This can enable quality assurance during mix design optimization for structural applications involving significant bending loads.

4. CONCLUSIONS

This study investigated the influence of GGBFS incorporation and drying methodology on the physical, mechanical, and microstructural characteristics of fly ash-based geopolymer aggregates and concrete. The following conclusions can be drawn:

- GGBFS addition (0% to 20%) to fly ash-based geopolymer aggregates significantly enhanced their properties: aggregate crushing value (25.84% to 20.8%), impact value (26.8% to 24.7%), abrasion value (15.34% to 13.67%), and water absorption (10.39% to 7.01%) for oven-dried mixes.
- Oven drying consistently resulted in superior aggregate properties compared to ambient air drying: crushing value (20.8% vs. 26.04%), impact value (24.7% vs. 27.49%), abrasion value (13.67% vs. 16.52%), and water absorption (7.01% vs. 10.61%) for 80% fly ash - 20% GGBFS mix.
- Compressive strength of geopolymer aggregate concrete increased with GGBFS content: 80% fly ash - 20% GGBFS oven-dried mix exhibited maximum strength (44.64 MPa), showing 26.31% and 14.28% enhancements over 100% fly ash mix for oven-dried and ambient dried samples, respectively.
- Split tensile and flexural strengths followed similar trends: 80% fly ash - 20% GGBFS oven-dried mix demonstrated optimal performance with 29.46% and 21.67% tensile strength enhancements and 12–15% higher flexural strength over ambient drying.
- Strong positive correlations between compressive strength and split tensile strength (R^2=0.906) and flexural strength (R^2=0.898) were observed, indicating simultaneous enhancement of mechanical properties.
- Regression equations accurately predicted split tensile (1–3% variation) and flexural strengths (2–4% variation) based on compressive strength data, substantiating the precision of the developed models for reliable forecasting.

In conclusion, the 80% fly ash - 20% GGBFS oven-dried geopolymer aggregate mix exhibited optimal physical, mechanical, and durability properties, with strong correlations enabling accurate performance predictions for structural applications. The findings establish that a controlled oven drying method and synergistic GGBFS addition can produce superior-quality fly ash-based geopolymer aggregates with reliable strength forecasting models.

ETHICS

There are no ethical issues with the publication of this manuscript.

DATA AVAILABILITY STATEMENT

The authors confirm that the data that supports the findings of this study are available within the article. Raw data that support the finding of this study are available from the corresponding author, upon reasonable request.

CONFLICT OF INTEREST

The authors declare that they have no conflict of interest.

FINANCIAL DISCLOSURE

The authors declared that this study has received no financial support.

USE OF AI FOR WRITING ASSISTANCE

Not declared.

PEER-REVIEW

Externally peer-reviewed.

REFERENCES

[1] Bagheri, S. M., Koushkbaghi, M., Mohseni, E., Koushkbaghi, S., & Tahmouresi, B. (2020). Evaluation of environment and economy viable recycling cement kiln dust for use in green concrete. *J Build Eng, 32*, 101809. [CrossRef]

[2] Venkatesh, C., Nerella, R., & Chand, M. S. R. (2021). Role of red mud as a cementing material in concrete: A comprehensive study on durability behavior. *Innov Infrastruct Solut, 6*(1), 13. [CrossRef]

[3] Xu, L. Y., Qian, L. P., Huang, B. T., & Dai, J. G. (2021). Development of artificial one-part geopolymer lightweight aggregates by crushing technique. *J Clean Prod, 315*, 128200. [CrossRef]

[4] Shivaprasad, K. N., Das, B. B., & Krishnadas, S. (2021). Effect of curing methods on the artificial production of fly ash aggregates. In *Recent Trends in Civil Eng: Select Proc of TMSF 2019* (pp. 23–32). Springer Singapore. [CrossRef]

[5] Harrison, E., Berenjian, A., & Seifan, M. (2020). Recycling of waste glass as aggregate in cement-based materials. Environ Sci Ecotechnol, 4, 100064. [CrossRef]

[6] Dong, Q., Wang, G., Chen, X., Tan, J., & Gu, X. (2021). Recycling of steel slag aggregate in portland cement concrete: An overview. *J Clean Prod, 282*, 124447. [CrossRef]

[7] Li, Z., Zhang, W., Jin, H., Fan, X., Liu, J., Xing, F., & Tang, L. (2023). Research on the durability and sustainability of an artificial lightweight aggregate concrete made from municipal solid waste incinerator bottom ash (MSWIBA). *Constr Build Mater, 365*, 129993. [CrossRef]

[8] Xu, L. Y., Huang, B. T., Lao, J. C., Yao, J., Li, V. C., & Dai, J. G. (2023). Tensile over-saturated cracking of Ultra-High-Strength Engineered Cementitious Composites (UHS-ECC) with artificial geopolymer aggregates. *Cem Concr Compos, 136*, 104896. [CrossRef]

[9] Tajra, F., Abd Elrahman, M., & Stephan, D. (2019). The production and properties of cold-bonded aggregate and its applications in concrete: A review. *Constr Build Mater, 225*, 29–43. [CrossRef]

[10] Qian, L. P., Xu, L. Y., Huang, B. T., & Dai, J. G. (2022). Pelletization and properties of artificial lightweight geopolymer aggregates (G.P.A.): One-part vs. two-part geopolymer techniques. *J Clean Prod, 374*, 133933. [CrossRef]

[11] Ma, X., Da, Y., He, T., Su, F., & Wan, Z. (2024). Improvement of harmlessness and resource utilization of incineration fly ash by high temperature sintering. *J Build Eng, 84*, 108589. [CrossRef]

[12] Biernacki, J. J., Vazrala, A. K., & Leimer, H. W. (2008). Sintering of a class F fly ash. *Fuel, 87*(6), 782–792. [CrossRef]

[13] Aungatichart, O., Nawaukkaratharnant, N., & Wasanapiarnpong, T. (2022). The potential use of cold-bonded lightweight aggregate derived from various types of biomass fly ash for preparation of lightweight concrete. *Mater Lett, 327*, 133019. [CrossRef]

[14] Huang, H., Yuan, Y., Zhang, W., & Gao, Z. (2019). Bond behavior between lightweight aggregate concrete and normal weight concrete based on splitting-tensile test. *Constr Build Mater, 209*, 306–314. [CrossRef]

[15] Kwek, S. Y., Awang, H., Cheah, C. B., & Mohamad, H. (2022). Development of sintered aggregate derived from POFA and silt for lightweight concrete. *J Build Eng, 49*, 104039. [CrossRef]

[16] UNE (2003). *Lightweight aggregates - Part 1: Lightweight aggregates for concrete, mortar, and grout*. UNE-EN-13055-1.

[17] Bekkeri, G. B., Shetty, K. K., & Nayak, G. (2023). Synthesis of artificial aggregates and their impact on performance of concrete: a review. *J Mater Cycles Waste Manag, 25*, 1–24. [CrossRef]

[18] Gomathi, P., & Sivakumar, A. (2014). Synthesis of geopolymer based class-F fly ash aggregates and its composite properties in concrete. *Arch Civ Eng, 60*(1), 55–75. [CrossRef]

[19] Vasugi, V., & Ramamurthy, K. (2014). Identification of admixture for pelletization and strength enhancement of sintered coal pond ash aggregate through statistically designed experiments. *Mater Des, 60*, 563–575. [CrossRef]

[20] Geetha, S., & Ramamurthy, K. (2013). Properties of geopolymerised low-calcium bottom ash aggregate cured at ambient temperature. *Cem Concr Compos, 43*, 20–30. [CrossRef]

[21] Asadizadeh, M., Clements, C., Hedayat, A., Tunstall, L., Gonzalez, J. A. V., Alvarado, J. W. V., & Neira, M. T. (2023). The effect of class F fly ash on the geopolymerization and compressive strength of lightweight aggregates made from alkali-activated mine tailings. *Constr Build Mater, 395*, 132275. [CrossRef]

[22] Colangelo, F., Messina, F., & Cioffi, R. (2015). Recycling of MSWI fly ash by means of cementitious double step cold bonding pelletization: Technological assessment for the production of lightweight artificial aggregates. *J Hazard Mater, 299*, 181–191. [CrossRef]

[23] Gomathi, P., & Sivakumar, A. (2015). Accelerated curing effects on the mechanical performance of cold bonded and sintered fly ash aggregate concrete. *Constr Build Mater, 77*, 276–287. [CrossRef]

[24] Gesoğlu, M., Özturan, T., & Güneyisi, E. (2007). Effects of fly ash properties on characteristics of cold-bonded fly ash lightweight aggregates. *Constr Build Mater, 21*(9), 1869–1878. [CrossRef]

[25] Qian, L. P., Huang, B. T., Xu, L. Y., & Dai, J. G. (2023). Concrete made with high-strength artificial geopolymer aggregates: Mechanical properties and failure mechanisms. *Constr Build Mater, 367*, 130318. [CrossRef]

[26] BIS. (1963). *Standard method of test for aggregates for concrete: Part IV Mechanical properties*. Bureau of Indian Standards, New Delhi. BIS I.S.: 2386 (Part IV)-1963.

[27] Terzić, A., Pezo, L., Mitić, V., & Radojević, Z. (2015). Artificial fly ash based aggregates properties influence on lightweight concrete performances. *Ceram Int, 41*(2), 2714–2726. [CrossRef]

[28] Mukkala, P., Venkatesh, C., & Habibunnisa, S. (2022). Evaluation of mix ratios of light weight concrete using geopolymer as binder. *Mater Today Proc, 52*, 2053–2056. [CrossRef]

[29] Gomathi, P., & Sivakumar, A. (2015). Accelerated curing effects on the mechanical performance of cold bonded and sintered fly ash aggregate concrete. *Constr Build Mater, 77*, 276–287. [CrossRef]

[30] Khanna, A. R., Satyanarayana, G. V. V., Raju, Y. K., & Ramanjaneyulu, N. (2023, September). Experimental investigation on mix design of foam concrete to fix ingredients for various densities. In A.I.P. *Conf Proc Vol. 2754*, No. 1. A.I.P. Publishing. [CrossRef]

[31] Venkatesh, C., Ruben, N., & Chand, M. S. R. (2020). Red mud as an additive in concrete: comprehensive characterization. *J Korean Ceram Soc, 57*(3), 281–289. [CrossRef]

[32] Venkatesh, C., Nerella, R., & Chand, M. S. R. (2020). Experimental investigation of strength, durability, and microstructure of red-mud concrete. *J Korean Ceram Soc, 57*(2), 167–174. [CrossRef]

[33] Ramanjaneyulu, N., Rao, M. S., & Desai, V. B. (2019). Behavior of self-compacting concrete partial replacement of coarse aggregate with pumice lightweight aggregate. *Int J Recent Technol Eng, 7*(6C2):434–440.

[34] Özkan, H., Kabay, N., & Miyan, N. (2022). Properties of cold-bonded and sintered aggregate using washing aggregate sludge and their incorporation in concrete: A promising material. *Sustainability, 14*(7), 4205. [CrossRef]

[35] Zhang, H., Zhao, Y., Meng, T., & Shah, S. P. (2016). Surface treatment on recycled coarse aggre-

gates with nanomaterials. *J Mater Civ Eng, 28*(2), 04015094. [CrossRef]

[36] Priyanka, M., Muniraj, K., & Madduru, S. R. C. (2022). Influence of geopolymer aggregates on micro-structural and durability characteristics of O.P.C. concrete. *J Build Pathol Rehabil, 7*(1), 13. [CrossRef]

[37] Strokova, V., Zhernovsky, I., Ogurtsova, Y., Maksakov, A., Kozhukhova, M., & Sobolev, K. (2014). Artificial aggregates based on granulated reactive silica powders. *Adv Powder Technol, 25*(3), 1076–1081. [CrossRef]

[38] Sahoo, S., & Selvaraju, A. K. (2020). Mechanical characterization of structural lightweight aggregate concrete made with sintered fly ash aggregates and synthetic fibres. *Cem Concr Compos, 113*, 103712. [CrossRef]

[39] Li, J., Niu, J., Wan, C., Liu, X., & Jin, Z. (2017). Comparison of flexural property between high performance polypropylene fiber reinforced lightweight aggregate concrete and steel fiber reinforced lightweight aggregate concrete. *Constr Build Mater, 157*, 729–736. [CrossRef]

[40] Punlert, S., Laoratanakul, P., Kongdee, R., & Suntako, R. (2017, September). Effect of lightweight aggregates prepared from fly ash on lightweight concrete performances. In *J Phys Conf Ser Vol. 901, No. 1, p. 012086*. I.O.P. Publishing. [CrossRef]

[41] Sravya, Y. L., Manoj, T., & Rao, M. S. (2021). Effect of temperature curing on lightweight expanded clay aggregate concrete. *Mater Today Proc, 38*, 3386–3391. [CrossRef]

[42] ASTM. (2019). *Standard specification for Portland cement. ASTM International, West Conshohocken*. ASTM C150, C150M-19a.

[43] ASTM. (2022). *Standard specification for coal FA and raw or calcined natural pozzolan for use in concrete*. ASTM International, West Conshohocken. ASTM C 618.

[44] ASTM. (2018). *Standard specification for slag cement for use in concrete and mortars*. ASTM International, West Conshohocken. ASTM C989, C989M-18a.

[45] BIS. (2016). *Specification for coarse and fine aggregates from natural sources for concrete*. Bureau of Indian Standards, New Delhi. BIS IS 383-2016.

[46] Shivaprasad, K. N., & Das, B. B. (2018). Determination of optimized geopolymerization factors on the properties of pelletized fly ash aggregates. *Constr Build Mater, 163*, 428–437. [CrossRef]

[47] BIS. (2002). *Part- IV Specification for methods of test for aggregates for concrete: Mechanical tests*. Bureau of Indian Standards, New Delhi. BIS IS 2386-2002.

[48] BIS. (2002). *Part- III Specification for methods of test for aggregates for concrete: Physical tests*. Bureau of Indian Standards, New Delhi. BIS IS 2386-2002.

[49] BIS. (2019). *Specification for mix design guidelines for concrete*. Bureau of Indian Standards, New Delhi. BIS IS 10262–2019.

[50] BIS. (1959). Specification for methods of tests for strength of concrete. Bureau of Indian Standards, New Delhi. BIS IS 516–1959.

[51] Chava, V., & Chereddy, S. S. D. (2023). Effect of calcination on the physical, chemical, morphological, and cementitious properties of red mud. *J Sustain Constr Mater Tech, 8*(4), 297–306. [CrossRef]

[52] Chava, V., Mv, S. R., Munugala, P. K., & Chereddy, S. S. D. (2024). Effect of mineral admixtures and curing regimes on properties of self-compacting concrete. *J Sustain Constr Mater Tech, 9*(1), 25–35. [CrossRef]

[53] BIS. (1999). *Specification for splitting tensile strength of concrete—method of test*. Bureau of Indian Standards, New Delhi. BIS IS 5816-1999.

[54] Durga, C. S. S., Venkatesh, C., Muralidhararao, T., & Bellum, R. R. (2023). Crack healing and flexural behaviour of self-healing concrete influenced by different bacillus species. *Res Eng Struct Mater, 9*(4), 1459–1475. [CrossRef]

[55] Ruben, N., Venkatesh, C., Durga, C. S. S., & Chand, M. S. R. (2021). Comprehensive study on performance of glass fibers-based concrete. *Innov Infrastruct Solut, 6*(2), 112. [CrossRef]

[56] Chaitanya, B. K., Sivakumar, I., Madhavi, Y., Cruze, D., Venkatesh, C., Naga Mahesh, Y., & Sri Durga, C. S. (2024). Microstructural and residual properties of self-compacting concrete containing waste copper slag as fine aggregate exposed to ambient and elevated temperatures. *Infrastructures, 9*(5), 85. [CrossRef]

[57] Li, Y., Huang, L., Gao, C., Mao, Z., & Qin, M. (2023). Workability and mechanical properties of GGBS-RFBP-FA ternary composite geopolymer concrete with recycled aggregates containing recycled fireclay brick aggregates. *Constr Build Mater, 392*, 131450. [CrossRef]

[58] Nicula, L. M., Manea, D. L., Simedru, D., Cadar, O., Ardelean, I., & Dragomir, M. L. (2023). The advantages of using GGBS and ACBFS aggregate to obtain an ecological road concrete. *Coatings, 13*(8), 1368. [CrossRef]

[59] Abdollahnejad, Z., Mastali, M., Woof, B., & Illikainen, M. (2020). High strength fiber reinforced one-part alkali activated slag/fly ash binders with ceramic aggregates: Microscopic analysis, mechanical properties, drying shrinkage, and freeze-thaw resistance. *Constr Build Mater, 241*, 118129. [CrossRef]

[60] Erdem, S., Dawson, A. R., & Thom, N. H. (2012). Influence of the micro- and nanoscale local mechanical properties of the interfacial transition zone on impact behavior of concrete made with different aggregates. *Cem Concr Res, 42*(2), 447–458. [CrossRef]

[61] Criado, M., Aperador, W., & Sobrados, I. (2016). Microstructural and mechanical properties of alkali activated Colombian raw materials. *Materials, 9*(3), 158. [CrossRef]

[62] Gao, X., Yu, Q. L., & Brouwers, H. J. H. (2016, August). Development of alkali activated slag-fly ash mortars: mix design and performance assessment. In *4th Int Conf Sustain Constr Mater Tech, SCMT 2016* (p. S167). [CrossRef]

[63] Elsharief, A., Cohen, M. D., & Olek, J. (2005). Influence of lightweight aggregate on the microstructure and durability of mortar. *Cem Concr Res, 35*(7), 1368–1376. [CrossRef]

[64] Abd Razak, R., Al Bakri, A. M., Kamarudin, H., Is-

mail, K. N., Hardjito, D., & Zarina, Y. (2016). Performances of Artificial Lightweight Geopolymer Aggregate (ALGA) in O.P.C. Concrete. *Key Eng Mater, 673*, 29–35. [CrossRef]

[65] Sitarz, M., Urban, M., & Hager, I. (2020). Rheology and mechanical properties of fly ash-based geopolymer mortars with ground granulated blast furnace slag addition. *Energies, 13*(10), 2639. [CrossRef]

[66] Bellum, R. R., Venkatesh, C., & Madduru, S. R. C. (2021). Influence of red mud on performance enhancement of fly ash-based geopolymer concrete. *Innov Infrastruct Solut, 6*(4), 215. [CrossRef]

[67] Barbarey, M. S., Seleman, M. M. E. S., El Kheshen, A. A., & Zawrah, M. F. (2024). Utilization of ladle furnace slag for fabrication of geopolymer: Its application as catalyst for biodiesel production. *Constr Build Mater, 411*, 134226. [CrossRef]

[68] Bellum, R. R., Al Khazaleh, M., Pilla, R. K., Choudhary, S., & Venkatesh, C. (2022). Effect of slag on strength, durability and microstructural characteristics of fly ash-based geopolymer concrete. *J Build Pathol Rehabil, 7*(1), 25. [CrossRef]

J Sustain Const Mater Technol, Vol. 9, Issue. 2, pp. 106–113, June 2024

Journal of Sustainable Construction Materials and Technologies
Web page info: https://jscmt.yildiz.edu.tr
DOI: 10.47481/jscmt.1501623

JSCMT
Journal of Sustainable Construction Materials and Technologies

Research Article

Evaluation of the effect of para-aramid and micro-polyolefin fibers on permanent displacement in stone mastic asphalt

Sepehr SAEDI*

Department of Civil Engineering, Altinbas University, İstanbul, Türkiye

ARTICLE INFO

Article history
Received: 15 March 2024
Revised: 20 May 2024
Accepted: 04 June 2024

Key words:
Fatigue, micro-polyolefin, para-aramid, rutting, static creep, stone mastic asphalt

ABSTRACT

This study examines the role of fibers formed from para-aramid and micropolyethylene in enhancing the performance of stone mastic asphalt (SMA) mixtures against permanent deformation. The use of SMA mixtures has the potential to mitigate permanent deformation and plasticity. Marshall tests, static creep tests, fatigue tests, and wheel track tests were conducted on samples prepared using the modified Marshall design method to achieve the research objectives. According to the test results, Samples containing 1.5% of the fiber mixture's total weight exhibited greater strength than other samples. Additionally, these samples demonstrated the most minor displacement against rutting among all prepared samples. Based on these findings, incorporating fibers containing Para-aramid and Micro-polyolefin in SMA mixtures can enhance the performance of this type of mixture against permanent deformations.

Cite this article as: Saedi, S. (2024). Evaluation of the effect of para-aramid and micro-polyolefin fibers on permanent displacement in stone mastic asphalt. *J Sustain Const Mater Technol*, 9(2), 106–113.

1. INTRODUCTION

A multitude of factors influences road longevity. Variances in soil composition, traffic volume, vehicle types, and precipitation levels along different road sections can lead to diverse drawbacks and deficiencies. Failure to inspect, evaluate, and maintain roads promptly can lead to rapid deterioration. This results in significant financial losses and leads to dissatisfaction among road users. Hence, utilizing new asphalt technologies becomes imperative to extend the lifespan of roads and minimize road maintenance expenses. In the 1970s, researchers developed Stone Mastic Asphalt (SMA) mixtures to mitigate road pavement issues. This type of mixture offers significant advantages, including high stability, resistance to permanent deformation, and resilience against rutting [1]. SMA is a gap-graded asphalt mixture characterized by a substantial coarse aggregate, maximizing interlocking between aggregates to establish an efficient load distribution network. The stone skeleton is filled with a bitumen mastic mixture containing filler, to which fibers are added. This addition ensures sufficient stability of the bitumen and prevents drainage of the binder during transport and placement. Typically, SMA consists of a high proportion of coarse aggregates and a minimal amount of fine aggregates, resulting in a particle grading commonly known as gap-graded [2]. Fibers serve multiple purposes in SMA mixtures, including reinforcement, enhancing tensile strength, extending fatigue life, and preventing bitumen drainage. Mineral and cellulosic fibers are the most frequently utilized types within SMA mixtures [3]. Polypropylene fibers, for example, are known to have a beneficial effect on enhancing the resistance of SMAs against rutting [4]. Adding Proplast (Proplast is a highly porous material composed of a Teflon fluorocarbon.) as an additive to SMA mixtures improves their resistance to permanent deformations and reduces settlement caused by rutting [5].

***Corresponding author.**
*E-mail address: sepehr.saedi@altinbas.edu.tr

Table 1. Aggregate characteristics

Characteristic	Code	Unit	Results	Requirement
Coarse specific gravity	ASTM C-127-15 [18]	gr / cm^3	2.751	
Fine specific gravity	ASTM C-128-15 [19]	gr / cm^3	2.747	
Filler specific gravity	ASTM C-128-15 [19]	gr / cm^3	2.750	
Los Angeles	ASTM C-131 [20]	%	16	30 max.
Water absorption	ASTM C-127-15 [18]	%	0.85	2 max.
Flat and elongated	ASTM D-4791 [21]	%	12	5 max.
Crushed content (two faces)	ASTM D-5821 [22]	%	96	90 min.

Laboratory research indicates that using carbon fibers improves the resistance of SMAs to permanent deformations and enhances the load-bearing capacity of the surface layer [6]. The addition of glass fiber improves the properties of SMA mixtures by reducing instability, increasing flow value, and decreasing voids in the mix [7]. Furthermore, adding fiber enhances fatigue properties by increasing resistance to cracking and permanent deformation in bituminous mixtures [6]. Based on conducted studies, using 0.4% basalt fibers in SMA (Stone Mastic Asphalt) mixtures improves their resistance to permanent deformations up to 40 °C. Thus, it significantly prevents the formation of rutting in the wheel path [8]. The use of ethylene-vinyl acetate in SMA mixtures leads to an increase in dynamic modulus and resistance against the rutting phenomenon [9]. The results of uniaxial dynamic creep tests at temperatures of 25, 40, and 60 °C on SMA samples containing FRP (Fiber Reinforced Polymer) fibers plus Viatop (a pelletized blend of natural cellulose fibers and bitumen) indicate that the mentioned additive combination leads to an increase in the load-bearing capacity of the surface layer. These additives play an instrumental role in enhancing the resistance of these mixtures against rutting [10]. Natural fibers can indeed significantly enhance the rut resistance of SMAs. Adding natural fibers to pavement can increase structural resistance against pavement distress [11]. Studies have shown that the combination of basaltic and cellulose fibers has increased the resistance of SMA mixtures against the phenomenon of rutting. Recent research has shown that combining crumb rubber fibers and glass fibers improves the dynamic modulus of Stone Mastic Asphalt (SMA) mixtures [12]. Laboratory research has demonstrated that incorporating a mixture of polypropylene and aramid fibers into hot-mix asphalt enhances its mechanical properties [13]. Research indicates polyolefin-aramid composite fibers resist fatigue cracking within the blend [14]. Several studies have examined the impact of polyolefin-aramid fibers and hydrated lime on porous asphalt mixtures' functional and mechanical performance [15]. The test results indicate that mixtures modified with aramid fibers improve fatigue performance compared to the virgin mixture [16]. Research suggests that despite higher initial costs associated with SMA mixtures containing fibers, repair and maintenance costs are reduced considering the improved performance characteristics of these mixtures. Ultimately, this results in a lower life cycle cost [17]. The use of fibers to enhance the characteristics of asphalt mixtures continues by researchers in various parts of the world. This research aims to investigate the possibility of using fibers that, in addition to being cost-effective, can be easily added to SMA mixtures during the mixing stages, creating a homogeneous mixture.

2. MATERIALS AND METHODS

2.1. Aggregates

Basalt aggregates sourced from Uskumruköy in the western part of İstanbul, Türkiye, were used in this study. Samples underwent qualitative mechanical tests, and the outcomes are detailed in Table 1.

The grading curve depicted in Figure 1 illustrates the aggregate gradation used in the mixture [16].

As depicted in Figure 1, the curves represented by black lines delineate the upper and lower limits of the gradation stipulated in the code. In contrast, the red lines and dark dots illustrate the gradation curves of the aggregates used.

2.2. Binder

In this study, the binder used is 50/70, produced by Tupras Company. The physical characteristics of the used binder are outlined in Table 2.

2.3. Additive

Fibers, including Para-aramid and Micro-polyolefin, are formed from long molecular chains of poly-phenylene terephthalamide, and the inter-chain bonds significantly strengthen the material. These fibers derive some of their high strength from hydrogen bonds between neighboring carbonyl groups of polymer chain molecules. These interactions significantly impact the structure of stiff and sturdy molecules that typically create sheet-like structures. SIRJAN NANO Company, IRAN, provided the fibers used in this study. Some physical properties of the fibers, including Para-aramid and Micro-polyolefin, utilized in this research are presented in Table 3. A fiber image is provided in Figure 2.

2.4. Mix Design

In this research, the Marshall modification method [23]. It was employed to determine the optimal bitumen percentage for the mixture. The volume of air-filled spaces in compacted samples emerges as the paramount design parameter for SMA mixtures [24].

Marshall samples were prepared by gradually adding bitumen at a rate of 0.5%, ranging from 4.5% to 7% by weight

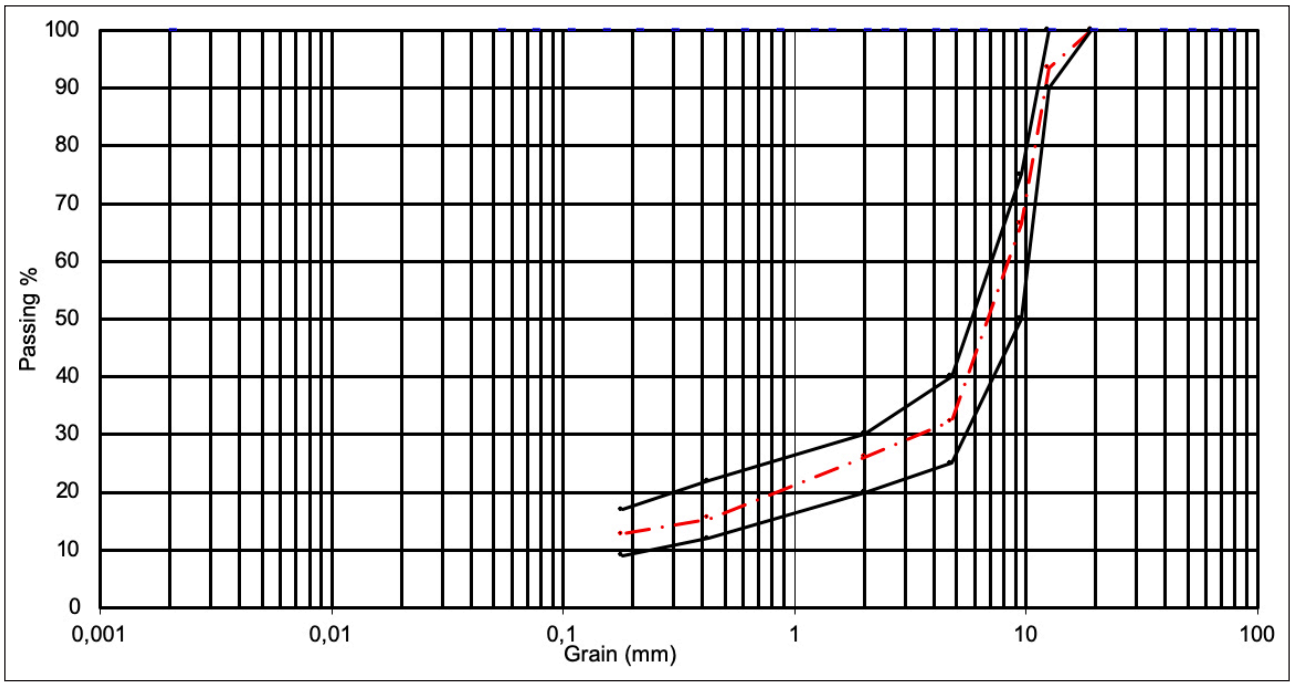

Figure 1. Granulometric curve.

Table 2. The physical properties of 50/70 binder

Test	Code	Unit	Results
Ductility	ASTM D-113	cm	**100+**
Softening point (ring and ball)	ASTM D-36	˚C	49
Penetration at 25 °C	ASTM D-5	mm / 10	60
Flash point	ASTM D-92	˚C	280
Specific gravity	ASTM D-70	gr / cm^3	1.01
Solubility in trichloroethylene	ASTM D-2042	%	**99**

Table 3. Properties of fiber

Properties	Values
Fiber length (mm)	6–19
Black density (g/cm^3)	2.6
Tensile stress (Mpa)	750–900
Flash point (°C)	500

of the mixture. Afterward, the samples were compacted by applying 50 blows to both surfaces. Following determining the optimal bitumen content through preliminary tests, fibers were added to the aggregates at percentages of 0.5, 1, 1.5, and 2 of the total weight. In line with the research objectives, 130 Marshall and six samples of slab shape were prepared. In Figure 3, the image of the prepared samples is shown.

2.5. Marshall Quotient

The Marshall quotient is a parameter to estimate the stiffness of the asphalt mixture against permanent deformation (Fig. 4). By increasing the value of it, it can be said that the resistance of the asphalt mixture against permanent deformation has been improved [25].

Figure 2. Fiber Image www.sirjannano.com.

2.6. Static Creep

The static creep test is crucial to assessing asphalt mixtures' durability under static loads (Fig. 5). In this evaluation, a uniaxial load is applied to the specimen, removed, and the resulting permanent deformation is measured. The creep modulus derived from this test enables the prediction of asphalt mixtures' susceptibility to thermal cracking and rutting. In our investigation, we adhered to the ASTM D6927 standard procedure for conducting the static creep test. Here, specimens were subjected to a 150 kPa compressive load at 25 °C for 3600 seconds, with deformation values

Figure 3. Sample prepare.

Figure 4. Marshall quotient test.

Figure 5. Static creep test.

recorded after this duration. The static creep values for the specimens were determined using Equation (1) [26].

Ecq (t)

$$= \frac{\sigma}{\varepsilon c(t)} \quad (1)$$

$E_{cq\,(t)}$: Creep Modulus in Time t (MPa), σ: Stress (MPa), $\varepsilon_{c\,(t)}$: Strain in Time t

2.7. Wheel Track Test

The wheel track test used prepared samples measuring 500 mm in length, 180 mm in width, and 50 mm in height. Approximately twelve hours before initiating the test, the samples were exposed to a temperature of 60 °C. The LCPC device was set up so that each wheel applied a force of 500 N to the samples. A laboratory-tired compactor provided the compaction for the samples. Typically, the tire was rolled over each sample for 30,000 cycles, exerting a load of 500 N to a pneumatic tire inflated to 600 kPa. This study conducted the LCPC test for each prepared mixture at various cycle intervals, specifically at 1000, 3000, 5000, 10,000, 30,000, and 50,000 cycles [27] (Fig. 6).

2.8. Fatigue Test

Asphalt samples endure repeated loading during the indirect tensile fatigue test until failure is reached (Fig. 7). Various stress sources are applied to the samples throughout this process. The fatigue life (N_f) is subsequently calcu-

Figure 6. LCPC test.

lated based on the stress level that triggers failure, which can be derived from the following equation [28].

$$N_f = K_1 \left(\frac{1}{\sigma}\right)^{K_2} \quad (2)$$

where: N_f: Fatigue life, K_1, K_2: Material properties dependent coefficients, σ: Stress

3. RESULTS

3.1. SMA Design Results

The mixing process steps were performed using the modified Marshall method, and the optimal bitumen amount was calculated. These calculations are detailed in Table 4.

As expected, the optimal bitumen percentage increased with the increase in fiber percentage.

3.2. The Marshall Quotient Results

As depicted in Figure 8, samples containing 1.5% fibers, Para-aramid, and Micro polyolefin have notably enhanced the Marshall Quotient. Consequently, it can be inferred that these fibers strengthen the stiffness of the mixture, thereby potentially contributing to the improvement of its resistance against deformations. The results show that samples containing 1.5% fibers Marshall Quotient increased by 26% compared to non-additive samples.

3.3. The Results of Static Creep

Marshall samples were prepared and subjected to a uniaxial static creep test. The results, showing the permanent deformations caused by static loading, are presented in Figure 9.

Figure 7. Indirect tensile fatigue test.

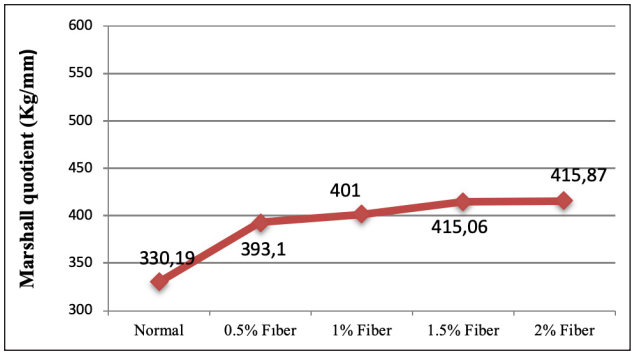

Figure 8. The results of the Marshall quotient.

As illustrated in Figure 9, upon applying load to the sample, there was an initial increase in instantaneous deformation, followed by a period where the rate of deformation increase slowed down. The findings indicated that the rise in instantaneous deformations in fiber sam-

Table 4. Results of Marshall's design

Mix type	Non. add.	0.5% fiber	1% fiber	1.5% fiber	2% fiber
Optimal bitumen (%)	6.59	6.67	6.74	6.79	6.81
Marshall stability (Kg)	1050	1195	1240	1295	1310
Flow (mm)	3.18	3.04	3.09	3.12	3.15
Air voids (%)	4	3,76	3,38	3.18	3.09
Voids in the mineral aggregate (%)	14.52	14,37	14.1	13.96	13.9
Voids filled with asphalt (%)	72.44	73.86	75.99	77.22	77.72

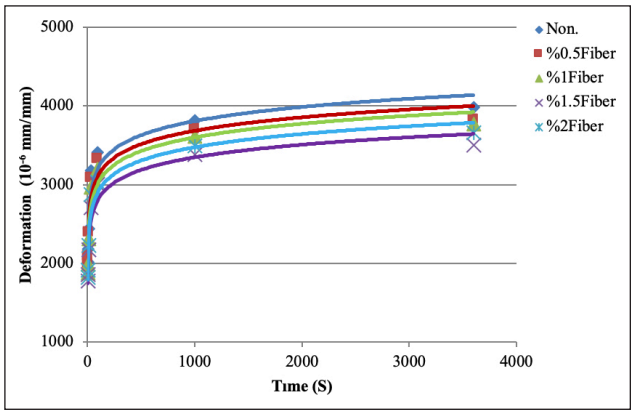

Figure 9. Static creep test results.

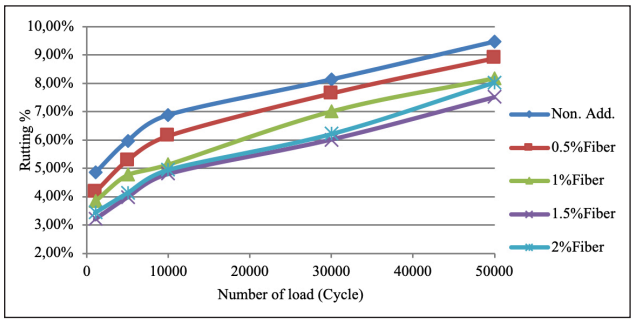

Figure 10. The results of the LCPC test.

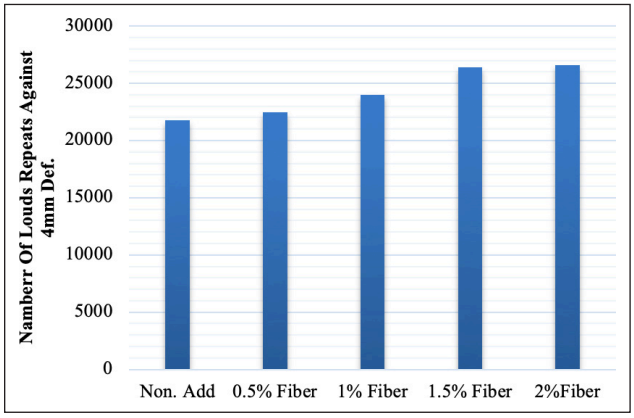

Figure 11. Fatigue test results.

ples was lower than those without additives. In samples with additives compared to those without, the amount of these changes at the end of 3600 seconds showed a reduction of approximately 4%, 5.5%, 12%, and 8%, respectively. Adding fibers to the mixture has enhanced the bonding between bituminous aggregates, resulting in the modified mixture exhibiting more excellent resistance under creep loads. Therefore, it can be concluded that adding fibers containing Para-aramid and Micro-polyolefin enhances the resistance of SMAs against the phenomenon of rutting caused by static loads from heavy vehicles.

3.4. The Results of the Wheel Track Test

The results of the wheel track rutting test conducted using the LCPC method are presented in Figure 10.

The rutting on the asphalt surface resulting from 30,000 wheel passes should not exceed 6%, according to the LCPC method. Based on the graphs, it is evident that samples containing fibers with Para-aramid and Micro-polyolefin exhibited superior resistance to rutting. Based on the curves from the Rutting test using the LCPC method, only the samples containing 1.5% fibers could meet the conditions specified in the LCPC test standard. According to the comparative curves, incorporating 1.5% of these fibers in SMAs reduces the percentage of rutting in 30,000 load cycles by 26% compared to samples without additives. Additionally, the analysis of the results revealed that the percentage of rutting increased in samples with a rate exceeding 1.5%. The fibers have enhanced the mixture's resistance to permanent deformation by increasing its hardness. This test's results further validate the Marshall index test findings. Increasing the amount of fibers in the mixture reduces the friction between aggregates and mastic.

3.5 The result of Fatigue Test

The results of the indirect tensile fatigue test are depicted in Figure 11. The test was conducted at a temperature of 25 degrees Celsius using a prepared sample, with loading repeated until a deformation of 4 mm was observed in the samples. As the weight percentage of fiber increased, the number of loading cycles until complete deformation also increased. Furthermore, increasing the weight percentage of fibers, particularly those containing Para-aramid and Micro-polyolefin, led to more loading cycles until complete deformation ensued.

Experimental results indicated that including fibers containing Para-aramid and Micro-polyolefin improved the stiffness of the SMA mixture. Analysis of the resulting graph reveals that augmenting the number of fibers containing para-aramid and micro-polyolefin in SMA mixtures increased the load repetition cycle by 22% in the samples. Fibers reinforce the asphalt mix, resulting in improved durability. As a result of stresses acting in various directions, samples with additives experience lower stress concentration and fatigue failure compared to those without additives. Fatigue cracks are a significant contributor to pavement failure. A 30% increase in such failures can impair the performance of asphalt surfaces, necessitating repair operations. Employing protective methods becomes unavoidable [29]. Hence, enhancing fatigue resistance can substantially mitigate maintenance costs. Based on the fatigue test results, it is evident that incorporating para-aramid and micro-polyolefin fibers into Stone Mastic Asphalt (SMA) can effectively lower the maintenance costs associated with these pavement types.

4. CONCLUSONS

This study aimed to evaluate the effects of Para-aramid and Micro-polyolefin fibers on Stone Mastic Asphalts' fatigue and rutting properties. Below are the results of the investigation.

Incorporating fibers containing Para-aramid and Micro-polyolefin as additives to the SMA mixture enhanced the Marshall index parameter of this mixture type. This improvement suggests potential reinforcement against permanent deformations, contingent upon other necessary conditions being met.

The research results demonstrate that adding a combination of Para-aramid and Micro-polyolefin fibers to SMA mixtures enhances their resistance to deformation caused by heavy static loads.

Results from the rutting test revealed that samples without additives exhibited the highest rate of rutting, while those containing 1.5% fibers showed the lowest. Notably, the samples containing 1.5 fiber met the 6% rutting limit specified in the standard for hot asphalt mixtures, as determined by the rutting test conducted via the LCPC method.

Incorporating Para-aramid and Micro-polyolefin fibers into SMA mixtures enhances their fatigue resistance against repeated loading. Consequently, these fibers can reduce repair and retrofitting costs attributed to fatigue-related deterioration.

Those containing 1.5% Para-aramid and Micro-polyolefin fibers exhibited the most favorable outcomes among the prepared samples. However, increasing the fiber percentage disrupts the uniform texture of SMA mixtures, thereby diminishing the fibers' effectiveness in enhancing the mixture's resistance to permanent deformations.

Based on the results obtained from the conducted physical and functional tests, it can be concluded that incorporating fatty fibers containing Para-aramid and Micro-polyolefin into SMA mixtures can effectively contribute to reducing maintenance costs associated with these mixtures.

The research results indicated that this mixture exhibits significantly enhanced resistance to permanent deformations and demonstrates good resilience to rutting in hot climate areas with heavy traffic.

ETHICS

There are no ethical issues with the publication of this manuscript.

DATA AVAILABILITY STATEMENT

The authors confirm that the data that supports the findings of this study are available within the article. Raw data that support the finding of this study are available from the corresponding author, upon reasonable request.

CONFLICT OF INTEREST

The authors declare that they have no conflict of interest.

FINANCIAL DISCLOSURE

The authors declared that this study has received no financial support.

USE OF AI FOR WRITING ASSISTANCE

Not declared.

PEER-REVIEW

Externally peer-reviewed.

REFERENCES

[1] Valkering, C.P., Lancon, D. J. L., Dehilster, E. & Stoker, D.A. (1990). Rutting resistance of asphalt mixes containing non-conventional and polymer-modified binders (with discussion and closure). J *Assoc Asph Paving Technols, 59*, 590–609.

[2] Mokhtari, A. & Nejad, F. M. (2012). Mechanistic approach for fiber and polymer modified SMA mixtures. *Constr Building Mater, 36*, 381–390. [CrossRef]

[3] Putman, B. J. & Amirkhanian, S. N. (2004). Utilization of waste fibers in stone matrix asphalt mixtures. *Resour Conserv Recycl, 42*(3), 265–274. [CrossRef]

[4] Tapkin, S., Çevik, A., Uşar, Ü. & Gülşan, E. (2013). Rutting prediction of asphalt mixtures modified by polypropylene fibers via repeated creep testing by utilising genetic programming. *Mater Res, 16*, 277–292. [CrossRef]

[5] Saedi, S., Sadeghian Asl, G., & Yasrobi, S. H. (2018). The combined effect of SBS and proplast in improving the stone mastic asphalt performance. *Quarterly J Transportation Eng, 10*(2), 385–399.

[6] Aboutalebi Esfahani, M., & Mirian, V. (2021). Evaluation of glass fibers, ethylene vinyl acetate and their combination on stone mastic asphalt. *Australian J Civil Eng, 19*(2), 134–147. [CrossRef]

[7] Ma, R., Haldenbilen, S., & Zengin, D. (2023). Investigation of usability of mineral fiber in stone mastic asphalt. *Revista de la Construcción, 22*(3), 569–580. [CrossRef]

[8] Cetin, A., Evirgen, B., Karslioglu, A., & Tuncan, A. (2021). The effect of basalt fiber on the performance of stone mastic asphalt. *Period Polytech Civ Eng, 65*(1), 299–308. [CrossRef]

[9] Chegenizadeh, A., Tokoni, L., Nikraz, H., & Dadras, E. (2021). Effect of ethylene-vinyl acetate (EVA) on stone mastic asphalt (SMA) behaviour. *Constr Build Mater, 272*, 121628. [CrossRef]

[10] Saedi, S., & Oruc, S. (2020). The influence of SBS, viatop premium and FRP on the improvement of stone mastic asphalt performance. *Fibers, 8*(4), 20.

[11] AlSaadi, I., Tayh, S. A., Jasim, A. F., & Yousif, R. (2023). The use of natural fibers in stone mastic asphalt mixtures: a review of the literature. *Archives Civil Eng, 69*, 347–370.

[12] Morea, F., Nosetti, R., Gonzalez, L., & Sánchez, A. (2023). Performance analysis of non-conventional Stone Mastic asphalt (SMA) elaborated with crumb rubber bitumen or by mean of glass macrofibers addition. *Constr Build Mater, 400*, 132654. [CrossRef]

[13] Klinsky, L. M. G., Kaloush, K. E., Faria, V. C., & Bardini, V. S. S. (2018). Performance characteristics of fiber modified hot mix asphalt. *Constr Build Mater, 176*, 747–752. [CrossRef]

[14] Jia, H., Sheng, Y., Guo, P., Underwood, S., Chen, H., Kim, Y. R., Li, Y., & Ma, Q. (2023). Effect of synthetic fibers on the mechanical performance of asphalt mixture: A review. *J Traffic Transportation Eng, 10*(3), 331–348. [CrossRef]

[15] Slebi-Acevedo, C. J., Lastra-González, P., Calzada-Pérez, M. A., & Castro-Fresno, D. (2020). Effect of synthetic fibers and hydrated lime in porous asphalt mixture using multi-criteria decision-making techniques. *Materials, 13*(3), 675. [CrossRef]

[16] Noorvand, H., Salim, R., Medina, J., Stempihar, J., & Underwood, B. S. (2018). Effect of synthetic fiber state on mechanical performance of fiber reinforced asphalt concrete. *Transportation Res Record, 2672*(28), 42–51. [CrossRef]

[17] Ahmadinia, E., Zargar, M., Karim, M. R., Abdelaziz, M., & Ahmadinia, E. (2012). Performance evaluation of utilization of waste Polyethylene Terephthalate (PET) in stone mastic asphalt. *Constr Build Mater, 36*, 984–989. [CrossRef]

[18] ASTM. (2012). Standard Test Method for Density, Relative Density (Specific Gravity), and Absorption of Coarse Aggregate. *American Society for Testing and Materials*: West Conshohocken, PA, USA.

[19] ASTM. (2015). Standard test method for relative density (specific gravity) and absorption of fine aggregate. *American Society for Testing and Materials*: West Conshohocken, PA, USA.

[20] ASTM. (2006). Standard test method for resistance to degradation of small-size coarse aggregate by abrasion and impact in the Los Angeles machine. *American Society for Testing and Materials*: West Conshohocken, PA, USA.

[21] ASTM. (2010). Standard Test Method for Flat Particles, Elongated Particles, or Flat and Elongated Particles in Coarse Aggregate. *American Society for Testing and Materials*: West Conshohocken, PA, USA.

[22] ASTM. (2000). Standard test method for determining the percentage of fractured particles in coarse aggregate. *American Society for Testing and Materials*: West Conshohocken, PA, USA.

[23] Dibaj, S. M., & Kavussi, A. (2012). An optimized mix design method for emulsified bituminous mixtures. *Quarterly J Transportation Eng, 4*(1), 23–34.

[24] ASTM. (2006). Standard Test Method for Sieve Analysis of Fine and Coarse Aggregates. *American Society for Testing and Materials*: West Conshohocken, PA, USA.

[25] Saedi, S., & Oruc, S. (2022). Investigating the Possibility of Using Roof Shingles Waste and Fibers in Stone Mastic Asphalt Pavements. *Int J Transportation Eng, 9*(3), 681–691.

[26] Ghasemi, M., & Marandi, S. M. (2011). Laboratory investigation of the properties of stone matrix asphalt mixtures modified with rgp–sbs. *Digest J Nanomaterials Biostructures, 6*(4), 1823–1834.

[27] Sengul, C. E., Oruc, S., Iskender, E., & Aksoy, A. (2013). Evaluation of SBS modified stone mastic asphalt pavement performance. *Constr Build Mater, 41*, 777–783. [CrossRef]

[28] Oruç, Ş., Yılmaz, B., & Sancak, K. (2022). Characterization and rheological behavior of asphalt binder modified by a novel cyclic borate ester additive. *Constr Build Mater, 348*, 128673. [CrossRef]

[29] Behiry, A. E. A. E. M. (2012). Fatigue and rutting lives in flexible pavement. *Ain Shams Eng J, 3*(4), 367–374. [CrossRef]

Journal of Sustainable Construction Materials and Technologies
Web page info: https://jscmt.yildiz.edu.tr
DOI: 10.47481/jscmt.1499749

JSCMT
Journal of Sustainable Construction Materials and Technologies

Research Article

Experimental investigation of the effect of longitudinal tensile reinforcement ratio on ductility behaviour in GPC beams

Ahmet ÖZBAYRAK*[1], Ali İhsan ÇELİK[2], Mehmet Cemal ACAR[3], Ahmet ŞENER[2]

[1]*Department of Civil Engineering, Erciyes University Faculty of Engineering, Kayseri, Türkiye*
[2]*Department of Construction, Kayseri University, Tomarza Mustafa Akıncıoğlu Vocational College, Kayseri, Türkiye*
[3]*Department of Construction, Kayseri University, Technical Science Vocational College, Kayseri, Türkiye*

ARTICLE INFO

Article history
Received: 14 April 2024
Revised: 24 May 2024
Accepted: 04 June 2024

Key words:
Compressive and flexural strength, ductility, geopolymer concrete, reinforced concrete beam, strain limit

ABSTRACT

This research first determined the strength of the cylindrical geopolymer concrete materials under compressive stresses. Secondly, conventional and geopolymer-reinforced concrete beams were manufactured in different reinforcement ratios, and their mechanical properties were compared under bending. The main aim of this study is to experimentally compare the effect of reinforcement ratio on the ductility behavior of an alkali-activated geopolymer concrete (GPC) beam with that of an ordinary Portland cement (OPC) beam. First, balanced reinforcement calculations were made considering the mechanical properties obtained from the material tests. The load-displacement, moment-curvature, and crack development results obtained from beam tests are interpreted with this information. OPC and GPC beams exhibited similar strength and crack development behavior. However, the behavior of GPC and OPC concretes differs regarding the ductility index. Therefore, to achieve similar ductility in the conduct of GPC and OPC beams, the balanced reinforcement ratio and section dimensions of GPC beams should be chosen to be larger than OPC.

Cite this article as: Özbayrak, A., Çelik, A. İ., Acar, M. C., & Şener, A. (2024). Experimental investigation of the effect of longitudinal tensile reinforcement ratio on ductility behaviour in GPC beams. *J Sustain Const Mater Technol*, 9(2), 114–127.

1. INTRODUCTION

The production of Ordinary Portland Cement (OPC) harms the environment, which has sparked intense interest in creating new varieties of "green" geopolymer concrete. It is necessary to demonstrate the applicability of current design procedures or develop new design methodologies if geopolymer concretes are widely used in practice [1]. Davidovits invented geopolymer concrete (GPC) with superior properties in 1974 by using materials such as Silicon (Si) and Aluminium (Al) rich fly ash activated with alkaline liquids instead of Portland cement (OPC) as a binder in concrete [2–4]. Alkaline liquids are concentrated aqueous alkali hydroxide or silicate solutions with soluble alkali metals, usually based on sodium (Na) or potassium (K). Highly alkaline liquids dissolve silicon and aluminum atoms in the source materials and form the geopolymeric binder. Efficiency in the production of geopolymer concrete is highly dependent on the types of aluminosilicate sources and activators [5, 6]. The raw material used as a source, alkaline solution concentrations, and curing conditions play an essential role in increasing the strength of geopolymer concrete by improving the polymerization process. The experimental results demonstrate that geopolymer concrete's mechanical qualities rise as the activator/binder ratio increases and the water/binder ratio decreases [7]. However,

***Corresponding author.**
*E-mail address: ozbayrak@erciyes.edu.tr

the development of this material is still in its infancy. Further progress is needed to deal with the safety risk associated with the activating solution's high alkalinity and the polymerization reaction's hypersensitivity to temperature [8–10]. The advantages of geopolymer concrete are its high compressive and tensile strength, rapid strength gain, low shrinkage, and high temperature and chemical resistance [11–15]. Despite these advantages, the practical use of geopolymer concrete is quite limited. The main reason for its limited practical use is insufficient research on building elements, design, and application studies [16].

In the literature research, shear and bending behaviors of fly ash-based geopolymer-reinforced concrete beams were investigated structurally under chemical composition, reinforcement ratio, glass fiber content, and steel fiber use. The first studies on the structural behavior of fly ash-based geopolymer concrete beams were made by Sumajouw et al. [17] They tested the bending behavior of six reinforced concrete beams with variable reinforcement ratios. As a result, it was determined that the flexural strength increased depending on the increase in the reinforcement ratio, as in the behavior of conventional reinforced concrete beams. In another study, sixteen reinforced concrete geopolymer beams with varying tensile reinforcement ratios (0.64–2.69%) and concrete compressive strength (37–76 MPa) were tested by M. Sumajouw and Rangan [18]. The effect of reinforcement ratio on geopolymer concrete beams in terms of bending capacity and ductility was similar to conventional reinforced concrete beams. In parallel studies, it has been reported that the flexural behavior of fly ash-based geopolymer concrete beams is identical to traditional reinforced concrete beams, such as initial cracking load, crack width, load-deflection relationship, bending stiffness, ultimate load, and failure mode [19–27]. The bending behaviors of geopolymer-reinforced and cementitious reinforced concrete beams were investigated by numerical analysis (ANSYS APDL) and confirmed by experimental studies. The deflection in the GPC beam was higher than in the OPC beam, and better crack propagation was found in the GPC beam than in the OPC beam. The applied specifications state the hat GPC beam is a better alternative material for the beam [28]. It was determined by Jeyasehar et al. [29] that the initial crack load of geopolymer concrete beams was higher when compared to conventional cement-based concrete beams, but crack width, mid-span deflection, and final load were lower.

Another study for bending and deflection calculations evaluated the applicability of the ACI 318-2019 code for geopolymer concrete beams. It has been stated that a suitable model is needed to calculate the flexural strengths and deflections of geopolymer concrete beams after the first crack formation [30]. When adding glass fiber or steel fiber and hybrid propylene while manufacturing fly ash-based geopolymer-reinforced concrete beams, the bending capacity increased by 30–35% [31, 32]. Sathish Kumar et al. [33] experimentally tested the shear strength of geopolymer concrete beams by adding triple-blended hybrid fibers. Fracture beams were compared by adding steel and polypropylene fiber at different rates. As a result, combining hybrid fibers improved the shear strength and changed the fracture type of the beams from shear to bending. However, the disadvantage of GPC beams is that they exhibit a more ductile behavior than OPC beams, and as a result, more small cracks occur in GPC beams compared to OPC beams [34].

On the other hand, the research conducted by Mourougane et al. [35] revealed that geopolymer concrete beams have higher shear strength in the range of 5–23% than conventional cement-based concrete beams. Based on research on a series of shear-critical geopolymer concrete beams with varying longitudinal and transverse reinforcement ratios, Chang concluded that the calculation method applied for conventional concrete beams could also be safely used to predict the shear strength of geopolymer concrete beams [36]. In the results of direct shear tests (shear aperture ratio) conducted by Visintin et al. [1], it was determined that the shear friction properties of the geopolymer concrete used in the experimental research behaved similarly in range to the shear friction properties of the commonly used OPC concrete.

This study compared the flexural behaviors of OPC (3 specimens) and GPC (3 specimens) beams with various reinforcement ratios, targeting an average strength of 30 MPa. To calculate the balanced reinforcement ratio, the compressive strength and mechanical properties of OPC and GPC concrete were determined by conducting preliminary material tests on cylindrical samples of Ø100 x 200 mm dimensions. This way, the stress-strain relationship and stress block design parameters of fly ash-based GPC and OPC were investigated for the balanced reinforcement ratio calculation. The equivalent pressure block height (a) at the moment of strain corresponding to the maximum stress of the cylindrical GPC specimens is approximately 30% higher than that of the OPC specimens [37]. Therefore, the balanced reinforcement ratio calculated for GPC concrete was larger. At the end of the experimental study, GPC beams were compared with OPC beams in load-displacement and moment-curvature relations. Similarities and differences were revealed regarding behavior and strength [38]. Although GPC beams exhibit similar properties to OPC beams in terms of maximum strength and crack development, increasing the beam section and reinforcement ratio is necessary for similar ductility in behavior.

1.1. Research Significance

In recent years, it has been revealed that geopolymer concrete (GPC) has superior properties compared to Portland cement concrete (OPC). However, more research is needed before GPC can be used in any area where OPC is used. With the increasing population and rapid urbanization, the demand for concrete is increasing exponentially. In addition, due to OPC production, 7–8% of CO_2 emissions are essential in improving the effect of greenhouse gases in the atmosphere. For these reasons, research on using fly ash material in the waste product class in concrete production is essential in making concrete more environmentally friendly. Previous studies have shown that the mechanical characteristics of geopolymer concrete, such as compressive strength and tensile strength, are superior to those of OPC concrete [39–45]. However, compared to

Table 1. Chemical components of fly ash

Components	%
SiO_2, x	59.2
Al_2O_3, y	20.3
Fe_2O_3, z	7.65
The sum of x, y, z	87.1
CaO	1.87
MgO	2.21
SO_3	0.19
Na_2O	1.56
K_2O	2.36
Cl^-	0.05
LOI (loss of ignition)	3.23
Fineness (>45 μm)	17.4

typical cement-based concrete, geopolymer concrete has a lower elastic modulus [37, 41, 46–48]. Using geopolymer concrete as a structural element has no detrimental effect on load-bearing capacity, and the geopolymer concrete members could be safely designed following existing standards of practice [49]. However, more research is needed to accelerate the use of geopolymer concrete in large-scale field applications and provide more practical and cost-effective design guidelines for its use in structural members.

In the Research Significance section of the manuscript, the authors state the purpose of their study, which is to investigate the mechanical performance of GPC beams reinforced with steel bars. The survey results will assist in understanding the behavior of GPC beams and their load-carrying capacity and ductility. This information could potentially lead to the developing of more optimized and sustainable structural designs for buildings and infrastructures. Therefore, the study is significant as it advances construction materials and engineering knowledge.

2. MATERIALS AND METHODS

2.1. Materials

Low calcium fly ash (ASTM Class F) supplied from the İsken Sugözü Power Plant was used as the primary material in the production of geopolymer concrete. The chemical composition of the fly ash determined for this power plant based on XRF analysis is given in Table 1. Accordingly, the sum of x, y, and z being more than 70% indicates that the ash taken from the İsken Sugözü Power Plant meets the targeted strength and behavior requirements. Its specific gravity was 2.35 on average.

The research used a mixture of NaOH and Na_2SiO_3 solutions as an alkali activator. NaOH grains in the form of pallets used in sodium hydroxide solution are 98% pure. To prepare a 14 M sodium hydroxide solution, 560 grams of NaOH was added to 1 Liter of water. Before adding the NaOH solution to the concrete mix, it was kept at room temperature for 24 hours. The mixing ratios of the Na_2SiO_3 solution are Na_2O=13.5–15%, SiO_2=27–30%, H_2O=48–50% and the mass density is 1510 kg/m^3. Crushed stone with a 7–11 mm diameter was used as coarse aggregate, and river sand was used as fine aggregate. To reduce the absorption of water and chemicals by the aggregate, the moisture content of the fine aggregate was kept as close to the saturated surface dry as possible.

2.2. Mixing Ratios

To reach the optimum ratio of various components of GPC concrete, preliminary studies have been conducted and published [50]. Accordingly, the parameters held constant in the current study include the aggregate content by weight (0.75), the ratio of fine aggregate to total aggregate (0.35), the proportion of alkali to fly ash by mass (0.60), and the ratio of Na_2SiO_3 to NaOH (1.5). The amount of material required to produce 1 m^3 of GPC concrete according to the above ratios is given in Table 2 in kg.

While preparing the mixture, primarily coarse aggregate, fine aggregate, and fly ash were mixed for 3 minutes in a 125 dm^3 concrete mixer. Afterward, the previously prepared Na_2SiO_3 and NaOH solutions were added to the mixture mortar one after the other for two more minutes. No water or plasticizer was added to the mixture during the total mixing period of 5 minutes. In the literature, it has been recommended that alkaline liquid be prepared by mixing sodium silicate and sodium hydroxide solutions and reacting thoroughly for at least 24 hours before use [22]. However, such an application was not made in the study since it was determined to accelerate the setting time. Furthermore, since 14 M sodium hydroxide causes the presence of excess NaOH ions, it leads to rapid and early precipitation of the aluminosilicate gel, leading to rapid hardening and inhibiting the formation of other geopolymeric precursors [51].

2.3 Experiment Samples

GPC and OPC beams with dimensions of 150 mm width, 200 mm depth, and 1100 mm span length were produced, targeting a compressive strength of 30 MPa as the intended strength and varying tensile reinforcement ratios. Tensile reinforcement ratios were determined as the lower limit (0.003), the upper limit (0.02), and a value between both specified in the ACI 318 specification [52, 53]. 2Ø8 longitudinal reinforcement was used in the compression region of all samples produced. The transverse reinforcement (stirrup) is adjusted to be 8Ø8/150 mm in each beam. The research tested six beams using three different GPC and OPC beams that matched each other. The transverse reinforcements were sized so that the concrete cover was 25 mm. The cross-section and reinforcement information of the beams are given in Table 3, and the longitudinal and transverse reinforcements are placed in Figure 1.

Table 2. GPC mixing ratios (kg/m^3)

Class F fly ash	Sodium silicate solution	Sodium hydroxide solution	Extra added water	Plasticizer	Fine aggregate	Coarse aggregate
406	146	97	–	–	643	1194

Table 3. Beam geometry and reinforcement information

Group	Sample name	Reinforcements		Tensile reinforcement ratio	Curing	ρmin	ρb	0.85xρb
		Compression reinforcement	Tensile reinforcement					
1	OPC1	2Ø8	2Ø8	0.003	28 days	0.0028	0.025	0.021
	OPC2	2Ø8	3Ø14	0.017	28 days			
	OPC3	2Ø8	2Ø18	0.019	28 days			
2	GPC1	2Ø8	2Ø8	0.003	24h 90 °C			
	GPC2	2Ø8	3Ø14	0.017	24h 90 °C			
	GPC3	2Ø8	2Ø18	0.019	24h 90 °C			

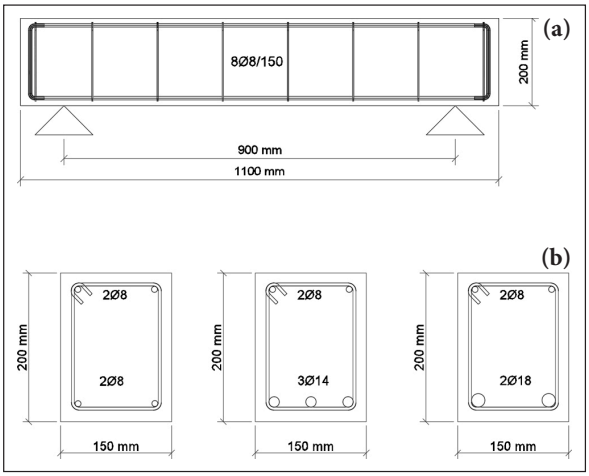

Figure 1. **(a)** Beam longitudinal section and transverse reinforcements, **(b)** Beam cross-sections and longitudinal reinforcements.

Table 4. Reinforcement properties under axial tension

Rebar diameter (mm)	f_y (MPa)	f_u (MPa)	ε_p (%)	f_u / f_y
Ø8	424	541	37.5	1.27
Ø14	453	572	32.8	1.26
Ø18	456	564	24.4	1.24

f_y: Yield strength; f_u: Tensile strength; ε_p: Unit elongation at break.

In the experimental study, B420c reinforcement was used following the standards, and the tensile strength/yield strength ratio was determined to be between 1.15 and 1.35. The ratio of yield strength, tensile strength, unit elongation at break, and tensile strength to yield strength of the longitudinal and transverse reinforcements used in the research are in Table 4.

2.4. Casting and Curing

Geopolymer-reinforced concrete beams were poured into plywood molds with dimensions of 150x200x1100 mm in the laboratory. A bottle-type vibrator was used to compact the concrete. The average slump value was determined as 21 cm in the measurements made during casting. Curing was done in a laboratory oven at 90 °C for 24 hours without mold removal. The research recommended curing after a rest period of 0–5 days after casting. To obtain the best results regarding compressive strength, geopolymer samples were kept for four days before curing [54]. Traditional reinforced concrete beams were produced in a ready-mixed concrete plant. The concrete is placed in the prepared beam molds, and the curing stages are shown in Figure 2.

2.5. Experiment Setup and Loading Procedure

The precise span length of tested beams is 900 mm and simply supported, fixed at one end, and sliding joint at the other. The load was applied to the beam by a 300 kN servo-hydraulic actuator from a single loading point in the middle of the span (Fig. 3). The ratio obtained by dividing

Figure 2. Placing and curing concrete in molds.

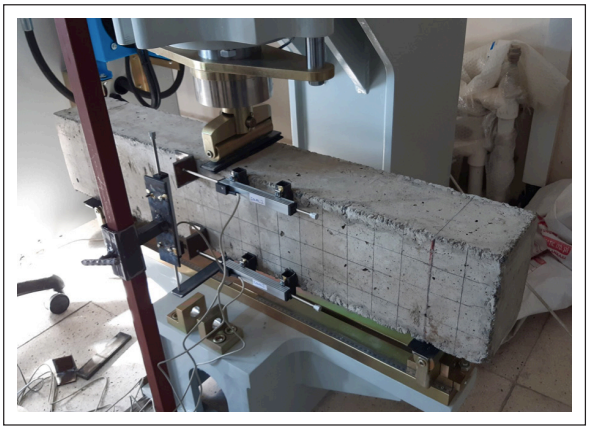

Figure 3. Experiment setup and measuring instruments.

the shear span (a=0.9/2=0.45) by the average adequate depth (d=0.175) is found to be a/d=0.257 (considering the variation in sufficient depth, ±0.04). The beam's cross-sectional height (0.2 m) is not greater than 1/4 of its clear span (0.9/4=0.225 m), so it is classified as a standard beam. To prevent local crushing of the concrete, hard rubber, and leather belts are placed between the steel rollers and the concrete surface in the loading and bearing areas. The load was applied by controlling the displacement of the actuator at a rate of 2 mm/s until 50 mm of deflection occurred. Next, two LVDTs (Linear Variable Data Transformers) were placed on the middle span upper and lower beam faces to determine the moment-curvature relationship by measuring the shortening in the upper fibers of the beam and the elongation in the lower fibers. Again, a third LVDT was added to the experimental setup to determine the load-deflection relationship by taking vertical measurements from the beam middle span. The measurements taken during the experiment were transferred to the computer with the help of a data logger.

3. RESULTS

3.1 Material Tests

Material tests are essential in the interpretation of beam behavior and strength. For this reason, three Ø 100 x 200 mm cylindrical specimens were prepared for each group, and unit strain, modulus of elasticity, Poisson's ratio, and compressive strength were calculated [37, 55]. The weight, unit volume weight, and slump values measured from the average of the samples in each group before the tests are given in Table 5. It has been determined that GPC and OPC are similar in unit volume weight.

The characteristic strength properties, corresponding to the targeted 30 MPa and the obtained strengths, are provided in Table 6 by averaging the concrete samples in each group. The ratio of transverse strain to longitudinal strain (Poisson), modulus of elasticity, and ductility due to deformation were obtained differently in GPC and OPC samples. In the calculation of the elastic modulus, firstly, 40% of the maximum stress (fck) is taken, and the elastic stress limit (fd) is determined (Fig. 4).

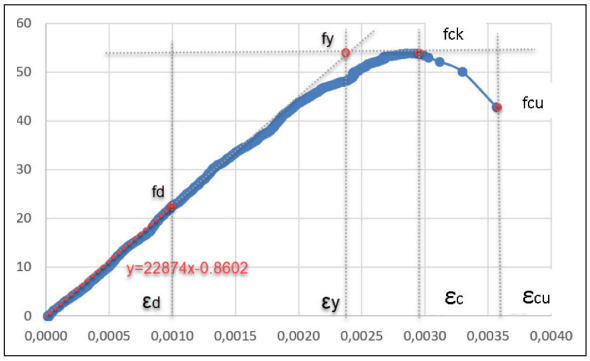

Figure 4. Example calculation of elastic modulus and ductility from the concrete stress-strain curve.

Table 5. Average slump and unit volume mass

Group name	Slump cm	Weight kg	Unit volume mass kg/m^3
OPC	16	3.662	2330
GPC	21	3.739	2380

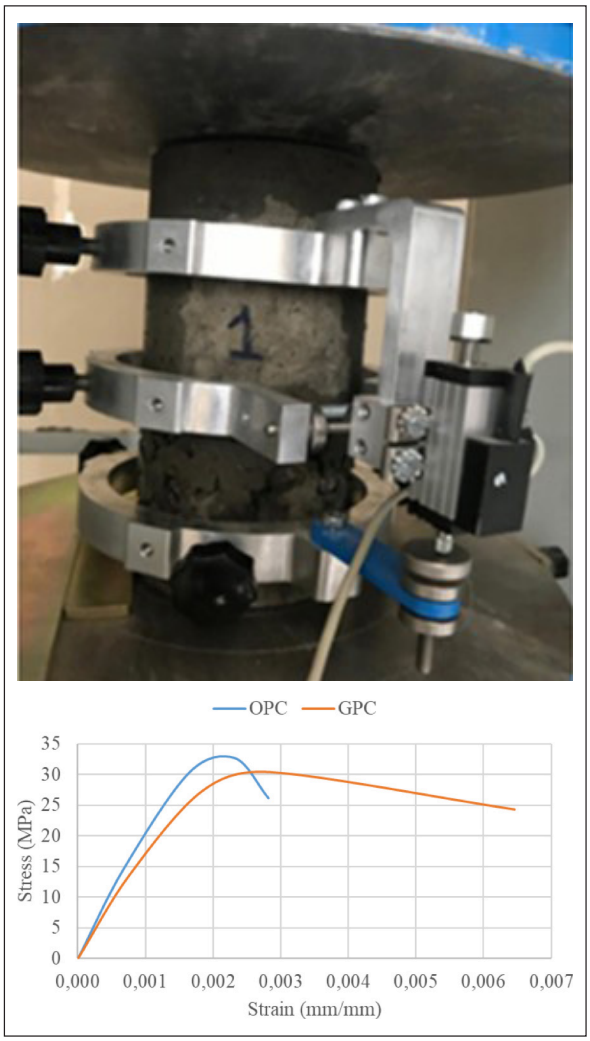

Figure 5. Stress-strain curves.

Table 6. Characteristic strength properties of materials (MPa - mm/mm)

Group name	E_c	f_d	f_y	f_{ck}	f_{cu}	v_c
OPC	19128	14.71	30.34	32.70	26.16	0.20
GPC	16913	13.69	27.40	30.43	24.34	0.30
Group name	**E_s**	**ε_d**	**ε_y**	**ε_c**	**ε_{cu}**	**$\mu=\varepsilon_{cu}/\varepsilon_y$**
OPC	210000	0.00068	0.00165	0.00232	0.00282	1.71
GPC	210000	0.00077	0.00185	0.00284	0.00646	3.50

E_c: Concrete modulus of elasticity; E_s: Steel modulus of elasticity; v_c: Poisson's ratio; f_d: Concrete elastic stress; f_y: Concrete yield stress; f_{ck}: Concrete maximum stress; f_{cu}: Concrete ultimate stress; ε_d: Concrete strain corresponding to elastic stress; ε_y: Concrete yield strain; ε_c: Concrete strain corresponding to maximum stress; ε_{cu}: Concrete strain corresponding to ultimate stress; μ: Material ductility (compression ductility).

Table 7. Balanced reinforcement ratios (N-mm)

Group name	ε_s	ε_{cu}	$\varepsilon_{cu} E_s$	k_1	d	x	a	f_{cd}	ρ_b
OPC	0.0018	0.00282	592.20	0.821	175	105.70	86.79	21.8	0.0258
GPC	0.0008	0.00646	1357.3	0.837	175	135.96	113.8	20.3	0.0312

Then, a trend line (red line) was added to fd from the starting point (0, 0) of the stress-strain graph, and the equation of this line was displayed. The modulus of elasticity was calculated by finding the expression y/x in this equation. Ductility is the ratio of ultimate strain (εu) to yield strain (εy). εcu is the strain of the ultimate stress (fcu), corresponding to approximately 85% of the fco. εy is the strain corresponding to the yield stress (fy). fy is the intersection point of the trend line for which the elastic modulus is calculated, and the line that passes horizontally through the axis corresponds to fck (gray lines). In the equation y=22874x-0.8602, the value of x=εy is obtained by substituting the value of fck for y. Thus, the ductility value was calculated from the experimental data of the stress-strain curve using the formula μ=εu/εy.

A comparison of the average stress-strain curves of GPC and OPC concrete samples is given in Figure 5. The strain corresponding to the maximum stress of GPC is more significant than that of OPC.

3.2. Balanced Reinforcement Ratio

Only a few studies on the stress-block parameters for fly-ash-based GPC under heated curing conditions have been reported in the literature, even though there have been many studies on the rectangular stress-block parameters for conventional Portland concrete [56, 57]. Nevertheless, the research findings demonstrate that it is still appropriate and highly accurate to design GPC beams using the ACI standards for concrete structures [58].

In the cylinder compression tests, the maximum deformations (εcu) of GPC and OPC concretes at ultimate load are different (Table 6). This table shows that according to GPC (0.00646), the balanced reinforcement ratio calculation will differ from OPC (0.00282), depending on the ultimate strain corresponding to the concrete crushing change. It is important to make balanced reinforcement calculations to prevent brittle fractures in beams. Equation 1 represents the calculation of x, the depth of the compressive stress block based on the strain values of steel and concrete at yield and crushing. Equation 2 represents the calculation of the balanced reinforcement ratio (ρb) using the strain values of concrete at crushing obtained from cylinder pressure tests. The main reason for the different balanced reinforcement ratios is that the crushing strain values of GPC and OPC concrete differ, resulting in different values of ρb.

$$\frac{d}{x} = \frac{\varepsilon_{sy} + \varepsilon_{cu}}{\varepsilon_{cu}} \times \frac{E_s}{E_s} \quad and \quad x = \frac{a}{k_1} \tag{1}$$

$$\rho_b = \frac{A_{sb}}{bd} = 0.85 k_1 \frac{f_{cd}}{f_{yd}} \times \frac{\varepsilon_{cu} E_s}{\varepsilon_{cu} E_s + f_{yd}} \tag{2}$$

The coefficient k1, the ratio between the average and maximum stress, was calculated in Eq. 3 according to ACI 318 for the characteristic cylindrical compressive strength fck >28 MPa.

$$k_1 = (1.05 - 0.007 f_{ck}) \geq 0.65 \tag{3}$$

The calculated balanced reinforcement ratio values are given in Table 7. Accordingly, it is seen that the tensile reinforcement ratios (ρ<ρb) of all beam samples shown in Table 3 are below the balanced reinforcement ratio. In this case, tensile failure is expected to occur in all beams.

The equivalent compressive block height (a) of the GPC samples at the moment of maximum stress is greater than that of the OPC samples. However, Figure 6 shows that the GPC samples achieve their ultimate load capacity at lower deflection values than the OPC samples (Fig. 6a). Using more tensile reinforcement in GPC beams is necessary to achieve similar ductility with OPC beams. For this reason, the balanced reinforcement ratio of GPC beams is higher than that of OPC beams. However, this inference is applicable for fracture scenarios due to bending. In cases of fracture due to shear, the situation is different. Table 7 shows that the reinforcement in GPC does not yield at the point of concrete crushing. Additionally, the strain of GPC concrete at the end of crushing is greater than that of OPC concrete

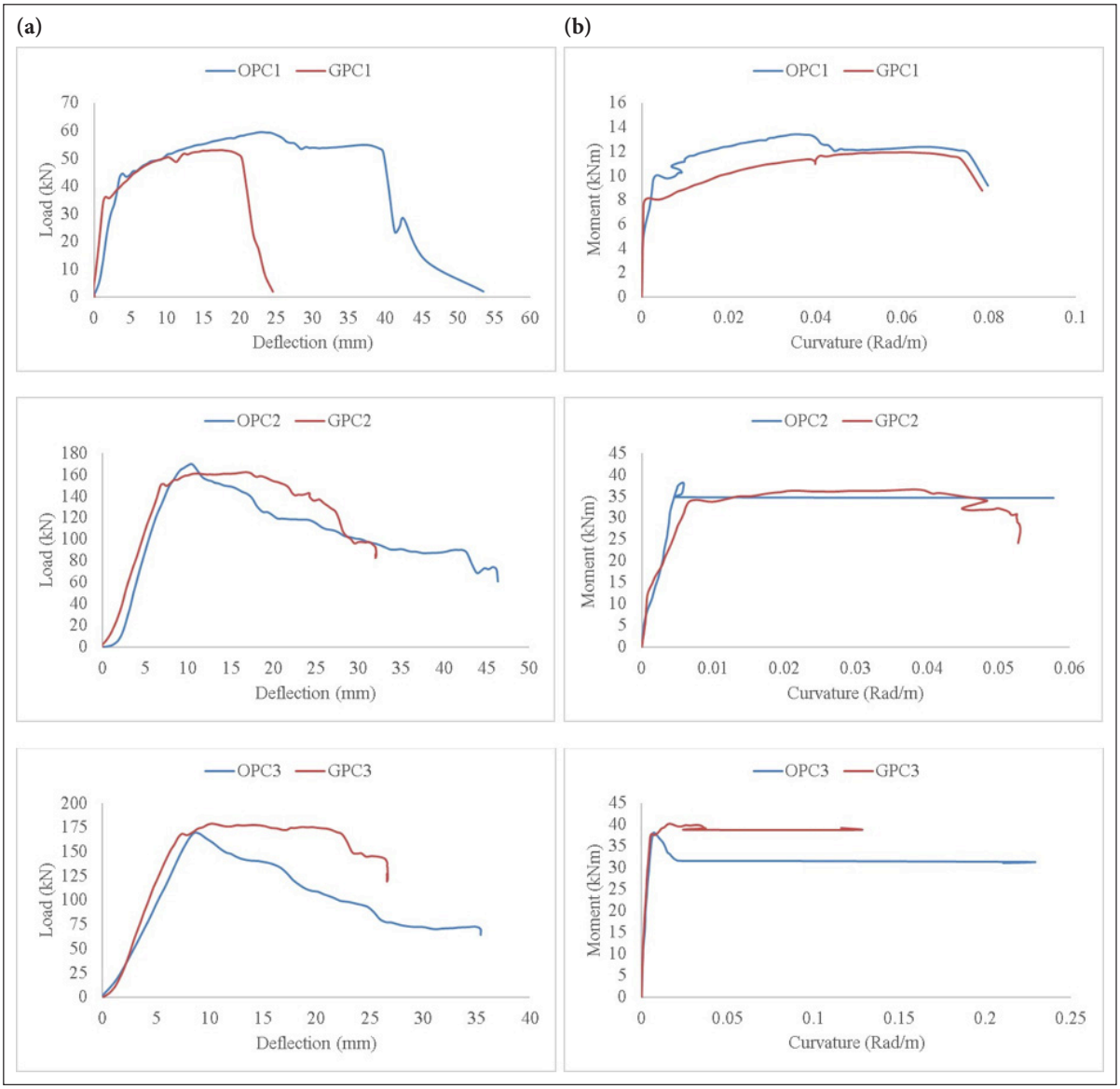

Figure 6. **(a)** Load displacement curves, **(b)** Moment curvature relationship.

due to its slightly lower modulus of elasticity, indicating that GPC is weaker regarding shear. It has been determined that the reinforcement in OPC concrete beams reaches the total yield strain at the ultimate load capacity.

3.3. Beam Tests

The load-displacement and moment-curvature graphs of the beam samples with different reinforcement ratios are as given in Figure 6.

For values of a concrete compressive strength less than 50MPa, the maximum reinforcement ratio defined in ACI 318 is 0.02 [52, 53]. This condition must be met for a tensile fracture to occur under the influence of ductile behavior. Therefore, the deformation capacity of GPC beams is lower than OPC beams, and the need for tensile reinforcement is higher. However, the balanced reinforcement ratio calculated for GPC (ρb=0.031) exceeds the limit value (ρ=0.02) given in ACI 318 for OPC. In this case, GPC beam section dimensions should be more significant than OPC beam section dimensions to provide sufficient ductility.

The strains corresponding to compressive stresses in geopolymer concrete are higher than in conventional concrete. For this reason, geopolymer concrete's material ductility (compression ductility) was greater than conventional concrete's (Table 6). In the first experiments, where the reinforcement ratio is low (0.003), the GPC1 beam has a deflection capacity of less than the OPC1 beam (Fig. 6a). The OPC concrete in the compression zone reached its fracture strength after the reinforcement in the tensile zone yields. Concrete crushing in the compression zone in GPC can reach similar strength due to considerably large than in OPC. As a result, the yielding of tensile reinforcement is the determining factor in GPC beams, which produce a

Table 8. Moment values for reinforcement yielding (M_y)

kNm	OPC1	GPC1	OPC2	GPC2	OPC3	GPC3
Experimental M_y	10.0	8.12	37.9	34.1	37.6	37.1
Analytical M_y	7.10	–	29.2	–	32.0	–

later compressive strength response than OPC beams. As a result, the beam collapses from oblique tensile failure before reaching the maximum compression fracture. In experiments second and third, the increase in reinforcement ratios increased the load-carrying capacity of the beams and became a determinant of flexural stiffness. However, the shear tension failure occurred (Fig. 6a).

Due to the high ductility of the material, GPC beams show lower stiffness in the compression region and reach the moment-carrying capacity earlier than OPC beams for similar curvature values. The curvature values of the GPC and OPC beams were found to be close to each other since the failure of the first beams occurred due to the reinforcement yielding in the tension zone (Fig. 6b). However, the tension reinforcement ratio increased in the second and third beams. Due to the high ductility value in GPC, the compressive stresses formed in the upper beam fiber remained at lower levels for curvature values similar to those of OPC. This high ductility reduced the strength contribution of the concrete in the compression zone during bending. As a result, the load in GPC beams is carried mainly by the tension reinforcement. In the second and third experiments, the beams reached the bearing capacity at higher curvature values than the OPC beams (Fig. 6b).

Oblique tensile and shear compression fractures occurred in beam samples due to shear and flexural cracks (a/d=2.57). In the GPC1 and OPC1 samples, flexural tensile fracture occurred due to the rupture of the reinforcement by yielding. In the other beam samples (GPC2-OPC2 and GPC3-OPC3), only shear cracking occurred without bending cracks, resulting in sudden power depletions (Fig. 7). The inclined crack formed in the body in the first stage progressed rapidly and caused brittle fractures. As a result, shear compression collapses occurred in the beams without yielding the tensile reinforcements. However, the bearing capacity moment values increased due to increased reinforcement ratios (Table 8).

When the tests are examined in terms of load-displacement relations in Figure 6, it is seen that only in the first experiments is a load below the shear capacity applied to the beams. The way the beams break is a flexural tensile failure, which confirms this situation. In the second and third experiments, shear pressure fracture occurred due to the load applied to the beams above the shear strength (Fig. 7). The maximum analytical shear loads that OPC beams with the properties specified in the research can carry were calculated as 162 kN.

4. DISCUSSION

As a result of the material and beam tests, it was determined that geopolymer concrete (GPC) has a similar strength to conventional concrete but exhibits different behavior characteristics. Specifically, the increase in material ductility (compression ductility) according to cylinder pressure tests caused a decrease in section ductility in beam bending tests. While the energy consumption capacity of GPC was higher in compressive strength tests, conventional concrete (OPC) performed better in energy consumption in beam tests focused on flexural strength.

Since the modulus of elasticity of GPC is lower and the strain corresponding to the maximum compressive stress is more significant than that of OPC concrete, the flexural stiffness is lower than that of OPC. This condition shows that the GPC-reinforced concrete beam will deflect more under the effect of bending. The calculations in the previous sections demonstrated the necessity of increasing the tensile reinforcement to exhibit similar stiffness to the OPC beam. In addition, increasing the flexural reinforcement alone may not be sufficient for the required stiffness not to exceed the reinforcement upper limit (0.02) set by regulations such as ACI318 and TS500. In this case, it may be necessary to increase the section dimensions for sufficient flexural stiffness. However, the experiments were terminated due to shear damage, especially in the last two experiments. This does not affect the flexural findings based on the material tests. Future studies should support these findings by conducting studies in which flexural fractures of beams can be observed.

4.1. Parameters Considered for OPC and GPC

4.1.1. Material Tests

- Compressive Strength: The compressive strength of GPC, determined through material tests, was comparable to that of OPC.
- Elastic Modulus: The elastic modulus of GPC was lower than that of OPC, as indicated by the values obtained from cylindrical samples [59–64].
- Poisson's Ratio: The Poisson's ratio of GPC was higher than that of OPC [65–68].
- Strain at Maximum Stress: The strain value corresponding to the maximum stress of GPC was higher than that of OPC [69, 70]. This difference increased as it approached the ultimate strain.
- Ductility: The increased yield and ultimate state strain values of GPC improved its ductility [71, 72]. Consequently, the equivalent pressure block height of GPC was greater than that of OPC, indicating that GPC beams would reach their bearing capacity at lower deflection values. Therefore, more tensile reinforcement is required to achieve similar ductility with OPC beams, resulting in a higher balanced reinforcement ratio for GPC.

4.1.2. Beam Tests

- Reinforcement Ratios: Three different reinforcement ratios were used in beam experiments. Beams in the first group failed due to flexural tensile fractures follow-

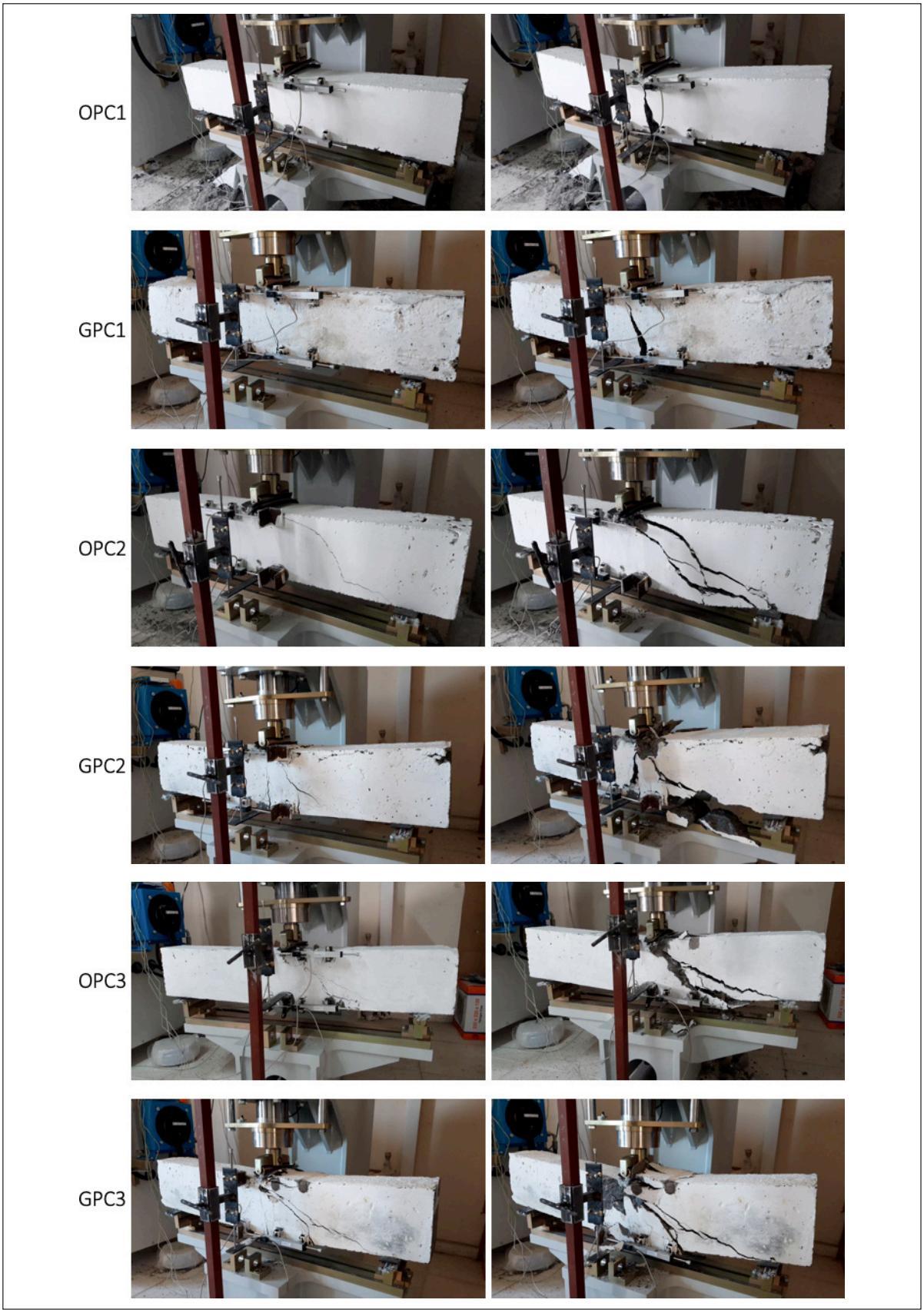

Figure 7. Crack development (left image: during the experiment, right image: at the end of the experiment).

ing reinforcement yield. In the last two groups, failure occurred due to shear pressure fractures in the beams without reinforcement yielding.

- Deflection Values: GPC beams reached maximum bearing capacity at lower deflection values than OPC beams [73, 74]. This indicates that the section ductility of GPC beams is lower despite higher material ductility [20, 75].
- Energy Consumption: The decrease in section ductility negatively affected energy consumption. In the first experiment, moment-curvature graphs were similar because the concrete was crushed when the reinforcement yielded. However, the graphs differed in the last two tests as the concrete collapsed according to the shear and compressive strength before reinforcement yield. The demand for compressive strength due to high deformation from GPC material tests led to decreased section ductility by consuming energy before OPC.

4.2. Advantages and Weaknesses of GPC over OPC

4.2.1. Advantages

- Higher Ductility: GPC exhibits higher material ductility, enhancing its energy consumption capacity in compressive strength tests.
- Environmental Benefits: GPC production is typically more environmentally friendly, as it can utilize industrial waste products such as fly ash and slag [76–78].

4.2.2. Weaknesses

- Lower Elastic Modulus: GPC's lower elastic modulus leads to higher deflections under load, reducing its flexural stiffness compared to OPC.
- Section Ductility: GPC beams have lower section ductility, negatively impacting their performance in flexural applications. The high material ductility of GPC, observed in cylinder tests, delays the compressive strength response in flexural tests, causing earlier energy depletion in shear and tensile effects.
- Design Adjustments: To achieve similar stiffness and ductility to OPC beams, GPC beams require more tensile reinforcement and potentially larger cross-sectional dimensions.

4.3. Recommendations for Beam Design and Standards

Given the experimental findings, it is crucial to consider the implications of these differences in practical applications:

4.3.1. Reinforcement Ratio and Standards Compliance

- The balanced reinforcement ratio limit should be strictly adhered to per standards such as ACI 318. The experiments indicated a higher balanced reinforcement ratio for GPC, suggesting a need for careful design adjustments.
- The designs used in the experiments might not fully comply with ACI standards due to the higher reinforcement ratios. Future designs should aim for compliance to ensure valid comparisons and safe structural performance.

4.3.2. Cross-Sectional Dimensions

- The conclusion that beam dimensions should be increased for GPC is based on the need for sufficient flexural stiffness. While this approach may address the immediate stiffness issues, it is important to consider it within the framework of standard design practices.
- The suggestion to enlarge cross-sectional dimensions must be carefully evaluated, particularly when the beam is completely bending. If the reinforcement ratio in the beam is lower than the balanced reinforcement ratio, the behavior of the beam could differ significantly.

4.3.3. Future Research Directions

- The current findings are valuable and highlight key differences between GPC and OPC. However, definitive statements should be avoided until further studies, particularly those observing flexural failures in beams, are conducted.
- Future research should focus on verifying these findings with larger sample sizes and varied loading conditions to develop a more comprehensive understanding of GPC's behavior under different structural demands. By incorporating these considerations and adhering to established standards, the structural applications of GPC can be optimized to leverage its advantages while mitigating its weaknesses.

5. CONCLUSIONS

The high ductility of the material in geopolymer concretes causes a delay in the response of the compressive strength due to deflection. The increase in curvature causes a collapse in the form of tension and shear. The delayed pressure response on the beam's neutral axis causes the beam's energy to be depleted in shear and tensile effects before reaching the maximum compressive strength. All the obtained findings related to strength and deformation support each other. In general, GPC and OPC concrete exhibit similar behavior in terms of tensile and shear strengths. Still, the delayed compressive strength demand due to the ductility of GPC concrete reduces its section ductility and energy absorption capacity. For these reasons, it was determined that the balanced reinforcement ratio in GPC beams should be increased. In this case, larger sizes of GPC beams should be produced compared to OPC beams to have similar bending strength and energy consumption properties to prevent brittle fractures and maintain the upper limit of the reinforcement of 0.02. As a result, GPC concrete with low modulus of elasticity and high strain properties achieves similar stress values to OPC concrete ($\sigma = E.\varepsilon$). Although there is no significant difference in strength, they differ in deflection.

- High Ductility and Delayed Response: The high material ductility of geopolymer concrete (GPC) causes a delay in the compressive strength response due to deflection. This delay and increased curvature lead to tension and shear collapses.
- Energy Depletion in Shear and Tensile Effects: The delayed pressure response on the beam's neutral axis causes the beam's energy to be depleted in shear and tensile effects before reaching maximum compressive strength.
- Consistency of Findings: All findings related to strength

and deformation support each other. GPC and OPC concrete exhibit similar behavior in terms of tensile and shear strengths.

- Reduced Section Ductility: Due to the material ductility of GPC concrete, the delayed compressive strength demand reduces its section ductility and energy absorption capacity.
- Balanced Reinforcement Ratio: The balanced reinforcement ratio in GPC beams should be increased to achieve bending strength and energy consumption properties similar to those of OPC beams.
- Larger Beam Sizes: Larger GPC beams should be produced compared to OPC beams to achieve similar bending strength and energy consumption properties. This necessity arises because the modulus of elasticity of GPC is lower, and the strain corresponding to the maximum compressive stress is more significant than that of OPC concrete. Consequently, the flexural stiffness is lower, leading to more deflection under bending.
- Stress and Strain Relationship: GPC concrete with a low modulus of elasticity and high strain properties achieves similar stress values to OPC concrete ($\sigma = E.\varepsilon$). However, they differ in deflection despite similar strength.
- Flexural Reinforcement and Section Dimensions: Increasing the tensile reinforcement in GPC beams is necessary to exhibit similar stiffness as OPC beams. However, merely increasing flexural reinforcement may not suffice for the required stiffness due to regulatory limits. Therefore, increasing section dimensions may be needed for adequate flexural stiffness. This consideration is based on calculations and is consistent with the results of the material tests, even though some experiments were terminated due to shear damage.
- Comparative Behaviour: Geopolymer concrete unit weight, maximum compressive and flexural strengths, crack development, and fracture patterns are similar to conventional reinforced concrete structures. Deflection and ductility values differ between GPC and OPC. GPC beams require a higher balanced reinforcement ratio or larger section dimensions to achieve ductility, similar to OPC beams.
- Recommendations for Future Studies: Further studies should be conducted better to understand the behavior of geopolymer structural carrier system elements. This will help optimize the use of GPC in structural applications and ensure compliance with design standards. Additionally, future studies should focus on flexural fractures of beams to support and expand on the current findings.

As a result, geopolymer concrete unit weight, maximum compressive and flexural strengths, crack development, and fracture patterns are similar to conventional reinforced concrete structures. However, the deflection and ductility values are different in terms of behavior. Therefore, to achieve similar ductility in the behavior of GPC and OPC beams, the balanced reinforcement ratio or section dimensions of GPC beams should be chosen to be larger than OPC. Further studies on the subject should be increased better to understand the behavior of geopolymer structural carrier system elements.

ACKNOWLEDGMENTS

We want to thank Kayseri Beton firm and Önder Işık and Hasan Şahbaz for their contribution to the project.

ETHICS

There are no ethical issues with the publication of this manuscript.

DATA AVAILABILITY STATEMENT

The authors confirm that the data that supports the findings of this study are available within the article. Raw data that support the finding of this study are available from the corresponding author, upon reasonable request.

CONFLICT OF INTEREST

The authors declare that they have no conflict of interest.

FINANCIAL DISCLOSURE

This research was financially supported by the Kayseri University Projects Unit (BAP-FKB-2020-1013).

USE OF AI FOR WRITING ASSISTANCE

Not declared.

PEER-REVIEW

Externally peer-reviewed.

REFERENCES

[1] Visintin, P., Mohamed Ali, M. S., Albitar, M., & Lucas, W. (2017). Shear behavior of geopolymer concrete beams without stirrups. *Constr Build Mater, 148*, 10–21. [CrossRef]

[2] Lloyd, N., & Rangan, B. (2010). Geopolymer concrete: A review of development and opportunities. In *35th Conference on Our World in Concrete and Structures*, pp. 25–27.

[3] Kotwal, A. R., Kim, Y. J., Hu, J., & Sriraman, V. (2015). Characterization and early age physical properties of ambient cured geopolymer mortar based on Class C fly ash. *Int J Concr Struct Mater, 9*(1), 35–43. [CrossRef]

[4] Luhar, S., Chaudhary, S., & Luhar, I. (2019). Development of rubberized geopolymer concrete: Strength and durability studies. *Constr Build Mater, 204*, 740–753. [CrossRef]

[5] Madheswaran, C. K., Ambily, P. S., Dattatreya, J. K., & Ramesh, G. (2015). Experimental studies on behaviour of reinforced geopolymer concrete beams subjected to monotonic static loading. *J Inst Eng India Ser A, 96*(2), 139–149. [CrossRef]

[6] Duxson, P., Fernández-Jiménez, A., Provis, J. L., Lukey, G. C., Palomo, A., & Van Deventer, J. S. J. (2007). Geopolymer technology: The current state of the art. *J Mater Sci, 42*(9), 2917–2933. [CrossRef]

[7] Pham, D. Q., Nguyen, T. N., Le, S. T., Pham, T. T., & Ngo, T. D. (2021). The structural behaviours of steel reinforced geopolymer concrete beams: An experimental and numerical investigation. *Structures, 33*, 567–580. [CrossRef]

[8] Tyson, S., & Tayabji, S. (2010). Geopolymer Concrete (No. FHWA-HIF-10-014). United States. Federal Highway Administration.

[9] Al Bakri, A. M., Kamarudin, H., Bnhussain, M., Nizar, I. K., Rafiza, A. R., & Zarina, Y. (2012). The processing, characterization, and properties of fly ash based geopolymer concrete. *Rev Adv Mater Sci, 30*(1), 90–97.

[10] Ryu, G. S., Lee, Y. B., Koh, K. T., & Chung, Y. S. (2013). The mechanical properties of fly ash-based geopolymer concrete with alkaline activators. *Constr Build Mater, 47*, 409–418. [CrossRef]

[11] Fernandez-Jimenez, A., Palomo, A., & Lopez-Hombrados, C. (2006). Engineering properties of alkali-activated fly ash concrete. *ACI Mater J, 103*(2), 106. [CrossRef]

[12] Hardjito, D., Wallah, S., Sumajouw, D., & Rangan, B. (2004). On the development of fly ash-based geopolymer concrete. *Mater J, 101*(6), 467–472. [CrossRef]

[13] Hardjito, D., Wallah, S., Sumajouw, D., & Rangan, B. (2004). Properties of geopolymer concrete with fly ash as source material: Effect of mixture composition. *Spec Publ, 222*, 109–118.

[14] Delair, S., Prud'homme, É., Peyratout, C., Smith, A., Michaud, P., Eloy, L., Joussein, E., & Rossignol, S. (2012). Durability of inorganic foam in solution: The role of alkali elements in the geopolymer network. *Corros Sci, 59*, 213–221. [CrossRef]

[15] Cheng, T. W., & Chiu, J. P. (2003). Fire-resistant geopolymer produced by granulated blast furnace slag. *Miner Eng, 16*(3), 205–210. [CrossRef]

[16] Ma, C. K., Awang, A. Z., & Omar, W. (2018). Structural and material performance of geopolymer concrete: A review. *Constr Build Mater, 186*, 90–102. [CrossRef]

[17] Sumajouw, D. M. J., Hardjito, D., Wallah, S. E., & Rangan, B. V. (2005). Behaviour and strength of reinforced fly ash-based geopolymer concrete beams. *Australian Structural Engineering Conference 2005*, pp. 453.

[18] Sumajouw, M. D. J., & Rangan, B. V. R. (2006). Low-calcium fly ash-based geopolymer concrete: Reinforced beams and columns. *Curtin Univ Technol.* https://espace.curtin.edu.au/bitstream/handle/20.500.11937/23928/19466_downloaded_stream_558.pdf

[19] Dattatreya, J., Rajamane, N., Sabitha, D., Ambily, P., & Nataraja, M. (2011). Flexural behaviour of reinforced geopolymer concrete beams. *Int J Civ Struct Eng, 2*(1), 138–159.

[20] Yost, J. R., Radlińska, A., Ernst, S., Salera, M., & Martignetti, N. J. (2013). Structural behavior of alkali activated fly ash concrete. Part. Structural testing and experimental findings. *Mater Struct, 46*(3), 449–462. [CrossRef]

[21] Kumaravel, S., & Thirugnanasambandam, S. (2013). Flexural behaviour of reinforced low calcium fly ash based geopolymer concrete beam. *Glob J Res Eng, 13*(8), 8–14.

[22] Kumaravel, S., Thirugnanasambandam, S., & Jeyasehar, A. (2014). Flexural behavior of geopolymer concrete beams with GGBS. *IUP J Struct Eng, 7*(1), 45–54.

[23] Yodsudjai, W. (2014). Application of fly ash-based geopolymer for structural member and repair materials. *13th Int Ceram Congr - Part F, 92*, 74–83. [CrossRef]

[24] Madheswaran, C., Ambily, P., Rajamane, N., & Arun, G. (2014). Studies on flexural behaviour of reinforced geopolymer concrete beams with lightweight aggregates. *Int J Civ Struct Eng, 4*(3), 295–305. [CrossRef]

[25] Hutagi, A., & Khadiranaikar, R. B. (2016). Flexural behavior of reinforced geopolymer concrete beams. *Int Conf Electr Electron Optim Tech*, ICEEOT 2016, 3463–3467. [CrossRef]

[26] Kumar, P. U., & Kumar, B. S. (2016). Flexural behaviour of reinforced geopolymer concrete beams with GGBS and metakaoline. *Int J Civ Eng Technol, 7*(6), 260–277.

[27] Zhang, H., Wan, K., Wu, B., & Hu, Z. (2021). Flexural behavior of reinforced geopolymer concrete beams with recycled coarse aggregates. *Adv Struct Eng, 24*(14), 3281–3298. [CrossRef]

[28] Alex, A. G., Gebrehiwet, T., Kemal, Z., & Subramanian, R. B. (2022). Structural performance of low-calcium fly ash geopolymer reinforced concrete beam. *Iran J Sci Technol Trans Civ Eng, 46*(1) 1–12. [CrossRef]

[29] Jeyasehar, C., Saravanan, G., & Salahuddin, M. (2013). Development of fly ash based geopolymer precast concrete elements. *Asian J Civ Eng (BHRC), 14*(4), 605–616

[30] Zinkaah, O. H., Araba, A., & Alhawat, M. (2021). Performance of ACI code for predicting the flexural capacity and deflection of reinforced geopolymer concrete beams. *IOP Conf Ser Mater Sci Eng, 1090*(1), 012067. [CrossRef]

[31] Srinivasan, S., Karthik, A., & Nagan, D. S. (2014). An investigation on flexural behaviour of glass fibre reinforced geopolymer concrete beams. *Int J Eng Sci Res Technol, 3*(4), 1963–1968.

[32] Devika, C. P., Deepthi, R. (2015). Study of flexural behavior of hybrid fiber reinforced geopolymer concrete beam. *Int J Sci Res (IJSR), 4*(7), 130–135.

[33] Kumar, V. S., Ganesan, N., & Indira, P. V. (2021). Shear strength of hybrid fibre-reinforced ternary blend geopolymer concrete beams under flexure. *Materials, 14*(21), 6634. [CrossRef]

[34] Abraham, R., Raj, S., & Abraham, V. (2013). Strength and behaviour of geopolymer concrete beams. *Int J Innov Res Sci Eng Technol, 2*(1), 159–166.

[35] Mourougane, R., Puttappa, C., Sashidhar, C., & Muthu, K. (2012). Shear behaviour of high strength GPC/TVC beams. *Proc Int Conf Adv Arch Civ Eng, 21*, 142.

[36] Chang, E. H., Sarker, P., Lloyd, N., & Rangan, B. V. (2009). Bond behaviour of reinforced fly ash-based geopolymer concrete beams. *Concrete Solutions 09, The 24th Biennial Conf of the Concrete Inst of Australia*, pp. 1–10.

[37] Çelik, A. İ., Özbayrak, A., Şener, A., & Acar, M. C. (2022). Effect of activators in different ratios on compressive strength of geopolymer concrete. *Can J Civ Eng, 50*(2), 69–79. [CrossRef]

[38] Çelik, A. İ., Özbayrak, A., Şener, A., & Acar, M. C. (2022). Numerical analysis of flexural and shear behaviors of geopolymer concrete beams. *J Sustain Constr Mater Technol, 7*(2), 70–80. [CrossRef]

[39] Shrestha, R., Baweja, D., Neupane, K., Chalmers, D., & Sleep, P. (2013). Mechanical properties of geopolymer concrete: Applicability of relationships defined by AS 3600. *Concrete Inst of Australia-Biennial Conf,* 3600(2014), 3600.

[40] Chi, M. (2012). Effects of dosage of alkali-activated solution and curing conditions on the properties and durability of alkali-activated slag concrete. *Constr Build Mater, 35*, 240–245. [CrossRef]

[41] Farhan, N. A., Sheikh, M. N., & Hadi, M. N. S. (2019). Investigation of engineering properties of normal and high strength fly ash based geopolymer and alkali-activated slag concrete compared to ordinary Portland cement concrete. *Constr Build Mater, 196*, 26–42. [CrossRef]

[42] Zhang, P., Gao, Z., Wang, J., Guo, J., Hu, S., & Ling, Y. (2020). Properties of fresh and hardened fly ash/slag based geopolymer concrete: A review. *J Clean Prod, 270*, 122389. [CrossRef]

[43] Okoye, F. N., Durgaprasad, J., & Singh, N. B. (2015). Mechanical properties of alkali activated flyash/Kaolin based geopolymer concrete. *Constr Build Mater, 98*, 685–691. [CrossRef]

[44] Erfanimanesh, A., & Sharbatdar, M. K. (2020). Mechanical and microstructural characteristics of geopolymer paste, mortar, and concrete containing local zeolite and slag activated by sodium carbonate. *J Build Eng, 32*, 101781. [CrossRef]

[45] Amran, M., Al-Fakih, A., Chu, S. H., Fediuk, R., Haruna, S., Azevedo, A., & Vatin, N. (2021). Long-term durability properties of geopolymer concrete: An in-depth review. *Case Stud Constr Mater, 15*, e00661. [CrossRef]

[46] Wardhono, A., Gunasekara, C., Law, D. W., & Setunge, S. (2017). Comparison of long-term performance between alkali activated slag and fly ash geopolymer concretes. *Constr Build Mater, 143*, 272–279. [CrossRef]

[47] Meng, Q., Wu, C., Hao, H., Li, J., Wu, P., Yang, Y., & Wang, Z. (2020). Steel fibre reinforced alkali-activated geopolymer concrete slabs subjected to natural gas explosion in buried utility tunnel. *Constr Build Mater, 246*(3), 118447. [CrossRef]

[48] Nguyen, K. T., Ahn, N., Le, T. A., & Lee, K. (2016). Theoretical and experimental study on mechanical properties and flexural strength of fly ash-geopolymer concrete. *Constr Build Mater, 106*, 65–77. [CrossRef]

[49] Mo, K. H., Alengaram, U. J., & Jumaat, M. Z. (2016). Structural performance of reinforced geopolymer concrete members: A review. *Constr Build Mater, 120*, 251–264. [CrossRef]

[50] Acar, M. C., Şener, A., Özbayrak, A., & Çelik, A. İ. (2020). The effect of zeolite additive on geopolymer mortars. *J Eng Sci Des, 8*(3), 820–832. [CrossRef]

[51] Lee, W. K. W., & Van Deventer, J. S. J. (2002). Structural reorganisation of class F fly ash in alkaline silicate solutions. *Colloids Surf A Physicochem Eng Asp, 211*(1), 49–66. [CrossRef]

[52] ACI Committee 318. (2014). ACI 318-14: *Building Code Requirements for Structural Concrete and Commentary*.

[53] Turkish Standarts. (2000). Requirements for design and construction of reinforced concrete structures. TS-500.

[54] Bhushan H. Shinde, & Dr. Kshitija N. Kadam. (2015). Properties of fly ash based geopolymer mortar. *Int J Eng Res, 4*(7), 971–974. [CrossRef]

[55] Özbayrak, A., Kucukgoncu, H., Atas, O., Aslanbay, H. H., Aslanbay, Y. G., & Altun, F. (2023). Determination of stress-strain relationship based on alkali activator ratios in geopolymer concretes and development of empirical formulations. *Structures, 48*, 2048–2061. [CrossRef]

[56] Prachasaree, W., Limkatanyu, S., Samakrattakit, A., & Hawa, A. (2014). Development of equivalent stress block parameters for fly-ash-based geopolymer concrete. *Arab J Sci Eng, 39*, 8549–8558. [CrossRef]

[57] Tempest, B., Gergely, J., & Skipper, A. (2016). Reinforced geopolymer cement concrete in flexure: A closer look at stress-strain performance and equivalent stress-block parameters. *PCI J, 61*(6), 30–43. [CrossRef]

[58] Tran, T. T., Pham, T. M., & Hao, H. (2019). Rectangular stress-block parameters for fly-ash and slag based geopolymer concrete. *Structures, 19*, 143–155. [CrossRef]

[59] Hardjito, D., & Rangan, B. V. (2005). Development and properties of low-calcium fly ash-based geopolymer concrete. *Curtin University of Technology, pp. 1–94*.

[60] Farooq, F., Rahman, S. K. U., Akbar, A., Khushnood, R. A., Javed, M. F., alyousef, R., alabduljabbar, H., & aslam, F. (2020). A comparative study on performance evaluation of hybrid GNPs/CNTs in conventional and self-compacting mortar. *Alex Eng J, 59*(1), 369–379. [CrossRef]

[61] Viet Hung, T., Duy Tien, N., & Van Dong, D. (2017). Experimental study on section curvature and ductility of reinforced geopolymer concrete beams. *Sci J Transp, 8*, 3–11.

[62] Fernández-Jiménez, A. M., Palomo, A., & López-Hombrados, C. (2006). Engineering properties of alkali-activated fly ash concrete. *ACI Mater J, 103*(2), 106–112. [CrossRef]

[63] Liu, Y., Shi, C., Zhang, Z., Li, N., & Shi, D. (2020). Mechanical and fracture properties of ultra-high performance geopolymer concrete: Effects of steel fiber and silica fume. *Cem Concr Compos, 112*, 103665. [CrossRef]

[64] Sofi, M., van Deventer, J. S. J., Mendis, P. A., & Lukey, G. C. (2007). Engineering properties of inorganic polymer concretes (IPCs). *Cem Concr Res, 37*(2), 251–257. [CrossRef]

[65] Mohammed, A. A., Ahmed, H. U., & Mosavi, A. (2021). Survey of mechanical properties of geopolymer concrete: A comprehensive review and data analysis. *Materials, 14*(16), 4690. [CrossRef]

[66] Verma, M., Dev, N., & Research, O. (2021). Geopolymer concrete: A sustainable and economic concrete via experimental analysis. https://www.researchsquare.com/article/rs-185150/v1 [CrossRef]

[67] Ding, Y., Dai, J. G., & Shi, C. J. (2016). Mechanical properties of alkali-activated concrete: A state-of-the-art review. *Constr Build Mater, 127*, 68–79. [CrossRef]

[68] Cong, X., Zhou, W., & Elchalakani, M. (2020). Experimental study on the engineering properties of alkali-activated GGBFS/FA concrete and constitutive models for performance prediction. *Constr Build Mater, 240*, 117977. [CrossRef]

[69] Xin, L., Xu, J. Y., Li, W., & Bai, E. (2014). Effect of alkali-activator types on the dynamic compressive deformation behavior of geopolymer concrete. *Mater Lett, 124*, 310–312. [CrossRef]

[70] Ou, Z., Feng, R., Mao, T., & Li, N. (2022). Influence of mixture design parameters on the static and dynamic compressive properties of slag-based geopolymer concrete. *J Build Eng, 53*, 104564. [CrossRef]

[71] Huda, M. N., Jumat, M. Z. Bin, & Islam, A. B. M. S. (2016). Flexural performance of reinforced oil palm shell & palm oil clinker concrete (PSCC) beam. *Constr Build Mater, 127*, 18–25. [CrossRef]

[72] Yap, S. P., Bu, C. H., Alengaram, U. J., Mo, K. H., & Jumaat, M. Z. (2014). Flexural toughness characteristics of steel–polypropylene hybrid fibre-reinforced oil palm shell concrete. *Mater Des, 57*, 652–659. [CrossRef]

[73] Liu, Y., Zhang, Z., Shi, C., Zhu, D., Li, N., & Deng, Y. (2020). Development of ultra-high performance geopolymer concrete (UHPGC): Influence of steel fiber on mechanical properties. *Cem Concr Compos, 112*, 103670. [CrossRef]

[74] Bhutta, A., Borges, P. H. R., Zanotti, C., Farooq, M., & Banthia, N. (2017). Flexural behavior of geopolymer composites reinforced with steel and polypropylene macro fibers. *Cem Concr Compos, 80*, 31–40. [CrossRef]

[75] Zhang, H., Wan, K., Wu, B., & Hu, Z. (2021). Flexural behavior of reinforced geopolymer concrete beams with recycled coarse aggregates. *Adv Struct Eng, 24*(14), 3281–3298. [CrossRef]

[76] Özbayrak, A., Kucukgoncu, H., Aslanbay, H. H., Aslanbay, Y. G., & Atas, O. (2023). Comprehensive experimental analysis of the effects of elevated temperatures in geopolymer concretes with variable alkali activator ratios. *J Build Eng, 68*, 106108. [CrossRef]

[77] Aslanbay, Y. G., Aslanbay, H. H., Özbayrak, A., Kucukgoncu, H., & Atas, O. (2024). Comprehensive analysis of experimental and numerical results of bond strength and mechanical properties of fly ash based GPC and OPC concrete. *Constr Build Mater, 416*, 135175. [CrossRef]

[78] Cecen, F., Özbayrak, A., & Aktaş, B. (2023). Experimental modal analysis of fly ash-based geopolymer concrete specimens via modal circles, mode indication functions, and mode shape animations. *Cem Concr Compos, 137*, 104951. [CrossRef]

J Sustain Const Mater Technol, Vol. 9, Issue. 2, pp. 128–137, June 2024

Journal of Sustainable Construction Materials and Technologies
Web page info: https://jscmt.yildiz.edu.tr
DOI: 10.47481/jscmt.1500347

JSCMT
Journal of Sustainable Construction Materials and Technologies

Research Article

Mechanical properties of kevlar and jute fiber reinforced concrete

Shamsoon FAREED[1], Bilal ZAHID[2], Asad-ur-Rehman KHAN*[1]

[1]*Department of Civil Engineering, NED University of Engineering and Technology, Karachi, Pakistan*
[2]*Department of Textile Engineering, NED University of Engineering and Technology, Karachi, Pakistan*

ARTICLE INFO

Article history
Received: 10 March 2024
Revised: 29 May 2024
Accepted: 02 June 2024

Key words:
Compressive strength, fiber reinforced concrete, jute fibers, kevlar fibers, tensile strength

ABSTRACT

Concrete, due to its inherent brittleness, exhibits relatively low tensile strength. Fibers have been used extensively to improve their mechanical properties as they helped to reduce the crack width. Textile industries produce a lot of natural and synthetic fiber waste, which can be utilized to produce better-performing fiber-reinforced concrete. Therefore, in this study, a detailed experimental investigation has been carried out to study the compressive, tensile, and flexural properties of the Kevlar and jute fiber reinforced concrete. Concrete specimens with a mix design ratio of 1:1.43:1.89 and a water-cement ratio of 0.6 were cast. Jute fibers with lengths of 10 mm, 15 mm, and 25 mm and three different concentrations of 0.1%, 0.25%, and 0.5% by volume of concrete were used. In contrast, Kevlar fibers with lengths of 10 mm, 15 mm, and 20 mm and three different concentrations of 1%, 1.5%, and 2.5% by volume of concrete were used. It was found that both Kevlar and Jute fibers contributed positively towards controlling the crack initiation and propagation, suggesting using fibers in concrete for enhanced mechanical properties and performance.

Cite this article as: Fareed, S., Zahid, B., & Khan, A. R. (2024). Mechanical properties of kevlar and jute fiber reinforced concrete. *J Sustain Const Mater Technol*, 9(2), 128–137.

1. INTRODUCTION

Concrete is a brittle material exhibiting minor strains and deficient tensile capacity. To reduce the effect of this brittleness, incorporating short, discrete, discontinuous fibers into the concrete matrix has become increasingly popular [1]. The fibers used in concrete may be commonly classified as metallic, textile, and natural fibers [2]. The metallic fibers in concrete include steel, amorphous, etc. In contrast, textile and natural fibers include Kevlar, Jute, coconut, palm tree, etc.

It has been a well-established fact that when concrete is reinforced with short, discrete, and discontinuous fibers, the addition of fibers results in the formation of bridges across the crack, thus reducing the inherent brittleness associated with concrete. When the load is applied and cracks are formed, the randomly oriented fibers arrest the crack formation and propagation, thus improving strength and ductility [3]. It has been observed that the cracks of textile-reinforced concrete are thinner than those of steel-reinforced concrete, making the surface more durable [4].

Textile-reinforced concrete originated from a German institute focusing on Textile technology. The initial work on textile-reinforced concrete structures began in the 1980s. In 1982, the first patent for textile-reinforced concrete design was granted for transportation-related safety items meant to be reinforced with materials other than steel. In 1996, two concrete canoes using textile reinforcement were created by students of German University. In 1996, a boat competition, Concrete Canoe Regatta, was held in Dresden, Germany, during which the textile-reinforced concrete gained public attention [5].

***Corresponding author.**
*E-mail address: asadkhan@neduet.edu.pk

Walton and Majumdar [6] conducted an experimental investigation to study the properties of cement composites reinforced with Kevlar fibers under different curing conditions. Based on the study, it was found that Kevlar-reinforced concrete specimens exhibited good strength and ductility even in adverse environments.

Chaudhary conducted an experimental investigation to study the mechanical properties of Kevlar fiber-reinforced concrete (KFRC) [7]. For this purpose, KFRC, which has a fiber content of 2%, 4%, 6%, 8%, 10%, 12%, and 14%, was used in preparing concrete specimens. It was found that with the increase in the Kevlar fiber, the concrete compressive strength of up to 16% was observed.

Uchida et al. [8] also conducted an experimental investigation to study the mechanical properties of ultra-high-strength fiber-reinforced concrete using aramid fibers. Aramid fibers of different shapes and sizes were incorporated into the concrete mixture to examine the properties of fresh and hardened fiber-reinforced concrete. Based on the study, it was found that the concrete reinforced with aramid fibers of 3 mm length and 3% fiber content had the highest compressive and flexural strength when compared with different lengths and concentrations of aramid fibers.

Zakaria et al. [9] carried out an experimental study to examine the mechanical properties of jufiber-reinforced concrete (JFRC). For this purpose, jute fibers with lengths of 10 mm, 15 m, and 2 mm and three concentrations of 0.1%, 0.25%, 0.50%, and 0.75% were used to evaluate the compressive, tens,ile, and flexural strength. The concrete was prepared with two different ratios of cement/ sand/ brick chips (1:2:4, 1:1.5:3) and water/cement ratios (0.60 and 0.55). It was observed that for both ratios, the concrete compressive strength increased for the case of the concrete specimen having 15 mm jute fiber with 0.10% concentration. However, the concrete compressive strength decreased when fiber lengths of 20 mm and 25 mm with a fiber content of 0.25, 0.50 and 0.75% were used.

Dayananda et al. [10] also investigate the behavior of JFRC. The specimens were prepared with jute fibers having fiber concentrations of 0.5%, 1%, and 2% and were tested after 7, 28, 56, and 90 moist curings. It was observed that the concrete compressive strength decreased with the increase in the Jute content, and after 7 and 28 moist curing, the concrete compressive strength of the JFRC specimen decreased with the rise in jute content. However, the concrete compressive strength of Jute fibers increased when specimens were cured for 56 days, in the case of specimens with fiber contents of up to 1%. This trend of increase in compressive strength again shows a decline when the specimen was cured for 90 days.

Zhang et al. [11] investigated using jute fibers on the mechanical properties of high-strength concrete. It was observed that using the jute fibers in high-strength concrete proved to be efficient in reducing the micro-cracks and porosity and delaying the initiation and crack propagation. Kim et al. [12] investigated using regular strength and high-fluidity concrete using jute fibers. It was found that the influence of the use of the jute fiber was more prominent in the high fluidity concrete compared to the normal strength concrete when comparing compressive and tensile strength. Razmi and Mirsayar [13] invested in the fracture properties of JFRC specimens. Based on the detailed experimental investigation, it was found that the use of the jute fiber possesses a positive influence against crack growth in addition to the improved compressive and tensile splitting strength when compared with plain specimens. Rahman and Azad [14] investigated the impact of jute fiber length on the mechanical properties of concrete. He concluded that jute fibers with a length of 10 mm were most influential in increasing the concrete compressive and tensile strength compared to the plain concrete specimens. In contrast to the above findings, however, Faiq [15] concluded the decremental pattern in concrete compressive and tensile strength using the jute fibers.

Li et al. [16] investigated the influence of kevlar, carbon, and hybrid fiber-reinforced concrete specimens under static and quasi-static loading. It was found that using Kevlar fiber with carbon fiber significantly improved both static and dynamic compressive strength of concrete specimens as compared to when the specimens were prepared separately with Kevlar and carbon fibers. Li et al. [17] also investigated the influence of using Kevlar fibers in concrete specimens under static and high-rate loading. They found that the specimens prepared with 12 mm and 24 mm fiber lengths show similar static properties. However, under high rate loading, the specimens prepared with fibers having 24 mm length exhibited higher strain energies than those prepared with 12 mm fibers. Konczalski and Piekarski [18] investigated the influence of Kevlar fibers on the tensile properties of ordinary Portland cement and found that using Kevlar significantly improves the elastic modulus and fracture energy.

Pakistan, whose economy is mainly boosted by the export of its textile products, has an abundance of textile-related wastage, which, if not correctly recycled, goes to already polluted landfills. Therefore, this investigation studies the uniaxial compressive, splitting tensile, and flexural tensile strength of Kevlar and JFRC. Furthermore, the influence of jute and kevlar fiber lengths and percentage of fiber content (by volume) on the properties of jute and KFRC was also studied. As discussed above, few studies have focused on using jute and Kevlar fibers in concrete.

2. MATERIALS AND METHODS

2.1. Kevlar Fiber Reinforced Concrete Specimens

The investigation presented herein aims to investigate the mechanical properties (compression and tension) of concrete reinforced with Kevlar fibers. For this purpose, concrete was prepared with Kevlar, which has fiber lengths of 10 mm, 15 mm, and 20 mm. Furthermore, to study the influence of the fiber quantity on the mechanical properties of concrete, three different concentrations of Kevlar fibers, 1%, 1.5%, and 2.5% concentration by volume of concrete were used in concrete casting.

To study the behavior of KFRC under uniaxial compression and splitting tensile, cylinders having a diameter of 100 mm and height of 200 mm were used and tested as per C39

Table 1. Constituents of concrete mix

Constituent	Quantity
Water	272.4 kg/m^3
w/c ratio	0.6
Coarse aggregates	858 kg/m^3
Fine aggregates	649 kg/m^3
Cement	454 kg/m^3
Super plasticizer	222 mL

Table 2. Physical properties of coarse and fine aggregates

Properties	Coarse aggregates	Fine aggregates
Loose density	1886 kg/m^3	2002 kg/m^3
Saturated bulk specific gravity	2.66	2.4
Dry rodded density	1905 kg/m^3	2120 kg/m^3
Absorption	0.78	0.968

and C496 ASTM Standards [19, 20], whereas prisms having a cross-section of 75 mm × 75 mm and length of 300 mm were used to study the flexural behavior as per C78 ASTM standard [21]. A total of sixty (60) cylindrical specimens, 30 each for uniaxial compression and splitting tension, were cast such that three specimens for concrete without Kevlar fibers and a set of 3 for each fiber length and fiber concentration. Similarly, 30 prism specimens with varying percentages and concentrations of Kevlar fibers used for compression and splitting tensiles were also cast and tested under three-point bending.

The specimens used in this study were prepared with concrete with a mix proportion of 1:1.43:1.89 and a water-to-cement ratio (w/c) of 0.6. The details of the concrete mix are provided in Table 1. The concrete was prepared with ordinary Portland cement coarse and fine aggregates. As discussed above, percentages and concentrations were used for specimens with Kevlar fibers. The physical properties of coarse and fine aggregates and the chemical properties of the ordinary Portland cement used in the study are provided in Table 2 and Table 3, respectively. The Kevlar fibers used in this study have a yarn count of 20/2 NeC, 1440 kg/m^3 tensile modulus density, and tenacity of 70500 MPa and 2920 MPa, respectively. All specimens were tested after 28 days of moist curing as per ASTM standards [19].

2.2. Jute Fiber Reinforced Concrete Specimens

Uniaxial compression and splitting tension tests were carried out per ASTM standards to study the mechanical properties of concrete made with jute fibers. Cylinders with a diameter of 100 mm and a height of 200 mm were used and tested as per ASTM Standards.

The specimens were cast from concrete, having a mixed proportion of 1:1.43:1.89 and a w/c of 0.6. Initially in yarn or twine form, a locally available jute was used for preparing concrete with three different yarn lengths of 10 mm, 15 mm, and 25 mm and three different concentrations of 0.1%, 0.25%, and 0.5%. In total, sixty (60) specimens were cast out of which

Table 3. Chemical composition of cement

Component	Content (%)
Lime (CaO)	60.9%
Silica (SiO_2)	20.8%
Alumina (Al_2O_3)	5.1%
Iron Oxide (Fe_2O_3)	3.2%
Magnesia (MgO)	3%
Sulphur trioxide (SO_3)	1.7%

Table 4. Properties of Jute yarn used in preparing concrete specimens

Parameters	3-Plied yarn
Diameter (mm)	0.1
Weight (lb)	0.27
Spindle count (lb / one spindle of 14400)	77
Linear density (tex)	2651
Count (Ne)	0.22
Twist per inch (TPI)	1.87
Moisture content (%)	2.76
Moisture regain (%)	2.85
Force (N)	366
Extension (%)	6.04
Stress value (N/ m^2)	28152307
Strain value	0.06
Elastic modulus (GPa)	0.46

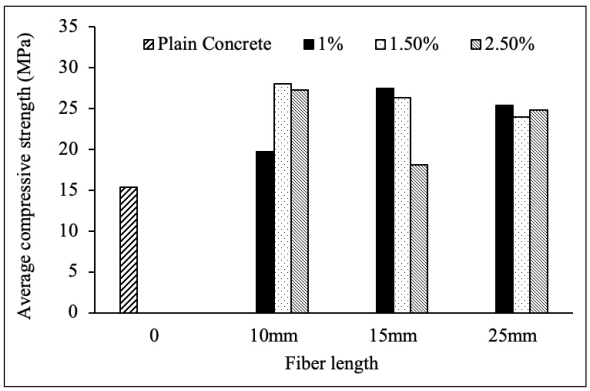

Figure 1. Relationship exhibiting the influence of the fiber volume and length on the average compressive strength of KFRC specimens.

27 cylinders were used for uniaxial compression tests and 27 for the splitting tensile test. Three specimens were cast and tested for each fiber length and volume after 28 days of moist curing. Plain concrete specimens 3 for each compressive and tensile testing were also used for comparison.

Two different types of jute yarn in twine were locally available: 3-plied and 4-plied. The three plied twine yarns were used in the experimental program, and their properties are provided in Table 4. The properties of the 3-plied yarn were determined as per ASTM standards [14].

Table 5. Average uniaxial compressive strength of KFRC

	Fiber length				Fiber length		
	0	10 mm	15 mm	25 mm	10 mm	15 mm	25 mm
	Average concrete compressive strength (MPa)				% Increase w.r.t Plain concrete		
Fiber percentage							
0%	15.35	–	–	–	–	–	–
1%	–	19.8	27.5	25.3	28.70	79.3	65.1
1.50%	–	28.1	26.3	24.0	82.9	71.3	56.5
2.50%	–	27.3	18.1	24.8	77.8	18.1	61.6

Table 6. Average splitting tensile strength of KFRC

	Fiber length				Fiber length		
	0	10 mm	15 mm	25 mm	10 mm	15 mm	25 mm
	Average splitting tensile strength (MPa)					% Increase w.r.t. Plain concrete	
Fiber percentage							
0%	1.81	–	–	–	–		
1%	–	2.32	1.56	1.53	28.2	-13.8	-15.5
1.50%	–	2.35	2.14	1.62	29.8	18.2	-10.5
2.50%	–	2.30	1.63	2.72	27.1	-9.9	50.3

3. RESULTS AND DISCUSSION

Results of experimental investigations carried out during the study on KFRC and JFRC are presented in terms of uniaxial compressive strength, splitting tensile strength, and flexural tensile strength.

3.1. Kevlar Fiber Reinforced Concrete Specimens

3.1.1. Compressive Strength

The concrete compressive strength of plain concrete and KFRC specimens prepared with different fiber contents and fiber lengths are shown in Figure 1. In general, the positive influence of the use of the Kevlar fibers was observed on the concrete compressive strength as the specimens having Kevlar fibers exhibited higher compressive strength as compared to the plain concrete without any fibers, irrespective of the fiber lengths and fiber content used in preparing concrete specimens. An increase in concrete compressive strength was observed in specimens with the increase in the fiber contents for 10 mm long Kevlar fibers. In contrast, it was the opposite for 15 mm fibers, as concrete specimen strength decreased with increased fiber content. However, when a fiber length of 25 mm was used, the effect of fiber content was insignificant as almost similar strengths were observed. Maximum strength was obtained when 10 mm fibers were used at 1.5% content by volume. Strengths in a similar range were observed for the cases of 10 mm fibers at 2.5% and 15 mm fibers at 1%.

Table 5 compares the concrete compressive strength of specimens with 1%, 1.5%, and 2.5% Kevlar fibers concerning the plain concrete specimens. Maximum strength gain compared to plain concrete without fibers was 78% to 83% for the cases mentioned in the preceding paragraph. This shows a significant increase in the compressive strength of KFRC, and it can be implied that Kevlar fibers can be used in concrete to improve its stability.

Figure 2 shows the failure patterns exhibited by KFRC specimens under uniaxial compression. It was observed that, as expected, the plain concrete specimen under uniaxial compression exhibited excessive crushing before failure. However, with the addition of Kevlar fibers, a significant reduction in crushing was observed with the failure of the specimen, resulting in the rupture of junk pieces from the concrete specimen, as seen in Figure 2.

3.1.2. Splitting Tensile Strength

The experimentally exhibited splitting tensile strengths of plain and KFRC specimens are shown in Figure 3. Figure 3 shows that, in general, KFRC specimens exhibited higher splitting tensile strength than plain concrete specimens. It was also observed that no definite relationship was demonstrated between the fiber content and length of Kevlar fibers on the tensile strength of the KFRC specimens.

It was further observed that the inclusion of the fibers positively influences the splitting tensile strength of the concrete for all the percentages of 10 mm long fibers, 1.5% of 15 mm long fibers, and 2.5% of 25 mm long fibers. For the case of 10 mm long fibers, the gain in splitting tensile strength was similar, showing no effect on the percentage of fibers used.

In addition to the strength, the inherent brittleness of concrete was also improved as the inclusion of the fibers

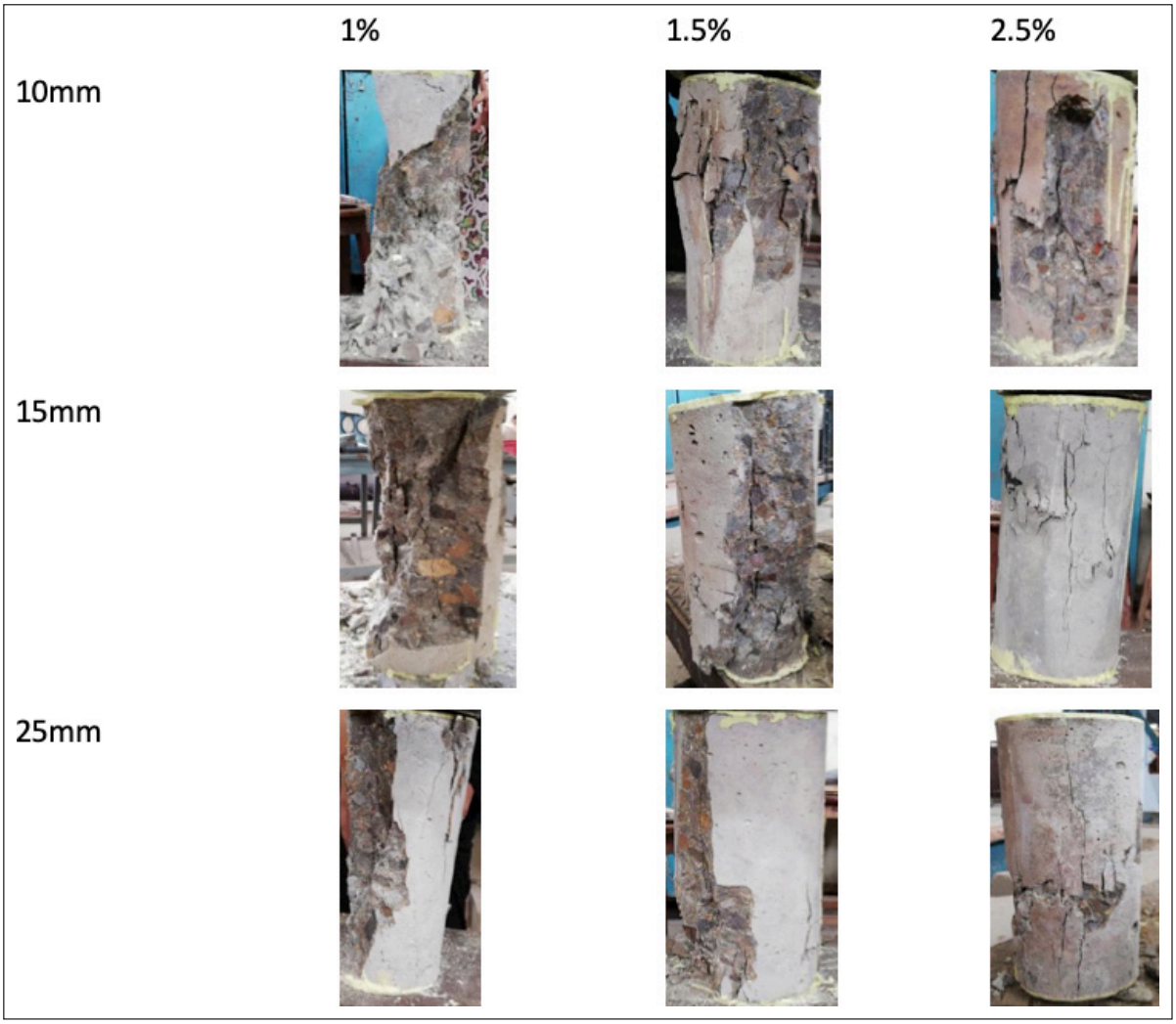

Figure 2. Failure pattern exhibited by KFRC specimens made with different fiber content and fiber lengths under uniaxial compression.

delayed the failure of the specimen, as several cracks were observed before complete failure, reflecting the effectiveness of the Kevlar fibers used. The failure pattern of the KFRC specimens under splitting tensile can be seen in Figure 4.

Table 6 compares the concrete splitting tensile strength of KFRC with 1%, 1.5%, and 2.5% Kevlar fibers concerning the plain concrete specimens. Maximum strength gain compared to plain concrete without fibers was 30% to 50% for the cases mentioned in the preceding discussion. This shows a significant increase in the splitting tensile strength of KFRC, and the use of Kevlar fibers delayed the initiation of cracking and, ultimately, the failure.

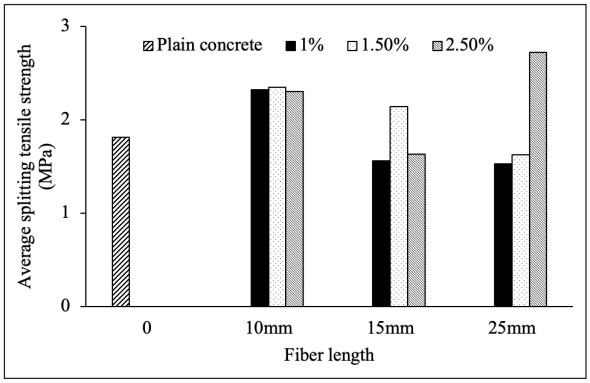

Figure 3. Relationship exhibiting the influence of the fiber volume and length on the average splitting tensile strength of KFRC specimens.

3.1.3. Flexural Tensile Strength

The flexural strengths of the plain concrete and KFRC specimens are shown in Figure 5. It was found that Kevlar fibers significantly reduced the concrete flexural strength, irrespective of the fiber contents and fiber lengths used in preparing the specimens when compared with the plain concrete specimens. Only marginal gain in strength was noted in the case of 25 mm fibers at 1% and 1.5% concentration.

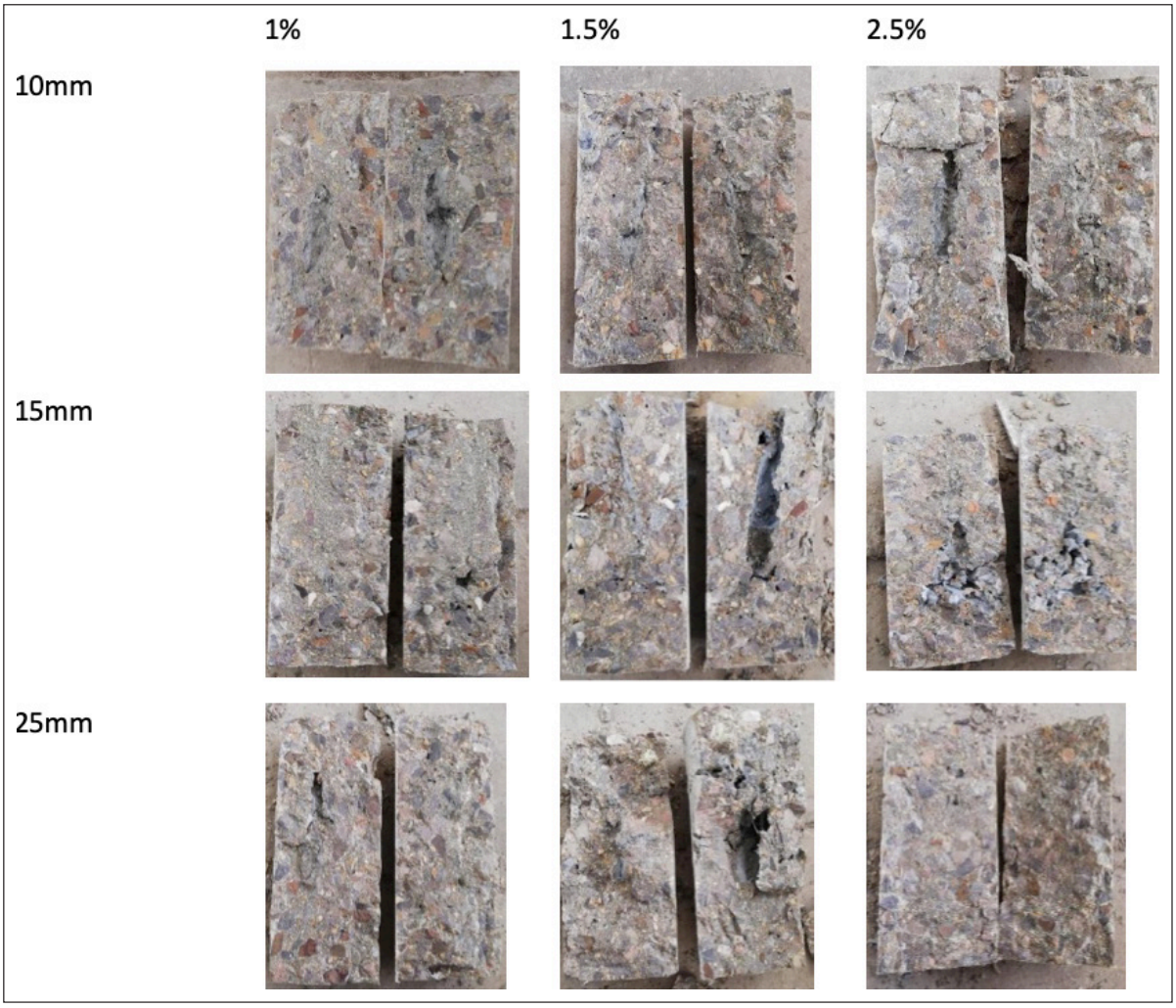

Figure 4. Failure patterns were exhibited by KFRC specimens made with different fiber content and fiber lengths under splitting tensile.

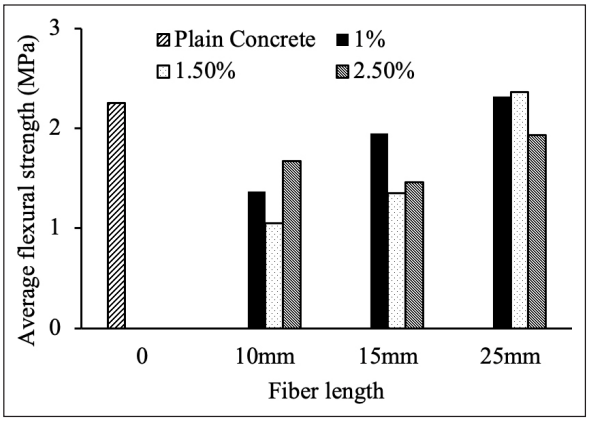

Figure 5. Relationship exhibiting the influence of the fiber volume and length on the average flexural strength of KFRC specimens.

Table 7 compares the concrete flexural strength of specimens with 1%, 1.5%, and 2.5% Kevlar fibers concerning the plain concrete specimens. In general, no significant influence of Kevlar fibers used in the study was observed on the flexural strength of the specimens investigated when compared with plain concrete specimens, except 25 mm fibers specimens having fibers content of 1.0% and 1.5%, in which a marginal increase of 2.7% and 4.9% respectively was observed in the flexural strength. This is in contrast to the splitting tensile strengths observed. This may be due to the uneven distribution of Kevlar fibers during the casting of specimens to be tested in flexure, as the gain in strength and overall behavior of fiber-reinforced concrete depends on the uniform distribution of fibers in concrete.

3.2. Jute Fiber Reinforced Concrete Specimens

3.2.1. Compressive Strength

The compressive strength of plain concrete and JFRC specimens is shown in Figure 6. As can be seen, in general, using the Jute fibers in concrete proved beneficial in increasing the concrete compressive strength irrespective of the fiber length and concentrations used in preparing the

Table 7. Average flexural strength of KFRC

	Fiber length				Fiber length		
	0	10 mm	15 mm	25 mm	10 mm	15 mm	25 mm
	Average flexural strength (MPa)				% Increase w.r.t Plain concrete		
Fiber percentage							
0%	2.25	–	–	–	–		
1%	–	1.37	1.95	2.31	-39.1	-13.3	2.7
1.50%	–	1.05	1.35	2.36	-53.3	-40.0	4.9
2.50%	–	1.67	1.46	1.953	-25.8	-35.1	-13.3

Table 8. Average uniaxial compressive strength of JFRC

	Fiber length				Fiber length		
	0	10 mm	15 mm	25 mm	10 mm	15 mm	25 mm
	Average compressive strength (MPa)				Increase w.r.t Plain concrete		
Fiber percentage							
0%	14.82	–	–	–	–	–	–
0.1%	–	26.75	38.44	25.77	80.50	159.4	73.9
0.25%	–	25.97	36.79	22.83	75.2	148.2	54.0
0.50%	–	25.25	28.32	22.45	70.4	91.1	51.5

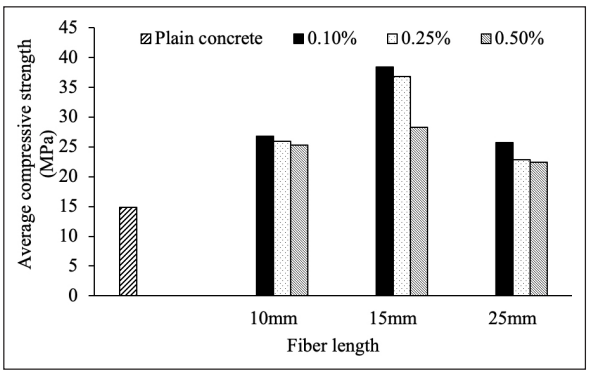

Figure 6. Relationship exhibiting the influence of the fiber volume and length on the average compressive strength of JFRC specimens.

Figure 7. Typical failure pattern exhibited by **(a)** plain concrete and **(b)** JFRC specimens under uniaxial compression.

specimens. However, the gain in strength reduces with the increase in fiber content for all lengths. A maximum increase in the concrete compressive strength was observed for specimens with Jute fibers with a length of 15 mm at all concentrations of fibers. Strength gain is reduced with the increase in the percentage of fibers used. A similar trend was observed when 10 mm and 25 mm fiber lengths were used, with the highest strength at 0.1%. Reduction in strength for 0.25% and 0.5% fibers was found to be marginal compared to 0.1% fibers, indicating that the influence of the percentage of fibers used is insignificant for 10 mm and 25 mm long fibers.

Table 8 compares the concrete compressive strength of specimens with 0.1%, 0.25%, and 0.5% jute fibers concerning the plain concrete specimens. Maximum strength gain compared to plain concrete without fibers was 159% to 148% for 15 mm long fibers at 0.1% and 0.25% fiber contents, respectively. For fiber lengths of 10 mm and 25 mm, gain in strength is in the range of 51% to 80%, which is less than strength gain for 15 mm fibers but is still significant. This significant increase in the compressive strength of JFRC demonstrates that jute fibers can be used in concrete to have performance in terms of compressive strength.

The increase in concrete compressive strength with the inclusion of the Jute fibers may be attributed to the fact that plain concrete specimens under uniaxial compression fail due to excessive lateral deformations, resulting in concrete crushing, as seen in Figure 7. However, the inclusion of the

Table 9. Average splitting tensile strength of JFRC

	Fiber length				Fiber length		
	0	10 mm	15 mm	25 mm	10 mm	15 mm	25 mm
	Average tensile strength (MPa)				% Increase w.r.t Plain concrete		
Fiber percentage							
0%	2.01	–	–	–			
0.1%	–	3.47	3.12	3.46	72.6	55.2	72.1
0.25%	–	3.66	2.35	2.78	82.1	16.9	38.3
0.50%	–	2.85	3.79	3.28	41.8	88.6	63.2

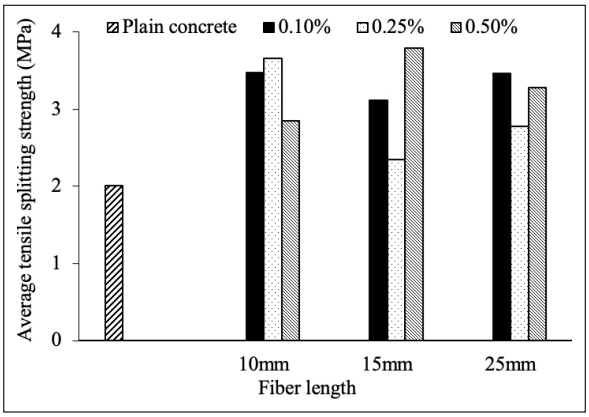

Figure 8. Relationship exhibiting the influence of the fiber volume and length on the average splitting tensile strength of JFRC specimens.

Figure 9. A typical failure pattern is exhibited by **(a)** plain concrete and **(b)** JFRC specimens under tensile splitting.

Jute fibers controlled excessive lateral deformations. As such, a higher magnitude of the force is required to fail the specimen, thus increasing the concrete compressive strength.

3.2.2. Splitting Tensile Strength

The splitting tensile strength of plain and JFRC specimens is shown in Figure 8. In general, it was found that with the addition of the Jute fibers, the splitting tensile strength also increased irrespective of the length of fibers and their percentages. However, no definite relationship was observed between the fiber lengths and concentration on the splitting tensile strength of concrete with the addition of the jute fibers.

For 10 mm long fibers, tensile strength was almost similar, at 0.1% and 0.25%, while it decreased by 0.5%. For 15 mm and 25 mm long fibers, strength decreased at 0.25% and then increased again at 0.5%. Strengths for 15 mm and 25 mm fibers were almost similar.

Table 9 compares the splitting tensile strength of specimens with 0.1%, 0.25%, and 0.5% jute fibers concerning the plain concrete specimens. Maximum strength gain compared to plain concrete without fibers was 89% in 15 mm fibers at 0.5%, followed by 82% in 10 mm fibers at 0.25%, 72.6 in 10 mm fibers at 0.1%, and 72.1% in 15 mm fibers at 0.1%. The minimum strength gain was 17% in 15 mm fibers at 0.25%. Gain in splitting tensile strength followed a trend similar to the one KFRC and again indicated that using Jute fibers delayed the initiation of cracking in tension and, ultimately, the failure.

Figure 9 shows the typical failure pattern of plain concrete and JFRC specimens with different fiber content and lengths under tensile splitting. As can be seen with the inclusion of the fibers, the number of cracks increases on the surface, indicating that higher resistance to tensile cracking was provided by the jute fibers used in concrete specimens, which was delayed, and the cracks were fine and distributed.

4. CONCLUSIONS

The investigation presented aimed at studying the behavior of JFRC and KFRC specimens under uniaxial compression, splitting tension, and flexure. Based on the detailed experimental investigation, it was observed that adding Kevlar fibers increased the compressive, tensile, and flexural strength of concrete specimens when compared with plain concrete specimens. In this investigation, the effect of the Kevlar and Jute fibers on the compressive and tensile strengths was studied using varying lengths of the fibers, the fiber content, and the volume of concrete. Conclusions drawn from the study are as follows:

- The use of Kevlar and Jute fibers in concrete was found to have a positive influence on the compressive and tensile (splitting and flexural) strengths of concrete.

- For KFRC, fibers of 10 mm length performed better under uniaxial compression and splitting tension. No strength gain was noted in flexural tension for all the fiber lengths and proportions. Therefore, using 10 mm long fibers at 1.5% content by volume is recommended for KFRC.
- For JFRC, fibers of 15 mm length performed better under uniaxial compression, while fibers of 10 mm and 15 mm length performed better-splitting tension. Therefore, 10 mm and 15 mm long fibers at 0.1% content by volume are recommended for use in JFRC.
- Both Kevlar and Jute fibers contributed positively towards controlling the crack initiation and propagation compared to plain concrete specimens, suggesting using fibers in concrete for enhanced mechanical properties and performance.

ACKNOWLEDGMENT

Assistance provided by the Department of Civil Engineering and Department of Textile Engineering, NED University of Engineering and Technology, Karachi, Pakistan, is duly acknowledged by the authors in the pursuit of the work.

ETHICS

There are no ethical issues with the publication of this manuscript.

DATA AVAILABILITY STATEMENT

The authors confirm that the data that supports the findings of this study are available within the article. Raw data that support the finding of this study are available from the corresponding author, upon reasonable request.

CONFLICT OF INTEREST

The authors declare that they have no conflict of interest.

FINANCIAL DISCLOSURE

The authors declared that this study has received no financial support.

USE OF AI FOR WRITING ASSISTANCE

Not declared.

PEER-REVIEW

Externally peer-reviewed.

REFERENCES

[1] Afroughsabet, V., & Ozbakkaloglu, T. (2015). Mechanical and durability properties of high-strength concrete containing steel and polypropylene fibers. *Constr Build Mater, 94*, 73–82. [CrossRef]

[2] Awwad, E., Mabsout, M., Hamad, B. S., & Khatib, H. (2011). Preliminary studies on using natural fibers in sustainable concrete. *Lebanese Sci J, 12*(1), 109–117.

[3] Wafa, F.F. (1990). Properties & applications of fiber reinforced concrete. *Eng Sci, 2*(1), 49–63. [CrossRef]

[4] Raupach, M., & Cruz, C.M. (2016). Textile-reinforced concrete: Selected case studies. In T. Triantafillou (Ed.), Textile Fibre Composites in Civil Engineering, In *Textile fiber composites in civil engineering* (pp. 275–299). Woodhead Publishing. [CrossRef]

[5] Scheerer, S., Schladitz, F., & Curbach, M. (2015). Textile reinforced concrete - From the idea to a high performance material. In W. Brameshuber (Ed.). *Proceedings of the FERRO-11 & 3rd ICTRC (PRO 98)* (pp. 7–10). RILEM Publications.

[6] Walton, P., & Majumdar, A.J. (1978). Properties of cement composites reinforced with Kevlar fibres. *J Mater Sci, 13*, 1075–1083. [CrossRef]

[7] Chaudhary, S., & Sharma, A.K. (2019). An experimental study on mechanical properties of kevlar fiber in concrete. *Int J Eng Res Technol, 8*(7), 710–712.

[8] Uchida, Y., Takeyama, T., & Dei, T. (2010). Ultra high strength fiber reinforced concrete using aramid fiber. In B. H. Oh, et al. (Ed.). *Proceedings of FraMCoS-7* (pp. 1492–1496). Korea Concrete Institute.

[9] Zakaria, M., Ahmed, M., Hoque, M., & Islam, S. (2017). Scope of using jute fiber for the reinforcement of concrete material. *Textiles Cloth Sustain, 2*, 1–10. [CrossRef]

[10] Dayananda, N., Gowda, B. K., & Prasad, G. E. (2018). A study on compressive strength attributes of jute fiber reinforced cement concrete composites. *IOP Conf Ser Mater Sci Eng, 376*(1), 012069. [CrossRef]

[11] Zhang, T., Yin, Y., Gong, Y., & Wang, L. (2020). Mechanical properties of jute fiber-reinforced high-strength concrete. *Struct Concr, 21*(2), 703–712. [CrossRef]

[12] Kim, J., Park, C., Choi, Y., Lee, H., & Song, G. (2012). An investigation of mechanical properties of jute fiber-reinforced concrete. In G. Parra-Montesinos, H. W. Reinhardt, A. E. Naaman, (Eds.). *High Performance Fiber Reinforced Cement Composites 6: HPFRCC 6* (pp. 75–82). Springer. [CrossRef]

[13] Razmi, A., & Mirsayar, M. (2017). On the mixed mode I/II fracture properties of jute fiber-reinforced concrete. *Constr Build Mater, 148*, 512–520. [CrossRef]

[14] Rahman, S., & Azad, A. (2018). Investigation on mechanical strength of jute fiber reinforced concrete JFRC compared to plain concrete. *Int J Sci Eng Res, 9*, 560–564.

[15] Faiq, L. S. (2018). Study of the mechanical properties of jute fiber reinforced cement composites. *Eng Technol J, 36*(12A), 1244–1248. [CrossRef]

[16] Li, Y. F., Yang, K. H., Hsu, P. Y., Syu, J. Y., Wang, S. J., Kuo, W. S. & Tsai, Y. K. (2023). Comparing mechanical characterization of carbon, kevlar, and hybrid-fiber-reinforced concrete under quasistatic and dynamic loadings. *Buildings, 13*(8), 2044. [CrossRef]

[17] Li, Y. F., Syu, J. Y., Huang, C. H., Huang, Y. R., & Tsai Y. K. (2023). A study on mechanical behavior of Kevlar fiber reinforced concrete under static and high-strain rate loading. *Int J Prot Struct, 14*(3), 407–437. [CrossRef]

[18] Konczalski, P., & Piekarski, K. (1982). Tensile properties of Portland cement reinforced with Kevlar fibers. *J Reinf Plast Comp, 1*(4), 378–384. [CrossRef]

[19] Standard, A. (2010). *Standard test method for compressive strength of cylindrical concrete specimens*. ASTM C39.

[20] Norma, A. (2004). *Standard test method for splitting tensile strength of cylindrical concrete specimens*. C496/C496M-11

[21] ASTM Int. (2010). Standard test method for flexural strength of concrete (using simple beam with third-point loading). *Am Soc Test Mater*, ASTM Michigan.

J Sustain Const Mater Technol, Vol. 9, Issue. 2, pp. 138–143, June 2024

Journal of Sustainable Construction Materials and Technologies
Web page info: https://jscmt.yildiz.edu.tr
DOI: 10.47481/jscmt.1398732

JSCMT
Journal of Sustainable Construction Materials and Technologies

Research Article

Evaluation of antimicrobial properties in coatings for operating room surfaces

Halit COZA*

Department of Architecture, Pamukkale University Faculty of Architecture and Design, Denizli, Türkiye

ARTICLE INFO

Article history
Received: 01 December 2023
Revised: 17 January 2024
Accepted: 26 April 2024

Key words:
Acrylic, alkyd, antimicrobial properties, epoxy, infection control, operating room, polyurethane

ABSTRACT

This article highlights the crucial significance of upholding sterility in operating rooms (ORs) to minimize infection risks and uphold patient safety. Putting a spotlight on the pivotal role of antimicrobial coatings, the research delves into the examination of four frequently used coatings—polyurethane, acrylic, alkyd, and epoxy—across various surfaces within ORs. The study evaluates the antimicrobial properties of these coatings against 20 contaminant bacteria, uncovering diverse impacts on different strains. While these coatings may not inherently possess antimicrobial characteristics, formulations enriched with agents like 1,2-benzisothiazol-3(2H)-one (BIT) and 2-octyl-2H-isothiazol-3-one (OIT) demonstrate active resistance against bacterial growth. The results highlight the efficacy of acrylic and epoxy coatings, specifically in impeding bacterial proliferation. These findings affirm the practical utility of antimicrobial coatings in vital healthcare settings, providing valuable insights into their potential to elevate hygiene, safety, and efficiency in ORs. The study advocates for ongoing exploration of innovative coatings and antimicrobial agents, underscoring the importance of adhering to cleaning protocols and healthcare regulations for optimal effectiveness.

Cite this article as: Coza, H. (2024) Evaluation of antimicrobial properties in coatings for operating room surfaces. *J Sustain Const Mater Technol*, 9(2), 138–143.

1. INTRODUCTION

Creating and maintaining a sterile environment in an operating room (OR) is paramount for reducing the risk of infections and ensuring patient safety. Modern clean operating rooms must meet specific requirements for layout, floor, walls, and facilities, as well as selecting building materials and addressing hand washing room considerations [1]. The careful selection of building materials for the OR floor and walls plays a crucial role, with a focus on incorporating antimicrobial properties to enhance hygiene. Among the preferred materials for the OR floor, certain types of vinyl flooring are engineered with antimicrobial features, providing an easily cleanable and impermeable surface that resists bacterial growth. Flooring, formulated with antimicrobial agents, contributes to a durable and hygienic surface, resistant to chemicals and easy to clean [2]. For the walls of the OR, antimicrobial paints with additives inhibiting bacterial and fungal growth are applied to enhance hygiene [2, 3]. Solid surface wall systems, such as non-porous and seamless wall panels, are chosen to prevent microbial growth, offering ease of maintenance.

In the construction and maintenance ORs, the strategic application of various coatings, such as polyurethane, acrylic, alkyd, and epoxy, is essential to meet the specific demands of this critical healthcare environment. Polyurethane coatings, prized for their durability and chemical resistance, find utility in surfaces requiring robust protec-

***Corresponding author.**
*E-mail address: hcoza@pau.edu.tr

tion against chemicals and frequent cleaning, such as cabinets and medical equipment [4]. Acrylic coatings, known for their quick drying time and versatility, may be chosen for walls or ceilings in ORs where a fast-drying and easy-to-apply solution is advantageous. With low odor and toxicity, acrylic coatings contribute to a cost-effective and aesthetically pleasing environment [5].

Alkyd coatings, being oil-based, are suitable for metal surfaces within the OR, offering reliable adhesion and protection against corrosion [6, 7]. They are commonly applied to metal components of furniture and medical devices. Epoxy coatings, renowned for exceptional durability and chemical resistance, are prevalent in ORs, particularly on floors and walls. The impermeable surface created by epoxy coatings resists chemicals, stains, and microbial growth, meeting the stringent hygiene requirements of operating rooms [8]. Each of these coatings plays a vital role in enhancing the functionality, durability, and cleanliness of different surfaces within the operating room, contributing to the overall safety and efficiency of healthcare practices. While not inherently possessing antimicrobial properties, these coatings can contribute significantly to creating a hygienic environment in ORs [9]. Some formulations of coatings can be enriched with antimicrobial agents like silver ions, imparting the surfaces with the ability to resist the growth of bacteria and fungi actively [10–12]. This is particularly advantageous when applied to surfaces requiring frequent cleaning.

Establishing antimicrobial surfaces could be one of the keys to helping prevent further contagious incidents and breakouts. An antimicrobial surface must ensure that pathogenic contamination is eliminated or lowered to a minimum. Different antimicrobial agents are often added to coating formulas to prevent microbial growth. There are now various antimicrobial substrates on the market. It is worthwhile investigating the efficacy and precision of these products. Meanwhile, the use of antimicrobial agents is expanding, as is research into their antibacterial characteristics and components [11]. This study has designed an experiment to test the antimicrobial properties of polyurethane, acrylic, alkyd, and epoxy coatings. It has been investigated whether the bacteria will survive or proliferate, and if they don't, how long will it take to be diminished on a surface coated with the substances. This study has been conducted on four types of coatings, observing 20 types of contaminant bacteria.

2. MATERIALS AND METHODS

2.1. Materials

Four different types of coatings used frequently in hospitals and ORs surfaces (polyurethane, acrylic, alkyd, and epoxy) were purchased from commercial sources. The information and the ingredients of the coatings investigated are listed in Table 1. For evaluation of the surfaces antibacterial effectivity 20 different microorganisms were used (Table 2). The microorganisms were obtained from ATCC culture collection.

2.2. Samples Preparation

Coatings were administered to four wooden panels measuring 5×5 cm each and allowed to dry for a period of 10 hours at room temperature (Fig. 1). This procedure was repeated three times. The panels were subsequently sterilized via autoclave, and bacterial suspensions were sprayed onto the surfaces, left to dry at room temperature. Sampling was conducted after 24 hours of bacterial attachment.

2.3. Evaluation of Antimicrobial Activity

For this research, a total of 20 diverse microorganisms were employed to contaminate the four coated panels. Subsequent to the contamination, the surface was allowed to stand undisturbed for 24 hours before repeating the swab sampling. The results were quantified as $\log_{10}$kob/cm^2 through the generation of serial dilutions with maximum recovery diluent. These diluted samples were then inoculated onto plate count agar (tryptone glucose yeast agar CM0325, Oxoid). using the spread plate technique and incubated at 37°C for 24 hours.

3. RESULTS AND DISCUSSION

This study aimed to evaluate and determine the duration of the antimicrobial effect of different coatings that can be used operating rooms and hospitals. The data obtained from polyurethane and acrylic, coated panels at the end of 6 hours are shown in Table 3. The data obtained from alkyd, and epoxy coated panels at the end of 6 hours are shown in Table 4.

Examining the antibacterial properties of polyurethane, acrylic, alkyd, and epoxy coatings reveals varying impacts on different bacterial strains. Polyurethane coating is most effective against *Listeria monocytogenes 3b* but less so against *Proteus mirabilis*. Acrylic coating significantly reduces *Staphylococcus aureus* counts, while *Salmonella typhimurium* shows the least response. Alkyd coating strongly affects *Staphylococcus aureus* but minimally impacts *Methicillin resistant S.aureus*. In the case of epoxy coating, *Streptococcus epidermidis* experiences the greatest reduction, while *Salmonella typhimurium* exhibits a less pronounced response. The coatings, ranked by their average percentage reduction in bacterial counts across all tested strains, exhibit varying levels of antibacterial efficacy. Acrylic coating leads with an impressive average reduction of 94.26%, followed closely by Alkyd and Epoxy coatings at 90.79% and 90.58%, respectively. In contrast, Polyurethane coating shows a somewhat lower average reduction at 74.79%. Based on the polyurethane ingredient list, it appears that the antibacterial properties of polyurethane coating may not be directly attributed to the listed components. The primary antibacterial effects might be due to the physical characteristics of the coating or other factors not explicitly mentioned in the provided ingredient list.

The Acrylic ingredient list contains antimicrobial agents such as 1,2-benzisothiazol3(2H)-one (BIT), Zinc Pyrithione [13], and 2-octyl-2H-isothiazol-3-one (OIT). These components likely contribute to the observed antibacterial

Table 1. Coatings ingredient used within the scope of the study.

Polyurethane-hardtop XP		Acrylic-jotashield topcoat silk	
Ingredient	**Concentration**	**Ingredient**	**Concentration**
Xylene	≥10–≤15	Alcohols, C16-18 and C18-unsatd., ethoxylated	≤0.1
N-butyl acetate	≤10	1,2-benzisothiazol-3(2h)-one (BIT)	<0.05
Ethylbenzene	≤5	zinc pyrithione	≤0.024
Titanium dioxide	≤5	2-octyl-2h-isothiazol-3-one (OIT)	≤0.0024
Hydrocarbons, C9, aromatics	≤4.1		
N-butyl methacrylate	<1		
2-Propenoic acid, 2-methyl-, 2- (dimethylamino)ethyl ester, polymer with butyl 2-propenoate, compd. with polyethylene glycol hydrogen maleate C9-11-alkyl ethers	<1		
Decanedioic acid, 1,10-bis (1,2,2,6,6-pentamethyl-4-piperidinyl) ester, mixt. with 1-methyl 10- (1,2,2,6,6-pentamethyl-4-piperidinyl) decanedioate	≤0.3		
Oleic acid, compound	≤0.1		
Maleic anhydride	≤0.1		
Alkyd - Pilot II		**Epoxy - Jotamastic 80**	
Ingredient	**Concentration**	**Ingredient**	**Concentration**
Hydrocarbons, C9-C12, n-alkanes, isoalkanes, cyclics, aromatics (2–25%)	≥25–≤50	Epoxy resin (MW ≤700)	≥10–<25
Titanium dioxide	≥10–≤25	Titanium dioxide	≤10
Xylene	≤3	Hydrocarbons, c9-unsatd., polymd	≤10
Hexanoic acid, 2-ethyl-, zinc salt, basic	≤0.3	Xylene	≤10
		2-methylpropan-1-ol	≤5
		Benzyl alcohol	≤3
		Ethylbenzene	≤3
		Epoxy resin (MW 700–1200)	≤3
		2-Propenoic acid, 2-methyl-, 2- (dimethylamino)ethyl ester, polymer with butyl 2-propenoate, compd. with polyethylene glycol hydrogen maleate C9-11-alkyl ethers	≤0.3
		Oleic acid, compound	≤0.1

Table 2. Bacterial cultures used in antimicrobial analysis

Microorganism	Gram type
E.coli	Gram negative
E.coli O157	Gram negative
Bacillus subtilis	Gram positive
Bacillus cereus	Gram positive
Staphylococcus aureus	Gram positive
Methicillin resistant *S.aureus*	Gram positive
Vancomycin resistant Enterococcus faecium	Gram positive
Streptococcus epidermidis	Gram positive
Listeria monocytogenes 3b	Gram positive
Salmonella enteritidis	Gram negative
Salmonella typhimurium	Gram negative
Campylobacter jejuni	Gram negative
Geobacillus stearothemophilus	Gram positive
Shigella flexneri	Gram negative
Cronobacter sakazakii	Gram negative
Pseudomonas aeruginosa	Gram negative
Proteus mirabilis	Gram negative
Acinetobacter baumanii	Gram negative
Vibrio parahemolyticus	Gram negative
Yersinia enterocolitica	Gram negative

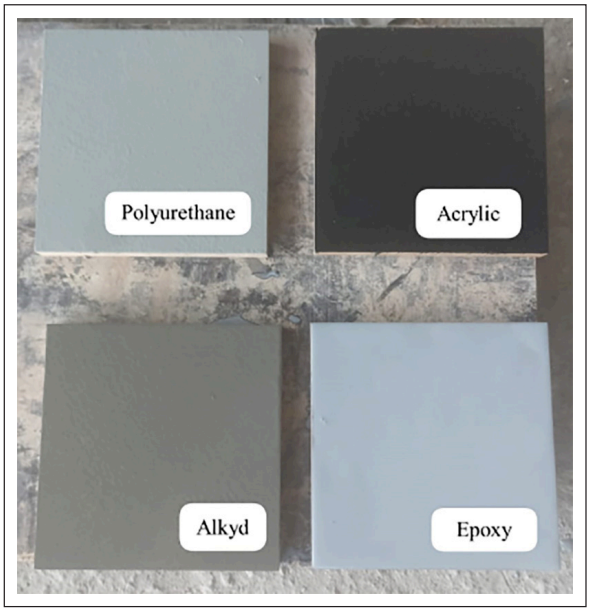

Figure 1. Polyurethane, acrylic, alkyd, and epoxy coated panels.

Table 3. Bacterial growth dynamics on polyurethane and acrylic surfaces over time

Bacteria name	Polyurethane					Acrylic		
	Initial count	Logarithmic level	2. h	4. h	6. h	2. h	4. h	6. h
E.coli	8200000	6.913813852	3700000	37000	3700	990000	9900	990
E.coli O157	6900000	6.838849091	6600000	66000	6600	820000	8200	820
Bacillus subtilis	3000000	6.477121255	2300000	23000	2300	850000	8500	850
Bacillus cereus	5500000	6.740362689	2500000	25000	2500	220000	2200	220
Staphylococcus aureus	6300000	6.799340549	2200000	22000	2200	760000	7600	760
Methicillin resistant S.aureus	6800000	6.832508913	6400000	64000	6400	100000	1000	100
Vancomycin resistant Enterococcus faecium	8900000	6.949390007	2200000	22000	2200	680000	6800	680
Streptococcus epidermidis	5400000	6.73239376	7800000	78000	7800	260000	2600	260
Listeria monocytogenes 3b	6900000	6.838849091	2800000	28000	2800	700000	7000	700
Salmonella enteritidis	1000000	6	3900000	39000	3900	460000	4600	460
Salmonella typhimurium	9200000	6.963787827	9100000	91000	9100	510000	5100	510
Campylobacter jejuni	5700000	6.755874856	7000000	70000	7000	260000	2600	260
Geobacillus stearothemophilus	6100000	6.785329835	9500000	95000	9500	770000	7700	770
Shigella flexneri	4800000	6.681241237	4300000	43000	4300	390000	3900	390
Cronobacter sakazakii	1400000	6.146128036	1500000	15000	1500	160000	1600	160
Pseudomonas aeruginosa	1700000	6.230448921	5900000	59000	5900	580000	5800	580
Proteus mirabilis	700000	5.84509804	2200000	22000	2200	820000	8200	820
Acinetobacter baumanii	3900000	6.591064607	6900000	69000	6900	430000	4300	430
Vibrio parahemolyticus	5100000	6.707570176	5000000	50000	5000	640000	6400	640
Yersinia enterocolitica	8200000	6.913813852	3900000	39000	3900	540000	5400	540

properties of the Acrylic coating. The concentrations mentioned suggest a careful formulation to provide effective antimicrobial action while minimizing potential adverse effects. BIT is a commonly utilized biocide applied to industrial products with broad antimicrobial activity [14, 15]. BIT has been shown to react with thiol-containing proteins on target microorganisms and is especially effective against actively metabolizing bacteria [16, 17]. It is widely used in food packaging, industrial and consumer products like adhesives, laundry and dish detergents, cleaning and disinfectants, air fresheners, personal care products and sunscreens, paints, and industrial lubricants [18, 19]. OIT is a coordination complex of isothiazolone and has antibacterial and fungicidal properties [20]. It is used as a biocide in cooling-tower water, paints, cutting oils, cosmetics, and shampoos, and for leather preservation [20]. According to a CLH report published by the Chemicals Regulation Division United Kingdom, 2-octyl-2H-isothiazol-3-one ex-

Table 4. Bacterial growth dynamics on alkyd and epoxy surfaces over time

Bacteria name	Alkyd					Epoxy		
	Initial count	Logarithmic level	2. h	4. h	6. h	2. h	4. h	6. h
E.coli	8200000	6.913813852	610000	6100	610	64000	640	64
E.coli O157	6900000	6.838849091	880000	8800	880	59000	590	59
Bacillus subtilis	3000000	6.477121255	630000	6300	630	18000	180	18
Bacillus cereus	5500000	6.740362689	870000	8700	870	60000	600	60
Staphylococcus aureus	6300000	6.799340549	250000	2500	250	99000	990	99
Methicillin resistant S.aureus	6800000	6.832508913	330000	3300	330	65000	650	65
Vancomycin resistant Enterococcus faecium	8900000	6.949390007	320000	3200	320	75000	750	75
Streptococcus epidermidis	5400000	6.73239376	550000	5500	550	44000	440	44
Listeria monocytogenes 3b	6900000	6.838849091	370000	3700	370	94000	940	94
Salmonella enteritidis	1000000	6	470000	4700	470	32000	320	32
Salmonella typhimurium	9200000	6.963787827	100000	1000	100	25000	250	25
Campylobacter jejuni	5700000	6.755874856	690000	6900	690	95000	950	95
Geobacillus stearothemophilus	6100000	6.785329835	380000	3800	380	58000	580	58
Shigella flexneri	4800000	6.681241237	840000	8400	840	76000	760	76
Cronobacter sakazakii	1400000	6.146128036	530000	5300	530	67000	670	67
Pseudomonas aeruginosa	1700000	6.230448921	400000	4000	400	25000	250	25
Proteus mirabilis	700000	5.84509804	220000	2200	220	91000	910	91
Acinetobacter baumanii	3900000	6.591064607	250000	2500	250	29000	290	29
Vibrio parahemolyticus	5100000	6.707570176	530000	5300	530	84000	840	84
Yersinia enterocolitica	8200000	6.913813852	220000	2200	220	24000	240	24

hibited strong antibacterial activity against *Escherichia coli*, *Staphylococcus aureus*, and *Pseudomonas aeruginosa* [21].

Alkyd coating is composed of a blend of hydrocarbons, titanium dioxide, xylene, and a zinc salt. Although hydrocarbons and titanium dioxide may not exhibit direct antibacterial properties, the inclusion of xylene [22] and the zinc salt [23, 24] suggests a potential contribution to the observed antibacterial effects. The overall performance of the coating is likely influenced by the specific formulation and interactions among these components.

The epoxy coating contains a mix of components, including some with potential antimicrobial properties. However, the overall antibacterial efficacy is likely influenced by the combination and interactions of these components. Based on this information, none of these materials are inherently antibacterial and they all require proper care and maintenance to keep them hygienic. Some products may claim to have antibacterial features, but they may not be effective or long-lasting. Therefore, it is important to follow the manufacturer's instructions and use suitable cleaners for each material. A substantial proportion of antimicrobial coatings finds widespread use in the construction industry, particularly in the creation of both interior and exterior coatings designed to provide protection against microbial threats. There is a projected significant increase in the demand for antimicrobial coatings, especially in sectors such as hospitals, operating rooms, nursing homes, daycares, and other medical applications where maintaining a stringent standard of hygiene is imperative [11, 25]. In these crucial environments, the common practice involves integrating various antimicrobials into paint formulations to enhance the resilience of products against potential microbial attacks. Antimicrobial agents play a crucial role in reducing the likelihood of microbial growth on coated surfaces, thereby ensuring a hygienic and sterile environment in medical settings [26–28]. While selecting these coatings, consideration of their compatibility with cleaning protocols, surface types, and adherence to healthcare regulations is crucial. Collaborating with infection control experts ensures that these coatings contribute effectively to the overall hygiene and safety standards of the operating room. Regular cleaning and disinfection practices further enhance the antimicrobial efficacy of these coatings, collectively fortifying the OR against potential infections.

4. CONCLUSION

This study investigated the pivotal role of antimicrobial coatings—polyurethane, acrylic, alkyd, and epoxy—in cultivating a hygienic environment within operating rooms and hospital settings. Applied strategically across diverse surfaces, these coatings significantly contributed to overall functionality, durability, and cleanliness, enhancing healthcare safety and efficiency. The experimental assessment of antimicrobial properties against 20 contaminant bacteria yielded noteworthy results. While the coatings may not inherently possess antimicrobial traits, formulations enriched with agents like BIT and OIT demonstrated active resistance against bacterial growth, emphasizing their potential in promoting hygiene. Results showed varying degrees of antimicrobial efficacy, with acrylic and epoxy coatings particularly excelling in inhibiting bacterial proliferation. The incorporation of antimicrobial agents notably enhanced the coatings ability to create surfaces resilient to microbial growth, highlighting their practical applications in critical healthcare settings like ORs.

ETHICS

There are no ethical issues with the publication of this manuscript.

DATA AVAILABILITY STATEMENT

The authors confirm that the data that supports the findings of this study are available within the article. Raw data that support the finding of this study are available from the corresponding author, upon reasonable request.

CONFLICT OF INTEREST

The authors declare that they have no conflict of interest.

FINANCIAL DISCLOSURE

The authors declared that this study has received no financial support.

USE OF AI FOR WRITING ASSISTANCE

Not declared.

PEER-REVIEW

Externally peer-reviewed.

REFERENCES

[1] Yang, J., Qing, Y. (2002). Study on Modern Clean Operating Room. *J Prac Med Tech*, *1*, 64.

[2] Bäumler, W., Eckl, D., Holzmann, T., & Schneider-Brachert, W. (2022). Antimicrobial coatings for environmental surfaces in hospitals: A potential new pillar for prevention strategies in hygiene. *Crit Rev Microbiol, 48*(5), 531–564. [CrossRef]

[3] Coza, H. (2023). Timeline approach for antimicrobial paints applied on surfaces. *J Sustain Constr Mater Technol, 8*(2), 107–111. [CrossRef]

[4] Reinstadtler, S., Williams, C., & Olson, A. (2015). *Polyurethane coatings*. ASM International eBooks. [CrossRef]

[5] Jackson, U. *Understanding and controlling acrylic drying time*. https://justpaint.org/de/understanding-and-controlling-acrylic-drying-time/

[6] Hofland, A. (2012). Alkyd resins: From down and out to alive and kicking. *Prog Org Coat, 73*(4), 274–282. [CrossRef]

[7] Montemor, M. (2014). Functional and smart coatings for corrosion protection: A review of recent advances. *Surf Coat Technol, 258*, 17–37. [CrossRef]

[8] Floorings Solutions. *The sanitary benefits of epoxy flooring for hospitals and clinics and hospitals*. https://flooringsolutions.ph/blog/epoxy-clinics-hospitals/

[9] Maamori, M. A., Majdi, H. S., Kareem, A., & Saud, A. N. (2023). Modification of acrylic paint by acetamide to be antibacterial used for medical applications. *6th International Conference on Nanotechnologies and Biomedical Engineering*.

[10] Pică, A., Guran, C., Ficai, D., Ficai, A., & Oprea, O. (2013). Decorative antimicrobial coating materials based on silver nanoparticles. *UPB Sci Bull, 75*(1), 35–42.

[11] Johns, K. (2003). Hygienic coatings: The next generation. *Surf Coat Int, 86*(2), 101–110. [CrossRef]

[12] Davidson, K., Moyer, B., Ramanathan, K., Preuss, A., & Pomper, B. (2007). Formulating coatings with silver-based antimicrobials: A systematic approach. *J Coat Technol Res, 4*(1), 56–62.

[13] National Cancer Institute. *Pyrithione zinc*. https://www.qeios.com/read/OYFZ98

[14] Collier, P. J., Ramsey, A. J., Austin, P., & Gilbert, P. (1990). Growth inhibitory and biocidal activity of some isothiazolone biocides. *J Appl Bacteriol, 69*(4), 569–577. [CrossRef]

[15] Shimizu, M., Shimazaki, T., Yoshida, T., Ando, W., & Konakahara, T. (2012). Synthesis of 1, 2-benzisothiazolin-3-ones by ring transformation of 1, 3-benzoxathiin-4-one 1-oxides. *Tetrahedron, 68*(21), 3932–3936. [CrossRef]

[16] Paulus, W. (2005). *Directory of microbicides for the protection of materials: A handbook*. Springer. [CrossRef]

[17] Collier, P. J., Ramsey, A., Waigh, R. D., Douglas, K. T., Austin, P., & Gilbert, P. (1990). Chemical reactivity of some isothiazolone biocides. J Appl Bacteriol, *69*(4), 578–584. [CrossRef]

[18] Ayadi, M., & Martin, P. (1999). Pulpitis of the fingers from a shoe glue containing 1, 2-benzisothiazolin-3-one (BIT). *Contact Dermatitis, 40*(2), 115–116. [CrossRef]

[19] Appendini, P., & Hotchkiss, J. H. (2002). Review of antimicrobial food packaging. *Innov Food Sci Emerg Technol, 3*(2), 113–126. [CrossRef]

[20] ChemicalBook. *2-Octyl-2H-isothiazol-3-one*. https://www.chemicalbook.com/ChemicalProductProperty_EN_CB3221648.htm

[21] ECHA. (2018). *CLH report - Substance Name: octhilinone (ISO); 2-octyl-2H-isothiazol-3-one; [OIT]*. https://echa.europa.eu/documents/10162/df62dc1e-b657-a288-7050-b7763e8ec8eb

[22] Aminsobhani, M., Razmi, H., Hamidzadeh, F., & Rezaei Avval, A. (2022). Evaluation of the antibacterial effect of xylene, chloroform, eucalyptol, and orange oil on *enterococcus faecalis* in nonsurgical root canal retreatment: An *ex vivo* study. *BioMed Res Int*, *2022*, 8176172. [CrossRef]

[23] Lavaee, F., Ghapanchi, J., Motamedifar, M., & Sharifzade Javidi, M. (2018). Experimental evaluation of the effect of Zinc salt on ınhibition of streptococcus mutans. *J Dent* (Shiraz), 19(3), 168–173.

[24] Almoudi, M. M., Hussein, A. S., Sarmin, N. I. M., & Hassan, M. I. A. (2023). Antibacterial effectiveness of different zinc salts on Streptococcus mutans and Streptococcus sobrinus: An *in-vitro* study. *Saudi Dent J, 35*(7), 883–890. [CrossRef]

[25] Davidson, K., Moyer, B., Ramanathan, K., Preuss, A., & Pomper, B. (2007). Formulating coatings with silver-based antimicrobials: A systematic approach. *J Coat Technol Res, 4*(1), 56–62.

[26] Snyder, D., Barrett L., Sianawati, E. *Antimicrobial coatings*. https://www.pcimag.com/articles/87237-antimicrobial-coatings

[27] C. Vielkanowitz. (2008). New silver based antimicrobial systems for hygiene coatings. *American Coatings Conference*. Charlotte, NC.

[28] J. Baghdachi, D. Clemans. (2006). Formulation and evaluation of antimicrobial waterborne and high solids coatings. *Smart Coatings Conference*. Orlando.

J Sustain Const Mater Technol, Vol. 9, Issue. 2, pp. 144–158, June 2024

Journal of Sustainable Construction Materials and Technologies
Web page info: https://jscmt.yildiz.edu.tr
DOI: 10.47481/jscmt.1495140

JSCMT
Journal of Sustainable Construction Materials and Technologies

Research Article

Determining the importance levels of criteria in selection of sustainable building materials and obstacles in their use

Serkan YILDIZ, Gülnaz Şengül GÜNEŞ*

Department of Real Estate Development and Management, Ankara University, Ankara, Türkiye

ARTICLE INFO

Article history
Received: 12 March 2024
Revised: 05 May 2024
Accepted: 09 May 2024

Key words:
Building material, factor analysis, relative importance, sustainability

ABSTRACT

The construction industry has become the focal point of sustainability as one of the largest consumers of natural resources and waste producers. A sustainable construction industry is possible with the sustainability of building materials, which is the main factor controlling the construction management process. In this research, the importance levels of a total of 17 criteria under the headings of economic, environmental, and social sustainability in terms of sustainability of building materials and the importance levels of 11 obstacles to the use of sustainable materials were investigated through a survey conducted with the participation of 60 people. Whether there were differences between the participants' opinions was investigated through inferential analysis. In ranking criteria according to their importance level, the health of workers and citizens, safety in construction and operation, and toxic emissions took the first three places. The risks of higher initial cost, total cost, and extra time are the biggest obstacles to using sustainable materials. In addition, the obstacles were subjected to factor analysis, and a model consisting of four factors was created. The study revealed the criteria for sustainable material selection and the barriers to sustainable material use in a holistic manner. In this respect, it is evaluated that it will be a guide for governments, local governments, building material manufacturers, designers, contractors, and ultimately users to achieve a more sustainable construction sector.

Cite this article as: Yıldız, S., & Güneş, G. Ş. (2024) Determining the importance levels of criteria in selection of sustainable building materials and obstacles in their use. *J Sustain Const Mater Technol*, 9(2), 144–158.

1. INTRODUCTION

The world population, estimated to be around 600 million in the 1700s [1], today exceeds 8 billion. This insane population growth and the accompanying industrial revolution have led to an uncontrolled development process focused on unlimited production and consumption. This process has put significant pressure on the environment. It has created major environmental problems such as the rapid depletion of natural resources, pollution of air, water, and soil, the spread of chemicals and heavy metals throughout the environment, the destruction of forests and agricultural areas, global warming and acid rain, desertification, and the destruction of the ozone layer [2, 3]. In addition to these environmental problems, the rapidly increasing population, which cannot be satisfied in the countryside, has piled up in cities to work. This has led to unmanageable and unplanned urban growth [4]. Cities have become potential centers for many social, environmental, and economic problems, such as inequality, unemployment, poverty, inadequate infrastructure and services, traffic chaos, violence, crime, and disease [5, 6]. This economic development model has been based on people's desire to continuously raise their living standards without limits, on a policy

***Corresponding author.**
*E-mail address: gsengul@ankara.edu.tr

of unlimited production and overconsumption of natural resources, and on destroying the basis of life of living beings. The World Commission on Environment and Development (WCED) report "Our Common Future," published in 1987, emphasized the need to change this model. The report contended that sustainable development should encompass apparent consideration and definition of the social, economic, and ecological facets, defining it as fulfilling present needs while safeguarding the capacity of future generations to fulfill their own [7].

Buildings, particularly in urban areas, are significant consumers of energy and natural resources, contributing to air, water, and soil pollution through waste generation [8]. The statistics reveal that buildings account for 45% of global energy consumption and 50% of water usage. Additionally, they are responsible for 23% of urban air pollution, 50% of greenhouse gas emissions, 40% of water pollution, and 40% of solid waste generation [9]. These alarming figures have prompted initiatives to enhance the sustainability of the construction industry as a whole and individual buildings. "sustainable design" and "sustainable architecture" have emerged to systematically solve the environmental, social, and economic problems associated with our built environment and buildings. Sustainable design is defined as the design of products, services, and the built environment by the principles of social, economic, and environmental sustainability, that is, in a way that serves both present and future generations to achieve a healthy and quality life [10]. On the other hand, sustainable architecture is designing sustainable buildings to reduce the total environmental impact during the entire life cycle, from the production of building materials to the construction, use, and demolition of the building [11]. The goal of sustainable architecture is to create buildings that are sensitive to their environment, minimize the destruction of nature, use all-natural resources such as energy, materials, water, and land most economically and efficiently [12] and expresses an approach that adapts to the surrounding nature, climate, society, and culture [13].

The first and essential condition for producing sustainable architectural works is the selection of sustainable materials [14–16]. Research shows that by selecting construction materials compatible with sustainability principles, for example, CO_2 emissions can be reduced by up to 30% [17]. Otherwise, efforts to build sustainable buildings will be ineffective [14, 18, 19]. On the other hand, the material selection process is very challenging and complex since building materials are the main factor affecting many criteria expected from a building, such as being safe, economical, durable, aesthetic, and functional. With the addition of sustainability in this process, sustainable material selection becomes one of the most challenging tasks in a building project [20]. This situation necessitates a good understanding of the relationship between sustainability and building materials, and this study was carried out to serve this purpose.

The study highlights the significance of environmental, social, and economic factors impacting building material sustainability alongside barriers to their adoption. It assessed 17 criteria covering these sustainability aspects and identified 11 obstacles to material use in Türkiye. Furthermore, factor analysis categorized these barriers into common groups. The data collected through the questionnaire study were obtained from 60 people with different demographic characteristics, including engineers and architects, real estate workers and contractors operating in the construction sector, and faculty members working in related faculties. In the research, inferential analyses were obtained with T and Anova Tests, and the barriers in selecting sustainable materials were tested by factor analysis. In the last stage, all criteria' Index of Relative Importance (IRI) was determined. This research is vital in ranking the requirements for sustainable material selection in Türkiye, identifying the barriers, and selecting the similarities or differences between the criteria choices of participants with different demographic characteristics. Unlike previous studies that only focused on criteria selection or barriers, a holistic approach was used by including the participants' demographic characteristics. It also aims to fill the gap in the literature by conducting research with participants in Türkiye.

Within the scope of the study's design, the relationship between sustainable architectural design and sustainable materials is examined in section 2, and previous studies in the literature are reviewed. In section 3, the study materials and methods are presented, the findings are evaluated, and the results are discussed in section 4. Considering that sustainability is closely related to the local, the study is critical primarily because it was conducted in Türkiye. On the other hand, unlike the literature, the study analyzed the participants' views according to their demographic characteristics and created a model for the barriers to using sustainable materials. In these respects, the study will make a significant contribution to the literature, and the results of the study will be a guide for efforts to make the construction sector more sustainable.

2. THEORETICAL FRAMEWORK AND STUDIES IN THE LITERATURE

As hybrid and electric cars are changing the automobile industry, sustainable architecture is changing the construction industry [21]. According to Bourdeau (1999), the main characteristics of a sustainable architectural product are meeting human health and comfort at the highest level, aiming to improve the quality of human life, being energy and resource-efficient, protecting biodiversity, minimizing waste production, longevity, and using recycled and recyclable materials [22]. Sustainable housing offers many benefits, such as improving quality of life and property value, ensuring affordability, fostering human development, reducing natural disaster risks, and encouraging sustainable urban growth [23]. In the framework developed by Kim and Rigdon (1998) as a guideline for sustainable design, three basic principles of "Economy of Resources, Life Cycle Design, and Humane Design" and strategies and methods related to these principles have been developed. The relationship between sustainability and building materials has been examined through these principles (Table 1) [24].

Table 1. Sustainable design framework [24]

Principles		
Economy of resources	Life cycle design	Humane design
Strategies		
Energy conservation	Prebuilding phase	Preservation of natural conditions
Water conservation	Building phase	Urban design / Site planning
Material conservation	Post building phase	Design for human comfort
Methods		

2.1. The Principle of the Economy of Resources

Covering only 2% of the world's landmass, cities consume 75% of resources, producing greenhouse gas clouds and billions of tons of solid and toxic waste. For example, 125 times the area of London is required to re-supply the resources consumed [25]. The principle of resource conservation, which was developed in response to this excessive human consumption, aims to reduce the use of non-renewable resources and ensure their conservation throughout the life cycles of buildings consisting of design, construction, construction, and demolition. The objectives of sustainable building design include reducing resource inputs, recycling resource outputs, and reducing environmental pollution through effective waste management [26].

The principle of resource conservation consists of methods related to energy, water, and material conservation strategies [24]. The energy conservation strategy aims to use more renewable energy throughout the building life cycle [27]. When the relationship between energy conservation and building materials is examined, it is seen that both the energy consumed during the production, transportation, and transformation of building materials and the contribution of materials to energy saving during the use of the building should be addressed. Energy is inevitably used to process all building materials [28]. There is a vast difference between the energy used to build a house made of locally available material, such as adobe or rammed earth, and the energy used to create a steel construction house. In sustainable design, it is essential to use materials that require less energy to produce and transport [29]. Within the framework of energy conservation, Kim and Rigdon (1998) recommend the use of materials with low embodied energy; the selection of materials that require little energy for their production, transportation, maintenance, and repair and are obtained from local sources; attention to insulation materials used to reduce heat gains and losses; and the use of energy-saving materials in systems such as heating, cooling, air conditioning, and lighting [24].

In addition to the increase in world population, per capita water use, industrial and production activities, and urbanization, the decrease in precipitation and change in precipitation regimes due to climate change put the world's freshwater resources under tremendous pressure [30]. For example, Türkiye's water per capita has decreased from 4,000 m^3 to 1,500 m^3 in the last 20 years. Türkiye's population is expected to reach 100 million in 2030. With the decrease in precipitation, Türkiye is expected to approach the category of water-poor countries with a per capita water amount of 1100 m^3 [31]. The water conservation strategy aims to reduce the amount of water buildings use throughout their life cycle. Just like in energy, there is also embedded water for building materials. It is possible to define embodied water as water consumed during the cultivation and extraction of raw materials for building materials, manufacturing and transportation of products, and construction. Research shows that most of this water (92%) is consumed for material production [32]. For 1 m^3 of concrete, the embedded water reaches 11 tons; for 1 m^2 of glass with a thickness of 4 mm, 3.4 tons; and for 1 m^3 of timber, 20.1 tons [33]. These figures indicate the importance of water conservation in selecting building materials.

Material conservation is crucial to ensure that the design meets sustainability criteria. It is vital for sustainability that building materials are durable, easy to maintain and maintain, recycled, and recyclable [34]. According to Stahel (1990), materials should be recyclable, reusable, locally sourced, produced outside extensive centralized facilities, and positively impact user health and comfort level [29]. They prefer materials that have a long lifetime and are easy to maintain, resulting in less need for renovation. In this way, problems such as the embedded energy and water required to produce the new material, carbon dioxide emissions during manufacturing, local environmental impact due to raw material extraction, and pollution during the transportation and processing of the material are avoided [28].

2.2. The Principle of Life Cycle Design

The principle of life cycle design is based on the transformation of resources from one form in which they are helpful to another in which they can be useful so that their useful life continues without ever ending. Materials are considered one of the most critical inputs to the life cycle process. All stakeholders, from owners to designers, contractors to users, should seek assurance that the materials used in buildings are the best materials for the environment on a "cradle to grave" basis. Under ideal conditions, it is part of the process that buildings are built with materials from recycling other buildings and are recyclable. However, it is naturally impossible to design an utterly closed building life cycle that eliminates the need for new materials. However, adhering to life cycle principles means reducing the consumption of energy, water, and resources required to produce new materials and reducing the production of solid waste and harmful emissions. The life cycle design principle

comprises pre-building, building, and post-building phases [24]. The building design is realized in the pre-building phase, and the selected materials are evaluated regarding their environmental impact. In this phase, the raw materials should consist of renewable resources, environmentally harmless materials with low embodied energy and water, and long-lasting and durable materials requiring less replacement and maintenance. The building phase is concerned with the environmental, social, and economic impacts that arise during the transformation of materials into manufacturing using labor. This phase aims to establish a waste management system that includes collecting and recycling material waste. Care is also taken to ensure that building materials and materials used during manufacturing, such as adhesives and binders, do not contain toxins that could harm the health of construction workers and users. In the post-building phase, the aim is to recycle materials after the end of the useful life of the building, thus reducing the use of new natural resources and energy.

2.3. The Principle of Humane Design

The first two principles prioritize efficiency and conservation, while the design principle for people encompasses the entire ecosystem, including individuals, plants, and wildlife [24]. Research indicates that the quality of the environment influences people's health, well-being, economic prosperity, and lifestyle [35]. Making sustainability viable involves aligning it with people's needs and cultural values [36]. The strategies within this principle involve conserving natural environments, urban design, and designing for human comfort [24]. Sustainable selection of building materials can help preserve the natural ecosystem and protect vulnerable areas [37]. Designing buildings in harmony with their environment, considering topography, climatic data, and natural and artificial elements aids in selecting materials correctly, prolonging their service life, using them effectively, and avoiding unnecessary labor and costs [38]. Urban design and land planning strategies involve transitioning from building to city scale, requiring materials that respect local characteristics [24]. The design strategy for human comfort focuses on interior spaces, where people spend 70% of their lives selecting materials to enhance thermal, visual, and auditory comfort. Proper thermal insulation materials reduce mechanical heating and cooling systems, while utilizing natural light reduces the need for additional lighting, promoting healthy biorhythms [39]. Additionally, materials used in door, window, and wall systems play a crucial role in providing auditory comfort by mitigating noise.

2.4. Studies in the Literature

Studies in the literature reveal that more importance should be given to selecting sustainable materials. A study conducted in Türkiye concluded that using sustainable materials and building elements is insufficient even in LEED-certified projects [40]. Therefore, it seems appropriate to investigate the crucial factors in using sustainable materials and their barriers. There are a limited number of studies on this issue in the literature. Akadiri (2015) examined the main barriers to selecting sustainable building materials in Nigeria. A survey conducted among professionals in the construction sector showed that the most critical barriers to selecting sustainable materials are the perception of extra cost and the need for knowledge of sustainable materials [41]. Kuppusamy et al. [42] concluded that the main barriers to using green building materials in Malaysia are high cost, lack of awareness, and lack of rules and regulations. The solutions are reducing the cost of green building materials and organizing education and training campaigns. In a similar study, Mohsin and Ellk (2018) found problems between designers' environmental awareness in building construction and realistic implementation due to administrative and technical reasons [43]. Dinh et al. [44] identified 11 obstacles to integrating sustainability criteria into material selection in Vietnam, one of the developing country examples. They concluded that four are of "high" importance. Mewomo et al. [45] evaluated sustainable building materials through 25 barriers they created. In the study, lack of awareness and knowledge, lack of local authority and government involvement, insufficient funding for research and development and education and training, lack of understanding of the net benefit, lack of qualified personnel or practitioners, and lack of building codes and regulations on innovation were considered as the most critical barriers. In their study, Gounder et al. [46] aimed to identify the main barriers to using sustainable materials in Australia. Using the relative importance index, exploratory factor analysis, and multinomial logistic regression analysis as research methods, the study reveals that the critical barriers to the use of sustainable materials are related to cost and profit considerations, the reluctance of key stakeholders to include these materials in construction projects, lack of incentives and government policies. In another study conducted in Nigeria, Eze et al. [47] identified resistance and information barriers, regulation and financing challenges in research and development, cost and market hurdles, insufficient government incentives, limited supplier availability, and barriers to expertise and labor as the primary obstacles hindering the adoption of sustainable materials.

Danso (2018), in his study on the determination of sustainability criteria, determined criteria by evaluating building materials based on their economic, social, and environmental sustainability [48]. Dinh et al. [44] ranked 18 criteria according to their importance. As a result of the research, it was concluded that the most crucial criterion is material price. Al-Atesh et al. [49] evaluated the criteria for sustainable building materials. Within the scope of the study, 29 criteria were ranked according to their importance with AHP. As a result of the research, it was concluded that environmental and economic criteria are more important than social criteria. When previous academic studies are evaluated, there has yet to be a consensus on the criteria for sustainable building materials selection and the barriers in this regard. It is seen that the barriers to the selection of sustainable materials vary from country to country and can also differ according to the opinions of the participants. In all these respects, there is a need for much more studies on the subject, especially on a national scale.

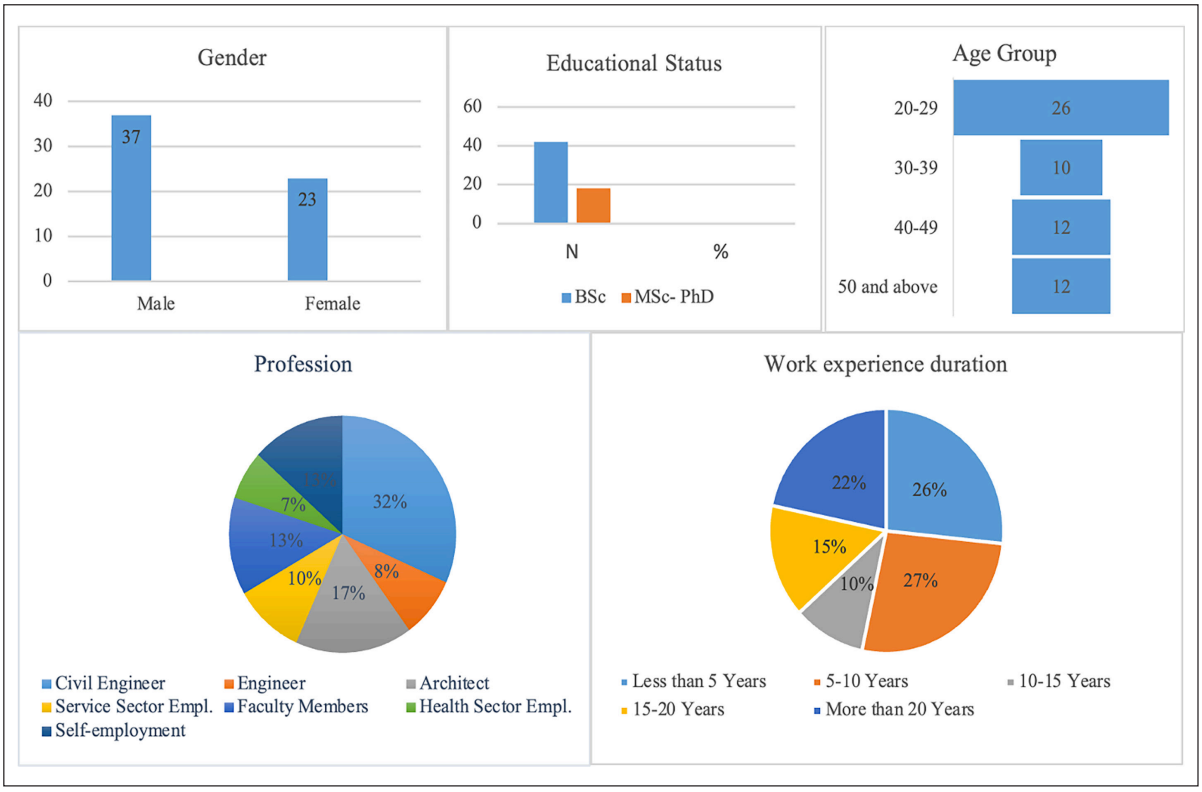

Figure 1. Demographic features of the participants.

3. MATERIAL AND METHODS

Dinh et al. [44] examined sustainable material selection and barriers to sustainable material use in Vietnam. In the study, it was seen that the criteria were determined based on a comprehensive literature study and existing criteria related to sustainability. Since Vietnam is a developing country, Vietnam has economic characteristics similar to Türkiye, so the scale used by Dinh et al. [44] was utilized in this study. Participants were asked to evaluate the importance levels of 17 criteria under the headings of environmental, social, and economic sustainability in terms of sustainability of building materials and the importance levels of 11 barriers to using sustainable materials. The evaluations used a 5-point Likert scale (1- Not important, 2- Slightly important, 3- Average important, 4- Very important, and 5- Very important). The survey was conducted with 60 participants with different demographic characteristics, and the collected data were analyzed using SPSS 29.0 (Statistical Package for Social Sciences) (SPSS, 2023). Descriptive analyses were made about the scales according to the characteristics of the participants. In the study, the reliability of the scales was also tested, and inferential analyses were made with independent sample T-Tests andT-testsTests after checking the normality of the data. The Index of Relative Importance (IRI) of all criteria was determined. In the last stage, to better understand the barriers to sustainable material selection, factor analysis was performed, factor weights were determined, and a model was created.

4. RESULTS

4.1. Demographic Findings

Demographic findings of the participants were obtained through descriptive analysis. Descriptive analysis expresses and summarizes a data set in quantitative numerical values or counting or ranking values in quantitative or graphic form [50]. Demographic findings of the participants are given in Figure 1. Accordingly, 62% of the participants were male. All the participants, who were predominantly (43%) between the ages of 20 and 29, were selected from those with a university education level or higher, as it was thought that they could better evaluate the issue of sustainability. In terms of work experience, more than half of the respondents have 0–10 years of experience, while 22% have more than 20 years of experience. When engineers and architects, real estate sector employees and contractors included in the service sector employees and self-employed, and faculty members working in related faculties are evaluated together, it is possible to say that almost all the participants are related to the construction sector.

4.2. Descriptive Statistics and Reliability Analysis Results of the Scales Used

The results of descriptive statistics and reliability coefficients of the scales used in the research are given in Table 2. The questions were 3.65, 3.86, 3.90, and 3.65 for economic, environmental, and social criteria and barriers to sustainable material use, respectively. As can be seen in the table, the reliability values of the scales were above the 0.5 limit

Table 2. Descriptive statistics and reliability values of the scales

Variable	N	Item number	Item mean	Item min.	Item max.	C. Alpha
Economic criteria	60	5	3.653	3.067	4.100	0.649
Environmental criteria	60	8	3.867	3.483	4.300	0.813
Social criteria	60	6	3.904	3.317	4.367	0.552
Barriers	60	11	3.652	3.100	4.033	0.789

Table 3. Mean and standard deviation values of the criteria

No	Criteria	N	Mean	SD
Ec1	Material price	60	4.1000	0.72952
Ec2	Material handling cost	60	3.7667	0.87074
Ec3	Cost during the construction phase	60	3.6000	1.21013
Ec4	Cost in operation and maintenance phase	60	3.7333	1.05552
Ec5	Cost further ing demolition phase	60	3.0667	1.19131
Econmean		60	3.6533	0.65062
En1	Energy consumption	60	3.6667	1.14487
En2	Water consumption	60	3.4833	1.15702
En3	Global warming	60	3.6500	1.20486
En4	Waste production management	60	3.8667	1.06511
En5	Toxic emissions	60	4.3000	0.94421
En6	Depletion of natural resources	60	4.0667	0.95432
En7	Acidification of soil and water	60	4.1167	0.99305
En8	Potential for recycling and reuse	60	3.7833	1.13633
Envmean		60	3.8667	0.70481
Sc1	Safety in construction and operation	60	4.3167	0.79173
Sc2	The health of workers and citizens	60	4.3667	0.78041
Sc3	LabLaborailability	60	3.6167	0.99305
Sc4	Aesthetics	60	3.3167	1.29525
Socialmean		60	3.9042	0.63127

SD: Standard deviation.

value suggested by Cronbach and Helmstater, indicating that the scales were reliable [51, 52]. While the reliability values are pretty high for environmental criteria, they are relatively low for social criteria.

The average scores of the criteria are presented in Table 3. Among the economic criteria, the criterion of the initial price of the material explained in the questionnaire as "The price that the contractor orders from the suppliers" has reached the highest average score, and the cost during the demolition phase has reached the lowest average score. Among the environmental criteria, the toxic emission criterion, "emission of poisons into the environment during the use of construction material," has the highest average, and water consumption has the lowest average. Among the social criteria, "Health of workers and citizens" and "aesthetics" received the highest and lowest average scores, respectively.

The average scores of the criteria related to the barriers to the use of sustainable materials are presented in Table 4. Among this criterion, "Risks of higher initial cost, total cost and extra time" has the highest mean score and "Refusal to change traditional criteria in material selection and construction methods" has the lowest mean score.

4.3. Inferential Analyses

Inferential analyses were conducted to determine whether participant evaluations changed according to demographic characteristics. For this purpose, it was first checked whether the data were usually distributed to decide whether parametric or nonparametric tests would be applied in inferential analyses. Different methods can be used to determine this. The most used of these methods is to check the Skewness and Kurtosis values of the data. The skewness and kurtosis values in Table 5 vary between –0.922 and 0.244. Hair et al. [53] reported that the data are considered customarily distributed if the skewness and kurtosis values are between +1 and –1. Therefore, it was accepted that the data were normally distributed for all four criteria, and inferential analyses with parametric tests were conducted.

Inferential statistics are statistics that obtain analytic expressions for estimation or hypothesis testing about the character of the statistical main population [54]. Inferential analysis tests compare the means of two or more groups and decide whether the difference between means is random or statistically significant. Since the data were normally distributed, the independent sample T-test was used for

Table 4. Mean and standard deviation values of barriers to sustainable material use

No	Criteria	N	Mean	SD
BAR1	Lack of database on environmental and social impacts of the material	60	3.8000	1.0051
BAR2	Limited availability of sustainable materials in the construction sector	60	3.7167	0.9223
BAR3	Lack of education, awareness, and knowledge of sustainable materials	60	3.8167	0.8335
BAR4	Lack of cost-effective software or toolkits for material selection	60	3.5167	1.0655
BAR5	Stakeholders focus only on economic criteria	60	3.9667	0.9382
BAR6	Lack of government support	60	3.4833	1.4081
BAR7	Lack of customer demand and awareness	60	3.8333	1.1956
BAR8	Lack of sustainable construction culture	60	3.5833	1.1541
BAR9	Refusal to change traditional criteria in the selection of materials and construction methods	60	3.1000	1.2171
BAR10	The evaluation process is too complex	60	3.3167	1.0655
BAR11	Higher initial cost, total cost, and extra time risks	60	4.0333	1.0571
Barmean		60	3.6515	0.6137

SD: Standard deviation.

cases with two groups in inferential analyses, and the Anova test was used for cases with more than two groups. The test results for the cases where the difference between the participants' opinions is significant are as follows:

The independent sample T-test was used to investigate whether there was a significant difference between the participants' opinions according to their gender. As a result of the test, a significant difference was found only for environmental criteria (Table 6). In this test, Levene's test sig (p) value greater than 0.05 indicates no difference between the groups, in which case the value in the first row is considered. The sig. The value in the first row is 0.035, meaning the difference is significant ($p<0.05$). For environmental criteria, men's average was 3.7, while women's average was 4.1.

The analysis, according to the age groups of the participants, was carried out using the ANOVA test. As a result of the test, the sig (p) value was less than 0.05, i.e., significant, for the economic, environmental, and sustainable material selection barriers criteria (Table 7). The averages of the participants according to age groups are presented in Table 8. Accordingly, the lowest mean for economic criteria was 3.31 for the age group above 50 years, and the highest mean was 3.88 for the age group 20–29 years. For environmental criteria, the lowest mean was 3.13 for those over 50, and the highest was 4.27 for the 20–29 age group. For the barriers to using sustainable materials, the lowest average was realized for those over 50 and the highest for the 30–39 age group.

The independent sample T-test was used to investigate whether there was a significant difference between the participants' opinions according to their education level. As a result of the test, a significant difference was found only for economic criteria and barriers to using sustainable materials (Table 9). For both criteria groups, the averages of those with master's and doctorate level education were higher than those with university degrees. The averages were 3.50 and 4.01 for economic criteria and 3.48 4.04 for barriers.

Table 5. Mean, kurtosis, and skewness values of the scales

	Statistic	SE
Economic mean		
Mean	3.8667	0.091
Skewness	-0.362	0.309
Kurtosis	-0.524	0.608
Environmentalmean		
Mean	3.8925	0.098
Skewness	-0.922	0.337
Kurtosis	0.393	0.662
Socialmean		
Mean	3.9042	0.08150
Skewness	-0.537	0.309
Kurtosis	0.244	0.608
Barriermean		
Mean	3.6515	0.079
Skewness	-0.117	0.309
Kurtosis	-0.705	0.608

SE: Standard error.

Table 6. T-test results according to the gender of the participants

	Levene's Test for equality of var.		T-test for equality of means		
	F	Sig.	t	df	Sig. (2-tailed)
Envmean					
Equal var. as.	1.809	0.184	-2.161	58	0.035
Equal var. not as.			-2.319	56.193	0.024

df: Degrees of freedom.

Table 7. Anova test results according to age groups of participants

	Sum of squares	df	Mean square	F	Sig.
Econmean					
Between groups	3.498	3	1.166	2.893	0.043
Within groups	22.571	56	0.403		
Total	26.069	59			
Envmean					
Between groups	10.896	3	3.632	11.047	0.000
Within groups	18.412	56	0.329		
Total	29.308	59			
Barmean					
Between groups	3.878	3	1.293	3.947	0.013
Within groups	18.340	56	0.328		
Total	22.218	59			

df: Degrees of freedom.

Table 8. Mean criteria scores of participants according to age groups

Criteria	Age group	N	Mean	SD
Econmean	20–29	26	3.8846	0.70011
	30–39	10	3.7400	0.55817
	40–49	12	3.4167	0.64079
	>50	12	3.3167	0.52194
	Total	60	3.6533	0.66472
Envmean	20–29	26	4.2740	0.50747
	30–39	10	3.8125	0.74594
	40–49	12	3.7604	0.51802
	>50	12	3.1354	0.60410
	Total	60	3.8667	0.70481
Barmean	20–29	26	3.8217	0.56538
	30–39	10	3.9273	0.44906
	40–49	12	3.4470	0.65608
	>50	12	3.2576	0.58767
	Total	60	3.6515	0.61365

SD: Standard deviation

Inferential analyses of the participants, according to the duration of work experience, were conducted using the ANOVA test. As a result of the research, a significant difference was found for economic and environmental criteria ($p<0.05$) (Table 10). Looking at the averages, the average of the group with 16–20 years of experience (3.11) was found to be the lowest, and the average of the group with 6–10 years of experience (3.90) was found to be the highest for economic criteria (Table 11).

Anova test was used to analyze whether the differences in the participants' opinions according to their professions were significant [55]. The test showed that the result was significant for economic criteria (Table 12). When the averages of the groups were analyzed, it was seen that the lowest average was found for engineers (3.28), and the highest average was found for faculty members (4.13). When the inferential analyses are analyzed in general, it is seen that there are differences in the opinions in general for economic criteria and, in some cases, for environmental criteria and barriers. For social criteria, there is a consensus.

4.4. Criteria to be Considered in the Selection of Sustainable Building Materials

As a result of inferential analyses, it was determined that the results, especially the economic criteria, differed signifi-

Table 9. T-test results according to the education level of the participants

	Levene's Test for equality of var.		T-test for equality of means		
	F	Sig.	t	df	Sig. (2-tailed)
Econmean					
Equal var. as.	0.550	0.461	-2.895	58	0.005
Equal var. not as.			-3.034	35.976	0.004
Barmean					
Equal var. as.	1.068	0.306	-3.563	58	0.001
Equal var. not as.			-3.793	37.371	0.001

df: Degrees of freedom.

Table 10. Anova test results according to participants' duration of work experience

	Sum of squares	df	Mean square	F	Sig.
Econmean					
Between groups	5.453	4	1.363	3.637	0.011
Within groups	20.617	55	0.375		
Total	26.069	59			
Envmean					
Between groups	7.474	4	1.868	4.706	0.002
Within groups	21.835	55	0.397		
Total	29.308	59			

df: Degrees of freedom.

cantly according to the demographic characteristics of the participants. In this case, the results can't be generalized. However, to obtain a general view, the relative importance indexes of the criteria were determined according to the formula below. Table 13 presents the relative importance of economic, environmental, and social criteria. Accordingly, the criterion with the highest relative importance is "S2 - Health of workers and citizens," and the barrier with the highest relative importance is "BAR11 - Higher initial cost, total cost, and extra time risks".

$$IRI = \Sigma W/A * N \quad (1)$$

IRI: Index of Relative Importance

W: The weights given by each participant for that proposition are 1- Not important, 2- Somewhat important, 3- Average important, 4- Very important, and 5- Very important.

A: The highest weight value. In this case, it is 5.

N: Total number of participants (60)

The relative importance indexes of the criteria to be considered in selecting sustainable building materials and their ranking accordingly are presented in Table 13. The top three criteria were the health of workers and citizens, safety in construction and operation, and toxic emissions. At the same time, water consumption, aesthetics, and cost during the demolition phase were the bottom three criteria.

The ranking of the barriers to using sustainable building materials according to their relative importance indexes is given in Table 14. The criterion "Risks of higher initial cost, total cost and extra time" has the highest relative importance, and "Refusal to change traditional criteria in material selection and construction methods" has the lowest relative importance.

4.5. Factor Analysis

In the last stage of the study, factor analysis was conducted to determine the barriers to using sustainable building materials. Factor analysis is the general name of a group of multivariate analysis techniques that aim to reduce many variables that are thought to be related to each other to a smaller number of basic dimensions to orotate the understanding and interpretation of these relationships [56].

In factor analysis, the first step is to examine the suitability of the data for factor analysis, that is, to check the factorability of the items. The most well-known method for this is to conduct sample suitability tests. The tests for the suitability of factor analysis are Bartlett's test of sphericity and Kaiser-Methe yer-Olkin (KMO) test. The results of the

Table 11. Averages of the participants according to the duration of their work experience

Criteria	N	Mean	SD
Econmean			
≤5	16	3.8625	0.75089
6–10	16	3.9000	0.61536
11–15	6	3.8333	0.46332
16–20	9	3.1111	0.44845
>20	13	3.3846	0.56250
Total	60	3.6533	0.66472
Envmean			
≤5	16	4.2813	0.56734
6–10	16	4.0391	0.52185
11–15	6	3.8333	0.83915
16–20	9	3.6111	0.51707
>20	13	3.3365	0.77793
Total	60	3.8667	0.70481

SD: Standard deviation.

Table 12. Anova test results according to participants' professions

	Sum of squares	df	Mean square	F	Sig.
Econmean					
Between groups	5.685	6	0.948	2.464	0.036
Within groups	20.384	53	0.385		
Total	26.069	59			

df: Degrees of freedom.

Table 13. Ranking of sustainable building material selection criteria according to their IRI

No	Criteria	IRI
Sc2	The health of workers and citizens	0.873
Sc1	Safety in construction and operation	0.863
Env5	Toxic emissions	0.860
Env7	Acidification of soil and water	0.823
Ec1	Material price	0.820
Env6	Depletion of natural resources	0.813
	Social	0.781
Env4	Waste production management	0.773
	Environmental	0.773
Env8	Potential for recycling and reuse	0.757
Ec2	Material handling cost	0.753
Ec4	Cost in operation and maintenance phase	0.747
Env1	Energy consumption	0.733
	Economic	0.731
Env3	Global warming	0.730
Sc3	Labor availability	0.723
Ec3	Cost during the construction phase	0.720
Env2	Water consumption	0.697
Sc4	Aesthetics	0.663
Ec5	Cost during the demolition phase	0.613

IRI: Index of Relative Importance.

sample suitability tests are given.MO that is used to test the suitability of the sample size in factor a. The KMO value must be higher than 0.50 to proceed with factor analysis. In this test, the KMO value was found to be 0.590. Bartlett's test tests the null hypothesis that "the original correlation matrix is the same as the identity matrix (all correlation coefficients are zero)" [56]. The Table 15 shows that this test is significant, meaning that it is suitable for factor analysis.

According to the commonalities table, each variable (item) has a common variance between 0 and 1. While items with commonalities above 0.50 explain more of the variance, items with commonalities lower than 0.50 may lead to more complex factors to interpret, or these items need to be eliminated. In Table 16, only one item with a commonality below 0.5 was identified (BAR4–0.484). Still, since the value was close to 0.5, it was decided to include all items in the analysis.

A good factor analysis is expected to explain the highest variance with the least number of factors. An analysis that explains 50–75% of the total variance is considered a good result in factor analysis. The table below shows the eigenvalues before and after factor extraction and after rotation (Table 17). These values roughly indicate the correlation between two variables. Also, there are four factors with eigenvalues greater than 1; the first factor explains 32% of the variance. The relative importance of the factors is equalized by rotation. The four factors explain 74% of the total variance (Table 17).

Interpreting factor loadings without rotation presents challenges. Rotating the matrix aids in achieving a more interpretable factor structure and optimizes the items in terms of explained variance post-rotation. Upon examination of the factor loading matrix rotated using the Varimax method, no instance was observed where an item exhibited strong loadings from multiple factors. In such cases, a minimum load difference of 0.1 is preferred, and items explaining multiple factors are systematically removed from the scale, one item at a time, with the matrix reassessed accordingly. However, such a scenario did not occur in this instance (Table 18).

An essential stage of factor analysis is naming the factors. Factors are named by examining the variables loading on the factors and determining the common point between the variables. In naming, care is taken to give the name that best expresses the meaning the variables loading on the factor want to emphasize. By naming the factors, the model shown in Figure 2 was obtained.

5. DISCUSSION

The research was conducted with 60 participants with different demographic characteristics. The participants were asked to evaluate the importance of 17 criteria under the headings of economic, environmental, and social sustainability in terms of sustainability of building materials. Participants also reported how important they found the barriers to using sustainable materials. Inferential analyses showed that participant opinions differed according to different demographic characteristics. This differenti-

Table 14. Ranking of the barriers to the use of sustainable building materials according to their IRI

No	Criteria	IRI
BAR11	Higher initial cost, total cost, and extra time risks	0.807
BAR5	Stakeholders focus only on economic criteria	0.793
BAR7	Lack of customer demand and awareness	0.767
BAR3	Lack of education, awareness, and knowledge of sustainable materials	0.763
BAR1	Lack of database on environmental and social impacts of the material	0.760
BAR2	Limited availability of sustainable materials in the construction sector	0.743
BAR8	Lack of sustainable construction culture	0.717
BAR4	Lack of cost-effective software or toolkits for material selection	0.703
BAR6	Lack of government support	0.697
BAR10	The evaluation process is too complex	0.663
BAR9	Refusal to change traditional criteria in the selection of materials and construction methods	0.620

Table 15. KMO and Bartlett tests' results

Kaiser-Meyer-Olkin measure of sampling adequacy.	0.590
Bartlett's test of sphericity	
Approx. Chi-Square	270.539
df	55
Sig.	0.000

KMO: Kaiser-Methe yer-Olkin; df: Degrees of freedom.

ation was most pronounced for economic criteria, whereas no significant differences emerged for social criteria. It was observed that female respondents attributed greater importance to environmental criteria than male respondents. Another result is that as the age of the participants increases, the level of importance they attribute to the criteria decreases. The most significant difference emerged for environmental criteria, with the average for the 20–29 age group being well above very important (4.27).

Table 16. Communalities

Criteria	Extraction
BAR1	0.815
BAR2	0.759
BAR3	0.773
BAR4	0.484
BAR5	0.782
BAR6	0.852
BAR7	0.815
BAR8	0.775
BAR9	0.575
BAR10	0.730
BAR11	0.719

Extraction Method: Principal Component Analysis.

Table 17. Total variance explained

Comp.	Initial eigenvalues			Extraction sums of Sq. loadings			Rotation sums of Sq. loadings		
	Total	% of var.	cum. %	Total	% of var.	cum. %	Total	% of var.	cum. %
1	3.734	33.949	33.949	3.734	33.949	33.949	2.623	23.845	23.845
2	1.745	15.861	49.809	1.745	15.861	49.809	2.072	18.838	42.683
3	1.526	13.877	63.686	1.526	13.877	63.686	1.860	16.910	59.594
4	1.076	9.781	73.467	1.076	9.781	73.467	1.526	13.873	73.467
5	0.700	6.364	79.831						
6	0.676	6.147	85.978						
7	0.579	5.265	91.243						
8	0.333	3.028	94.270						
9	0.299	2.715	96.985						
10	0.225	2.049	99.034						
11	0.106	0.966	100.000						

Extraction Method: Principal Component Analysis.

Table 18. Rotated factor loadings matrix

		Component			
		1	2	3	4
BAR1	Lack of database on environmental and social impacts of the material	0.288	-0.105	0.809	0.258
BAR2	Limited availability of sustainable materials in the construction sector	0.061	0.763	0.390	0.147
BAR3	Lack of education, awareness, and knowledge on sustainable materials	0.387	0.389	0.166	0.667
BAR4	Lack of cost-effective software or toolkits for material selection	0.610	0.164	0.255	0.141
BAR5	Stakeholders focus only on economic criteria	0.053	-0.082	-0.008	0.879
BAR6	Lack of government support	0.387	0.642	-0.380	0.383
BAR7	Lack of customer demand and awareness	0.864	-0.107	-0.214	0.107
BAR8	Lack of sustainable construction culture	0.862	0.086	0.118	0.109
BAR9	Refusal to change traditional criteria in the selection of materials and construction methods	0.610	0.315	0.321	0.028
BAR10	The evaluation process is too complex	0.048	0.846	0.006	-0.113
BAR11	Higher initial and total cost and risk of extra time	0.004	0.222	0.809	-0.127

Extraction Method: Principal Component Analysis. Rotation Method: Varimax with Kaiser Normalization. a. Rotation converged in 5 iterations.

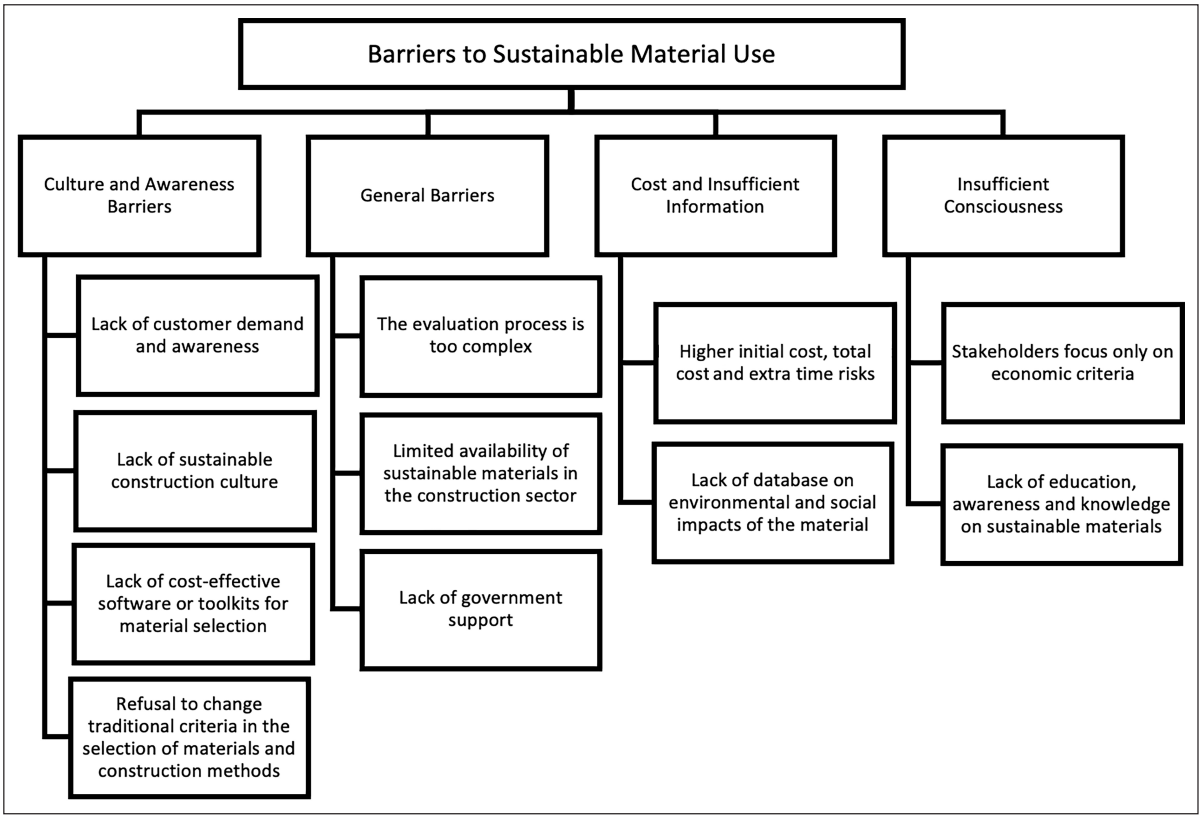

Figure 2. Model of barriers to sustainable material use (Source: Created by the authors).

In comparison, it was almost only necessary (3.14) for the over-50 age group. Since work experience is directly proportional to age, a similar pattern was observed for work experience. Respondents with a master's degree and higher education attributed greater importance to economic criteria. While there was a significant difference by occupation only for economic criteria, faculty members were the occupational group that attributed the highest importance. This differentiation between the participants' views identified by inferential analysis indicates that it would be helpful to conduct studies with a more significant number of participants.

On the other hand, it is pleasing that young people are more sensitive to sustainability. Nevertheless, conducting cross-sectional studies to see whether participants' views have changed over time would be helpful. There is always the possibility that other challenges participants face over time may have pushed sustainability to the background. The significant differences in participants' opinions on economic criteria, in general, maybe because the financial difficulties experienced by our country in recent years have affected different segments of society at various levels. A general conclusion is that people whose tasks are linked to sustainability should be carefully selected, as they can reflect their views on practice.

Although there were differences of opinion among the participants for some criteria, the relative importance of the criteria was found to get a general idea. The requirements with the highest relative importance were:

- The health of workers and citizens.
- Safety in construction and operation.
- Toxic emissions.

In this respect, the study conducted in Türkiye differs from other studies in the literature. This means that the country's dynamics should re-examine the study's structure. As a result, all three of the top three most important criteria are related to health and safety. This situation in the construction sector is quite alarming. The fact that building materials carry serious health risks increases the importance of this awareness. The following factors are considered influential in prioritizing criteria in this manner:

- With industrialization, the number of occupational accidents and diseases has increased significantly, and protecting workers' health and safety has been one of the most critical problems of working life since then. Occupational accidents affect the health and safety of everyone in the construction industry, including designers, architects, structural engineers, and construction site workers [57]. The construction sector ranks first in terms of the frequency of accidents causing death and permanent incapacity for work in Türkiye [58].
- The construction sector faces numerous risk factors that contribute to accidents. These include outdoor work under varying weather conditions, high turnover rates, work conducted at different elevations, constant movement of workers and materials, and a dispersed workforce with varying education levels [59]. These

factors, often intertwined with material selection, influence safety measures. For instance, opting for prefabricated materials reduces time spent at heights, while choosing easier-to-assemble materials minimizes on-site labor requirements.

- The link between occupational diseases and construction materials is significant, surpassing that of occupational accidents. Various materials used in construction, including cement, adhesives, wood and plaster dust, solvent and glue vapors, asbestos, heavy metals, and welding fumes, pose health risks to workers and users of completed structures. Exposure to these substances can result in severe conditions such as cancer, silicosis, asbestosis, skin allergies, bronchitis, nervous system disorders, and lead poisoning [60].

The last three ranked criteria were water consumption, aesthetics, and cost of demolition, with relative importance levels below 0.7. The conclusions reached regarding these are provided below:

- Water is one of the world's most precious natural resources. In Türkiye, projections indicate that per capita water availability may classify the country as water-poor [31]. Climate change simulations further forecast a rise in temperatures by up to 5 degrees Celsius nationwide, accompanied by a precipitation decline of up to 30% in the southern and western regions [61]. Given these forecasts, addressing water consumption is deemed crucial, necessitating heightened awareness and emphasis on conservation efforts
- Architectural beauty is more than just a visual delight. It's defined as "the harmony of everything and a certain harmony between all the elements of the building so that no part can be added, removed or changed without damaging the design" or "an impressive photograph of any relationship between lines, colors, and volumes" [62]. In this respect, aesthetics, like water consumption, is a criterion that should be given higher importance, as it's the architects' and urban planners' role to create functional, visually appealing, and harmonious structures.
- Demolition costs encompass various factors. However, compared to construction costs, demolition expenses are relatively low. Hence, it's common practice to assign minimal importance to demolition costs as a criterion in decision-making processes.

In ranking the barriers to using sustainable building materials according to the relative importance indexes, the criterion "Higher initial cost, total cost, and extra time risks" has reached the highest relative importance. "Refusal to change traditional criteria in material selection and construction methods" had the lowest relative importance. The results of the study are in line with the literature. In parallel with [41, 42, 46], "cost" factors are among the most critical barriers to the use of sustainable materials. The initial cost of sustainable materials is often higher than conventional ones, but a prevalent misconception is that sustainability always entails significantly higher expenses.

Additionally, uncertainty about future costs and availability can deter stakeholders from adopting sustainable materials. However, in the long term, buildings constructed with sustainable materials are more cost-effective due to the savings they provide. Transition difficulties are cited as barriers to the widespread adoption of sustainable materials. On the other hand, in this study, the participants attributed little importance to rejecting the traditional approach.

In the last stage of the study, the barriers to using sustainable building materials were subjected to factor analysis. Four factors explaining 73.5% of the total variance were identified. The factors were named cultural and awareness barriers, general barriers, cost, insufficient knowledge, and insufficient awareness by paying attention to the common points between the variables. It is evaluated that the model obtained will contribute to the literature in this regard.

6. CONCLUSIONS

While Türkiye's environmental pollution pressure is increasing, the bill resulting from its external dependence on energy is steadily rising. If this trend continues, the country is expected to become one of the water-stressed countries shortly. These three fundamental problems alone point to the need for Türkiye to make significant strides in sustainability. Like the rest of the world, the construction sector is one of the sectors where the need for sustainability is most evident. The first and most crucial step in achieving sustainability in the industry is the sustainable selection and use of materials that significantly affect construction management. The study is expected to make the construction industry sustainable by providing essential data to stakeholders on sustainable material selection and barriers to sustainable material use. It is thought that it would be beneficial to enrich the literature by conducting more extensive research in the future.

ETHICS

There are no ethical issues with the publication of this manuscript.

DATA AVAILABILITY STATEMENT

The authors confirm that the data that supports the findings of this study are available within the article. Raw data that support the finding of this study are available from the corresponding author, upon reasonable request.

CONFLICT OF INTEREST

The authors declare that they have no conflict of interest.

FINANCIAL DISCLOSURE

The authors declared that this study has received no financial support.

USE OF AI FOR WRITING ASSISTANCE

Not declared.

PEER-REVIEW

Externally peer-reviewed.

REFERENCES

[1] Klein Goldewijk, K., Beusen, A., Van Drecht, G., & De Vos, M. (2011). The HYDE 3.1 spatially explicit database of human-induced global land-use change over the past 12,000 years. *Glob Ecol Biogeogr, 20*(1), 73–86. [CrossRef]

[2] Elander, I., Gleeson, B., Lidskog, R., & Low, N. (2002). *Consuming cities—The urban environment in the global economy after the Rio Declaration* (1st ed.). Rutledge.

[3] Hoşkara, E., & Sey, Y. (2009). Ülkesel koşullar bağlamında sürdürülebilir yapım. *İtüderg/a, 7*(1), 50–61.

[4] Yazar, K. H. (2006). *Sürdürülebilir kentsel gelişme çerçevesinde orta ölçekli kentlere dönük kent planlama yöntem önerisi* [Doktora Tezi, Ankara Üniversitesi].

[5] Jian, Z., De-nong, Z., & Yu-kun, Z. (23–26 January, 1999). Opening a new epoch of architecture and culture in the 21st century. *Sub-theme Reports of the 20th UIA Congress: Architecture of the 21st Century*. Beijing, China.

[6] Blowers, A., & Pain, K. (1999). *The unsustainable city. Unruly Cities?* Order/Disorder.

[7] WCED. (1987). *Our common future. World commission on environment and development*. Sustainable Development.

[8] Vyas, S., Ahmed, S., & Parashar, A. (2014). BEE (Bureau of energy efficiency) and Green Buildings. *Int J Res, 1*(3), 23–32.

[9] Dixon, W. (2010). *The impacts of construction and the built environment*. Willmott-Dixon Group.

[10] McLennan, J.F. (2004). *The philosophy of sustainable design: The future of architecture*. Ecotone Publishing.

[11] Ji, Y., & Plainiotis, S. (2006). *Design for Sustainability*. Architecture and Building Press.

[12] Gür, N. V., & Aygün, M. (2008). Mimaride sürdürülebilirlik kapsamında değişken yapı kabukları için bir tasarım destek sistemi. *İtüderg/a, 7*(1), 74–82.

[13] Karslı, H. (2008). *Sürdürülebilir mimarlık çerçevesinde ofis yapılarının değerlendirilmesi ve çevresel performans analizi için bir model önerisi* [Yayımlanmamış Doktora Tezi]. Mimar Sinan Güzel Sanatlar Üniversitesi.

[14] Nassar, K., Thabet, W., & Beliveau, Y. (2003). A procedure for multi-criteria selection of building assemblies. *Autom Constr 12*(5), 543–560. [CrossRef]

[15] Treloar, G., Fay, R., Ilozor, B., & Love, P. (2001). Building materials selection: greenhouse strategies for built facilities. *Fac, 19*(3–4), 139–150. [CrossRef]

[16] Alibaba, H. Z., & Özdeniz, M. B. (2004). A building elements selection system for architects. *Build Environ, 39*(3), 307–316. [CrossRef]

[17] Wang, W., Zmeureanu, R., & Rivard, H. (2005). Applying multi-objective genetic algorithms in green building design optimization. *Build Environ, 40*(11), 1512–1525. [CrossRef]

[18] Van Kesteren, I. E. H. (2008). Product designers' information needs in materials selection. *Mater Design, 29*(1), 133–145. [CrossRef]

[19] González, M. J., & Navarro, J. G. (2006). Assessment of the decrease of CO2 emissions in the construction field through the selection of materials: Practical case study of three houses of low environmental impact. *Build Environ, 41*(7), 902–909. [CrossRef]

[20] Kibert, C. J. (2016). *Sustainable construction: green building design and delivery*. John Wiley & Sons. [CrossRef]

[21] Wang, N., & Adeli, H. (2014). Sustainable building design. *J Civ Eng Manag 20*(1), 1–10. [CrossRef]

[22] Bourdeau, L. (1999). Sustainable development and the future of construction: A comparison of visions from various countries. *Build Res Inf J, 27*(6), 354–366. [CrossRef]

[23] UN-Habitat. (2012). Going green: *A handbook of sustainable housing practice in developing countries*. UN-Habitat Publishing.

[24] Kim, J. J., & Rigdon, B. (1998). *Sustainable architecture module: Introduction to sustainable design*. National Pollution Prevention Center for Higher Education.

[25] Pearce, F. Eco-cities special: Ecopolis now. https://www.newscientist.com/article/mg19025561-600-eco-cities-special-ecopolis-now/.

[26] Özek Karadeniz, Y. (2010). *Geleneksel Afyonkarahisar evlerinin sürdürülebilir mimarlık ilkeleri bağlamında değerlendirilmesi* [Yüksek Lisans Tezi, Mimar Sinan Güzel Sanatlar Üniversitesi].

[27] Yellamraju, V. (2004). *Evaluation and design of double-skin facades for office buildings in hot climates* [Doctoral dissertation, Texas A&M University].

[28] Roaf, S., Fuentes, M., & Thomas, S. (2003). *Ecohouse 2: a design guide*. Architectural Press.

[29] Stahel, H. P. (1990). *Baukunst & Gesundheit*. AT Verlag.

[30] Anderson, J., & Thornback, J. (2012). *A guide to understanding the embodied impacts of construction products*. Construction Products Association.

[31] Bal, E. (2012, February 24). Su Hayattır, Hayatınızı Koruyun. https://web.archive.org/web/20161005163326/http://www.yesiloji.com/yesilhaber/su-hayattir-hayatinizi-koruyun/

[32] Bleby, M. "Embodied water" is the latest challenge for the building industry. https://www.afr.com/property/commercial/construction-s-next-cost-challenge-embodied-water-20230328-p5cvvm.

[33] Fuller, R. J., Crawford, R. H., & Leonard, D. (January, 2009). What is wrong with a big house. *Performative ecologies in the built environment: Sustainable research across disciplines: Proceedings of the 43rd Annual Conference of the Australian and New Zealand Architectural Science Association ANZAScA*. Launceston, Tasmania.

[34] Tönük, S. (2001). *Bina tasarımında ekoloji*. Yıldız Teknik Üniversitesi Basım-Yayın Merkezi.

[35] Toofan, S. (2014). Importance of humane design for sustainable landscape. *Int J Eng Technol, 6*(6), 508–511. [CrossRef]

[36] Oktay B., & Hoşkara, Ş. Ö. (2009). A model for measuring the sustainability level of historic urban quarters. *Eur Plan Stud, 17*(5), 715–739. [CrossRef]

[37] Jones, D. L. (1998). *Architecture and the environment: bioclimatic building design*. Laurence King Publication.

[38] Aktuna, M. (2007). *Geleneksel mimaride binaların sürdürülebilir tasarım kriterleri bağlamında değerlendirilmesi Antalya Kaleiçi evleri örneği* [Yüksek Lisans Tezi, Yıldız Teknik Üniversitesi].

[39] Atabay, B. (2010). *Doğal ve yapay ışığın mekanı anlamlandırma gücü ve bir arada bulunma dinamikleri* [Yüksek Lisans Tezi, İstanbul Teknik Üniversitesi].

[40] Hashi, M. N., & Kasapoğlu, E. (2023). Türkiye'de Leed Belgesi almış büro binalarının sürdürülebilir malzeme ve kaynak kullanımı bağlamında değerlendirilmesi. *Eksen Dokuz Eylül Üniv Mimar Fak Derg, 4*(1), 170–188. [CrossRef]

[41] Akadiri, P. O. (2015). Understanding barriers affecting the selection of sustainable materials in building projects. *J Build Eng, 4*, 86–93. [CrossRef]

[42] Kuppusamy, S., Chew, H. Y., Mari, T. S., & Chai, C. S. (2019). Implementation of green building materials in construction industry in Johor Bahru, Malaysia. *IOP Conf Ser Earth Environ Sci, 268*(1), 012006. [CrossRef]

[43] Mohsin, A. H., & Ellk, D. S. (2018). Identifying barriers to the use of sustainable building materials in building construction. *J Eng Sustain Dev, 22*(2), 107–115. [CrossRef]

[44] Dinh, T. H., Dinh, T. H., & Götze, U. (2020). Integration of sustainability criteria and life cycle sustainability assessment method into construction material selection in developing countries: The case of Vietnam. *Int J Sustain Dev Plan, 15*, 1145–1156. [CrossRef]

[45] Mewomo, M. C., Mogaji, I. J., Iruka, A., & Makanjuola, S. A. (2022). Barriers to the successful adoption of innovative building materials for sustainable construction: A review. *In Construction Industry Development Board Postgraduate Research Conference*. (pp. 103–112). Springer. [CrossRef]

[46] Gounder, S., Hasan, A., Shrestha, A., & Elmualim, A. (2023). Barriers to the use of sustainable materials in Australian building projects. *Eng Constr Archit Manag, 30*(1), 189–209. [CrossRef]

[47] Eze, E. C., Sofolahan, O., & Omoboye, O. G. (2023). Assessment of barriers to the adoption of sustainable building materials (SBM) in the construction industry of a developing country. *Front Eng Built Environ, 3*(3), 153–166. [CrossRef]

[48] Danso, H. (2018). Dimensions and indicators for sustainable construction materials: A review. *Res Dev Mater Sci, 3*(4), 286–294. [CrossRef]

[49] Al-Atesh, E. A., Rahmawati, Y., Zawawi, N. A. W. A., & Utomo, C. (2023). A decision-making model for supporting selection of green building materials. *Int J Constr Manag, 23*(5), 922–933. [CrossRef]

[50] Mann, P. S. (1995). *Introductory statistics*. Wiley. [CrossRef]

[51] Cronbach, L. J. (1951). Coefficient alpha and the internal structure of tests. *Psychometrika, 16*(3), 297–334. [CrossRef]

[52] Helmstadter, G. C. (1964). *Principles of psychological measurement*. Appleton-Century-Crofts.

[53] Hair, J. F., Black, W. C., Babin, B. J., Anderson, R. E., & Tatham, R. (2010). *Multivariate data analysis*. Pearson.

[54] Dodge, Y. (2003). *The Oxford dictionary of statistical terms* (6th ed.). Oxford University Press. [CrossRef]

[55] Hair, J.F., Anderson, R.E., Tatham, R.L., & Black, W.C. (1995). *Multivariate data analysis* (4th ed.). Prentice Hall.

[56] Kline, P. (2014). *An easy guide to factor analysis*. Routledge. [CrossRef]

[57] Gambatese, J. A., Behm, M., & Hinze, J. W. (2005). Viability of designing for construction worker safety. *J Constr Eng Manag, 131*(9), 1029–1036. [CrossRef]

[58] SSK. (n.d.) İstatistik yıllıkları. https://www.sgk.gov.tr/Istatistik/Yillik/fcd5e59b-6af9-4d90-a451-ee7500eb1cb4/

[59] Müngen, U. (2011). İnşaat sektörümüzdeki başlıca iş kazası tipleri. *Türk Müh Haber Derg, 469*(5), 32–39.

[60] Adisesh, A., Rawbone, R., Foxlow, J., & Harris-Roberts, J. Occupational health standards in the construction industry. https://www.researchgate.net/profile/Anil-Adisesh/publication/274700436_Occupational_Health_Standards_in_the_Construction_Industry/links/5aa40fe4aca272d448b8e7ab/Occupational-Health-Standards-in-the-Construction-Industry.pdf

[61] Şen, Ö. L., Bozkurt, D., Göktürk, O. M., Dündar, B., & Altürk, B. Türkiye'de iklim değişikliği ve olası etkileri. https://www.researchgate.net/profile/Bahadir-Altuerk/publication/322099836_Turkiye'de_Iklim_Degisikligi_ve_Olasi_Etkileri/links/5a44e280458515f6b0531a0e/Tuerkiyede-Iklim-Degisikligi-ve-Olasi-Etkileri.pdf

[62] Attia, M. M. (2000). *Aesthetic values in plastic arts*. Dar al-Faker al-Arabi.

J Sustain Const Mater Technol, Vol. 9, Issue. 2, pp. 159–169, June 2024

Journal of Sustainable Construction Materials and Technologies
Web page info: https://jscmt.yildiz.edu.tr
DOI: 10.47481/jscmt.1500907

Journal of Sustainable Construction Materials and Technologies

Research Article

Flexural and cracking behavior of reinforced lightweight self-compacting concrete beams made with LECA aggregate

Ningampalli RAMANJANEYULU*[1,2], M. V. Seshagiri RAO[1], V. Bhaskar DESAI[2]

[1]*Department of Civil Engineering, CVR College of Engineering, Hyderabad, India*
[2]*Department of Civil Engineering, Jawaharlal Nehru Technological University, Anantapur, India*

ARTICLE INFO

Article history
Received: 29 February 2024
Revised: 24 May 2024
Accepted: 05 June 2024

Key words:
Compressive strength, concrete, crack pattern, fly ash, light expanded clay aggregate

ABSTRACT

In the current research, an attempt was made to examine the flexural and cracking behavior of reinforced lightweight self-compacting concrete (LWSCC) beams incorporating light-expanded clay aggregate (LECA) as a partial replacement for natural coarse aggregate (NCA). Mechanical properties such as compressive strength, split tensile strength, and flexural strength were evaluated, alongside fresh properties assessed using flow table, V-funnel, J-ring, and L-box tests. The study examined six beams, including a control mix, with LECA replacements of 5%, 10%, 15%, 20%, and 25%. The results indicate that compressive strength decreased with higher LECA content, from 44.56 MPa in the control mix to 32.73 MPa at 25% LECA. Flexural and split tensile strengths showed similar trends. Crack width increased with LECA content, from 1 mm in the control mix to 2 mm at 25% LECA, while density decreased. Flexural performance analysis revealed reduced ultimate load capacity and increased deflection with higher LECA proportions. The ductility index improved, suggesting enhanced flexibility. This study concludes that LECA can effectively replace NCA in LWSCC, though with a trade-off in strength and cracking behavior.

Cite this article as: Ramanjaneyulu, N., Rao, M. V. S. & Desai, V. B. (2024). Flexural and cracking behavior of reinforced lightweight self-compacting concrete beams made with LECA aggregate. *J Sustain Const Mater Technol*, 9(2), 159–169.

1. INTRODUCTION

Concrete made of lightweight materials weighs less than traditional Concrete. Lightweight Concrete has a unit weight of between 300 and 1900 kg/m^3, compared to 2200 to 2500 kg/m^3 for regular Concrete. Using lighter particles instead of heavier ones is one method for producing lightweight Concrete. The Light Expanded Clay Aggregate (LECA) is used instead of the normal-weight aggregates in the experiment to produce Lightweight self-compacting concrete (LWSCC) using expanded clay aggregate. Expanded clay aggregates have higher compressive strengths than a lot of lightweight aggregates. Structural concrete containing LECA can reduce heating and cooling costs by up to 50% and reinforce steel costs by 20%. Using LECA in self-compacting concrete reduces density and improves flexibility, but challenges include reduced compressive strength and increased cracking, requiring careful balance in mix design. [1–5]. A unique kind of clay that may expand is used to create Light Expanded Clay Aggregate (LECA). The pulverized coal and oil mixture heated the rotary or vertical shaft kiln to about 1200 °C before the clay was blended with an additive to make it bloat. The final product comprises rigid, spherical particles with a honeycomb-like inside and a thick, smooth surface texture. The developed cellular struc-

***Corresponding author.**
*E-mail address: rams.613@gmail.com

ture is held in place as the product cools and is employed as a lightweight aggregate. Lightweight Expanded Clay Aggregate (LECA) uses alternate sources of aggregates, such as LECA in Concrete, which is beneficial in achieving sustainable construction practices [6–8].

The experimental work utilizes LECA instead of normal-weight aggregates. Expanded clay aggregates have more compressive strength than many lightweight aggregates. Structural Concrete containing LECA can reduce heating and cooling costs by up to 50% and reinforcing steel costs by 20% [9–11]. Concrete's strength qualities decreased when LECA alone was used to replace coarse aggregates [12]. Mineral admixtures were employed to boost the strength qualities. The ideal fly ash content is 10% [13]. The importance of utilizing fly ash on higher-strength "lightweight self-compacting concrete" made using "Light Expanded Clay Aggregate."After researching the impacts of silica fume on "lightweight aggregate concrete," [14]. The ten percent silica fume is the ideal substance. [15], The steel fibers included in fractions of 0.0%, 0.50%, and 1.0% improved strength and "unit weight of lightweight concrete" as the steel fiber concentration rose. Lightweight aggregates have been used in place of stable aggregates [16]. The ratio of Lightweight aggregate increased, and Concrete's density and compressive strength dropped. Lightweight concrete boasts a lower weight than traditional concrete, with a unit weight spanning from 300 to 1900 kg/m^3.

The construction industry is expanding quickly worldwide, intending to build structures more efficiently and faster and for less money to boost economics and construction quality. Furthermore, the construction sector is looking into several options for this aim. One way to do this is to emphasize how long it takes for Concrete to cure. This can be done by adequately curing the substance to increase its early strength. There are numerous curative techniques available. Vacuum-cured LECA has a higher compressive strength than partially saturated surface-dried LECA [17]. The slump-flow of self-consolidating concrete made with LC1 (with a density of 1.58 g/cm^3) measured at 667 mm, while for LC2 (with a density of 2.07 g/cm^3), it measured at 608 mm. These findings indicate that when using the exact proportions of lightweight aggregates, the self-consolidating concrete exhibits greater flowability with lower-density lightweight coarse aggregates. This observation applies to both lightweight aggregate and conventional concrete. [18, 19]. The accelerated cure with boiling water has been tested [20]. The structural behavior of lightweight concrete using LECA has been investigated, demonstrating a reduction in concrete weight and cost while maintaining mechanical properties. [21], It can be utilized to increase early development strength. In areas with a water constraint, LECA can be internally cured [22]. In this study, boiling water is used to hasten the curing process. It presents numerous advantages in terms of durability, cost-effectiveness, and productivity at construction sites. Conversely, lightweight concrete can significantly decrease the structural load, reducing member sizes and simplifying construction processes. Consequently, lightweight concrete can lead to overall cost savings in construction projects. Traditionally, lightweight aggregate concrete is produced similarly to conventional concrete. However, this manufacturing approach often faces aggregate segregation issues due to the aggregates' low density. In contrast, by reducing the aggregate content, self-consolidating concrete can be produced with more powders. This typically results in a concrete mix with improved viscosity during the fresh stage and greater compressive strength as it hardens. Therefore, integrating lightweight aggregates into self-consolidating concrete is believed to enhance quality and produce high-strength lightweight concrete while mitigating segregation issues associated with lightweight aggregates [23, 24]. The paper suggests that integrating pumice as a partial replacement in self-compacting concrete beams can enhance flexural properties, potentially leading to more sustainable construction practices by utilizing less conventional, more environmentally friendly materials while maintaining structural integrity and performance [25].

The primary goal of this study is to review lightweight aggregates (LWA) used to make lightweight self-consolidating Concrete. In addition to identifying the physical qualities, LWA is compared. The effects of LWA usage on the characteristics of freshly poured and hardened Concrete will be investigated. Additionally, the LWSCC mix design procedure is examined. After evaluating the currently available material, the LWSCC material goods and mix design can be significantly improved. Incorporating LECA as a lightweight aggregate in self-compacting concrete is crucial for advancing sustainable construction. LECA reduces the concrete's overall weight, enhancing its workability and reducing structural load. This innovation allows for more efficient material use, lower transportation costs, and improved thermal insulation, aligning with modern demands for environmentally friendly and energy-efficient building materials. This study's novelty lies in its comprehensive analysis of reinforced lightweight self-compacting concrete (LWSCC) beams incorporating varying proportions of LECA. By evaluating mechanical properties, flexural performance, and cracking behavior, this research offers new insights into optimizing LWSCC mixes for enhanced structural efficiency, sustainability, and practical application in modern construction practices.

2. MATERIALS AND METHODS

2.1. Materials

The present study utilized 53-grade ordinary Portland cement (OPC). Furthermore, ordinary physical cement attributes were evaluated according to IS 12269-2013 [26]. The specific surface area of the cement, measured at 329 m^2/kg, was determined using Blaine's air permeability method. Additionally, the specific gravity of the cement was found to be 3.09 by IS 4031-1996 [27]. River sand, locally available and sieved up to 4.750 mm, was used as the "fine aggregate (FA)." Sand characteristics were evaluated using IS: 2386-1963. Coarse Aggregates (CA) with a maximum size of 12.5 mm and a specific gravity of 2.45, held at 10

mm, were locally sourced, employed, and conformed to Zone-II as per IS 383:2016 [28–39]. To examine the characteristics of light-expanded clay, ranging in size from 8 to 12 mm, evaluated according to IS-2386-PART-III-1963 [40] as shown in Tables 1 and 2. Superplasticizer, specifically a sulfonated naphthalene-based polymer, was employed as an agent for significant water reduction in compliance with ASTM C 494:2019 [41].

The present research considers lightweight expanded clay aggregate (LECA), a coarse aggregate formed of clay. At roughly 1200 °C, lightweight expanded clay aggregate (LECA) can be created within a rotary kiln. Burnt clay is broken down into tiny, airy, swollen particles that make up LECA. The LECA used in this study featured an 8–12 mm particle size distribution, a 332 kg/m³ bulk density, and an approximately 14.5% water absorption rate. These properties were crucial for achieving the concrete's desired lightweight and self-compacting characteristics, ensuring proper workability, reduced density, and enhanced thermal insulation for structural applications. A picture of a light-expanded clay aggregate is shown in Figure 1.

An unwanted consequence of burning pulverized coal in thermal power plants is fly ash, also known as fuel ash. Fly ash is composed of small siliceous and aluminous pozzolan particles. We used Class C fly ash for this experiment. Subbituminous coals create Class C fly ashes containing mostly free lime, tricalcium aluminate, quartz, and calcium alumino-sulfate glass (CaO). Class C fly ash, which includes more than 20% CaO, is often called high-calcium fly ash. Utilizing fly ash has several advantages, including producing dense concrete with a smooth surface, excellent strength, workability, and reduced CO_2 emissions and hydration heat. Two downsides are the increase in salt scaling and the use of air-entraining admixtures. Fly ash, which had a specific gravity of 2.1, was used to replace 10% of the weight of the cement. The CONPLAST SP 430 was employed in this investigation. It is used to make concrete more workable and is carefully formulated to provide significant water reductions of up to 25% without sacrificing workability. It also minimizes permeability, resulting in high-quality concrete.

2.2. Mix Design

The LWSCC mix proportions are essential for its application since the suggested proportions may alter the necessary qualities in both the fresh and hardened stages. To satisfy the self-compacting requirement, LWSCC must develop the requisite fresh features, such as filling capacity, passage ability, and segregation resistance. The Concrete's filling or flow ability refers to its capacity to move freely, fill the formwork, and support its weight. On the other hand, the capacity to travel through dense steel reinforcement sections without harming them or cluttering the area with formworks is called passage ability. Segregation resistance is the capacity to maintain homogeneity during transportation, placement, and subsequent placement without bleeding or separating. "The composition of the raw materials, the quantity of chemical and mineral admixtures, the types of aggregate utilized, packing density, water-to-cement ratio (W/C)," and design methods significantly impact LWSCC performance. Presently being used as per the curves given in the rational mix design procedure by Rao et al. [42].

Table 1. Cement physical properties

S. No.	Test performed	Test values
1	initial setting time	42 min
2	Specific gravity	2.79
3	Soundness of cement	5 mm
4	Standard consistency	32%
5	Fineness of cement	3.7%

Table 2. Physical characteristics of gravel, LECA, and coarse aggregates

S. No.	Name of the test	Test values		
		Gravel	LECA	Fine aggregates
1	Fineness modulus	6.39	5.82	3.11
2	Specific gravity	2.45	0.606	2.59
3	Bulk density	1415.6 kg/m³	332 kg/m³	1638.7 kg/m³
4	Water absorption	0.7%	14.5%	1.1%

Figure 1. Lightweight expanded clay aggregate (LECA).

2.3. Test Methods

2.3.1. Compressive Strength

According to BS 12390-3: 2009 [43], the compressive strength of red mud concrete was assessed using samples sized 150 × 150 × 150 mm. These samples were meticulously prepared and subsequently tested for their compressive strength in a specialized compressive testing machine, ensuring precise and reliable results.

2.3.2. Flexural Strength

The procedure for evaluating the flexural strength adhered to BS 1881-118: 1983 [44]. Samples measuring 100 × 100 × 500 mm were meticulously crafted and tested on a flexural testing machine. This method effectively determined the concrete's bending resistance, offering critical insights into its structural capabilities under load.

Table 3. Mix proportions of control mic and LWSCC

Mix designation	Cement	Fly ash	Fine aggregate (sand)	Normal coarse aggregates	Light-expanded clay aggregate (LECA)	Water	Super plasticizer
Control mix	428	182	885	700	0	192	9.44
LECA 5	428	182	885	664.8	11.65	192	9.44
LECA 10	428	182	885	629.8	23.30	192	9.44
LECA 15	428	182	885	594.8	30.80	192	9.44
LECA 20	428	182	885	559.8	46.60	192	9.44
LECA 25	428	182	885	594.8	58.25	192	9.44

Table 4. Nomenclature and detailing of LWSCRC beams

S. No.	Beam designation	Average cube strength (MPa)	B (mm)	Height D (mm)	d (mm)	Length (mm)	Ast (mm²)
1	Control mix	28.28	200	230	200	1000	314.20
2	LECA 5	30.24	200	230	200	1000	314.20
3	LECA 10	31.65	200	230	200	1000	314.20
4	LECA 15	33.17	200	230	200	1000	314.20
5	LECA 20	31.89	200	230	200	1000	314.20
6	LECA 25	28.28	200	230	200	1000	314.20

2.3.3. Split Tensile Strength

The split tensile strength was assessed following BS 1881-117: 1983 [45]. Cylindrical samples with dimensions of 150 mm diameter and 300 mm height were prepared and examined using a tensile testing apparatus. This testing was crucial for understanding the concrete's tensile strength, highlighting its ability to withstand tensile forces, which is vital for structural applications.

2.3.4. Load Frame Machine

A load frame setup consisting of parameters such as hydraulic loads and deflection measurements via Linear Variable Differential Transformer (LVDT) sensors is needed. The setup includes vertical and lateral loads of 1000 and 20 kN, respectively, and measures deflection and strain at multiple points on a specimen, ensuring comprehensive data collection during testing.

2.4. Preparation of Specimens

Selected lightweight self-compacting concrete mixes with various percentages of LECA aggregate replacement—such as the Control Mix, LECA 5, LECA 10, LECA 15, LECA 20, and LECA 25 combinations, and NC discussed in the previous section—were used to create RC beams of different depths, incorporating fly ash and natural and synthetic lightweight aggregates. All beams were cast in wooden molds. The compressive strength of the concrete in each beam was measured using cube samples. Three concrete cubes were cast during the casting of each beam. All beam and cube samples were de-molded after 24 hours and cured in a water tank for 28 days. The beams were made from different mixtures of natural and lightweight aggregates, fly ash, and HYSD steel bars of various diameters (8 mm for stirrups and 10 mm for primary reinforcement in compression and tension). After assembly, the reinforcing cages were placed in beam molds before the concrete was poured. The names of the beams are displayed in Table 3. Beam mold size and other details are shown in Table 4. The width of all six beams was 150 mm. The molds were cleaned before pouring concrete into the cast iron molds, and oil was applied to all surfaces. The molds were positioned on a flat surface. After the molds were filled with concrete, it flowed and settled. Excess concrete was removed with a trowel, and the top surface was leveled. Beams of size 200 x 230 x 1000 mm were cast. as shown in Figure 2. The beam dimensions, 200x230x1000 mm, 200 mm, and 230 mm, are the is the standard width and depth of beam popularity used in the construction industry, 1000 mm is the unit length and reinforcement details were chosen to simulate real-world structural elements closely, ensuring accurate evaluation of flexural, cracking, and load-carrying behaviors.

Figure 2. Mould with casted beam specimen.

2.5. Details of Reinforcement Bars for Beams

As is common knowledge, concrete is strong in tension yet fragile in compression. Therefore, adding reinforcement

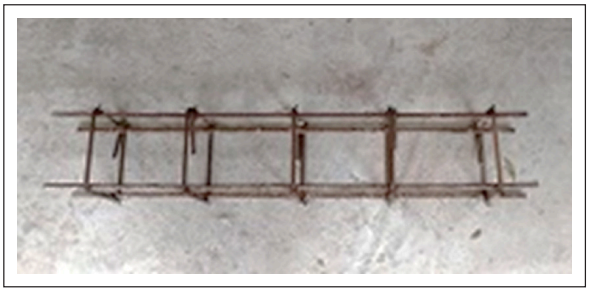

Figure 3. Reinforcement bars.

to Concrete makes a composite material with the "strength of concrete against compressive stress and the strength of reinforcement" against tensile stress. The reinforcement provided in the top and bottom is 2 bars of 12 mm diameter and 8 mm diameter stirrups at 200 mm center to center, as shown in Figure 3.

3. DISCUSSION ON RESULTS

3.1. Compressive Strength

According to the recommendations from EFNARC, the fresh properties of M40-grade concrete were successfully achieved. Extensive testing revealed that the compressive strength of this concrete grade at 28 days varied with the percentage of coarse aggregate replaced by Light Expanded Clay Aggregate (LECA). Specifically, the compressive strengths recorded were 44.56, 44.6, 45.2, 41.65, 36.1, and 32.73 N/mm² for replacement levels of 0%, 5%, 10%, 15%, 20%, and 25% respectively. This data indicates a trend where compressive strength tends to decrease as the replacement percentage of LECA increases beyond 10%. Additionally, it was observed that the rate of water absorption decreased as the grade of the concrete increased. This suggests that higher-grade concretes, likely due to their denser and more refined matrix, exhibit improved resistance to water penetration compared to lower grades. Moreover, when comparing self-compacting concrete (SCC) with lightweight self-compacting concrete (LWSCC), it was found that SCC exhibits significantly lower water absorption rates, indicating better performance in density and impermeability [1, 3, 15, 16]. The document further details the compressive strength of concrete using light-expanded clay aggregate, presenting results for five different replacement ratios in Figure 4. The methodology for determining the compressive strength involved calculating the maximum compressive load a specimen could withstand and dividing this value by the cross-sectional area of a 150 mm cube. This rigorous approach ensures an accurate assessment of the concrete's structural capabilities under compression, providing vital information for practical applications in construction.

Kumar et al. [46], found that the compressive strength of concrete using 100% lightweight coarse aggregate was 20% lower than that of the control concrete, which had an aggregate density of 2.07 g/cm³. Additionally, the strength was 31% lower when the aggregate density was 1.58 g/cm³.

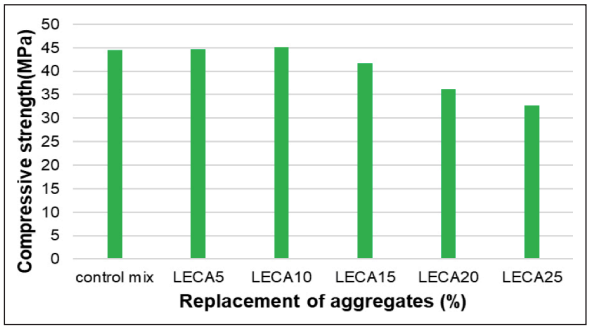

Figure 4. Compressive strength of LWSCC concrete of changed replacements.

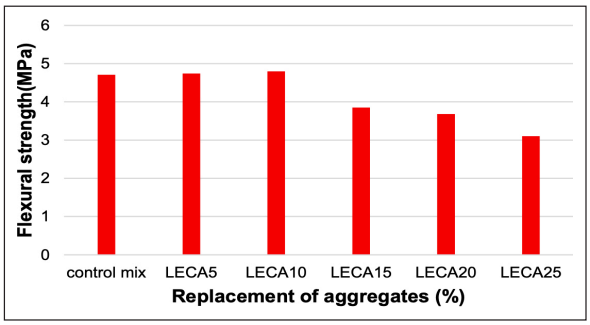

Figure 5. Flexural strength of concrete of different replacements.

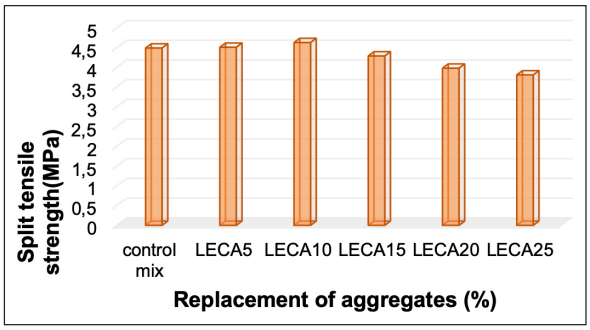

Figure 6. Split tensile strength of concrete of different replacements.

3.2. Flexural Strength Test

This study evaluated the flexural strength of lightweight expanded clay aggregate (LECA) concrete at different replacement levels of coarse aggregates. Beams with 100 mm x 100 mm x 500 mm were used for the flexural test. The replacements considered were 0% (control mix), 5%, 10%, 15%, 20%, and 25% LECA, as shown in Figure 5. The results indicate that the flexural strength of concrete decreases with increasing LECA replacement beyond 10%. The highest flexural strength was achieved at 10% LECA replacement, which is considered the optimum replacement level. This finding is corroborated by the data presented in Figure 5. At 10% replacement, the concrete attained a flexural strength of approximately 5.1 MPa, higher than the control mix and other replacement levels. This sug-

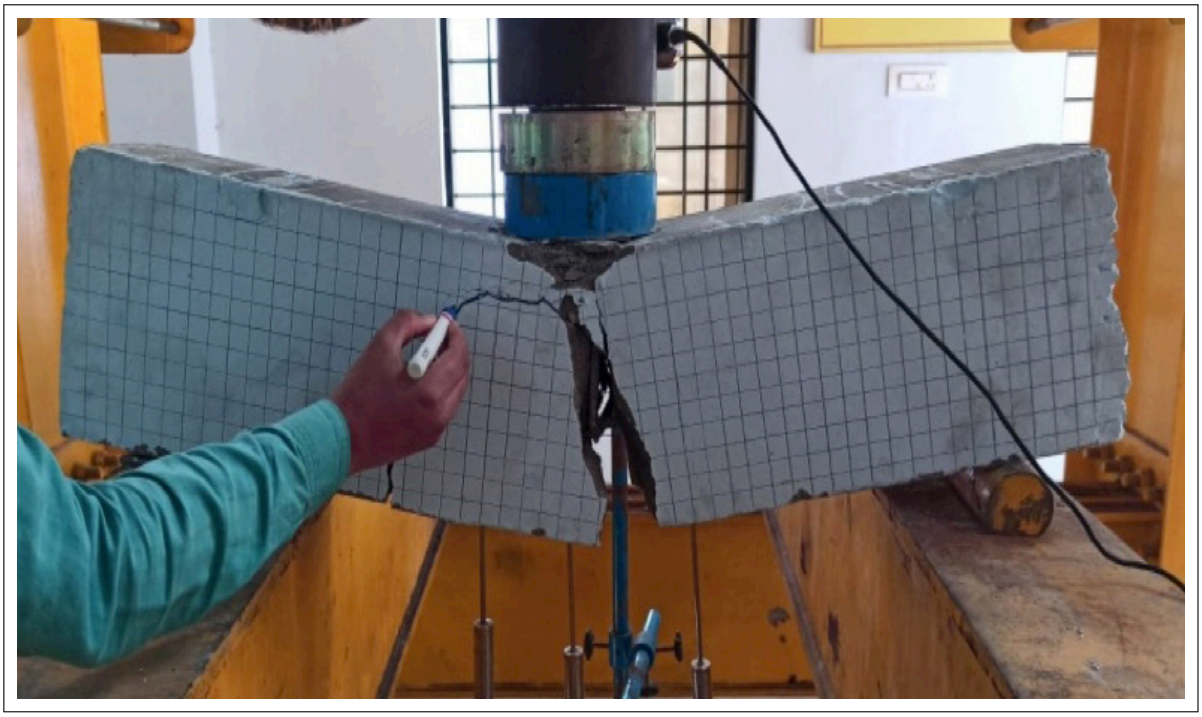

Figure 7. Crack pattern of beam control mix.

Figure 8. Crack pattern of beam LECA 5.

gests that a moderate incorporation of LECA can enhance the flexural strength of concrete [2, 4, 15, 16]. At lower replacement levels of 5% and 10%, the flexural strength remains relatively high and comparable to the control mix, indicating that LECA contributes positively to the structural integrity of concrete when used in small amounts. However, as the replacement level increases to 15%, 20%, and 25%, a noticeable decline in flexural strength is observed, with values dropping to approximately 4.2 MPa at 25% replacement. This decrease can be attributed to the increased presence of lightweight aggregate, which may reduce the density and bonding capacity within the concrete matrix. The trend in Figure 5 highlights the critical balance between achieving lightweight properties and

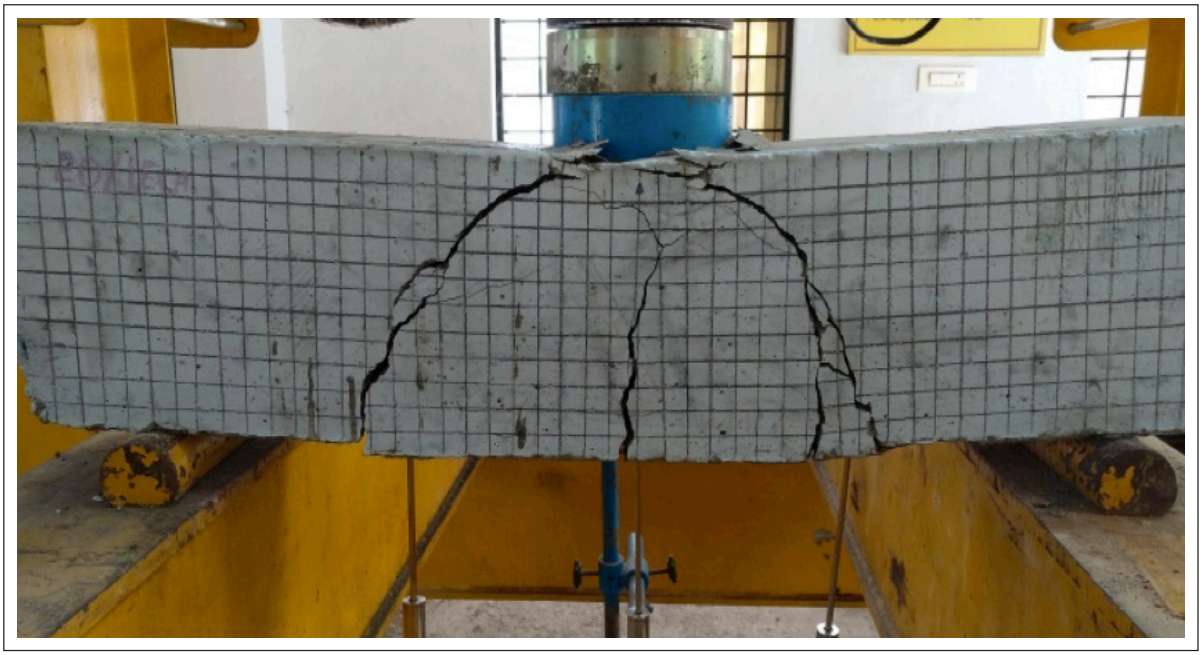

Figure 9. Crack pattern of beam LECA 10.

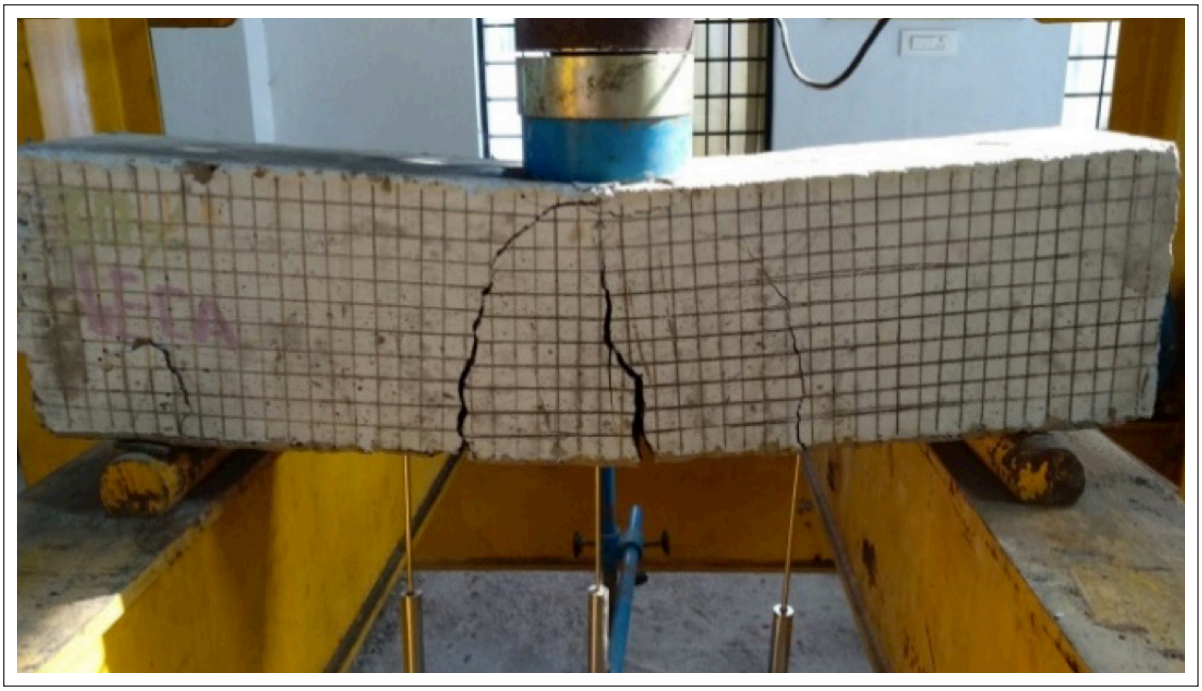

Figure 10. Crack pattern of beam LECA 15.

maintaining structural strength. While LECA is beneficial for reducing the weight of concrete and improving thermal insulation, its proportion must be carefully optimized to avoid compromising mechanical properties. Thus, a 10% replacement of conventional aggregates with LECA is identified as the most effective ratio, providing a good balance between enhanced flexural strength and lightweight characteristics.

3.3. Split Tensile Strength Test

The increase in split tensile strength with specific LECA replacement percentages, such as 10%, can be explained by the optimized strength of lightweight aggregates in the concrete matrix, as shown in Figure 6. The improved particle distribution and interlocking effect between the LECA particles and the cementitious matrix may enhance the overall tensile strength. The highest Split Tensile Strength Test

Figure 11. Crack pattern of beam LECA 20.

Table 5. Flexural performance of reinforced lightweight self-compacting concrete (LWSCC)

Beam designation	Ultimate state		Cracking state		Yielding state		Ductility index	
	Pu (kN)	Δu (mm)	Pcr (kN)	Δcr (mm)	Py (kN)	Δy (mm)	Δu/Δcr	Δu/Δy
Control mix	187.98	1	193.23	1	184.23	1.18	1.00	0.91
LECA 5	179.26	1.25	162.36	1.12	154.89	1.21	1.12	1.03
LECA 10	170.36	1.45	157.26	1.09	149.36	1.12	1.33	1.29
LECA 15	165.36	1.65	149.26	1.04	138.25	1.21	1.59	1.36
LECA 20	152.36	1.75	142.3	1.01	137.25	1.25	1.73	1.40
LECA 25	149.36	2.15	139.25	1	129.25	1.26	2.15	1.71

achieved at LECA 10 replacement is optimum replacement and strength, as shown in Figure 6. On the other hand, the decrease in split tensile strength observed for higher LECA replacement percentages, such as 20% and 25%, could be attributed to the increase in porosity and reduced interfacial bond strength between the aggregate and the matrix [2, 4, 15–17]. The lightweight nature of LECA can lead to increased voids and reduced cohesion, resulting in lower tensile strength values. The flexural and cracking behavior analysis revealed that higher LECA replacement levels increased crack widths and altered crack patterns. Beams with more LECA exhibited broader and more numerous cracks, indicating reduced structural integrity and load-bearing capacity. Overall, LECA contributes to more sustainable construction practices and resource conservation.

3.4. Flexural Behavior of LWSCC Reinforced Beams

Table 5 presents Reinforced Lightweight Self-Compacting Concrete (LWSCC) flexural performance with varying percentages of LECA (Lightweight Expanded Clay Aggregate) replacement. The data outlines several performance metrics across five different LECA replacement levels alongside a control mix. The ultimate state load capacity (Pu) decreases consistently as the LECA content increases. For example, the control mix has a Pu of 187.98 kN, while LECA 25 has a significantly lower value of 149.36 kN. This indicates a reduction in ultimate load-bearing capacity with higher LECA content, possibly due to the lower density and strength of LECA compared to traditional aggregates. Similarly, the cracking state load (Pcr) decreases from 193.23 kN in the control mix to 139.25 kN in the LECA 25 mix, highlighting reduced initial cracking resistance. The corresponding displacements at cracking (Δcr) slightly increase with more LECA, suggesting that higher LECA mixtures tend to have more flexibility before cracking. The yield load (Py) decreases in the yielding state, from 184.23 kN in control to 129.25 kN in LECA 25. Additionally, displacement at yield (Δy) increases, ranging from 1.18 mm to 1.26 mm. This could imply a decrease in stiffness with increased LECA replacement. The ductility indexes, Δu/Δcr and Δu/Δy, generally increase with more LECA content. For instance, Au/Acr rises from 1.00 in the control mix to 2.15 in LECA 25 and Au/Δy from 0.91 to 1.71, respectively. This suggests that higher LECA replacements contribute to increased ductility, which might benefit applications where flexibility and energy absorption are critical despite losing strength and stiffness. The above findings have import-

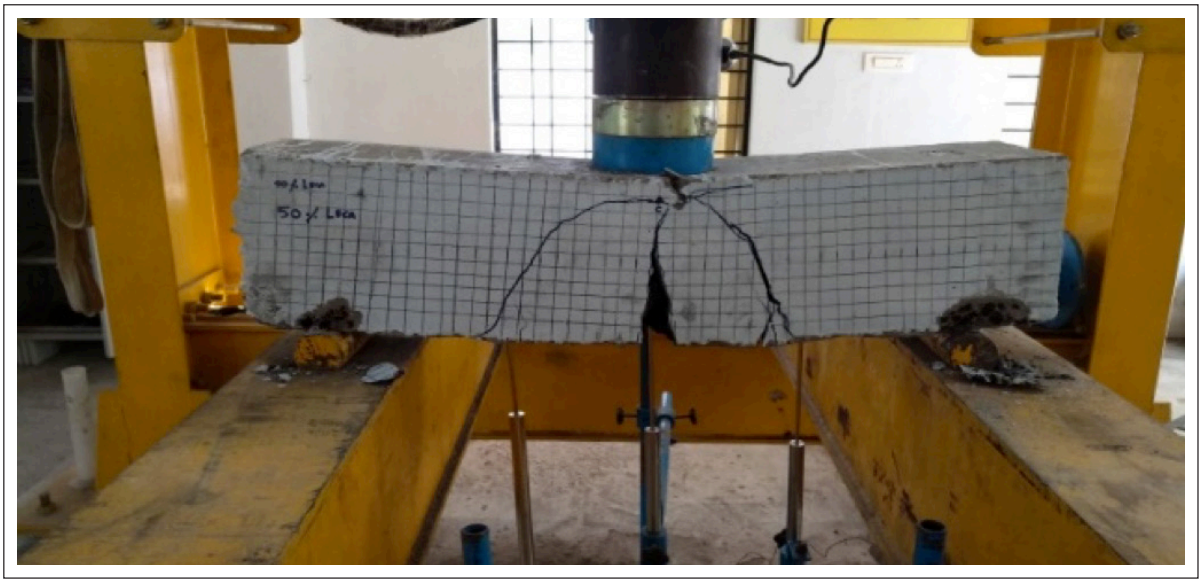

Figure 12. Crack pattern of beam LECA 25.

Table 6. Crack width values

Beam designation	Width of crack (mm)	Density kg/m³
Control mix	1	2312
LECA 5	1	1952
LECA 10	1.25	1915
LECA 15	1.55	1902
LECA 20	1.75	1899
LECA 25	2	1890

ant implications for the structural application of LWSCC. While higher LECA levels enhance ductility, they compromise load-bearing capacities and initial cracking resistance, which must be carefully considered in structural design and application. Kavyateja et al. [47]. The load-deflection behavior analysis showed that beams with higher LECA replacement levels had reduced ultimate load-carrying capacity and stiffness but increased ductility. For instance, beams with 25% LECA replacement exhibited lower load capacity and stiffness than the control mix but demonstrated more significant deflection before failure, indicating enhanced ductility. This trade-off highlights LECA's impact on structural performance.

Only flexure cracks and shear cracks, as can be seen from the figures, were created. Beams exhibited no web shear fracture development, as shown in Figure 7, Figure 8, Figure 9. Figure 10, Figure 11, and Figure 12. Because beams have a lower load-carrying capability, the data shows that crack breadth rose when the percentage of Light Expanded Clay Aggregate was replaced. The crack widths observed for the LWSCC beams with different LECA replacements were as follows: 1 mm for 0% replacement, 1 mm for 5% replacement, 1.25 mm for 10% replacement, 1.55 mm for 15% replacement, 1.75 mm for 20% replacement, and 2 mm for 25% replacement. It can be noted that as the LECA replacement percentage increased, the crack widths also increased gradually. Simultaneously, the density values of the LWSCC beams varied as follows: 2312 kg/m³ for 0% replacement, 1952 kg/m³ for 5% replacement, 1915 kg/m³ for 10% replacement, 1902 kg/m³ for 15% replacement, 1899 kg/m³ for 20% replacement, and 1890 kg/m³ for 25% replacement. Table 6 provides the crack width and densities. The density of the LWSCC beams decreased with increasing LECA replacement.

4. CONCLUSION

According to the findings of this investigation, the following conclusions were drawn:

1. The compressive strength of the lightweight self-compacting Concrete (LWSCC) is learned to be decreased by increasing the percentage of lightweight aggregate. In the case of Lightweight aggregate Concrete produced with sintered fly ash aggregate, the optimum compressive strength of LWSCC attained at 40% replacement is 29.46 N/mm² of M40 grade concrete.
2. Based on the results, it was discovered that replacing coarse aggregate with Light expanded clay aggregate (LECA) aggregate by control mix, 5%, 10%, 15%, 20%, and 25%, gradually reduced the densities of self-compacting Concrete.
3. As a generalization of these trials, it was found that the maximum load-bearing capacity of lightweight beam flexural elements is reduced by up to 35% compared to conventional beams.
4. The components of the lightweight reinforced concrete beams displayed behavior comparable to conventional concrete beams conventional-lightweight Concrete. At places where the bending moment was most significant, the first cracks appeared perpendicular to the neutral axis.

5. Flexural crack formations started as minute structures invisible to the human eye. The fracture widened as the ultimate stresses approached, but because longitudinal reinforcing was provided by indented steel bars, the crack diameters did not increase excessively.
6. With a percentage replacement of pumice aggregate, fracture width increased; it can be observed that with 15% LECA replacement, P/ reaches its highest value.
7. Load vs. deflection curves show that central deflections are more significant than side deflections. The maximum load values found during beam load frame testing exceeded those predicted by theory.
8. It can also be seen that as the proportion of LECA aggregates increased, the beams' maximum load-carrying capacity decreased.

ETHICS

There are no ethical issues with the publication of this manuscript.

DATA AVAILABILITY STATEMENT

The authors confirm that the data that supports the findings of this study are available within the article. Raw data that support the finding of this study are available from the corresponding author, upon reasonable request.

CONFLICT OF INTEREST

The authors declare that they have no conflict of interest.

FINANCIAL DISCLOSURE

The authors declared that this study has received no financial support.

USE OF AI FOR WRITING ASSISTANCE

Not declared.

PEER-REVIEW

Externally peer-reviewed.

REFERENCES

[1] Ramanjaneyulu, N., Rao, M. S., & Desai, V. B. (2019). Behavior of self-compacting concrete partial replacement of coarse aggregate with pumice lightweight aggregate. In Proceedings of the International Conference on Advances in Civil Engineering Vol. 21, pp. 23.

[2] Pavithra, A., & De Rose, D. J. (2018). Application of light expanded clay aggregate as replacement of coarse aggregate in concrete pavement. *Int J Eng Technol, 7*(4.2), 1–4. [CrossRef]

[3] Vijayalakshmi, R., & Ramanagopal, S. (2018). Structural concrete using expanded clay aggregate: A review. *Indian J Sci Technol, 11*(16), 121888. [CrossRef]

[4] Chaitanya, B. K., Sivakumar, I., Madhavi, Y., Cruze, D., Venkatesh, C., Naga Mahesh, Y., & Sri Durga, C. S. (2024). Microstructural and residual properties of self-compacting concrete containing waste copper slag as fine aggregate exposed to ambient and elevated temperatures. *Infrastructures, 9*(5), 85. [CrossRef]

[5] Chava, V., Rao, S., Munugala, P. K., & Chereddy, S. S. D. (2024). Effect of mineral admixtures and curing regimes on properties of self-compacting concrete. *J Sustain Constr Mater Technol, 9*(1), 25–35. [CrossRef]

[6] Real, S., Bogas, J. A., Gomes, M. G., & Ferrer, B. (2016). Thermal conductivity of structural lightweight aggregate concrete. *Mag Concr Res, 68*(15), 1–11. [CrossRef]

[7] Ramanjaneyulu, N., Desai, B., & Rao, M. S. (2021). Experimental investigations on lightweight self-compacting concrete produced with sintered fly ash aggregate. *Int J Eng Technol Manag Sci, 5*(5), 14–19. [CrossRef]

[8] Chava, V., & Chereddy, S. S. D. (2023). Effect of calcination on the physical, chemical, morphological, and cementitious properties of red mud. *J Sustain Constr Mater Technol, 8*(4), 297–306. [CrossRef]

[9] Wegian, F. M. (2012). Strength properties of lightweight concrete made with LECA grading. *Aust J Civ Eng, 10*(1), 11–22. [CrossRef]

[10] Shendy, M. E. (1991). A comparative study of LECA concrete sandwich beams with and without core reinforcement. *Cem Concr Compos, 13*(2), 143–149. [CrossRef]

[11] Durga, C. S. S., Venkatesh, C., Muralidhararao, T., Bellum, R. R., Rao, B. N. M. (2023). Estimation of durability properties of self-healing concrete influenced by different bacillus species. *Res Eng Struct Mater, 9*(4): 1489–1505. [CrossRef]

[12] Youssf, O., Hassanli, R., Mills, J. E., Ma, X., & Zhuge, Y. (2019). Cyclic performance of steel–concrete–steel sandwich beams with rubcrete and LECA concrete core. *J Compos Sci, 3*(1), 5. [CrossRef]

[13] Mortazavi, M., & Majlessi, M. (2013). Evaluation of silica fume effect on compressive strength of structural lightweight concrete containing LECA as lightweight aggregate. *Adv Mater Res, 626*, 344–349. [CrossRef]

[14] Ramanjaneyulu, N., Srigiri, K., & Rao, N. V. S. (2018). Strength and durability studies on light weight self-compacting concrete with LECA as partial replacement of coarse aggregate. *CVR J Sci Technol, 15*(1), 1–9. [CrossRef]

[15] Ashok, K., & Manoj, T. (2018). Study on strength properties of lightweight expanded clay aggregate concrete. *J Struct Eng, 7*(4), 7.

[16] Sravya, Y. L., Manoj, T., & Rao, M. S. (2021). Effect of temperature curing on lightweight expanded clay aggregate concrete. *Mater Today Proceed, 38*, 3386–3391. [CrossRef]

[17] Razak, R. A., Abdullah, M. M. A. B., Yahya, Z., & Hamid, M. S. A. (2017). Durability of geopolymer lightweight concrete infilled LECA in seawater exposure. In *IOP Conference Series: Materials Science and Engineering*, vol. 267, no. 1, p. 012012. IOP Publishing. [CrossRef]

[18] Lo, T. Y., & Cui, H. Z. (2004). Effect of porous lightweight aggregate on strength of concrete. *Material Letters, 58*(6), 916–919. [CrossRef]

[19] Lo, T. Y., Cui, H. Z., & Li, Z. G. (2004). Influence of aggregate pre-wetting and fly ash on mechanical properties of lightweight concrete. *Waste Manag, 24*(4), 333–338. [CrossRef]

[20] Kanagaraj, B., Anand, N., Praveen, B., Kandasami, S., Lublóy, E., & Naser, M. Z. (2023). Physical characteristics and mechanical properties of a sustainable lightweight geopolymer based self-compacting concrete with expanded clay aggregates. *Dev Built Environ, 13*, 100115. [CrossRef]

[21] Raju, K., Ramanjaneyulu, N., & Rao, M. S. (2022). Strength and durability studies on lightweight self-compacting concrete partially replacing coarse aggregate with sintered fly ash aggregate. *CVR J Sci Technol, 23*(1), 7–13.

[22] Hwang, C. L., & Hung, M. F. (2005). Durability design and performance of self-consolidating lightweight concrete. *Constr Build Mater, 19*, 619–626. [CrossRef]

[23] Caijun, S., & Yanzhong, W. (2005). Mix proportioning and properties of self-consolidating lightweight concrete containing glass powder. *ACI Mater J, 102*(5), 355–363. [CrossRef]

[24] Wang, H. Y. (2009). Durability of self-consolidating lightweight aggregate concrete using dredged silt. *Constr Build Mater, 23*, 2332–2337. [CrossRef]

[25] Kumar, T. V., & Ramanjaneyulu, N. (2022). Flexural behavior of self-compacting concrete beams partially replacing conventional aggregate with pumice aggregate. *CVR J Sci Technol, 22*(1), 8–21.

[26] Indian Standards. (2013). *Specification for 53 grade ordinary Portland cement*. IS 12269.

[27] Indian Standarts. (1996). *Specifications for a method of physical tests for hydraulic cement*. IS 4031-I.

[28] Indian Standards. (2016). *Specification for coarse and fine aggregates from natural sources for concrete*. IS 383.

[29] Venkateswara Rao, S., Seshagiri Rao, M. V., Ramaseshu, D., & Rathish Kumar, P. (2012). Durability performance of self-compacting concrete. *Mag Concrete Res, 64*(11), 1005–1013. [CrossRef]

[30] Pamu, Y., Kumar, V. S. S., Shakir, M. A., & Ubbana, H. (2022). Life cycle assessment of a building using Open-LCA software. *Mater Today Proc, 52*, 1968–1978. [CrossRef]

[31] Pamu, Y., & Alugubelli, S. (2023). A comparative study of environmental impacts due to conventional and sustainable concrete. *Mater Today Proc, 92*, 112–120. [CrossRef]

[32] Durga, C. S. S., Venkatesh, C., Muralidhararao, T., & Bellum, R. R. (2023). Crack healing and flexural behaviour of self-healing concrete influenced by different bacillus species. *Res Eng Struct Mater, 9*(4), 1477–1488. [CrossRef]

[33] Bellum, R. R., Al Khazaleh, M., Pilla, R. K., Choudhary, S., & Venkatesh, C. (2022). Effect of slag on strength, durability and microstructural characteristics of fly ash-based geopolymer concrete. *J Build Pathol Rehabil, 7*(1), 25. [CrossRef]

[34] Mukkala, P., Venkatesh, C., & Habibunnisa, S. (2022). Evaluation of mix ratios of light weight concrete using geopolymer as binder. *Mater Today Proc, 52*, 2053–2056. [CrossRef]

[35] Bellum, R. R., Venkatesh, C., & Madduru, S. R. C. (2021). Influence of red mud on performance enhancement of fly ash-based geopolymer concrete. *Innov Infrastruct Solut, 6*(4), 215. [CrossRef]

[36] Venkatesh, C., Nerella, R., & Chand, M. S. R. (2021). Role of red mud as a cementing material in concrete: A comprehensive study on durability behavior. *Innov Infrastruct Solut, 6*(1), 13. [CrossRef]

[37] Rao, T. M., Mahesh, K., Venkatesh, C., Durga, C. S. S., Reddy, B. R., Tejaswi, P. S., & Charandeepneelesh, R. (2023). Influence of water magnetization on mechanical and durability properties of fly ash concrete. *Mater Today Proc, 04*.194, 1–7.

[38] Venkatesh, C., Nerella, R., & Chand, M. S. R. (2020). Experimental investigation of strength, durability, and microstructure of red-mud concrete. *J Korean Ceram Soc, 57*(2), 167–174. [CrossRef]

[39] Venkatesh, C., Sri Rama Chand, M., Ruben, N., & Sonali Sri Durga, C. (2020). *Strength characteristics of red mud and silica fume based concrete. In Smart Technologies for Sustainable Development: Select Proceedings of SMTS 2019* (pp. 387–393). Springer Singapore. [CrossRef]

[40] BIS. (1963). *Standard methods for testing lightweight aggregates*. IS-2386.

[41] ASTM. (2019). *Standard specification for chemical admixtures for concrete*. ASTM C494.

[42] Rao, S. V., Rao, M. S., Ramaseshu, D., & Kumar, P. R. (2013). A rational mix design procedure for self-compacting concrete. *Cem Wapno Beton, 18*(5), 271–280.

[43] BS EN 12390-3. (2019). *Testing hardened concrete - Part 3: Compressive strength of test specimens*. EN 12390-3:2019.

[44] British Standarts. (1983). *Methods for determining the flexural strength of concrete.* BS 1881-Part 118.

[45] British Standarts (1983). *Methods for determining the split tensile strength of concrete*. 1881-Part 117.

[46] Kumar, V. R., Tejaswini, N., Madhavi, Y., & Kanneganti, J. B. C. (2022). Experimental study on self-compacting concrete with replacement of coarse aggregate by light expanded clay aggregate. *IOP Conf Ser Earth Environ Sci, 982*(1), 012006. [CrossRef]

[47] Kavyateja, B. V., Jawahar, J. G., Sashidhar, C., & Panga, N. R. (2021). Moment carrying capacity of RSCC beams incorporating alccofine and fly ash. *Pollack Periodica, 16*(1), 19–24. [CrossRef]

J Sustain Const Mater Technol, Vol. 9, Issue. 2, pp. 170–176, June 2024

Journal of Sustainable Construction Materials and Technologies
Web page info: https://jscmt.yildiz.edu.tr
DOI: 10.47481/jscmt.1485912

Research Article

Mechanical and microstructural properties of mortars: Obsidian powder effect

Talip ÇAKMAK, Ali GÜRBÜZ, Zafer KURT, İlker USTABAŞ*

Department of Civil Engineering, Recep Tayyip Erdoğan University, Rize, Türkiye

ARTICLE INFO

Article history
Received: 16 February 2024
Accepted: 18 March 2024

Key words:
Cement, mortar, obsidian, XRD

ABSTRACT

Concrete has been the world's most produced and utilized building material for years due to its economic and easy accessibility. However, it attracts attention due to the CO_2 emitted from cement, the raw material of concrete, during the production and consumption stages. Although there are different research studies to reduce this emission, one of the most logical solutions is to use pozzolanic materials with cement and reduce the need for cement. This paper investigated the general material characteristics of mortar samples generated by substituting obsidian powder with pozzolanic properties into cement at different ratios by weight. Mortar specimens with varying proportions of obsidian, such as 0%, 10%, 20%, and 30% by weight, were subjected to mechanical tests at 3, 7, 14, and 28 days. Material tests like X-ray diffraction (XRD) and scanning electron microscopy (SEM) were employed to characterize the material. As a result of the mechanical tests, 42.52 MPa compressive strength was obtained from the 28-day reference sample, while 44.331 MPa compressive strength was obtained from the mortar sample with 30% obsidian substitution. The outcomes of this paper noted that obsidian powder, which has pozzolanic properties, increased the mechanical strength of cementitious mortar specimens. This work indicates the suitability of using obsidian as pozzolan material with cement was determined.

Cite this article as: Çakmak, T., Gürbüz, A., Kurt, Z., & Ustabaş, İ. (2024). Mechanical and microstructural properties of mortars: Obsidian powder effect. *J Sustain Const Mater Technol*, 9(2), 170–176.

1. INTRODUCTION

If we have to list the materials that are most produced, used, and studied in the civil engineering discipline, it is clear that concrete is the most common material after water [1]. Concrete production, which is increasing with each passing day because it is cheap and durable, reached 32 billion tons in 2021 [2, 3]. Since traditional concrete cannot be produced without cement, cement production is increasing daily depending on concrete production. Today, as global warming and greenhouse gas effects have improved considerably, the impact of carbon footprints is gaining importance daily. In this context, CO_2 emissions from cement production and consumption constitute 7% of total emissions [4, 5]. Innovative technologies are needed to reduce cement production daily for a sustainable environment. Considering the advantages of traditional concrete produced with cement, one of the ideal solutions is to decrease the use of cement in the mix by using pozzolanic additives [6, 7]. Generally, materials with pozzolanic properties are known as not binders but gain binder properties when used with cement. Using pozzolanic materials in concrete production reduces the cost of cement and contributes to the durability properties of concrete, resulting in an ergonomic concrete output. Most importantly, it helps to reduce the amount of CO_2 emitted by diminishing the amount of cement produced.

***Corresponding author.**
*E-mail address: ilker.ustabas@erdogan.edu.tr

Table 1. Mixture calculations of the mortar series-produced

Mixture name	Binder (g)		Water (g)	CEN standard sand (g)	Water/ binder ratio
	Cement	Obsidian			
S1 (reference)	450	0	225	1350	0,5
S2	405	45	225	1350	0,5
S3	360	90	225	1350	0,5
S4	315	135	225	1350	0,5

There are many studies in which pozzolanic materials have been substituted with cement [8–12]. Ustabaş and Ömür [13] searched the changes in the strength and hydration heat of industrial waste by-products and obsidian powder that they substituted for cement. They stated that the strengths obtained from the samples produced by substituting 40% of pozzolanic materials such as obsidian, fly ash, and blast furnace slag into cement mortars were similar to those of unsubstituted cement mortars. Keçek et al. [14] examined the utilization of tuff as a mineral admixture in cement. They looked into the effect on strength values by substituting tuffs with different surface area values, which were ground at other times, into cement. The maximum strength of 37,45 MPa was obtained in 28 days in substituted cements. Zhao et al. [15] conducted a study to measure the pozzolanic activity of waste clay brick powders with different specific surface areas. They discovered that the strength values grew with the rise in surface area. Çullu et al. [16] used volcanic rocks as a substitute for cement at different ratios between 10%–50% to determine the pozzolanic properties of various types of volcanic rocks. They found that the ideal mixing ratio was 10%. Araújo et al. [17] observed an 11% higher increase in compressive strength compared to cement samples when the ceramic waste used as a cement substitute was 25% by weight. Aruntaş et al. [18] focused on the differences created by substituting blast furnace slag and hydrated lime into cement-based mortars and pastes. Although hydrated lime and blast furnace slag contributed to the concrete at some points within the scope of the study, it was observed that lower strength was obtained compared to the reference specimens.

A comprehensive literature review indicated that pozzolanic material experiments were conducted to determine the pozzolanic characteristics of waste and inert materials. Although there are various studies on common materials like fly ash, blast furnace slag, etc., there are few studies on innovative materials such as obsidian. This study investigates the substitution of obsidian, which has pozzolanic properties, into cement. Compressive strength, XRD, and SEM-EDS analysis results of concrete mortars were investigated.

2. MATERIALS AND METHODS

Within the scope of the study, concrete mortars were produced by substituting 10%, 20%, and 30% obsidian to cement. The obsidian rocks collected from nature were first crushed in a jaw crusher and pulverized by grinding in a ball mill. The material/ball weight ratio in the ball mill was 1/24. The information and mixing parameters of the mortar series used in the study are given in Table 1. The mortar specimens were cast according to ASTM C109 [19]. After casting, the mortars were left in the molds for 24 hours before being removed and water-cured in the curing pool.

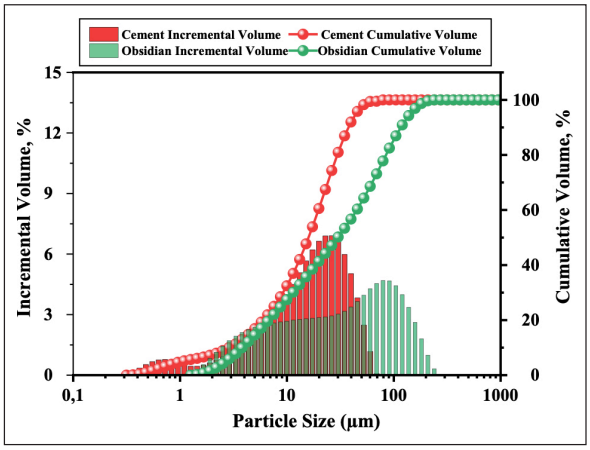

Figure 1. Cumulative volume and incremental volume granulometry curves of obsidian and cement.

2.1. Components

2.1.1. Obsidian

Obsidian rocks obtained from the Çağırankaya region of İkizdere District of Rize Province, Türkiye, were used in the study. The specific gravity of the ground obsidian powders is 2.6, and the average grain size is 53.786 µm. According to ASTM C618 [20], obsidian powder has N class natural pozzolanic properties as $SiO_2+Al_2O_3+Fe_2O_3$ >70, CaO<18, SO_3<4 and L.O.I<10. The granulometer curve of obsidian is given in Figure 1. The chemical contents obtained from XRF analysis of obsidian are given in Table 2.

2.1.2. Cement

The Portland cement type is CEM II/A-L 42.5 R, obtained from Trabzon Aşkale, which suits TS EN 197-1:2012 [21] requirements. The cement's specific gravity is 3.15 gr/cm^3, with an average particle size of 35.452 µm. The granulometer curve of the cement is given in Figure 1. Table 2 shows the chemical contents determined from XRF analysis of the materials employed as binders in the study. Also, the chemical phase structure of cement is depicted by XRD in Figure 2.

2.2. Methodology

In this study, The objective was to explore mortars' mechanical and microstructural qualities by inserting obsidian, which possesses pozzolanic capabilities, into cement at 10%, 20%, and 30% by weight. Mortar cube specimens of 50x50x50 mm^3 were cast in line with ASTM C109 [18], with four separate batches created using two different binders. For the mortars subjected to mechanical tests on other days, such as 3, 7, 14, and 28, 3 samples were poured in each series, and three compressive strengths were averaged. The experiments were carried out at Recep Tayyip Erdoğan University Building Materials Laboratory, and Figure 3 depicts a flow chart covering the working processes.

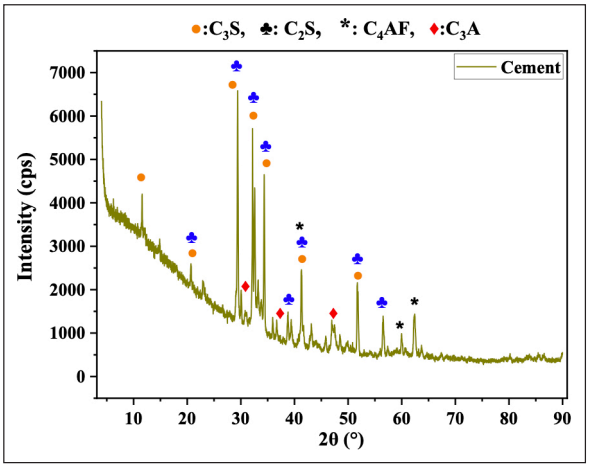

Figure 2. XRD pattern of the cement.

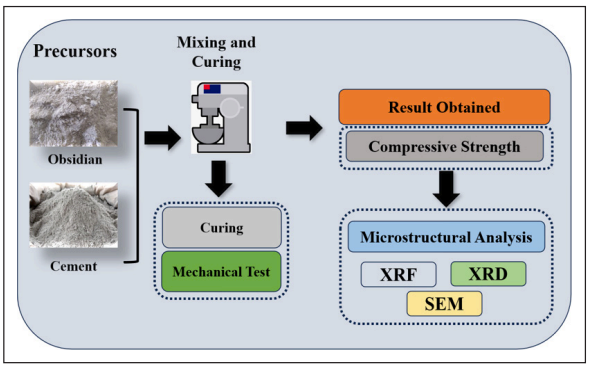

Figure 3. Flowchart of laboratory and test processes.

2.2.1. Mechanical Strength Experiments

The compressive tests were done on mortar specimens of dimensions (50x50x50 mm^3) previously cast and exposed to water curing on various days. All conditions, such as laboratory conditions, mixing water temperature, materials used, mechanical tests, etc., were implemented by requirement of ASTM C109 [18].

2.2.2. XRD Analysis

XRD analysis is one of the standard methods utilized to determine the characteristic mineral content of mortar samples. This study used a Rigaku SmartLab instrument (Cu-K-beta type PW1830, 2θ:4-90) for the analysis. The mortar samples were subjected to mechanical tests and ground in a ring grinder to prepare them for XRD analysis. 40 kV operating voltage, 0.02 step size, and 40 Ma emission current were selected as test parameters.

2.2.3. SEM Observations

The EOL JSM-6510 type SEM device was used to analyze the pores of mortar samples in which cement and obsidian were used as binders using a formal tone. The electron microscope has parameters like an accelerating voltage of 20 kV, a current emission of 0.9 nA, a magnification range of 5 to 1,000,000, and a resolution of 3 nm. To produce a clean image, the samples prepared for SEM examination were held at 50 °C for a specific time before vacuuming. The mortar samples were then put in the test equipment, covered with Au film, and examined under 50 to 10,000 magnification.

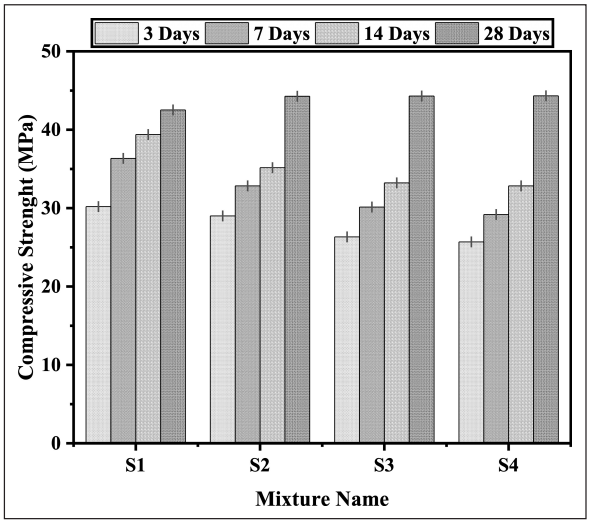

Figure 4. Compressive strength bar graphs of different mortar series for 3, 7, 14, and 28 days.

Table 2. Chemical composition of binders (%)

Chemical content	Obsidian	Cement
SiO_2	73,624	17,564
Al_2O_3	13,779	4,619
K_2O	5,296	1,006
Na_2O	3,959	–
Fe_2O_3	1,263	2,942
CaO	1,044	63,452
TiO_2	0,207	0,343
BaO	0,083	0,018
MgO	0,075	–
Mn_3O_4	0,055	0,051
SO_3	0,022	2,727
P_2O_5	0,02	0,118
SrO	0,018	0,023
L.O.I.	0,51	7,34

3. RESULTS AND DISCUSSION

3.1. Mechanical Strengths

Figure 4 demonstrates the compressive strengths of 50x50x50 mm mortar specimens generated by ASTM C109 at 3, 7, 14, and 28 days. Mechanical tests on mortar specimens were canceled if they exceeded the average value by more than ±10%. New specimens were cast to repeat the testing. Figure 4 illustrates that the maximum and lowest compressive strength values in 3 days were measured from the S1 and S4 series, respectively. At 3-day values, the compressive strength values of the S2, S3, and S4 series are 96%,

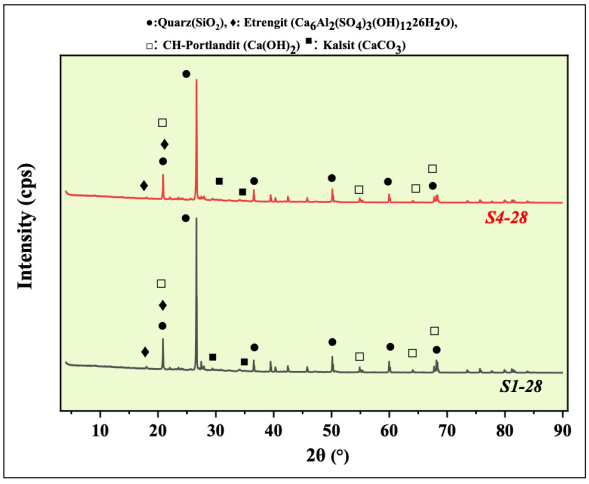

Figure 5. XRD patterns of S1 and S4 mortar samples.

87%, and 85%, respectively, compared to the strength of reference S1 which contains 100% cement. There is an inverse correlation between the amount of obsidian in the mixtures and the compressive strengths. The 7-day values show a similar trend to the 3-day compressive strengths. The compressive strength values of the S2, S3, and S4 series are 90%, 83%, and 80% respectively compared to the strength of S1. Obsidian content and compressive strength have an inverse relationship, similar to the 3-day values. However, it is seen that the proportional difference between the 7-day values and the reference sample increases. The 14-day strengths are identical to the three and 7-day strengths.

However, when 28-day strengths are analyzed, it is understood that there is a linear connection between obsidian content and compressive strength. The compressive strength values of the S2, S3, and S4 series are 104%, 104.1%, and 104.2% respectively compared to the strength of S1. When the research is evaluated according to TS EN 197-1 [21], the early compressive strength of the mortar specimens (7 days) should be more than the standard's requirement of 16 MPa, and the 28-day standard compressive strength should be more significant than 42.5 MPa. The 7-day and 28-day strengths of the reference control series S1 were 36,35 MPa and 42,52 MPa, respectively. When the other mixture series are considered, it is seen that the other series also have compressive strengths higher than the values required by the standard. Generally, the compressive strength of the obsidian-containing mortar specimens was lower than the reference specimen in the early age period but exceeded the reference specimen at 28 days. This demonstrates that obsidian advantages affect mortar specimens' compressive strength during the standard age period. Obsidian's favorable influence on compressive strength during the typical age period is assumed to be owing to its high SiO_2 concentration, which binds the free $Ca(OH)_2$ in the mixture and induces the development of extra binder gels [18].

ASTM C 270 [22] provides information about the minimum standards that cement mortars should have, and there are four categories of standards, particularly "M," "S," "N," and "O" for various field uses and mortar kinds. The "M" group has the highest strength requirement among the classes. Mortars in this group are required to have an average compressive strength of at least 17.2 MPa in 28 days. The other "S," "N," and "O" groups have minimum average compressive strengths of 12.4 MPa, 5.2 MPa, and 2.4 MPa, respectively. Given the compressive strength values of several series in Figure 4, it is seen that all series comply with ASTM C270 [22] standards, and all series are "M" group. Therefore, it is seen that the series produced within the scope of the study comply with the standards and can be applied in real life.

Ustabaş and Ömür [13] studied the impact of obsidian substitution on the heat of hydration and mechanical characteristics of cement mortar. In this study, 10%, 20%, 30%, 30%, 40%, and 50% by weight of obsidian, blast furnace slag, and fly ash were added to cement, and the hydration temperature and 2-, 7- and 28-day compressive strengths of mortars were investigated. The highest strength value was obtained from the reference sample containing 100% cement, while the order of magnitude of the strengths obtained from 40 wt% substitutions of fly ash, blast furnace slag, and obsidian were blast furnace slag, obsidian and fly ash, respectively. When the 2-, 7- and 28-day values are analyzed, it is noteworthy that there is an inverse relationship between the percentage increase in obsidian weight and compressive strength. Within the scope of our study, a similar relationship was found in 3, 7, and 14-day strengths. In this context, the values of the study are based on the literature.

Pehlivan [23] looked into the use of nano-silica in the manufacturing of calcined cement mortars by adding 10%, 20%, and 30% calcined clay and 0%, 0.5%, and 1% nano silicate to cement and examined 360-day compressive and flexural strengths. While 55.35 MPa compressive strength and 9.43 MPa flexural strength were obtained from the control specimen containing 100% cement, the series having 10% calcined clay and 1% nano-silica had the maximum compressive strength of 58.41 MPa and flexural strength of 9.75 MPa. When the strength values are analyzed in general, it is seen that there are decreases in compressive and flexural strengths when the additive ratio exceeds 10%. Aruntaş et al. [18] In their study, they substituted 10%, 20%, and 30% by weight of ground blast furnace slag and slaked lime to determine the effect of ground blast furnace slag and slaked lime on cement mortar. Compressive and flexural strengths were seen to decrease as the replacement rate soared. In this context, it is seen that our study is compatible with the literature. Dilek and Akpınar [24] investigated the effect of using waste bricks and glass as aggregates instead of normal aggregates on cement mortars. They obtained compressive strengths of 29.3 and 36.2 MPa in mortars where 100% of waste bricks and glass were used in 28 days. Although he received 30.24% and 13.81% lower compressive strength than the control sample, he received a significant result for a sustainable future. On the other hand, economy is one of the most critical criteria for determining building materials for engineering applications. When considered in terms of economy, cement has a significant share. From this perspective, the study results are promising for the future.

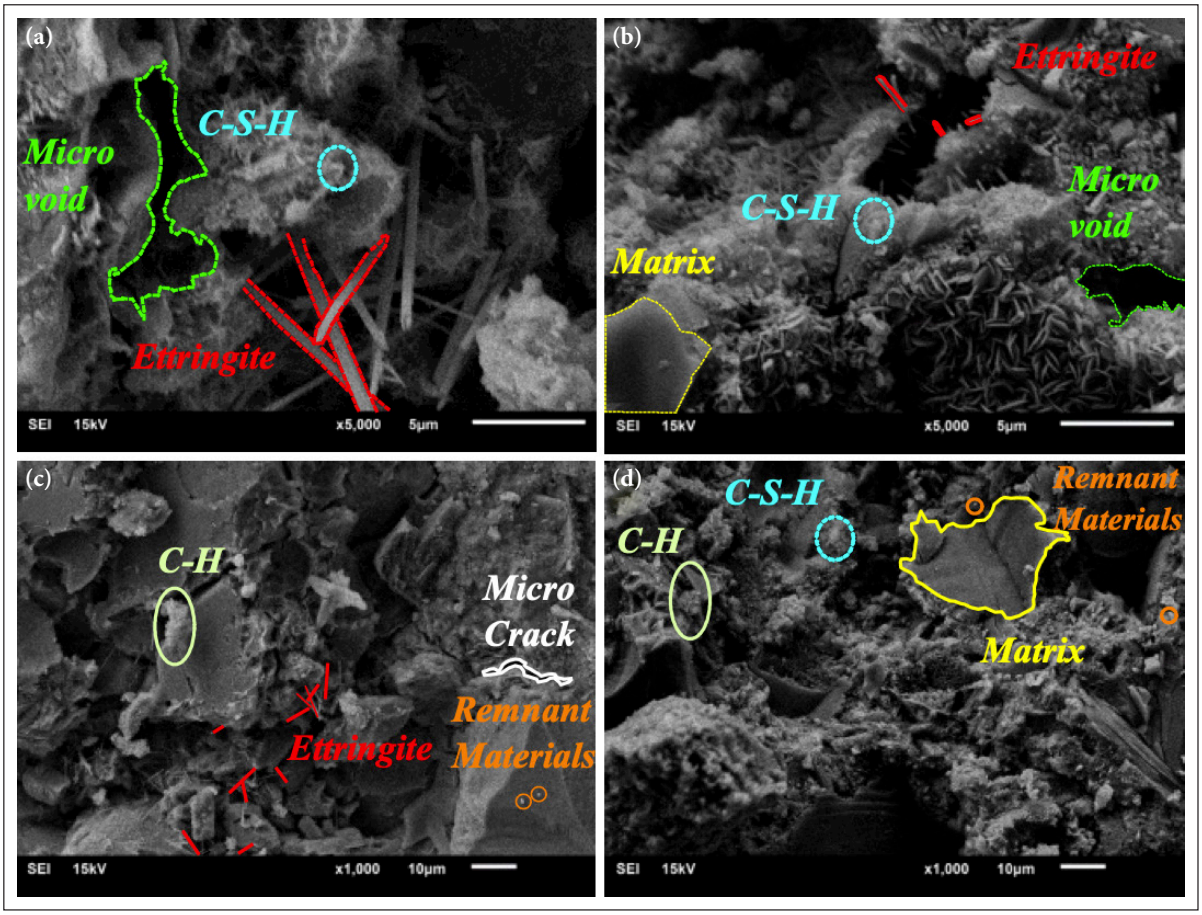

Figure 6. SEM images of S1-28 and S4-28 mortar samples.

3.2. XRD Analysis

The variables are monochromatic wavelength λ Cu-K-beta, model PW1830, 4°–90° 2Θ° angle range with automatic database for XRD analysis. 28-day-old cement and obsidian containing different mortar samples were scanned. The XRD patterns of the samples and their crystal structures are shown in Figure 5. When the model is examined in general, it is noteworthy that the most essential and central peak is Quarz (SiO_2), as well as the presence of structures such as CH-Portlandite and ettringite, which are hydration products. In the XRD model, it is seen that there are no non-hydrated materials, such as C_3S and C_2S, which are the primary base materials of the cement [25]. This indicates that the cement reacted completely and formed hydration products. Mortars containing obsidian, on the other hand, do not include any non-hydrated products. This suggests that obsidian substitution has no adverse effect on gel formation. Also, obsidian forms C-S-H gels by connecting free $Ca(OH)_2$ with its high SiO_2 content. Compared to the reference sample S1-28, the S4-28 sample with 30% obsidian substitution shows a decline in CH density and a rise in C-S-H content [26, 27]. It is thought that the primary source of quartz peaks in both mixtures in the XRD model is due to the CEN standard sand used in the mix.

3.3. SEM Analysis

28-day-old S1 mortar specimens containing 100% cement and S4 mortar specimens containing 30% obsidian substitution were analyzed using SEM to search the microstructural features. Figure 6 shows x1000 and x5000 zoomed SEM images of different regions. When the S1 sample containing 100% cement in Figure 6a is examined, the presence of microvoids, C-S-H gel, and ettringite structures in the structure is noteworthy. In Figure 6b, the structure of specimen S4 with 30% obsidian substitution shows C-S-H gel, micro-void, matrix, and ettringite structures similar to specimen S1. Etrengite is formed as a result of reactions between gypsum and aluminate phase. When gypsum is depleted, the remaining aluminate phase reacts with etrengite to form monosulfates or AFm [28]. As the density of these structures increases, the materials' mechanical and durability properties are adversely affected. When the dimensions of the structures are examined in detail, the density of ettringite in sample S4 is very low compared to S1. In this case, the compressive strengths obtained from the specimens and SEM images support each other. It is seen that the volume of microvoids in sample S4 is less than in sample S1. It is seen that the density of C-S-H gels in sample S4 is higher compared to sample S1. Figure 5c and Figure 5d show C-H (Portlandite), microcracks, matrix, ettring-

ite, and unreacted materials in samples S1 and S4. It can be seen that the density of unreacted materials in specimen S1 is higher than S4. This is known to have a negative effect on compressive strength. Similarly, the presence of C-H in S1 is higher than in S4. Binder materials with pozzolanic properties contribute to forming new C-S-H by binding C-H [29–31]. The low C-H density in the S4 series shows a relationship between the pozzolanic properties of obsidian. Depending on this situation, the strength properties also increase. The results obtained from SEM images support the results obtained from mechanical tests.

4. CONCLUSION

This work compared the mechanical and microstructural characteristics of cement and obsidian powder substitution mortar specimens. The results obtained from the mechanical testing and microstructural analysis (SEM, XRD) of the mortar specimens helped greatly to know the link between mechanical strength and microstructural characteristics.

The SEM images of the reference specimen and obsidian-substituted mortars clearly show the linear relationship between compressive strength and parameters such as C-S-H gel density, compact structure, low ettringite density, microcracks size, etc. Furthermore, due to the high SiO_2 content of obsidian, a pozzolanic material, the high density of C-S-H peaks in sample S4 in the XRD models of mortar samples demonstrates the favorable influence of pozzolanic materials on the mechanical strength of mortars. The study results show that substituting obsidian in concrete can positively improve mechanical strength in applications where early strength is not required. It is thought that different substitution rates and durability properties of obsidian can be studied in future studies.

ACKNOWLEDGMENTS

The authors of this work acknowledge every author of the works cited in this review.

ETHICS

There are no ethical issues with the publication of this manuscript.

DATA AVAILABILITY STATEMENT

The authors confirm that the data that supports the findings of this study are available within the article. Raw data that support the finding of this study are available from the corresponding author, upon reasonable request.

CONFLICT OF INTEREST

The authors declare that they have no conflict of interest.

FINANCIAL DISCLOSURE

The authors declared that this study has received no financial support.

USE OF AI FOR WRITING ASSISTANCE

Not declared.

PEER-REVIEW

Externally peer-reviewed.

REFERENCES

[1] Kurt, Z., Çakmak, T., Gürbüz, A., & Ustabaş, İ. (2022). Estimating the compressive strength of fly ash added concrete using artificial neural networks. *Celal Bayar Univ J Sci, 18*(4), 365–369.

[2] ISO. (2021). *Strategic Business Plan* (ISO Standart No. ISO/TC 283). https://committee.iso.org/files/live/sites/tc283/files/Documents/ISO_TC_283_Strategic_business_Plan_%20April2022.pdf

[3] Ustabas, İ., Demirci, M., Baltas, H., Demir, Y., Erdogdu, S., Kurt, Z., & Çakmak, T. (2022). Mechanical and radiation attenuation properties of conventional and heavy concrete with diverse aggregate and water/cement ratios. *Građevinar, 74*(8), 635–645. [CrossRef]

[4] Lee, N. K., Jang, J. G., & Lee, H. K. (2014). Shrinkage characteristics of alkali-activated fly ash/slag paste and mortar at early ages. *Cem Concr Compos, 53*, 239–248. [CrossRef]

[5] Kurt, Z., Ustabas, İ., & Çakmak, T. (2023). Novel binder material in geopolymer mortar production: Obsidian stone powder. *Struct Concr, 24*(4), 5600–5613. [CrossRef]

[6] Erdoğan, S. T., & Sağlık, A. Ü. (2013). Early-age activation of cement pastes and mortars containing ground perlite as a pozzolan. *Cem Concr Compos, 38*, 29–39. [CrossRef]

[7] Mielenz, R. C., Greene, K. T., & Schieltz, N. C. (1951). Natural pozzolans for concrete. *Econ Geol, 46*, 311–328. [CrossRef]

[8] Scholer, A., Lothenbach, B., Winnefeld, F., & Zajac, M. (2015). Hydration of quaternary Portland cement blends containing blast-furnace slag, siliceous fly ash and limestone powder. *Cem Concr Compos, 55*, 374–382. [CrossRef]

[9] Uzal, B., Turanlı, L., Yücel, H., Göncüoğlu, M. C., & Çulfaz, A. (2010). Pozzolanic activity of clinoptilolite: A comparative study with silica fume, fly ash and a non-zeolitic natural pozzolan. *Cem Concr Res, 40*, 398–404. [CrossRef]

[10] Caputo, D., Liguori, B., & Colella, C. (2008). Some advances in understanding the pozzolanic activity of zeolites: The effect of zeolite structure. *Cem Concr Compos, 30*, 455–462. [CrossRef]

[11] Marjanović, M., Komljenović, Z., Baščarević, V., Nikolić, R., & Petrović, N. (2015). Physical–mechanical and microstructural properties of alkali-activated fly ash–blast furnace slag blends. *Ceram Int, 41*, 1421–1435. [CrossRef]

[12] Ustabaş, İ. (2018). Effect of mineral additive use on permeation properties of concrete and the relationship between permeation and carbonation. *Turk J Mater, 3*(1), 38–52.

[13] Ustabaş, İ., & Ömür, İ. (2019). The effect of obsidian from Rize region on the hydration temperature of cement. *Nevsehir J Sci Technol, 8*, 78–87. [CrossRef]

[14] Keçek, İ., Özcan, A., Toprak, M. U., & Demirbilek, M. (2023). The use of Kütahya Çayca Tuff as a mineral additive to cement. *J Gumushane Univ Inst Sci Technol, 13*(2), 432–443.

[15] Zhao, Y., Gao, J., Liu, C., Chen, X., & Xu, Z. (2020). The particle-size effect of waste clay brick powder on its pozzolanic activity and properties of blended cement. *J Clean Prod, 242*, 118521. [CrossRef]

[16] Çullu, M., Bolat, H., Vural, A., & Tuncer, E. (2016). Investigation of pozzolanic activity of volcanic rocks from the northeast of the Black Sea. *Sci Eng Compos Mater, 23*(3), 315–323. [CrossRef]

[17] Araújo, R. A., de Menezes, A. L. R., Cabral, K. C., Nóbrega, A. K. C., Martinelli, A. E., & Dantas, K. G. M. (2019). Evaluation of the pozzolanic activity of red ceramic waste using mechanical and physicochemical methods. *Cerâmica, 65*, 461–469. [CrossRef]

[18] Aruntas, H. Y., Şahinöz, M., & Dayı, M. (2024). Investigation of the effect of ground blast furnace slag and slaked lime on cement dough and mortar properties. *J Polytech*. Advance online publication.

[19] ASTM Int. (2011). Standard test method for compressive strength of hydraulic cement mortars (Using 2-in. or [50-mm] Cube Specimens) (ASTM C109/C109M-11).

[20] ASTM Int. (2012). Standard specification for coal fly ash and raw or calcined natural pozzolan for use in concrete (ASTM C618-12a).

[21] Turkish Standards Institute. (2012). *Cement - Section 1: Compound, properties and conformity criteria of general cements* (TS EN 197-1:2012).

[22] ASTM Int. (2007). Standard specification for mortar for unit masonry. *United States American Society for Testing and Materials*, 2–13 (ASTM C270).

[23] Pehlivan, H. (2023). Kalsine kil katkılı çimento harçlarının üretiminde nano silika kullanımının araştırılması. *Euroasia J Math Eng Nat Med Sci, 10*(28), 1–12.

[24] Dilek, H., & Akpınar, P. (2023). A comparative study on the use of waste brick and glass in cement mortars and their effects on strength properties. *J Sustain Const Mater Technol, 8*(4), 269–277. [CrossRef]

[25] Koçak, Y. (2016). Effects of superplasticizer and trace on cement hydration. *Pamukkale Univ J Eng Sci, 23*(3), 184–192. [CrossRef]

[26] Dorum, A., Koçak, Y., Yılmaz, B., & Uçar, A. (2009). Effects of blast furnace slag on cement surface properties and hydration. *J Sci Technol Dumlupınar Univ*, (019), 47–58.

[27] Uzbaş, B., & Aydın, A. C. (2018). Investigation of mechanical properties of concrete with fly ash and silica fume by XRD. *Sinop Univ J Sci Technol, 3*(2), 1–22.

[28] Demirel, Ö., & Demirhan, S. (2021). Investigation of microstructural properties of high-volume fly ash blended cement mortars including micronized calcite. *J Fac Eng Archit Gazi Univ, 36*(4), 2255–2269.

[29] Kırgız, M. S. (2011). Literature research on the determination of hydration compounds of substituted and admixed cement pastes using scanning electron microscopy. *J Eskisehir Osmangazi Univ Fac Eng Archit, 24*(1), 72–90.

[30] Dorum, A., Koçak, Y., Yılmaz, B., & Uçar, A. (2010). The effect of electrokinetic properties on fly ash additive cement hydration. *Gazi Univ J Fac Eng Archit, 25*(3), 449–457.

[31] Günel, G., Alakara, E. H., Demir, İ., & Sevim, O. (2024). Effect of recycled cement mortar powder on cement-bonded composites. *Polytech J, 27*(2), 533–543. [CrossRef]

J Sustain Const Mater Technol, Vol. 9, Issue. 2, pp. 177–198, June 2024

Journal of Sustainable Construction Materials and Technologies
Web page info: https://jscmt.yildiz.edu.tr
DOI: 10.47481/jscmt.1363935

JSCMT
Journal of Sustainable Construction Materials and Technologies

Research Article

Analyzing an efficient mix design for the production of quality asphalt concrete: A means of reducing roads' maintenance cost

Abiodun Joseph KILANI*[1], Akinniyi Akinjide ADELANI[2], Oladipupo Seun OLADEJO[3], Bolanle Deborah IKOTUN[1], Ademilade OLUBAMBI[4]

[1]Department of Civil Engineering, University of South Africa, Florida Campus, South Africa
[2]Department of Civil Engineering, Federal University of Technology, Akure, Ondo State, Nigeria
[3]Department of Civil Engineering, Ladoke Akintola University of Technology, Ogbomoso, Nigeria
[4]Department of Civil Engineering Science, University of Johannesburg, Auckland Park Kingsway Campus, South Africa

ARTICLE INFO

Article history
Received: 25 September 2023
Revised: 29 April 2024
Accepted: 07 May 2024

Key words:
Aggregates, asphalt concrete, binder and wearing course, cost estimation, mix design

ABSTRACT

Poor road design is the bedrock for strength deformation and formation of potholes in road pavement systems. The best choice of aggregates for asphalt concrete production contributes significantly to road pavement stability, sustainability, and durability at its serviceability lifestyle. The use of critical design and analysis techniques for the production of asphalt concrete is one of the standard means of eradicating the defect of roads' pavement deformation in the global construction industries. This study reveals the hidden knowledge about the standard formulation and mix design required for producing durable asphaltic concrete pavements. In the experiment, three different mix designs were used to make quality asphalt concrete for the road's binder pavement construction. This was done to ascertain the best quality aggregates required to produce durable asphalt concrete to construct binder road's pavement. Also, the aggregates used for the production of quality asphalt concrete for the construction of road's wearing course pavements were formulated using two mix designs. The results of the experiments proved that the asphalt concrete made with the aggregate formulated for the binder course from the first mix design yielded the best outcome, which is suggested for the global production of quality and standard asphalt concrete for road' binder pavements' construction. Although the formulated aggregates for the wearing course's asphalt production were made from the two mix designs, however, the obtained results from the first mix design were satisfactory fell within the specified limits. This made it the best mix design for industrial practice. In addition, the accuracy and efficiency of the results obtained relied so much on the standard of estimation made to produce quality asphalt concrete, which cost up to $270,830.00 at Chainages 26 + 700 to 26 + 925. All the experimental results proved that application of standard aggregates' mix design in road pavement construction helps in preventing the problems of deformation, cracks, and other defects on the roads' pavement system. Also, applying the first formulated mix design used in this study will help in maintaining the sustainable, durable, stable, and flexible road pavement in the global communities. Likewise, the government's constant expenditure on road pavement maintenance will be reduced.

Cite this article as: Kilani, A. J., Adelani, A. A., Seun Oladejo, O., Ikotun, B. D., & Olubambi, A. (2024). Analyzing an efficient mix design for the production of quality asphalt concrete: A means of reducing roads' maintenance cost. *J Sustain Const Mater Technol*, 9(2), 177–198.

***Corresponding author.**
*E-mail address: abiodun_kilani@yahoo.com

1. INTRODUCTION

Asphalt concrete is a composite mixture of aggregates with standard mineral resources banded together with asphalt and Portland cement or epoxy [1]. As investigated by [2], a material with the potential capacity to revolutionize the method of road construction is known as asphaltic cement (hot mixed). It consists of aggregates mixed uniformly with asphalt–cement coated. Asphalt concrete possesses some potential properties that make it durable and last longer. Lying of asphalt – concrete, on road courses has been improving the level of road surfaces and smoothing them against damage. The smooth road surface is commonly constructed with little expense and high-standard quality asphalt for easy transportation of goods and services [3]. In the construction industries today, asphaltic concrete surfaces (binder and wearing courses) are referred to as the most durable surfaces typically constructed for the smooth driving of automobiles and transportation of goods and services. Asphalt is a versatile material with suitable properties for construction purposes. Its suitability is the construction of durable and flexible pavements that are far better for automobile rides than other pavements built from recycle and non-durable materials such as green asphalt and cement-concrete pavements. Riding on asphalt concrete pavement reduces the effects of tear and wear on vehicles and increases the efficiency of fuel used by car riding, making it more durable [4]. In residential lodges, manufacturing companies, and construction industries, asphaltic concrete is used to construct internal roads, inside and outer access, the floor of motor park centers, and the seal of water lodge buildings.

According to [5], road pavement analysis and design were carried out from the 1950s to the 1993s using the old version of the highway design manual of the American Association of the State, popularly known as AASHTO [5]. AASHTO manual was established to control the quality of asphalt produced for road pavement construction under the American Highways and geometrical design association [6]. Although AASHTO is a good manual for road pavement construction, some of its limitations reduce its efficient performance in service. One of its limitations is that it has no complex mix design for standard asphalt concrete production like the one in the recent AASHTO design manual. In the early 1990s, a Superpave asphalt concrete mix design was introduced into the construction system organized for road binder course classification. A Superpave road system is referred to as a road pavement with highly superior performing asphalt concrete built for smooth transportation of vehicles [7]. The Superpave road system was implemented by a research programming group for highway strategic design to reduce the rate of premature failure of the road pavement and the cost of its maintenance [8]. Despite the efficient strategic mix design introduced into the system and the application of suitable aggregates for the road's binder pavement construction, aggregate load stresses were still not reduced to the expected level. Instead, they were prone to more failures, resulting in creeping, cracking, and deflection of road pavement. To remove the problem of road pavement deformation, earlier before establishing the Superpave system, the Hveem mix design was introduced into the asphalt concrete production system. This mixed design (Hveem mix design) is a design technique established by a resident engineer called Francis Hveem, who worked as a highways engineer at the highways division of California in the United States of America (USA) in 1920–1930. Hveem mix design was established to use high quantities of asphalt binder to produce firmly thick asphalt concrete. This type of concrete has less strength to withstand stress from vehicles during loading, thus resulting in pavement deformation [9, 10]. Any deformation from the pavement produced by the Hveem mix design can lead to a high cost of maintenance. The Superpave design method is far better than this method.

In further investigations to remove this problem of road pavement deformation from highway systems, [11] designed and modeled the responses of asphalt concrete aggregates against deformation. It was conducted for pavement loading stages to work against deformations reflected from high temperatures and mixes' viscoelasticity asphalt pavement. The process was achieved using the finite element model. Yet, the model's efficiency against those defects was not totally met. Most of these tests were carried out using a specified mix design of AASHTO for binder and wearing layers of the roads' pavement [12]. Having observed deviations from the expected road pavement construction standards, a better aggregate mix design is required for the road pavement system's stability, sustainability, and durability. Thus, this is the trust of this study.

From the practical point of view, most of the maintenance works on road structures these days are commonly initiated by improper mix designs of asphaltic concrete aggregates, its poor production, their inaccurate mixing, their poor methods of laying and compacting courses of asphalt on road surfaces, and its poor aggregates durability confirmation. These defects have caused much damage to global societies, organizations, and industries. Among the damages are sudden accidents, potholes formation, vehicle parts destruction, and road surface swaying. The above damages have called for other standard alternatives for the smooth transportation of goods and services globally. At that time, other available means of transportation were heavily affected, and they were too loaded and busy. This has been increasing the road maintenance culture globally, thus inflating the price of goods and services transported and increasing the sale price of goods and commodities globally, most especially in Nigeria. This study aims to develop and analyze a global standard mix design for the production of quality asphalt concrete. It also help in minimizing the high cost of asphalt concrete for road pavement construction in the global international market. In connection with the aim, this study (1) determines the quality of the materials for asphalt concrete production, (2) actualizes the accurate mix design best for the production of asphalt concrete, (3) develops a new standard method at which asphaltic concrete can be produced to fall within the limit of recommended specification. (4) ascertain the quantity, quality, and cost of

Figure 1. **(a)** Set of Sieves **(b)** Sieve Shaking Machine **(c)** Weighing Balances **(d)** Bitumen Extraction Machine **(e)** Thermometer **(f)** Marshall Testing Machine.

asphalt concrete laid on road courses through the use of leveling instrument.

2. MATERIALS AND METHODS

2.1. Materials and Equipment

The materials and equipment used in this experiment are crushed aggregates of sizes ¾", ½", and 3/8"; quarry dust, uncrushed aggregate (sharp sand), bitumen, filler (soft sand), bitumen extraction machine, Marshall Testing machine, weighing balances, scapular, set of sieves, thermometer, leveling instrument, reading staff, site record book, and asphalt production plant. Some of these equipments are shown in Figure 1. For further clarification, a set of sieves is equipment with square apertures and wire screens, rigidly woven together in a cylindrical metal frame, generally used to determine the sizes of particles such as sand, gravel, and soil [13]. A sieve shaking machine is a device upon which a set of sieves is placed for efficient sieving of particles under steady power loading. Also, a weighing balance is a machine used to determine the mass of a particle, object, or material to calculate its weight easily. A bitumen extracting machine is a device that is usually used to remove the total quantities of bitumen from asphaltic concrete at a controlled temperature by extracting solvents such as petrol and kerosene. Likewise, a thermometer is a device used to determine the degree of hotness or coldness of the body or an object. In asphalt concrete production companies, it is usually used to assess the degree of hotness of asphalt produced before laying it as pavement on the road surface.

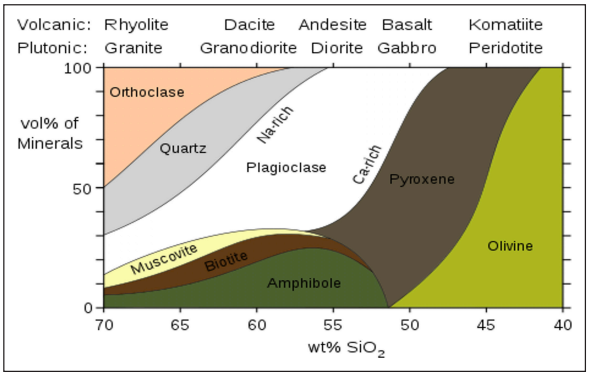

Figure 2. The levels of igneous rock assemblage of minerals [11].

2.1.1. Crushed Aggregates (Granite) of Sizes ¾", ½" and 3/8" Descriptions

Granite is a coarse-grained material extracted from hard igneous rock. It consists of microcline or orthoclase, mica, and quartz minerals. Granite is one of the most durable, oldest building materials. It is essentially used for offices and home luxuries because of its endurable beauty [14]. According to [15], granite is a grain stone called granum in Latin word. It is normally extracted from granitic rock that consists of major minerals such as amphibole, mica, quartz, and feldspar, which influence the interlocking process of the granite. Amphibole and mica formed the color minerals during the interlocking process, while quartz and feldspar formed the scattered dark biotite, often called hornblende. The coarse grain and a lighter–colored igneous rock is generally called Granitoid. A porphyritic texture granitic rock is known as granite porphyry [16]. The levels of igneous rock assemblage of minerals were presented as shown in Figure 2. The QAPF diagram of coarse-grained rocks was labeled according to the quantities of plagioclase feldspar alkali and quartz in half of the diagram. As alkali modern petrologic convention states, true granite consists of 35 to 90% of feldspar and 20–60% of quartz by volume.

The granitic rocks with more than 60% quartz are classified as quartz-rich granitoid or quartzite [17–19]. A typical granite (or metaluminous granite) is granite that is made up of alkali and aluminum metals, most especially potassium and sodium, as shown in the chemical reaction of $K_2O+Na_2O+CaO>Al_2O_3>K_2O+Na_2O$.The granite with less aluminum that developed into feldspar with alkali oxides, as shown in the chemical reaction of $Al_2O_3<K_2O+Na_2O$, is referred to as Peralkaline [20]. Granite possesses an average density of 2.65 to 2.75 g/cm^3 [21, 22]. It has over 200MPa compressive strength with a viscosity of 3 to 6 x 10^{20}Pa.S [23]. A dry granite melt at ambient pressure and temperature of 1215–1260^{0}C (2219–2300^{0}F) [24]. The melting temperature is usually reduced to 650^{0}C with the presence of water. Granite is poor in primary permeability but performs better in secondary permeability through fractures and cracks [25, 26].

2.1.1.1. Chemical Composition and Classifications of Crushed and Uncrushed Aggregates

Globally, the chemical composition of granite based on 2485 analyses was presented as shown in Table 1.

A ¾" crushed aggregate is a material for road and concrete construction with a 19.1mm size crush size. It is made of large stones and can be used to construct a base or sub-base in road pavement construction. It was classified as coarse gravel since its aggregate sizes fall between 16–64 mm and 19.1mm. It is also usually used to produce high-strength concrete [27, 28]. Likewise, the crushed aggregate of ½" size (12.5 mm) was classified as medium gravel due to its size gradation that is within 8–16 mm according to [27] and [28] classification. It is commonly used to supplement the performance of ¾" aggregate for high strength yielding during road pavement construction. With this, the base and sub-base materials of the road will be stronger and compatible. Also, the 3/8 crushed aggregate was classified into a medium gravel category ranging from 8–16 mm. Majorly, using ½" and 3/8" crushed aggregates supplements the structural function of ¾" aggregate in producing high-quality asphaltic concrete.

Moreover, the aggregates ranging from 2.36 mm to 0.6 mm were classified into coarse sand (uncrushed). ASTM classification states that 2.0 mm–0.5 mm of uncrushed aggregate is categorized and grouped into coarse sand material. The other uncrushed materials were sized to 0.30–0.075 mm and classified into fine sand and quarry dust. According to [28], the specified limit for these groups (other uncrushed materials) ranged from 0.25 mm–0.06 mm.

The mixture of these aggregates for asphalt production for road construction has highly increased the strength of the road surface pavement, especially the binder course. The classification of the aggregates used in this study proved to be of high quality and fit for experimental investigation and road courses" construction (binder and wearing courses). A quarry dust is defined as a waste obtained when the coarse aggregate (crushed granite) from rock material is being processed into sizes at the quarry [29]. The quarry dust used in this study was classified into 2.0–0.5 mm due to its presence of fine particles. They usually replaced sand (fine aggregate) for asphalt and concrete productions. It is gray and of grade A standard. It has no packaging type, but its formation is in the form of chips [28, 30]. The uncrushed material produced by asphalt concrete in this study is sharp sand. Sand is a granular loose material generally obtained from the disintegration of rock, which consists of smaller particles than gravel but has coarseness than silt and can be used to produce abrasive, mortar, and foundry molding [31]. The size of sand used in this experiment is 2.36–0.6 mm. Figure 3 shows the images of granite, sharp sand, and quarry dust used in this study.

Table 1. Chemical composition of granite [15]

Composition	SiO_2 (Silica)	Al_2O_3 Alumina	K_2O	Na_2O	CaO	FeO	Fe_2O_3	MgO	TiO_2	P_2O_5	MnO
% Constituent (%)	72.04	14.42	4.12	3.69	1.82	1.68	1.22	0.71	0.30	0.12	0.05

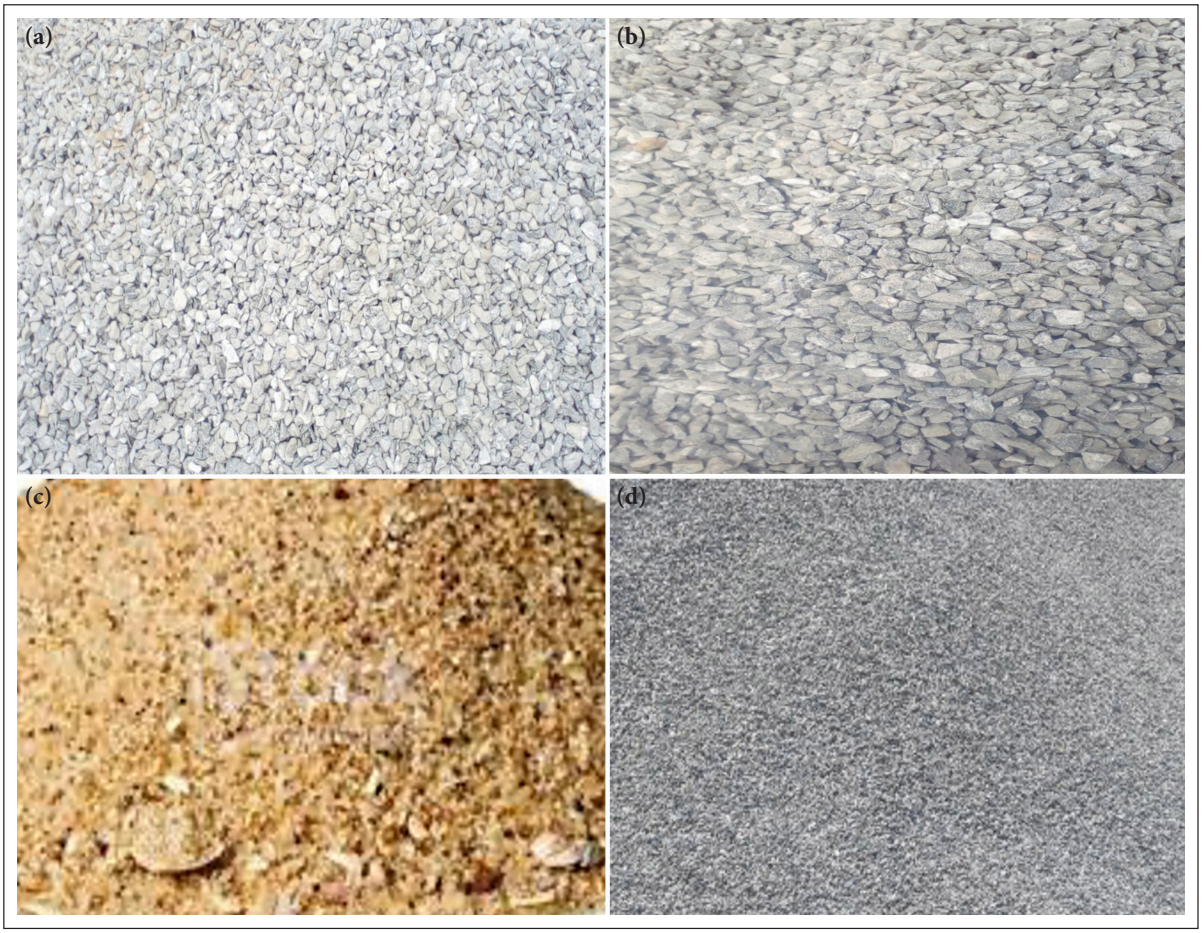

Figure 3. **(a)** Crushed Aggregate (1/2" granite) **(b)** Crushed aggregate (3/4" granite) **(c)** Sharp Sand **(d)** Quarry Dust.

2.1.2. Aggregates and Their Treatments

The crushed aggregates (sizes ¾", ½", and 3/8") used in this investigation were obtained from a quarry site very close to Okin, Oko, Ogbomoso, Oyo State, Nigeria. The obtained crushed aggregates were air-dried for four weeks in a cool, dry place around the quarry site. The air-dried aggregates were oven-dried again under 105 ^{0}C temperature to remove its optimum moisture content. The dried aggregates were removed from the oven, allowed to cool, and sieved to remove the clay particles and broken bottles. The sieved aggregates were stored around the quarry site in a cool, dry place. Also, the quarry dust used to produce asphalt concrete in this study was obtained from a quarry that belongs to Dutum Company Nigeria Limited at Okin, Oko, Ogbomoso, Oyo State, Nigeria. The same crushed aggregate treatment (granite) procedure was adopted for quarry dust treatment. Furthermore, the sand used in this research was obtained from a stream close to Dutum Company's quarry site at Okin, Ogbomoso. It was also Sun-dried for two weeks (14 days) like granite to dry its moisture content completely. The dried sand was sieved and kept in a cool, dry place until its usage. Likewise, the soft sand (filler) used in this investigation was to supplement the binding properties of asphalt aggregates for better production of quality asphalt. The soft sand was obtained around the Okin quarry site. The soft sand was treated as that of sharp sand. For standard production of asphalt concrete, the quality of bitumen supplied from the market were determined using the specified limit of 60–70 mm, 80–100 mm, 40–50 mm, 130–150 mm, and 180–200 mm.

2.2. Methodology

2.2.1. Determination of Quality of Bitumen Supplied for Asphalt Concrete Production

The higher the quality of bitumen is, the greater the quality of asphalt concrete that will be produced from it. Also, the more complex the needle penetration into the bitumen supplied, the higher the quality of the provided bitumen for asphalt concrete production. As conducted in the experiment, the quality of the provided 60–70 mm grade of bitumen with a heating temperature limit of 160–175 ^{0}C was determined through the bitumen penetration testing method. The small bitumen was taken into a small Can and heated to 150 ^{0}C on a Bunsen burner. The heated bitumen was poured into two or more Cans in equal quantities and cooled at 20 ^{0}C to 25 ^{0}C. The bitumen penetration machine was set in a good position for the experiment. The hap of plumb was attached to a penetrometer (penetration machine) at the base to maintain stability. The pin-tip of the penetration needle was well-positioned for easy penetration. The penetrometer

Table 2. First asphalt mix design for road binder course laying

Aggregate used with sizes (in inches)	Constituent (%)
¾" Aggregate (granite, crushed)	27
½" Aggregate (crushed)	18
3/8" Aggregate (crushed)	11
Quarry dust (uncrushed)	31.1
Sharp sand (uncrushed)	8
Bitumen content	4.9
Total	100

Table 3. Second asphalt mix design for road binder course laying

Aggregate used with sizes (in inches)	Constituent (%)
¾" Aggregate (granite, crushed)	25
½" Aggregate (crushed)	10
3/8" Aggregate (crushed)	13
Quarry dust (uncrushed)	37.4
Sharp sand (uncrushed)	10
Bitumen content	4.6
Total	100

was set to zero (0) to avoid inaccuracy in the reading results. Then, the pin-tip of the needle was set to coincide with that of the rod from the penetration scale and set to zero (0). The penetrometer rod was then released quickly and allowed to press the bitumen in the Can for 5 seconds. Immediately, the needle penetration was stopped at precisely 5 minutes. A rod positioned at the back of the penetration machine was pressed to touch the rod from the tip of the needle. Then, the needle penetration reading was taken immediately. This procedure was adopted and followed repeatedly for all the bitumen samples tested. The penetration values were measured in millimeters and recorded accordingly.

2.2.2. Asphalt Mix Design

The three mix proportions produced asphalt concrete for the road's binder pavement construction. For the construction of wearing pavement, two mix proportions were used to experiment with the quality production of asphalt pavement for the construction of Oko – Ogbomoso - Osogbo road by Dutum Company Nigeria Limited in agreement with ASTM: D692/D692M-20, D242/D242M-19 and D1073-16(2022) standard for the use of coarse aggregates, filler and fine aggregates for the production of asphalt concrete for road pavements construction respectively [32]; following the specification of FMW (1994)'s standard. After analyzing the asphaltic concrete aggregates, the best mix proportion among the three proportions used for producing asphaltic concrete was adopted for quality asphalt production. The best mix design was also adopted for the production of asphalt concrete for the road pavement wearing course's construction from the two mix designs evaluated.

2.2.2.1. Asphalt Concrete Mix Proportion for Binder Course

The first to the third trial mixes produced concrete at a quarry site around Okin-Oko, Ogbomoso. For efficient asphalt production, the crushed and uncrushed aggregates were placed into the asphalt plant in percentages, and asphalt concrete was produced using the three-mix design. During the first mix, ¾" aggregate (crushed) was placed inside the asphalt plant's mixer, occupying up to 27% of the total aggregates. Following this, about 18% of ½" aggregate (crushed) was placed inside the same asphalt plant's mixer. The two aggregates in the mixer were thoroughly mixed and prepared for the next stage. Then, about 11% of 3/8" aggregate (crushed) was added to the mixture of the aggregates in the asphalt plant mixer, and all the aggregates were thoroughly mixed for the second time. After a while, 31.1% and 8% of quarry dust and sharp sand were also added to the mixed aggregates in the asphalt plant mixer. All the aggregates (crushed and uncrushed) in the asphalt production plant's mixer were re-mixed for the third time to have a homogeneous composite. Then, about 4.9% of bitumen was added to the mixed aggregates in the asphalt plant mixer, remixed several times, and heated at high temperatures to produce quality asphalt concrete. Concrete was produced after the aggregates with bitumen have passed through the several stages of industrial processes in the asphalt plant. The concrete produced was discharged into the Lorries, transported them to the site where the pavements will be constructed. The mix designed adopted for this asphalt production is presented in Table 2. The second and third trial mixes were experimented following the steps used to produce asphalt concrete in the first mix design. Here, the aggregate mix proportion used to produce asphalt concrete differs from that of the first trial mix. This second trial mix comprises 25%, 10%, and 13% of ¾", ½", and 3/8" crushed aggregates and 37.4% and 10% of quarry dust and sand res, respectively. Also, the percentage of the bitumen added was about 4.6%. This percentage (4.6%) is lower than the first mix design. The third mix design used 27%, 15%, and 11% of ¾", ½", and 3/8"crushed aggregate, respectively. As used in the experiment, the sand and quarry dust percentages included in the mix were 10% and 32.2%, respectively. 4.8% of bitumen was added to the mixed aggregates before the aggregate's final processed to produce asphalt concrete for the binder pavement construction. This value (4.8%) is more than the percentage used in the second mix design (4.6%) by 0.2%. Tables 2–4 present the mix proportions for the production of asphalt concrete from first to third mix designs. To produce quality asphalt concrete for road-wearing pavement construction, the above procedures used for producing asphalt concrete for binder pavement construction were adopted. During the mixing of aggregates to produce asphalt concrete for wearing pavement construction, the volume of sand included in the mix was reduced, and that of quarry dust was increased. As shown in Table 5, 20% of ¾"–½" of crushed aggregate was used for the investigation, while the ½"–3/8" of crushed aggregates used were up to 27%. For smooth concrete production, 10% of sand and 42.2% of quarry dust were mixed thoroughly with the measure aggregates in the mixer to form a uniform composite. The initial mixed aggregates were mixed again thoroughly with 5.8% bitumen for the second time, after which it passed through series of stages before the asphalt concrete was produced. The asphalt concrete produced was

Table 4. Third asphalt mix design for road binder course laying

Aggregate used with sizes (in inches)	Constituent (%)
¾" Aggregate (granite, crushed)	27
½" Aggregate (crushed)	15
3/8" Aggregate (crushed)	11
Quarry dust (uncrushed)	32.2
Sharp sand (uncrushed)	10
Bitumen content	4.8
Total	100

Table 5. Asphalt mix design for road wearing course lying (first mix design)

Aggregate used with sizes (in inches)	Constituent (%)
¾" – ½"Aggregate (crushed)	20
½" – 3/8" Aggregate (crushed)	27
Quarry dust (uncrushed)	37.2
Sharp/soft sand (Filler) (uncrushed)	10
Bitumen content	5.8
Total	100

Table 6. Asphalt mix design for road wearing course lying (second mix design)

Aggregate used with sizes (in inches)	Constituent (%)
¾" – ½"Aggregate (crushed)	18
½" – 3/8" Aggregate (crushed)	22
Quarry dust (uncrushed)	49.4
Sharp/soft sand (Filler) (uncrushed)	5
Bitumen content	5.6
Total	100

transported to the site where the road-wearing pavement will be constructed. The second mix design was experimented with, to produce asphalt concrete for the construction of road's wearing course's pavement according to the proportion stated in Table 6.

2.2.3. Extraction Test and Asphalt Grain Analysis

2.2.3.1. Bitumen Extraction Test

The extraction of bitumen content from the freshly produced asphalt concrete was carried out to ascertain the quantity and quality of bitumen used to produce asphalt concrete for the sustainability of the Oko-Ogbomoso-Osogbo road which was under construction then in Nigeria. The following procedures were adopted: extract of bitumen from the asphalt concrete produced using three different mix designs. During the investigation, a certain quantity of asphalt concrete was taken from an asphalt production plant at Okin, Oko-Ogbomoso, Oyo State, Nigeria. The collected samples were heated on the bursen burner until their heat temperature read 150 ^{0}C on the thermometer. Then, the riffle box apparatus was set out to distribute the heated asphalt concrete evenly for easy testing. In each of the extraction test carried out, 1200 g of heated asphalt was measured on a weighing balance. The weighed samples were placed on clean trays and correctly positioned for testing. Also, the filter disc paper, which was used to protect the weighed sample from losing or dropping out during the bitumen extraction was weighed on a scale. The earlier measured 1200g heated asphalt concrete sample was transferred into the rotor bowl inside the centrifuge bitumen extracting machine. The weight of asphalt, together with that of the rotor bowl, was measured before testing. At that point, the bitumen-extracting machine was well-positioned for the test. After the machine positioning, a bitumen-extracting solvent (petrol or kerosene) was poured on the heated samples, which were earlier transferred into the rotor bowl, after which a new weighed filter disc paper was placed on top of the rotor bowl to prevent it from losing aggregates content of the sample testing. Also, it was used to avoid wasting bitumen during the extraction process. At this stage, the heated samples with solvent and disc paper placed inside the rotor bowl were covered with the extraction machine's lid. Then, the rotor bowl was keyed down with its lid using the nuts and bolts at the edge of the centrifuge bitumen-extracting machine. After properly tightening the nuts and bolts of the machine with the rotor bowl, it was powered on to start the extraction process. In the extraction process, the rotor machine motion speed was controlled, and it was gradually increased. This was done to prevent the escape of extract (solvent with bitumen) from the rotor bowl to the machine operators and laboratory technicians, which can lead to injury or burning of their skin. It was also observed that the higher the speed, the hotter the mixture of asphalt and solvent can lead to a fire outbreak. After 2–5 minutes of extraction, when the solvent might have washed the bitumen from the asphalt concrete away, the extraction machine was stopped, and the dissolved bitumen was drained from the mixture of solvent and asphalt in the rotor bowl. This process was repeated, and more solvent were poured on the aggregate in the bowl until no trace of bitumen was observed in the drained solvent after the extraction. The extraction process was stopped at the total draining of the bitumen from the sample. At the final stage, the extracted solvent was drained from the rotor machine, and the bowl and aggregates remained in the bowl after extractions were brought out from the machine. All the aggregates that escaped during the extraction process from the rotor bowl to the filter paper disc were brushed off into the bowl. Also, all the aggregate in the bowl was oven-dried at a steady and controlled temperature to dry off all its moisture content. After properly drying of the aggregate in the oven, the aggregates were removed, weighed, and kept in a cool, dry place for sieve analysis. At this time, the weight of the filter disc paper was also determined after the extraction process.

2.2.3.2. Sieve Analysis of Extracted Aggregates

After the bitumen extraction, the sieve analysis of asphalt concrete's aggregate was conducted as follows: The dry aggregate was taken from the oven and allowed to cool for some minutes. The specified sets of sieves, ranging from 3/4" (19.1 mm) to No. 200 (0.075 mm), were set as shown in Table 7.

Table 7. Sieve sizes arrangement in mm and inches

Sieve sizes in inches	3/4"	½"	3/8"	No. 7	No. 14	No. 100	No. 200
Sieve sizes in mm	19.1	12.7	9.5	2.3	1.18	0.60	0.075 or 75μm

Table 8. Set of sieve size for binder and wearing courses' asphalt aggregates

Source of aggregate	Binder and Wearing Course Aggregates												
Sieve sizes (mm)	38.1	25.4	20.0	12.7	10.0	6.35	2.36	1.18	600 μm	300 μm	150 μm	75 μm	Passing base plate

Then, the sets of sieves were placed on the electronic sieve shaking machine for sieve analysis. The oven-dried extracted aggregates were placed on a 19.1 mm sieve on top of the set. Then, a metallic cover was placed on top of the set sieve and tightened at both edges with the rods beside the sieve sets. The sieve shaker was powered on, and speeds were applied steadily to quickly sieve the aggregates. The retained aggregate on each set of sieves was measured and classified according to size. The values of aggregates from sieve analysis were compared with that of the specified standard stated by the Federal Ministry of Works (Federal Ministry of Works' Road Specification, 1994). The sizes of sieves specified for sieve analysis of the extracted aggregates from asphalt concrete for road binder and wearing course laying are shown in Table 8.

After the bitumen extraction process, the weights of aggregates observed were determined as follows:

The weight of asphalt concrete with solvent and rotor bowl in grams was represented by A, that is,

A = Weight of asphalt concrete + solvent + rotor bowl. The weight of the rotor bowl measured was represented by B, and then, the weight of the mixture (asphalt concrete + solvent) in the bowl was determined using Equation 1.

$$\text{Weight of mixture (asphalt concrete + solvent)}(C) = A - B \quad (1)$$

The weight of filter disc paper before testing was determined to be D, and its value after testing was determined to be E. Therefore, the weight of aggregate retained on the filter paper (F) was calculated using Equation 2.

$$\text{Weight of aggregate retained on the filter paper } (F) = E - D \quad (2)$$

Also, the weight of aggregates in the bowl after the bitumen extraction was G, while the weight of total aggregates in the bowl with filter paper was H. Then, the weight of bitumen in asphalt concrete tested was calculated using Equation 3.

$$\text{Weight of bitumen in asphalt concrete tested} = C - H \quad (3)$$

The percentage of bitumen used on the total weight of mixture (J) was determined using Equation 4.

Percentage of Bitumen used on the total weight of mixture (J)

$$= \frac{\text{Weight of Bitumen}}{\text{Weight of Mixture}} \times 100\%$$

$$= \frac{I}{C} \times 100\% \quad (4)$$

Also, the percentage of bitumen used on dry aggregate mixture was determined using Equation 5.

$$\text{Percentage of Bitumen on dry aggregate} \frac{\text{Weight of Bitumen}}{\text{Weight of Total aggregates in the bowl}} \times 100\% = \frac{I}{H} \times 100\% \quad (5)$$

2.2.4. Surveying Method of Determining the Cost of Asphalt Concrete Laid

The cost of asphalt concrete laid at the construction of the Ogbomoso – Osogbo – Oko Federal road was estimated for using the leveling method of measurement as prescribed by the regulation of the surveying department at Dutum Company Nigeria Limited, which is the contractor of the project. This study only considered the cost estimate of asphalt concrete laid at chainage 26 + 700 to chainage 26 + 925 of the road. During the survey measure, the road surface level was determined and recorded as the initial level before the commencement of asphalt lying. Also, after laying asphaltic concrete, the level of road pavement was retaken to determine the actual volume of asphalt concrete laid. In the leveling processes, the level instrument was fixed on its tripod stand and tight firmly as shown in Figure 4. Then, the leveling device was set accurately to cancel zero error. Then, the level instrument was put on a small pillar at chainage 26 + 700, referred to as the initial total benchmark (TBM). At the initial TBM, the first back sight of the road leveling was taken using staff and level equipment. Also, the road's high curvature (H.P.C.) was determined using a leveling device, staff, and measuring tape. A reduced internal level (R.I.L) of sights measurement was assumed to be 1012.500 for easy calculation. This value was used to determine the level of each point of the road at that location. Likewise, at chainage 26 + 700, around the TBM location, surveying staff was placed at the center of the road tip to do a reading from the level device, referred to as the first inter-sight of surveying measurement. The second inter-sight reading was taken when the staff instrument was placed at the road's right-hand side (R.H.S.), and the level device was used to take a reading from the staff. The following reading from the staff was taken at the road's left-hand side (LHS), called inter-sight reading. The values obtained were used to determine the R.I.L of all the sighted measurements. The above steps were repeated until there was a change of point in the measurement. These processes were carefully followed, and the readings were taken from Centre, RHS, and LHS until chainage 26 + 925 was reached. When there was a change in the reading level taken on the road from the staff sights, the previous foresight (FS) and the new backsight (BS) were taken for the measurement. The values obtained from the readings were tabulated as shown in Table 9.

Figure 4. **(a)** Survey Staff **(b)** Level device fixed on tripod stand **(c)** Taking of road levels by the chief surveyor.

After the asphalt concrete was laid, the above steps and methods were adopted for road leveling. This value was determined by the total volume of asphalt concrete laid (Fig. 5). The volume obtained from sight readings was used to estimate the cost of the asphalt concrete laid from chainage 26 + 700 to chainage 26 + 925, which is about 250 minutes. For accuracy of sight measurement, equation 6 was used to check the efficiency of the recorded values.

3. RESULTS AND DISCUSSIONS

The results of the investigation conducted on the three different aggregates mix designs for asphalt concrete production for binder course lying and that of two mix designs for wearing course pavements construction, together with their estimated costs obtained, are presented as follows.

3.1. Marshall Test Results on Asphalt Concrete for Binder Course

3.1.1. Marshall Test Results of Asphalt Concrete for Binder Course From First Aggregate Mix Design

The laboratory test results of the asphaltic concrete produced from the first mix design are presented in Tables 10, 11 and Figure 5. As shown in Table 10, the percentage of aggregate passing sieve sizes ¾" (19.1 mm), ½" (12.5 mm), 3/8" (9.5 mm), and ¼" (6.5 mm) were recorded as 86.4%, 66.7%, 57.88%, and 49.4% respectively. These values were within the specified limit of 70–100, 55–80, 47–70, and 40–60 percent, as stated by the Federal Ministry of Works and Housing for road-binder course pavement construction (1994). The results show that aggregates from the first mix design used to produce asphalt concrete are valuable with good structural properties to resist the stress generated through loading on road pavement during its serviceability life span (Fig. 5).

The specified limit approved for the aggregate passing sieve sizes No. 7 (2.38 mm), No. 14 (1.18 mm), No. 25 (0.60 mm), and No. 52 (0.30 mm) were ranged as 27–45, 20–34, 14–24 and 8–20 percents respectively by Federal ministry's specification. The percentages of aggregates passing through the sieve mentioned above sizes are 35.6%, 26.2%, 18.2%, and 13.6%, respectively. These values were perfectly fixed to the specified limit stated for the binder course aggregates for road construction according to the specifications of the Federal Ministry of Works and Housing (FMWH) road. The efficiency of these aggregates in road construction (significantly, the binder course) are shown in Figure 6 and are classified as fine aggregates. Likewise, the number of aggregates that passed through sieves No. 100 (0.150

Table 9. Format of recording Level values before and after asphaltic concrete lying

Back Sight (B.S.)	Inter Sight (I.S.)	Fore Sight (F.S.)	High Point of Curvature (HPC)	Reduce Internal Level (R.I.L)	Distance	Remarks

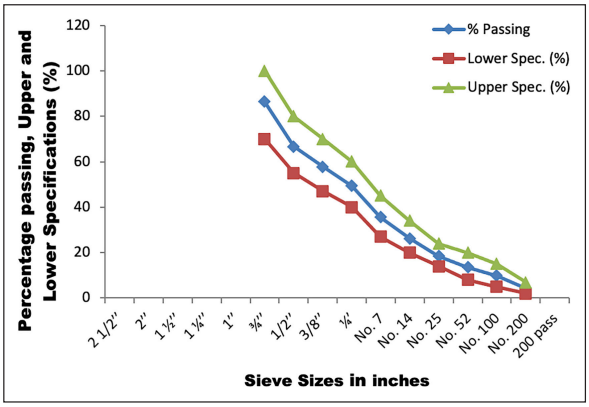

Figure 5. Chart of gradation result of asphalt concrete for road binder course laying from first mix design.

mm) and no. 200 (0.075 mm) also meet the specified limit of 5–15% and 2–7%, as stated for this classification. Aggregate passing through sieve No. 200 is referred to as clay. From the gradation result presented in Table 10, it was observed that all the aggregates used for the experiment were of high quality and suitable for asphalt concrete production for road binder pavement construction. As shown in Figure 6, all the aggregates' values presented were between the middle of the specified limit (envelope) for quality asphalt concrete production. This proves the first concrete mix design efficiently produces quality asphalt concrete for road binder course laying. Thus, this first mix design is highly recommended for global asphalt concrete production for the binder course of the road. As presented in Table 11, the bitumen content in the first mix design of asphalt concrete was calculated to be 4.9%. This is the bitumen content ex-

Table 10. Granisize analysis of asphalt concrete for road binder course laying from first mix design

Sieve size (inch)	Sieve size (mm)	Weight retained (g)	% Retained (%)	% Passing (%)	Specification
2 1/2"	63.5				
2"	50.6				
1 ½"	38.1				
1 ¼"	31.8				
1"	25.4	–	–	–	100
¾"	19.1	155	13.6	86.4	70–100
1/2"	12/7	225	19.7	66.7	55–80
3/8"	9.5	102	8.9	57.8	47–70
¼'	6.5	96	8.4	49.4	40–60
3/16"	4.76				
1/8"	3.45				
No. 7	2.36	157	13.8	35.6	27–45
No. 14	1.18	107	9.4	26.2	20–34
No. 25	0.600	89	7.8	18.4	14–24
No. 36	0.425				
No. 52	0.300	55	4.8	13.6	8–20
No. 72	0.212				
No. 100	0.150	43	3.8	9.8	5–15
No. 200	0.075	63	5.5	4.3	2–7
200 pass	0.075	49	4.3		

Contract: Ogbomoso–Osogbo–Oko Road Project; Sample Ref.: Binder Course; Location: Chainage 26+700 to chainage 26+925; Weight of total aggregate: 1141.4g

Table 11. Extracted Bitumen from asphalt concrete for road binder course laying from the first mix design

Reference	Description	Value	Unit
A	Weight of mixture+bowl	2010	g
B	Weigram bowl	870	g
C	Weight of mixture = A-B	1200	g
D	Weight of filter before testing	0.2	g
E	Weight of filter after testing	0.6	g
F	Weight of material retained by filter = E-D	0.4	g
G	Weight of aggregate in the bowl	1141	g
H	Weight of total aggregate = F+G	1141.4	g
I	Weight of bitumen = C-H	58.6	g
J	% of Bitumen on the total weight of mixture = I/C×100	4.9	%
K	% of Bitumen on dry aggregate = I/H×100	5.1	%

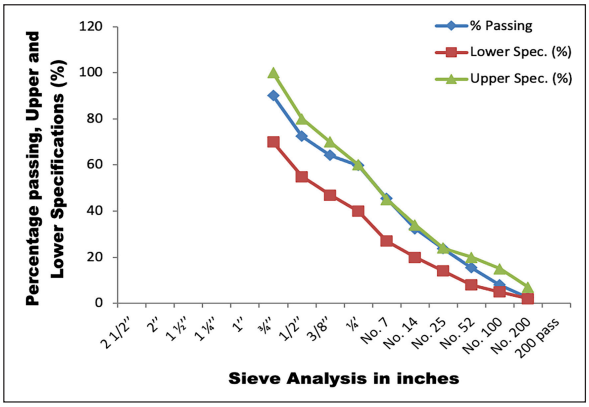

Figure 6. Chart showing the gradation result of asphalt concrete for road binder course laying formed from second mix design Grainsize.

tracted from 1200 g of asphalt concrete sample used. The result obtained is equivalent to the initial percentage used during the production of asphalt concrete (4.9%). As shown in the result, the quality of bitumen used in the first mix is accurate and efficient. The aggregates analysis and bituminous content results show that asphalt concrete produced from the first mix design is of high quality and is an efficient construction of a sustainable road's binder course layer.

3.1.2. Marshall Test Results of Asphalt Concrete for Road Binder Course Laying from Second Mix Design

The result of aggregates' analysis from the second mix design of asphalt concrete was wasted, as shown in Figure 6 and Tables 12, 13.

As shown in Table 12, the percentage of crushed aggregates passing sieve sizes ¾" (19.1 mm), ½" (12.5 mm), 3/8" (9.5 mm), and ¼" (6.5 mm) were 90%, 72.5%, 64.2%, and

Table 12. Grain size analysis of asphalt concrete for road binder course laying from second mix design

Sieve size (inch)	Sieve size (mm)	Weight retained (g)	% Retained (%)	% Passing (%)	Specification
2 1/2"	63.5				
2"	50.6				
1 ½"	38.1				
1 ¼"	31.8				
1"	25.4	–	–	–	100
¾"	19.1	114	10	90	70–100
1/2"	12/7	200	17.5	72.5	55–80
3/8"	9.5	95	8.3	64.2	47–70
¼'	6.5	52	4.5	59.7	40–60
3/16"	4.76				
1/8"	3.45				
No. 7	2.36	164	14.3	45.4	27–45
No. 14	1.18	150	13.1	32.3	20–34
No. 25	0.600	98	8.6	23.7	14–24
No. 36	0.425				
No. 52	0.300	95	8.3	15.4	8–20
No. 72	0.212				
No. 100	0.150	85	7.4	8.0	5–15
No. 200	0.075	64	5.6	2.4	2–7
200 pass	0.075	27	2.4		

Contract: Ogbomoso–Osogbo–Oko Road Project; Sample Ref: Binder Course; Location: Chainage 26+700 to chainage 26+925; Weight of total aggregate: 1144g

Table 13. Extracted Bitumen from asphalt concrete for road binder course lay from second mix design

Reference	Description	Value	Unit
A	Weight of mixture+bowl	1470	g
B	Weight of bowl	270	g
C	Weight of mixture = A-B	1200	g
D	Weight of filter before testing	1.0	g
E	Weight of filter after testing	2.0	g
F	Weight of material retained by filter = E-D	1.0	g
G	Weight of aggregate in the bowl	1143	g
H	Weight of total aggregate = F+G	1144	g
I	Weight of bitumen = C-H	56	g
J	% of Bitumen on the total weight of mixture = I/C×100	4.7	%
K	% of Bitumen on dry aggregate = I/H×100	4.9	%

Figure 7. Laying of asphalt concrete at the binder course.

59.7% respectively. Though the percentage of aggregates that passed ¾" sieve (90%) was within the specified limit (70–100%) set by FMWH on an excellent binder course of a road, the obtained values were so close to the upper limit of the specification. This implies that ¾" size aggregate has a higher volume in the third mix design formulated than other aggregates. This might cause ineffective compaction of aggregates during construction because the aggregate size is too big for perfect compatibility. The asphalt compaction quality will be improved if the aggregate percentage is reduced to 75–80% for accurate compaction. Also, the value of aggregate passing sieves ½" (72.5%), 3/8" (64.2%), and ¼" (59.7%) are within the Ministry's specified value, like 55–80%, 41–70%, and 40–60% as stated by FMWH. Although the values obtained are within the specified limit, the recorded values were too close to the edges of those specifications. As observed, some crushed aggregates are more significant than expected compared to the specified limit (Fig. 7). The aggregate values within the specified boundaries should be reduced to 65–72%, 58–62%, and 48–53% for perfect compaction of aggregates during the pavement construction at the binder course of the road. The categories of aggregates that passed through sieves No. 7, No. 14, No. 3,6, and No. 52 were found to perfectly satisfy the specified standard of uncrushed aggregate (sand) (2.4–0.5 mm,) which is in agreement with the findings of [33]. The percentage of aggregates that passed through the above set of sieves was calculated to be 45.4%, 32.3%, 23.3%, and 15.4%, respectively. Some aggregates that passed through sieve No. 7 are too big compared to others in the same category. As shown in Figure 7, the aggregate percentages specified to be within the limit of 27–45%, as stated by FMWH, are beyond the expected values. Therefore, there should be aggregate quantity reduction, which should range from 32–40%. Also, the value of aggregate passing sieve No. 14 (32.3%) is too close to the specified limit (20–34%) for perfect construction and compaction; it will be okay if it is reduced to 25–30%. Likewise, the values of aggregates passing sieves No. 25 and No. 52 have to be reduced and should fall within the range of 18–20% and 12–14% instead of 23.4% and 15.4% obtained. Percentages of other aggregates passing sieves No. 100 and No. 200 obtained (8.0% and 2.4%, respectively) are standard for producing sustainable asphaltic concrete compared with the specified limit approved by FMWH. The results analysis showed that the asphaltic concrete made from the second mix design is inefficient for the road's binder layer's construction, as the one produced from the first mix design. Therefore, the aggregate sizes formulated from the first mix design for asphalt concrete production are adopted to produce quality asphalt for the road's binder layer. Like the concrete made from the first mix design, the quantity of bitumen used to produce asphalt concrete through the second mix design was calculated to be 4.7%. This value is obtained through the bitumen extraction process. The value (4.7%) was 0.1% more than that obtained from concrete from the first mix design (4.6%).

3.1.3. Marshall Test Results of Asphalt Concrete for Road Binder Course from Third Mix Design

The aggregate analysis results and the bitumen content produced from the third mix design are shown in Tables 14, 15 and Figure 8. As presented in Table 13, the number of aggregates passing sieve sizes ¾", ½", 3/8", and ¼" were analyzed and classified as medium gravel. According to [33], the aggregates in this category were of sizes 8–16 mm. The percentages observed, 90.0%, 64.9%, 56.8%, and

Table 14. Granisize analysis of asphalt concrete for road binder course lay from third mix design

Sieve size (inch)	Sieve size (mm)	Weight retained (g)	% Retained (%)	% Passing (%)	Specification
2 1/2”	63.5				
2”	50.6				
1 ½”	38.1				
1 ¼”	31.8				
1”	25.4	–	–	100	100
¾”	19.1	108	10.2	90.0	70–100
1/2”	12/7	270	25.1	64.9	55–80
3/8”	9.5	88	8.1	56.8	47–70
¼’	6.5	79	7.3	49.5	40–60
3/16”	4.76				
1/8”	3.45				
No. 7	2.36	85	7.9	41.6	27–45
No. 14	1.18	88	8.2	33.4	20–34
No. 25	0.600	110	10.2	23.2	14–24
No. 36	0.425				
No. 52	0.300	100	9.3	13.9	8–20
No. 72	0.212				
No. 100	0.150	80	7.4	6.5	5–15
No. 200	0.075	70	6.5		2–7
200 pass	0.075				

Contract: Ogbomoso–Osogbo–Oko Road Project; Sample Ref: Binder Course; Location: Chainage 26+700 to chainage 26+925; Weight of total aggregate: 1078g

Table 15. Extracted Bitumen from asphalt concrete for road binder course lay from third mix design

Reference	Description	Value	Unit
A	Weight of mixture+bowl	1370	g
B	Weight of bowl	170	g
C	Weight of mixture = A-B	1200	g
D	Weight of filter before testing	1.0	g
E	Weight of filter after testing	2.5	g
F	Weight of material retained by filter = E-D	1.5	g
G	Weight of aggregate in the bowl	1075.0	g
H	Weight of total aggregate = F+G	1076.5	g
I	Weight of bitumen = C-H	123.5	g
J	% of Bitumen on the total weight of mixture = I/C×100	10.3	%
K	% of Bitumen on dry aggregate = I/H×100	11.5	%

49.5%, were within the specified limit of 70–100%, 55–80%, 47–70%, and 40–60% respectively, stated by FMWH for stability and durability of asphalt binder concrete. As shown in Figure 8, the quantity of aggregate passing sieve size ¾” was very close to the specified limit. A good value is expected to be within the specified envelope (lower and upper limit) as stated in the FMWH specification. This value must be reduced and should fall between the 78–85% range for quality production of asphalt concrete and efficient compassion and sustainability of the aggregates. Also, as shown in Table 14, the percentage of aggregates passing sieve sizes ½” and 3/8” (64.9% and 58.8%) were within the middle of the specified boundaries (lower and upper limit) that is 55–80% and 47–70% respectively. The values obtained were quality to produce asphalt concrete pavement. Also, the percentage of aggregate passing sieve ¼” is average, but it requires a bit of

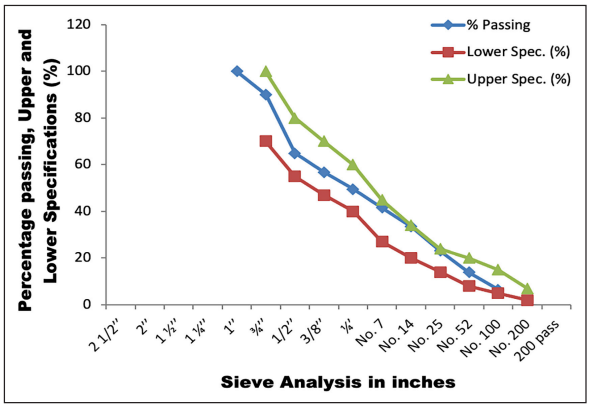

Figure 8. Chart showing the gradation result of asphalt concrete for road binder course laying from third mix design.

Table 16. Granisize analysis of asphalt concrete for road wearing course lying from the first mix design

Sieve size (inch)	Sieve size (mm)	Weight retained (g)	% Retained (%)	% Passing (%)	Specification
2 1/2”	63.5				
2”	50.6				
1 ½”	38.1				
1 ¼”	31.8				
1”	25.4				
¾”	19.1	–	–	100	100
1/2”	12/7	83	7.3	92.7	85–100
3/8”	9.5	100	8.8	83.9	75–92
¼’	6.5	121	10.7	73.2	62–82
3/16”	4.76				
1/8”	3.45				
No. 7	2.36	200	17.6	55.6	50–65
No. 14	1.18	157	13.8	41.8	36–51
No. 25	0.600	99	8.7	33.1	26–40
No. 36	0.425				
No. 52	0.300	117	10.3	22.8	18–30
No. 72	0.212				
No. 100	0.150	54	4.8	18.0	13–24
No. 200	0.075	89	7.8	10.2	7–14
200 pass	0.075	115	10.2		

Contract: Ogbomoso–Osogbo–Oko Road Project; Sample Ref: Wearing Course; Location: Chainage 26+700 to chainage 26+925; Weight of total aggregate: 1135g

adjustment (reduction) for its suitability for concrete production. Its value should be within the 50–52% range for more accuracy and compatibility.

All the aggregates that passed through sieves No. 7, No. 14, No. 25, and No. 52 were classified as fine aggregates using the size limit of 2.4–0.5 mm according to [34]. The t passed through these sieves was 41.6%, 33.4%, 23.2%, and 13%, respectively. The quantity of aggregate through sieve No.7 (41.6%) shows that the aggregates used need adjustment since their values were too close to the specified limit (27–45%). There should be a reduction in the aggregates' volume for accurate compatibility during the compaction of aggregates. The suggested reduction should be within the range of 35–39%. Likewise, the percentages of aggregates passing sieves No. 14 (33.4%) and No. 25 (23.2%) obtained were too close to the upper limit of the specification (20–34% and 14–24%). These values should be within the range of 20% for accurate and efficient compatibility. The compatibility rate of aggregate passing sieve No. 52 (13.9%) was correct compared to the 8–20% specification recommended by FMWH. Also, the obtained aggregates value (13.9%) fell within the middle of the specified limit (envelope) of 8–20% according to FMWH standards. The value of aggregate passing sieve No. 100 needs adjustment. The adjustment should be within 8.5–10% instead of 6.5%. The percentage of bitumen extracted from asphalt concrete produced from the third mix design is 11.5%. This value (11.5%) is more than the percentage of bitumen specified for average asphalt production from the third mix design, which is 4.8% (Tables 4 and 14). The increment is about 6.5%, which shows that the percentage of bitumen in asphalt concrete produced from the third mix design was not adequately controlled. For effectiveness, its bitumen is constantly controlled. Figure 7 shows the laying of asphalt concrete at the binder course.

Considering the three results of asphalt concrete obtained from the first, second, and third mix designs, the first mix design output is the best. It consists of accurate analysis results. Their aggregates were compatible and consisted of durable qualities. Therefore, the first mix design is recommended for producing concrete for road binder course construction. This experimental output is accurate and adequate for constructing global roads' binder courses with high sustainability and durability properties. Having obtained the first mix design as the best design method for stable binder pavement, this result is compared with other previous research outputs. According to [35], investigations were conducted to correct the properties of asphalt mix aggregates against fracture toughness. The results proved that applying lower asphaltic binder aggregates into road pavement construction reduced the intensity of concrete's fracture toughness but affected the stability and sustainability of its aggregate during tension. However, the output of this research negates the defect of fracture toughness as observed by [35]. In this experiment, no rutting defects were observed beneath the road binder pavement constructed with the concrete made from binder aggregate mix design.

Meanwhile, in the results of [36], there was a formation of 4% air voids and deep rutting deformation beneath the roads' binder pavement. This was increased with an

Table 17. Extracted bitumen from asphalt concrete produced for road-wearing course pavement construction using the first-wearing course mix design

Reference	Description	Value	Unit
A	Weight of mixture+bowl	2070	g
B	Weight of bowl	870	g
C	Weight of mixture = A-B	1200	g
D	Weight of filter before testing	0.2	g
E	Weight of filter after testing	0.6	g
F	Weight of material retained by filter = E-D	0.4	g
G	Weight of aggregate in the bowl	1135	g
H	Weight of total aggregate = F+G	1135.4	g
I	Weight of bitumen = C-H	64.6	g
J	% of Bitumen on the total weight of mixture = I/C×100	5.4	%
K	% of Bitumen on dry aggregate = I/H×100	5.7	%

increase in the rate of binder aggregate in the mix. Therefore, the value obtained in this study (especially from the first mix design) will significantly improve road pavement quality produced in construction industries. It was also observed that the output of this study satisfied the stability conducted through the Marshall testing. This is in line with the results of [37], which show that the application of cement aggregates improved the performance of asphalt concrete when loading during tension.

3.1.4. Granisize Analysis and Bitumen Extraction Test Results of Asphalt Concrete for Wearing Course Lying using the wearing course first mix design

The grain size analysis results and bitumen extraction test obtained from the asphalt concrete produced from asphalt mix design for the wearing course were presented as shown in Tables 16, 17 and 8. As shown in Table 16, the percentage of aggregates passing sieves ½" (12.5 mm), 3/8" (9.5 mm), and ¼" (6.5 mm) were calculated to be 92.7%, 83.9%, and 73.2% respectively. These values accurately fit the specified limits of 85–100%, 75–92%, and 62–82%, respectively, as stated by FMWH (1994). Thus, the aggregate used for the wearing course asphalt production is stable, effective, and durable. Likewise, the aggregates passing sieves No. 7 (2.36 mm), No. 14 (1.18 mm), No. 25 (0.6 mm), and No. 52 (0.30 mm), are 55.6%, 41.8%, 33.1%, and 22.8% respectively in value. These values were obtained after the grain size analysis, and they are within the specified envelope (that is, 50–65%, 36–51%, 26–40%, and 18–30%, respectively) stated by FMWH [38] for perfect asphalt concrete production for the wearing pavement. Therefore, the aggregates used in this experiment were suitable for asphalt concrete production for road construction in the global construction industries.

The experiment's output shows that aggregate passing sieves No. 100 and No. 200 possessed an excellent property for quality production of asphalt concrete for the wearing pavement construction. Considering the results, the values of aggregate passing sieve No. 100 and No. 200 (18.0% and 10.2%) were in line with the suggested specification according to FMWH (1994) standard, that is 13–24% and 7–14% respectively (Fig. 9). Also, as shown in Figure 9, it was observed that the aggregates used to produce asphalt concrete at the wearing zone of the road from the first mix design are of great potential for road construction. Therefore, it is recommended that the first mix designs used in this study be adopted to produce concrete for road-wearing pavement construction in the global construction industries. As shown in Table 17, the percentage of bitumen extracted recorded was 5.7%. This value is very close to the bitumen rate percentage or the production of asphalt concrete (5.8%). Therefore, the bitumen used to produce asphalt is excellent and efficient.

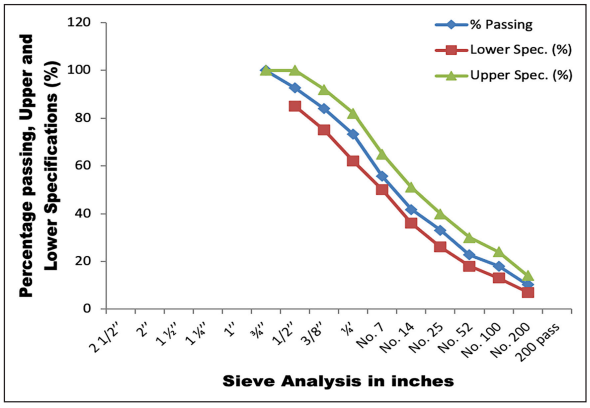

Figure 9. Chart showing the gradation result of asphalt concrete for road's road-wearing pavement construction using the wearing course mix design.

3.1.5. Grainsize Analysis and Bitumen Extraction Test Results of Asphalt Concrete for Wearing Course Lying Using the Wearing Course Second Mix Design

The results of the grain size analysis of asphalt concrete produced from the second mix design, as proportioned in Table 6, are presented in Tables 18, 19. According to Table 18, the percentage of aggregate passing sieve size 1.18 mm is more than that of the quantity specified in the 1994 asphalt production manual organized for the efficient production of quality asphalt concrete by the Federal Ministry of Works and Transportation Authority, Nigeria. This depreciation might have occurred due to the high proportions of quarry

Table 18. Granisize analysis of asphalt concrete for road-wearing pavement construction from the second mix design

Sieve Size (Inch)	Sieve Size (mm)	Weight Retained (g)	% Retained (%)	% Passing (%)	Specification
2 1/2”	63.5				
2”	50.6				
1 ½”	38.1				
1 ¼”	31.8				
1”	25.4				
¾”	19.1	–	–	100	100
1/2”	12/7	112.00	10.00	90.00	85–100
3/8”	9.5	98.56	08.80	81.20	75–92
¼’	6.5	176.96	15.80	65.40	62–82
3/16”	4.76				
1/8”	3.45				
No. 7	2.36	144.48	12.90	52.50	50–65
No. 14	1.18	4.59	0.41	52.09	36–51
No. 25	0.600	124.21	11.09	41.00	26–40
No. 36	0.425				
No. 52	0.300	256.59	22.91	18.09	18–30
No. 72	0.212				
No. 100	0.150	12.21	1.09	17.00	13–24
No. 200	0.075	42.56	3.80	13.20	7–14
200 pass	0.075	147.84	13.20		

Contract: Ogbomoso–Osogbo–Oko Road Project; Sample Ref: Wearing Course; Location: Chainage 26+700 to chainage 26+925; Weight of total aggregate: 1135g

Table 19. Extracted bitumen from asphalt concrete produced for road-wearing course pavement construction using the second-wearing course mix design

Reference	Description	Value	Unit
A	Weight of mixture+bowl	2080	g
B	Weight of bowl	880	g
C	Weight of mixture = A-B	1200	g
D	Weight of filter before testing	0.3	g
E	Weight of filter after testing	0.6	g
F	Weight of material retained by filter = E-D	0.3	g
G	Weight of aggregate in the bowl	1120	g
H	Weight of total aggregate = F+G	1120.3	g
I	Weight of bitumen = C-H	79.7	g
J	% of Bitumen on the total weight of mixture = I/C×100	5.64	%
K	% of Bitumen on dry aggregate = I/H×100	7.1	%

dust and filler (soft sand) used to produce asphalt concrete. Therefore, the second mix design is unsuitable for producing concrete with durable and flexible wearing pavement. Using the first mix design to create asphalt concrete will help the government and communities construct a durable wearing pavement against deformation, which can lead to constant maintenance and cost a lot. Also, the percentage of the bitumen content extracted from the asphalt concrete produced from the second mix design for wearing pavement construction (Table 6) was 1.5% more than its initial designed proportion, which is 5.6% (Table 19). Excess bitumen in the concrete signified that the asphalt production plant's discharge unit was poorly controlled or monitored for accurate production. From another perspective, it could be that the aggregates used for the production are very dry, leading to excess bitumen absorption to attain their satisfaction. It can be deduced that only the first design is accurate, standard, and effective for constructing quality and durable asphaltic road-wearing pavement.

3.1.6. The Importance of These Mixed Design Methods Against the Frequent Road Pavement Maintenance

The application of best mix designs used in this study for the construction of road binder and wearing pavements will

be a means of controlling premature pavement deterioration, such as cracks, potholes, and pavement shrinkage, which lead to its constant maintenance. This method is one of the best methods of controlling excessive spending on road pavement maintenance because it allows the right choice of valuable materials (crushed and uncrushed) to produce quality asphalt concrete for constructing durable road pavements. Also, the application of the best mix design discovered in this study for the production of asphalt concrete for the construction of asphalt pavements (binder and wearing) in highways construction industries is an excellent solution to the problem of premature pavement construction in the globe since the concrete produced using the best mix proportion of aggregates as shown in this study will produce concrete with high rigidity and durability properties which will prolong its lifespan and prevent the issue of constant road pavement maintenance. In addition to that, roads with poor-strength pavement will have a negative impact on the people of those communities. Its constant maintenance will affect the sales of some marketers, cause road trafficking, and increase the government expenditure. All these problems will be eradicated when the new method of asphalt concrete production is implemented in the global construction system.

Most of the materials used in this study are naturally endowed. They are so valuable, rigid, and of high standard. This shows its relevancy for the construction of a durable road pavement. Our natural resource, crushed and uncrushed aggregates, has contributed significantly to constructing rigid pavement. Using artificial or natural eco-friendly materials to produce asphalt concrete for road pavement construction, especially from green asphalt concrete production, will negatively affect the community's health and cause environmental pollution. Besides, the degradation of these materials, most significantly, the bitumen and asphalt made from recycled waste materials, will result in premature deterioration, leading to frequent maintenance of the road's pavement or its total rehabilitation, thus increasing the government's budget for road construction. The other limitation of using green asphalt concrete for the construction of road pavements is its high carbon emission rate from its carbonated recycled materials used to produce green emulsion bitumen for road pavement construction [39, 40]. This is unethical and unfriendly to humans and the environment. Since the materials used in this study to produce asphalt concrete are naturally endowed, they are not made from recycled waste materials. Therefore, asphalt concrete pavements are eco-friendly and not liable to carbon emissions. This makes it one of the best methods for producing durable, eco-friendly pavements.

3.1.7. Application of this Study's Findings to Global Road Pavements Construction Practice

Practicing road pavement construction with asphalt concrete produced from the best mix designs structured for the binder and wearing pavement construction according to the design findings of this study together with the use of asphalt concrete production manual organized by the Federal Ministry of Works and Transportation 1994 will help in producing the durable, sustainable, flexible, and mature road pavements without spending on its maintenance. Using this study method for road construction will also help control the high carbon emission rate in the environment, thus preventing global warming. In addition, most of the aggregates used to produce asphalt concrete in this study are naturally endowed, rigid, and have heavy weights to withstand stress generated during the roads' loading. From another perspective, most of the materials used to construct green asphalt–concrete pavements are made from recycled materials that are very fragile and prone to deterioration, decomposition, and carbon emission, which can increase the rate of global warming. To produce concrete for the construction of binder and wearing pavement, applying the first mix designs from each category is suitable for producing durable and sustainable pavements in temperate and cool environments, following the accurate procedures as explained in this study. It is advisable to carefully examine the climatic condition of the environment where pavement construction will occur before embarking on applying this method. It is essential to produce asphalt concrete that will be friendly to the climatic conditions of its construction environment. This will prevent constant maintenance of the road's pavements, encourage smooth vehicle movement, and extend the life span of the road's pavement.

3.1.8. Response of Asphalt Pavement to Climatic Conditions

Heating asphalt concrete to about 150^0C before laying for pavement construction is a means of increasing its rate of aggregates' compatibility after compaction. Using a standard compacting machine will play a vital role in increasing the strength of the pavement in construction against stress disturbances from heavy vehicles, which will prevent the formation of potholes and pavement cracking. This treatment will protect the asphalt pavement against hot and cold weather deformation. Any pavement constructed using the mix designs (first mix designs from both binder and wearing proportions) and materials from this study will develop high strength to withstand stress against deformation that usually occurs due to constant expansion and contraction of asphalt pavement during the hot and cold climatic conditions.

3.1.9 Results of road leveling at chainages 26 + 700 to 26 + 875 before and after the laying of asphalt concrete: For easy and accurate calculation of the thickness of asphalt concrete laid, two standard reduced internal levels (R.I.L) of 1013.506 and 1012.50 were introduced for efficient reduction of measured road levels before and after the laying of asphalt concrete at chainage 26 + 700 to chainage 26 + 875. The results of leveling measurements taken before and after laying asphalt concrete were presented as shown in Tables 20 and 21.

All the data presented in Tables 20 and 21 were used for accurate calculation of the volume of asphalt concrete laid and for their cost estimations

3.1.10. Calculating the Volume of Asphalt Concrete Laid at Chainages 26 + 700 to 26 + 875 Using Leveling Method

The volume of the road before laying asphalt concrete was determined using the leveling instrument for data measurement, as shown in Table 20. As presented in Table

Table 20. Measured Roads' Levels from chainage 26+700 to chainage 26+875 before the laying of asphalt concrete

Back sight B/S (mm)	Inter sight I/S (mm)	Fore sight F/S (mm)	High point of curvature (H.P.C.) (mm)	Reduced internal level (R.I.L.)	Road distance (m)	Remarks
2769			1016.275	1013.506		TBM on Top of a well at RHS
	1427			1014.848	26+700	Φ (Centre of the Road)
	1505			1014.770		Shoulder LHS
	0919			1015.356		Shoulder RHS
	1331			1014.944	26+725	Φ (Centre of the Road)
	1439			1014.836		Shoulder LHS
	1061			1015.214		Shoulder RHS
	1792			1014.483	26+750	Φ (Centre of the Road)
	1638			1014.637		Shoulder LHS
	1831			1014.444		Shoulder RHS
	2400			1013.875	26+775	Φ (Centre of the Road)
	2148			1014.127		Shoulder LHS
	2029			1014.246		Shoulder RHS
	2689			1013.586	26+800	Φ (Centre of the Road)
	2353			1013.922		Shoulder LHS
	2705			1013.570		Shoulder RHS
2277		2605	1015.947	1013.670		C. P (Change of Point)
	1671			1014.276	26+825	Φ (Centre of the Road)
	1541			1012.735		Shoulder LHS
	1357			1011.378		Shoulder RHS
	2140			1009.238	26+850	Φ (Centre of the Road)
	1965			1007.273		Shoulder LHS
	1927			1005.346		Shoulder RHS
	2431			1002.915	26+875	Φ (Centre of the Road)
	2169			1000.746		Shoulder LHS
	2429			998.317		Shoulder RHS
		2441		995.876		Total Bench Mark (TBM) on top of an iron line drain

20, the breadth of the road used was 12.8 m. The distance covered (D) from chainage 26 + 700 to chainage 26+875 was calculated to be 175 m. The volumes of the road surface were calculated for at the center (ϕ), left-hand side (LHS), and right-hand side (RHS) as shown in Table 22.

The volume at the center (Φ) of the road was calculated to be 175×12.8×1.77025=3965.36 m^3; That of the LHS of the road was calculated as 175×12.8×1.61800=3624.32 m^3. Also, the volume at the RHS of the road is estimated to be 175×12.8×1.7365=3889.76 m^3. The total volume of the road surface before laying asphalt was calculated to be 11,479.44 m^3. This value was obtained by adding the volume at the center of the road, its LHS and RHS equal to 3965.36 m^3+3624.32 m^3+3889.76 m^3=11,479.44 m^3. Likewise, the volume of the road surface after laying asphalt concrete was determined using the measured data from the leveling device in Table 21 as shown in Table 23. From the calculations made, the volume of asphalt concrete measured at the center (Φ) of the road which is 175×12.8 x 1.985125=4446.68 m^3; also, that of its LHS of the road was gotten from 175×12.8×1.84475=4132.240 m^3; and that of its RHS of the road was calculated as 175×12.8×1.7785=3983.84 m^3. The total volume of the road surface after the laying of asphalt concrete=4446.68 m^3+4132.240 m^3+3983.84 m^3=12 562.760 m^3. Therefore, the actual volume of asphalt concrete laid at chainage 26+700 to chainage 26+875=12, 562.760 m^3 -11,479.44 m^3=1083.320 m^3. The cost per 1 m^3 of asphalt concrete=$250.00. Therefore, the total cost of asphalt concrete laid on the road from chainage 26+700 to chainage 26+875=$250.00×1083.320 m^3=$ 270,830.00 which is 740×270,830=#200, 414, 200:00 (Table 23).

3.1.11. Limitations of this Study and Future Suggestions on Pavement Design

To ideally make use of this method for road pavement construction, the asphalt paving machine, which is commonly used for the construction of asphalt concrete on the road's surface, is required to retain high heat temperature to be able to lay the asphalt concrete on the road's surface perfectly. The high heat generation in this method contributes to the increase in high heat affecting the Island, thus exposing it to heat deficiency. Also, the application of mix design

Table 21. Measured Levels of the road from chainage 26+700 to chainage 26+875 after the laying of asphalt concrete

Back sight B/S (mm)	Inter sight I/S (mm)	Fore sight F/S (mm)	High point of Curvature (H.P.C.) (mm)	Reduced internal level (R.I.L.)	Road distance (m)	Remarks
2621			1815.121	1012.500		TBM on Top of a well at RHS
	1226			1813.895	26+700	Φ (Centre of the Road)
	1302			1813.819		Shoulder LHS
	0619			1814.502		Shoulder RHS
	1217			1813.904	26+725	Φ (Centre of the Road)
	1139			1813.982		Shoulder LHS
	1001			1814.120		Shoulder RHS
	1625			1813.496	26+750	Φ (Centre of the Road)
	1414			1813.707		Shoulder LHS
	2312			1812.809		Shoulder RHS
	1942			1813.179	26+775	Φ (Centre of the Road)
	2000			1813.121		Shoulder LHS
	2245			1812.876		Shoulder RHS
	2671			1812.450	26+800	Φ (Centre of the Road)
	2151			1812.970		Shoulder LHS
	1708			1813.413		Shoulder RHS
1272		1825		1813.296		C. P (Change of Point)
	1251			1813.317	26+825	Φ (Centre of the Road)
	1415			1813.153		Shoulder LHS
	1149			1813.419		Shoulder RHS
	2008			1812.560	26+850	Φ (Centre of the Road)
	1761			1812.807		Shoulder LHS
	1829			1812.739		Shoulder RHS
	2222			1802.933	26+875	Φ (Centre of the Road)
	1762			1812.806		Shoulder LHS
	2029			1812.536		Shoulder RHS
		1419		1813.149		Total Bench Mark (TBM) on top of an iron line drain

All the data presented in Tables 20 and 21 were used for accurate calculation of the volume of asphalt concrete laid and for their cost estimations.

in this study requires using a standard asphalt plant and a well-trained operation to proportion the aggregates and bitumen efficiently to produce quality asphalt concrete for the best pavement construction. Any deviation from this standard can produce low-quality asphalt concrete, which cannot be recycled or reused. In addition, the gravitational values of the aggregates used, as shown in this study, can differ from one location to another. This is because these aggregates are naturally endowed and have different gravitational values. These differences in values can negatively affect the products produced from the aggregates from one country to another, thus leading to the construction of less durable pavement and increasing the cost of pavement maintenance. Therefore, it is advisable to know the integrity value of an aggregate before its use in construction.

Furthermore, most of the materials used in this study are not renewable or recyclable, though they possess high resisting capacity against stress and deformation that can occur through loading. This value increases its durability properties. In case the initial pavement constructed is faulty, the asphalt concrete from the existing pavement cannot be recycled or renewed for the reconstruction of the new pavement—the building on of the payment required using new materials for the new construction.

Uture researchers should experiment with recycling and reusing old and weak pavement concrete made from natural materials to produce new durable asphalt concrete for road pavement construction. This will reduce the cost of road rehabilitation in construction industries.

4. CONCLUSION AND RECOMMENDATIONS

This study proved that the road pavement mix design used by the American Highway Design Association (AASHTO) from 1950 to 1993 is not complex enough for rugged pavement design and construction. A new standard design method is needed. Despite the mix design used for asphalt concrete production, the efficiency of aggregates and models used to neutralize the effects of creeping, cracks, and deflection of road pavement was not met. A better aggregate

Table 22. Calculating the volumes of the road's surface at the center, LHS, and RHS before the laying of asphalt concrete

Chainages (m)	Width of the road (m)	Height of the Road			Volume at Φ (m^3)	Volume at LHS (m^3)	Volume at RHS (m^3)
		Φ (center) (m)	LHS (m)	RHS (m)			
26+700	12.8	1.226	1.302	0.619	3965.36	3624.32	3889.76
26+725	12.8	1.217	1.139	1.001			
26+750	12.8	1.625	1.414	2.312			
26+775	12.8	1.942	2.000	2.245			
26+800	12.8	2.671	2.151	1.708			
26+825	12.8	1.251	1.415	1.149			
26+850	12.8	2.008	1.761	1.829			
26+875	12.8	2.222	1.762	2.029			
Total	102.4	14.162	12.944	13.892			
Average	12.8	1.77025	1.61800	1.7365			

LHS: Left-hand side; RHS: Right-hand side.

Table 23. Calculating the volumes of road surface after the laying of asphalt concrete at the center, LHS, and RHS of the road; the volume of asphalt concrete laid on the road

Chainages (m)	Width of the road (m)	Height of the Road			Volume before the laying of asphalt (m^3)	Volume after the laying of asphalt (m^3)	Volume of Asphalt concrete laid (m^3)
		Φ (center) (m)	LHS (m)	RHS (m)			
26+700	12.8	1.427	1.505	0.919	11,479.44	12,562.76	1083.320
26+725	12.8	1.331	1.439	1.061			
26+750	12.8	1.792	1.638	1.831			
26+775	12.8	2.400	2.148	2.029			
26+800	12.8	2.689	2.353	2.705			
26+825	12.8	1.671	1.541	1.357			
26+850	12.8	2.140	1.965	1.927			
26+875	12.8	2.431	2.169	2.429			
Total	102.4	15.881	14.758	14.228			
Average	12.8	1.985125	1.84475	1.7785			

mix design for road pavement's sustainability, durability, and stability is needed, and this was evaluated for the construction of a rigid pavement system in this study.

In the construction industries globally, most of the crushed aggregates (granites) used to produce asphalt concrete were not that rich in quality minerals such as amphibole, mica, quartz, and field spar, which boost the interlocking properties for compatibility in crush aggregates (granites). The crushed aggregates used in this study are rich in quality minerals, which makes them suitable for the best production of quality asphalt for rigid pavement formation. Other aggregates (uncrushed edged), such as sharp sand, quarry dust, and soft sand, possess the same qualities for better asphalt production.

As well know, the method of carrying out a product's design and production depends on the product's quality level. As used in this experiment, the percentage of crushed aggregates used ranged from 11–27% for 3/8", 1/2", and ¾" grades, contributing majorly to their efficiency in making the rigid and flexible asphaltic pavement. As used in this study, the application of many quarry dust (31.1%) for the production of asphalt concrete highly contributed to the compatibility of the aggregates used. Likewise, applying a small percentage of sand and bitumen in the mix gives room for an increase in the quality of asphalt concrete produced compared to concrete with second and third-mix designs. Leveling is one of the best methods of determining the accurate cost of asphalt concrete laid on road pavement.

As observed from the investigation results, all the Marshall Test results agreed with the standard of quality of products obtained as specified by the Federal Ministry of Works and Housing. This proves that the values of passed aggregates obtained using the first mix design, that is, 35.6%, 26.2%, 18.2%, and 13%, are so satisfactory with the value of mineral properties (amphibole, mica, quartz, and field spar) possessed together with well proportioning of the aggregates for better asphalt production. Other aggregates from the second and third mix designs were not appropriately proportioned. Applying the first asphalt mix

designs for binder and wearing pavements has dramatically influenced the quality of pavement rigidity in the global road construction industries.

Having predicted the amount of well-compacted asphalt concrete on road pavement at the initial project evaluation stage, the actual volume of asphalt laid was determined using the standard leveling method. The cost of materials and asphalt produced were evaluated with accurate calculations.

As observed from the findings of this study, the rigidity of road pavement depends solely on the sustainability capacity of its sub-base, base, sub-grade, binder, and wearing courses. The accurate and standard mix designs of the aggregate use for these layers were based on the basic principle of road pavement sustainability and durability. To conclude, the results of this study proved that a standard aggregate mix design of asphalt concrete is a crucial determinant of its durability, sustainability, rigidity, and stability. Therefore, it was suggested that the first asphalt concrete mix design used in this study with standard formulation, gradation, and proportion, which certified the specified boundary, is the best to be adopted to produce asphalt concrete for road binder course laying globally. Also, the formulation used in this study for the wearing course asphalt concrete production is recommended for asphalt concrete mixing for durable road pavement at the first wearing course. This will prevent frequent spending on road pavement maintenance.

The survey leveling method used in this experiment is one of the best methods for calculating the volume of asphalt concrete produced or laid without error. The outcome of this study proved that its application in construction industries would prevent unnecessary spending on road pavement resulting from poor cost estimation and inaccurate aggregate proportioning during asphaltic concrete production and laying. Therefore, it is recommended that the leveling method be adopted to estimate accurately the volume and thickness of asphalt concrete produced and laid in the global construction industries.

ETHICS

There are no ethical issues with the publication of this manuscript.

DATA AVAILABILITY STATEMENT

The authors confirm that the data that supports the findings of this study are available within the article. Raw data that support the finding of this study are available from the corresponding author, upon reasonable request.

CONFLICT OF INTEREST

The authors declare that they have no conflict of interest.

FINANCIAL DISCLOSURE

The authors declared that this study has received no financial support.

USE OF AI FOR WRITING ASSISTANCE

Not declared.

PEER-REVIEW

Externally peer-reviewed.

REFERENCES

[1] Virginia Asphalt Association (2022). *Publication of the Virginia Asphalt Association//Spring and Summer Issue 2022*. https://www.associationpublications.com/flipbook/vaa/springsummer2022/index.html

[2] Aguirre, M. A., Hassan, M. M., Shirzad, S., Mohammad, L. N., & Cooper, S. B. (2017). Performance of asphalt rejuvenators in hot-mix asphalt containing recycled asphalt shingles. *Transp Res Rec*, *2633*(1), 108–116. [CrossRef]

[3] Mivehchi, M., Wen, H., Wen, Y., & Wang, L. (2022). Study of measures to design asphalt mixes including high percentages of recycled asphalt pavement and recycled asphalt shingles. *Transp Res Rec, 2677*(1), 036119812211089. [CrossRef]

[4] Asphalt Paving Association of IOWA. *Benefits of asphalt*. https://www.apai.net/Files/content/Asphalt/Asphalt_Benefits_Page.pdf

[5] Huang H. Y. (2004). *Pavement Analysis and Design*. Pearson Prentice Hall.

[6] Tillamook County. *AASHTO Manual and Handout by Tillamook*. https://www.tillamookcounty.gov/publicworks/page/aashto-manual-handout

[7] HMA Paving and Contracting. *What is Superpave?* https://www.hmacontracting.com/news/what-is-superpave/

[8] Horak, E., & Emery, S. J. (2010). Forensic investigation to determine the reasons for premature failure in an asphalt surface layer. A case study. *Road Mater Pavement Des, 11*(3), 511–527. [CrossRef]

[9] Vallerga, B. A., Lovering, W. R. (1985). Evolution of the Hveem stabilometer method of designing asphalt paving mixtures. *Asphalt Paving Technol Proc, 54*, 243–265.

[10] Robert F., Kandhal P., Brown E., Lee D., & Kennedy T. (1996). *Hot mix asphalt materials, mixture design and construction*. National Asphalt pavement Association Education Foundation.

[11] Elseifi M. A., Al-Qadi L., & P. J. Yoo (2006). Viscoelastic modeling and field validation of flexible pavements. *J Eng Mech, 132*(2), 172–178. [CrossRef]

[12] Abu Abdo, A., Bayomy F., Nielsen R., Weaver, T., Jung, S. J., & Santi M. J. (July, 2009). Prediction of the dynamic modulus of Superpave mixes. *Proceedings of the 8th International Conference on the Bearing Capacity of Roads, Railways and Airfields (BCR2A '09)*. Champaign, USA. [CrossRef]

[13] Labmate. *Laboratory product - Particles sizing using laboratory test sieves*. https://www.labmate-online.com/news/laboratory-products/3/endecotts-ltd/particle-sizing-using-laboratory-test-sieves/43593

[14] Kovler, K. (2012). Does using coal fly ash in concrete construction present a radiation hazard? *Constr Build Mater 29*, 158–166. [CrossRef]

[15] Read, H. (1943). Meditations on granite: Part one. *Proc Geologist Assoc, 54*(2), 64–85. [CrossRef]

[16] Woo, I., Fleurisson, J. A., & Park, H. J. (2010). Influence of weathering on shear strength of joints in a porphyritic granite rock mass in Jechon area, South Korea. *Geosci J, 14*(3), 289–299. [CrossRef]
[17] Le Bas, M. J. & Streckeisen, A. L. (1991). The IUGS systematics of igneous rocks. *J Geol Soc, 148*(5), 825–833. [CrossRef]
[18] Silva, B., Rivas, T., & Prieto, B. (1999). Effects of lichens on the geochemical weathering of granitic rocks. *Chemosphere, 39*(2), 379–388. [CrossRef]
[19] Morad, S., El-Ghali, M. A., Caja, M. A., Al-Ramadan, K., & Mansurbeg, H. (2009). Hydrothermal alteration of magmatic titanite: Evidence from proterozoic granitic rocks, southeastern Sweden. *Can Mineral, 47*(4), 801–811. [CrossRef]
[20] Blatt, H., & Tracy, R. J. Petrology. igneous, sedimentary, and metamorphic. *Geol Mag, 134*(1), 121–142.
[21] Fukumoto, T. (1972). Effect of particle breakage on compaction density of decomposed granite soils. *Soils Found, 12*(3), 55–63. [CrossRef]
[22] Matsuda, T., & Shimizu, T. (2017). Study on correspondence between the evaluation of vibration sensation, average method, and measurement density of acceleration levels for impact vibration in prefabricated housing floor. *J Build Eng, 10*, 124–139. [CrossRef]
[23] Maluski, H. (1978). Behaviour of biotites, amphiboles, plagioclases and K-feldspars in response to tectonic events with the 40Ar-39Ar radiometric method. Example of Corsican granite. *Geochim Cosmochim, 42*(11), 1619–1633. [CrossRef]
[24] Leonard, R. J. (1929). Polygonal cracking in granite. *Am J Sci, 18*, 487–492. [CrossRef]
[25] Holland, J. G. (1967). Rapid analysis of the weardale granite. *Proc Yorkshire Geol Soc, 36*(1), 91–113. [CrossRef]
[26] Morrow, C. A., Moore, D. E., & Lockner, D. A. (2001). Permeability reduction in granite under hydrothermal conditions. *J Geophys Res: Solid Earth, 106*(B12), 30551–30560. [CrossRef]
[27] Karakaş, A., Smith M. R., L. Collis, L. (2020). Aggregates: Sand, gravel, and crushed rock aggregates for construction purposes (3rd edition). *Arab J Geosci, 13*, 11. [CrossRef]
[28] al-Swaidani A. M., Baddoura, M. K., Samira D. A., & Choeb, W. (2015). Acid resistance, water permeability and chloride penetrability of concrete containing crushed basalt as aggregates. *J Mater Sci Eng A, 5*(8). [CrossRef]
[29] Udaya Prakash, J., Ananth, S., Sivakumar, G., & Moorthy, T. (2018). Multi-objective optimization of wear parameters for aluminium matrix composites (413/B4C) using grey relational analysis. *Mater Today Proc, 5*(2), 7207–7216. [CrossRef]
[30] Huizn, M. E. (2022). Chips from the Quarry. *Rock Miner, 97*(6), 493–495. [CrossRef]
[31] Nyembwe, K. J., Makhatha, M. E., & Mageza, K. (2017). Waste foundry sand mineralogical characterisation: the impact of cast alloy, casting temperature and molding additive on the nature waste foundry sand. *Eng J, 21*(7), 1–14. [CrossRef]
[32] ASTM International. Road standards and paving standards. https://www.astm.org/products-services/standards-and-publications/standards/road-standards-and-paving-standards.html
[33] Shi, X., Mirsayar, M., Mukhopadhyay, A., & Zollinger, D. (2019). Characterization of two-parameter fracture properties of portland cement concrete containing reclaimed asphalt pavement aggregates by semicircular bending specimens. *Cem Concr Compos, 95*, 56–69. [CrossRef]
[34] Hewitt, M., Tarca, A., & Yohn, T. L. (2015). The effect of measurement subjectivity classifications on analysts' use of persistence classifications when forecasting earnings items. *Contemp Account Res, 32*(3), 1000–1023. [CrossRef]
[35] Abu Abdo A. M., Eckwright F., Jung S. J., Bayomy F., & Nielsen, R. (2014). Semi-circular notched beam-testing procedure for hot mixture asphalt. *Proc Inst Civ Eng Transp, 167*(1), 48–58. [CrossRef]
[36] Abu Abdo, A. M., & Khater, M. E. (2018). Enhancing rutting resistance of asphalt binder by adding plastic waste. *Cogent Eng, 5*(1), 1452472. [CrossRef]
[37] AASHTO. (2006). Standard method of test for determining the rheological properties of asphalt binder using a Dynamic Shear Rheometer (DSR) (AASHTO T315-06). https://store.accuristech.com/ecia/standards/aashto-t-315-06?product_id=1321092
[38] Federal Ministry of Works. (1994). *Specification for Roads and Bridges Construction*. FMWH, Nigeria.
[39] Nahkon K., & Jittichai R. (2017). Green assessment of thailand's highway infrastructure: A green growth index approach. *KSCE J Civ Eng, 21*(3), 2526–2537. [CrossRef]
[40] David, V.,Victor A., Jose N., & Ana, C. (2020). Assessment of eco-friendly pavement construction and maintenance using multi-recycled RAP mixtures. *Recycling, 5*(3), 17. [CrossRef]

J Sustain Const Mater Technol, Vol. 9, Issue. 2, pp. 199–210, June 2024

Journal of Sustainable Construction Materials and Technologies
Web page info: https://jscmt.yildiz.edu.tr
DOI: 10.47481/jscmt.1348260

JSCMT
Journal of Sustainable Construction Materials and Technologies

Review Article

Green building future: Algal application technology

Abuzer ÇELEKLİ*[1,2], İrem YEŞİLDAĞ[2], Özgür Eren ZARİÇ[2]

[1]*Environmental Research Center (GÜÇAMER), Gaziantep University, Gaziantep, Türkiye*
[2]*Department of Biology, Gaziantep University, Faculty of Art and Science, Gaziantep, Türkiye*

ARTICLE INFO

Article history
Received: 22 August 2023
Revised: 27 March 2024
Accepted: 19 April 2024

Key words:
Algae, bioenergy, CO_2 sequestration, photobioreactor, sustainable building

ABSTRACT

In the context of rising global energy demands driven by population growth and urbanization, the construction industry significantly contributes to greenhouse gas emissions during the construction phase and subsequent energy consumption. Fossil fuel dependency for heating and energy needs exacerbates climate change, necessitating urgent solutions. Algal technology emerges as a promising strategy for green building practices, addressing energy efficiency and emissions reduction. Algae's unique ability to absorb carbon dioxide (CO_2) through photosynthesis is harnessed by deploying photobioreactors on building exteriors. Studies indicate that each kilogram of dry algae consumes 1.83 kg of CO_2 while offering applications as organic fertilizer, oil, and protein sources. This technology not only diminishes CO_2 emissions but also transforms wastewater and generates bioenergy, catering to building energy requirements. Algal technology's economic and environmental significance becomes evident through carbon capture, energy generation, and circular waste management, aligning with sustainability principles. This study highlights the potential of algal technology to shape the future of environmentally conscious construction practices, providing avenues for reduced emissions, efficient energy utilization, and sustainable development.

Cite this article as: Çelekli, A., Yeşildağ, İ., & Zariç, Ö. E. (2024). Green building future: Algal application technology. *J Sustain Const Mater Technol*, 9(2), 199–210.

1. INTRODUCTION

Urban expansion is taking place globally faster, creating a disbalance in the sustainable climate mechanisms, which may result in natural disasters, causing acute social and economic losses. With the recent population growth and increasing urbanization and industrialization, more energy is needed [1]. During the 19th and 20th centuries, man learned to use focused points such as fossil fuel [2]. With industrial development and increased production, some problems have arisen on the planet and become more severe daily. Some consequences are increased disease and mortality caused by environmental pollution, acid rain, and the destruction of ecosystems and ozone [3]. Rapid urbanization will also cause the depletion of natural resources, particularly fossil fuels, due to the increase in energy consumption brought on by industrialization [4]. World Health Organization reports that 90% of the population in urban areas is breathing polluted air according to the air quality guidelines [5]. About 70% of Greenhouse emissions come from urban agglomerated centers [6]. Globally, buildings account for 40% of energy and material use, 33 % of CO_2 emissions, 25 % of wood harvesting, and 17% of freshwater usage [7]. However, it is projected that shortly, emissions from buildings in countries that are rapidly industrializing will surpass emissions from structures in wealthy nations. Historically, most emissions originated from developed countries [8]. Therefore, it is important

***Corresponding author.**
*E-mail address: celekli.a@gmail.com

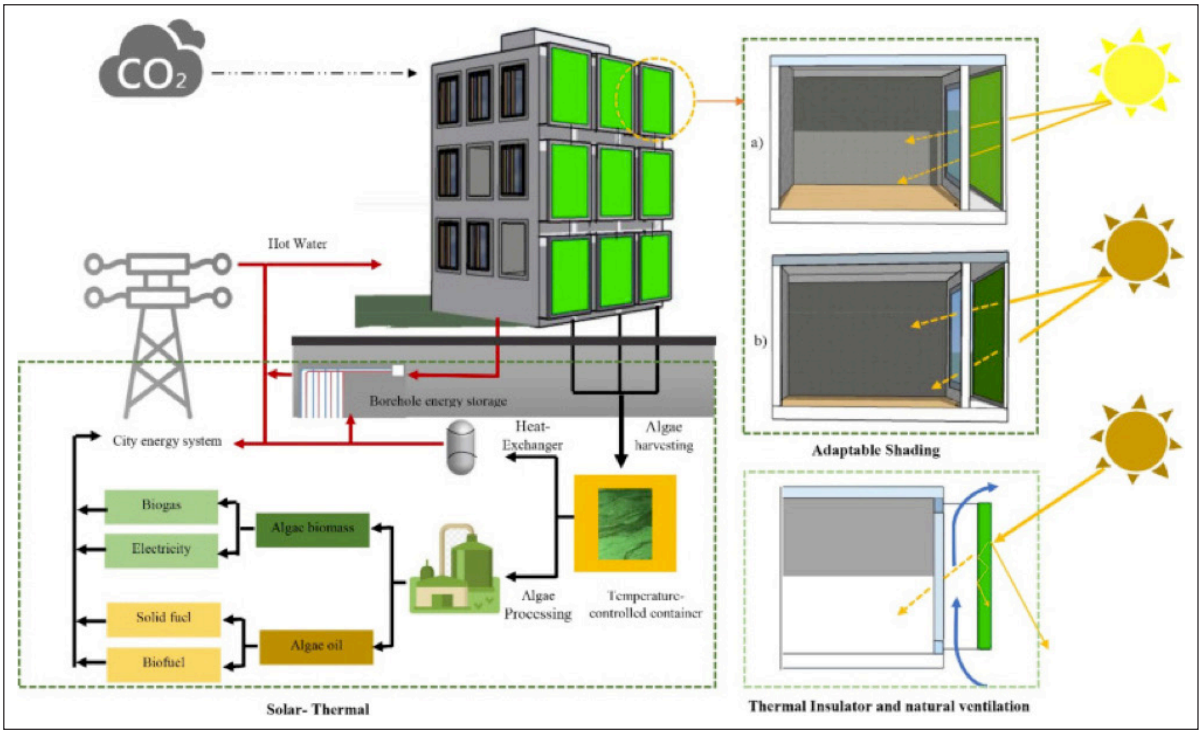

Figure 1. Algae can be grown in various settings, including closed-loop [22].

to plan and design new buildings and cities based on sustainable development features, such as self-sustainability, zero waste/zero emissions, environmental safeguarding, and green fuel and energy exercise [9]. Algae integration into buildings' external façade can sustain buildings and reduce energy consumption [10]. Incorporating algae into building exteriors promotes sustainability in the built environment and acts as a source of renewable energy [10]. Utilizing algae as a renewable energy source to produce electricity or offer other energy-related advantages inside buildings is called algae energy production for buildings [10]. Algae, photosynthetic organisms encompassing diverse species, play a crucial role in various ecological processes. They have garnered increasing attention for their potential applications in sustainable development, particularly in green building technology [11, 12]. Providing a detailed understanding of algae in the context of this discussion is paramount. Algae from the kingdom Protista exhibit various morphological and physiological characteristics. They can be unicellular, colonial, or multicellular, and their size can vary from microscopic to macroscopic scales [13]. Additionally, algae exhibit remarkable diversity in pigmentation, allowing them to thrive in diverse aquatic and terrestrial environments. Classification of algae is based on various criteria, including pigmentation, cell structure, and mode of reproduction. For instance, algae are commonly classified into several groups, such as Chlorophyta (green algae), Rhodophyta (red algae), Phaeophyta (brown algae), and Cyanobacteria (blue-green algae), each with distinct characteristics and ecological roles [14]. The types of algae relevant to green building applications encompass a broad spectrum, ranging from microalgae to macroalgae. Microalgae, such as Chlorella and Spirulina, are valued for their high photosynthetic efficiency and rapid growth rates, making them suitable candidates for biomass production and biofuel generation. Macroalgae, including kelp and seaweed, offer potential as sustainable construction materials due to their abundance, renewability, and unique mechanical properties. Harvesting algae involves various techniques tailored to the specific characteristics of the target species and intended applications [14]. These methods encompass traditional approaches, such as manual collection from natural habitats and innovative technologies like photobioreactors and biofilm cultivation systems. Advancements in harvesting methodologies aim to optimize biomass yield, minimize energy consumption, and enhance overall efficiency in algae cultivation processes. In summary, a comprehensive understanding of algae, encompassing their definition, characteristics, classification, and harvesting techniques, is essential for elucidating their role in green building technology. By integrating scientific knowledge with practical applications, researchers and practitioners can harness the potential of algae to promote sustainability and resilience in the built environment and functional food [15]. Algae-based alternative energy sources provide sustainable possibilities that can help solve pressing global problems such as resource depletion, pollution, and climate change [16]. With global warming, the importance of bioclimatic comfort has increased. An extremely promising strategy that substantially contributes to sustainability and the goal of a greener future is using algae as a source of electricity [17].

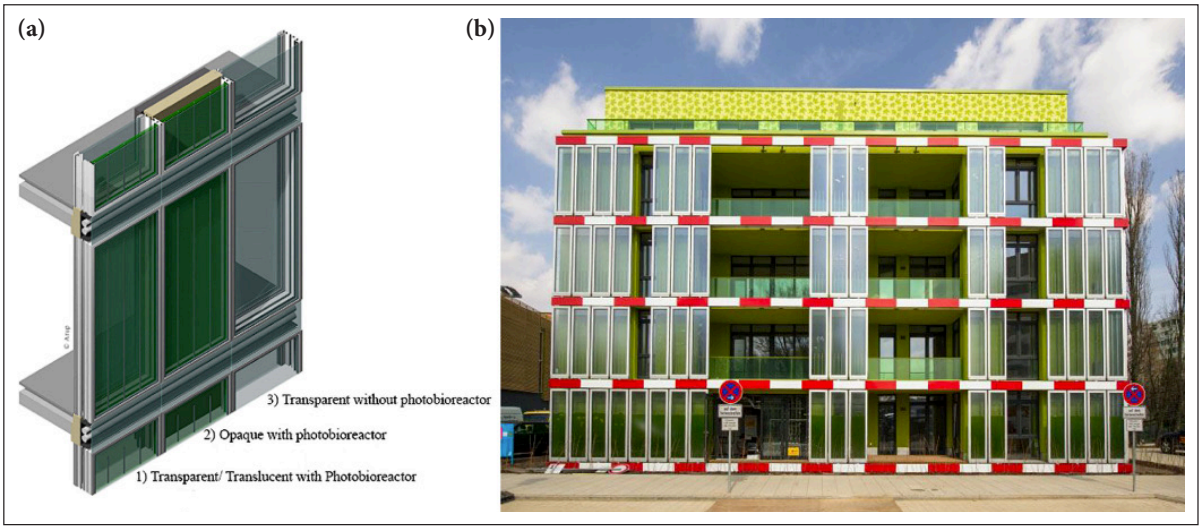

Figure 2. **(a)** Bio-panels [35] **(b)** Building façade in the algae application technology [36].

2. WHAT IS ALGAE APPLICATION TECHNOLOGY?

Algae application technology for buildings, commonly referred to as "bioarchitecture" or "algae-based building systems," includes incorporating algae and associated microorganisms as functional elements into the design and maintenance of buildings. In renewable energy, generating power by combining algae onto building façades is an eco-friendly and long-lasting solution [10]. There are essential applications for environmental sustainability, such as the biotechnological use of algae to purify harmful paints [11]. With the help of algae, energy can be produced directly on the exterior surfaces of buildings, as opposed to the standard photovoltaic systems, such as solar panels, which are mounted on building rooftops or open spaces to convert solar energy into electricity [18]. This developing field investigates algae's potential role in constructing and maintaining sustainable and energy-efficient buildings. A procedure known as transesterification can be used to turn the lipids (oils) that algae produce into biodiesel. Due to its ability to be generated responsibly and the fact that it does not compete with food crops for land, biodiesel made from algae is seen as a possible replacement for conventional fossil fuels [19]. The adaptability of algal energy production is one outstanding feature. Algae can be grown in various settings, including closed-loop photobioreactors and large-scale open ponds (Fig. 1) [20]. Because of their versatility, we can incorporate algal systems into multiple environments, including buildings [21]. For instance, it is possible to embed algae culture systems into building exterior façade designs, converting them into surfaces that produce energy [22].

Algal Application Technology offers a promising avenue for reducing dependence on finite fossil fuels and mitigating greenhouse gas emissions [12, 23]. Through algae cultivation, atmospheric CO_2 is utilized for photosynthesis and biomass accumulation, facilitating carbon capture and storage. Algae's rapid growth rates and adaptability to diverse environmental conditions enable efficient biomass production with minimal land and water requirements and provide information about water quality. Contributes to ecological protection in studies carried out within remote monitoring systems [24, 25]. This versatile biomass resource can be utilized across various sectors, including energy production, construction materials, biofuels, bioplastics, pharmaceuticals, space exploration, climate change causing human migration, and wastewater treatment, contributing to sustainability goals [26, 27].

Furthermore, algal cultivation systems facilitate nutrient recycling and wastewater remediation, reducing environmental pollution. However, the high initial capital investment and operational costs, coupled with energy-intensive extraction and processing processes, pose challenges to the widespread adoption and scalability of Algal Application Technology [28]. Technical obstacles such as contamination risks, nutrient imbalances, and environmental fluctuations necessitate ongoing research and development efforts. Additionally, large-scale algae production may compete with land and water resources needed for food production or natural ecosystems, potentially leading to environmental conflicts. Despite significant advancements, widespread commercialization faces barriers to economic viability, regulatory constraints, and market acceptance. Overall, addressing these challenges is crucial for realizing the full potential of Algal Application Technology in achieving sustainable development objectives.

3. PLACING ALGAE ON THE FACADE OF BUILDINGS

The process of placing algae outside of buildings includes these steps.

A growth medium or substrate would be created to support the growth and adhesion of the algae to the façade surface. This medium might provide algae's nutrients and a steady environment [29]. Specialized bioreactors or bio-panels would be created and built to house the algae on the building face. These bioreactors, which offer a regulated environment for algae growth, must be securely installed onto the façade (Fig. 2a) [30]. The building façade surface

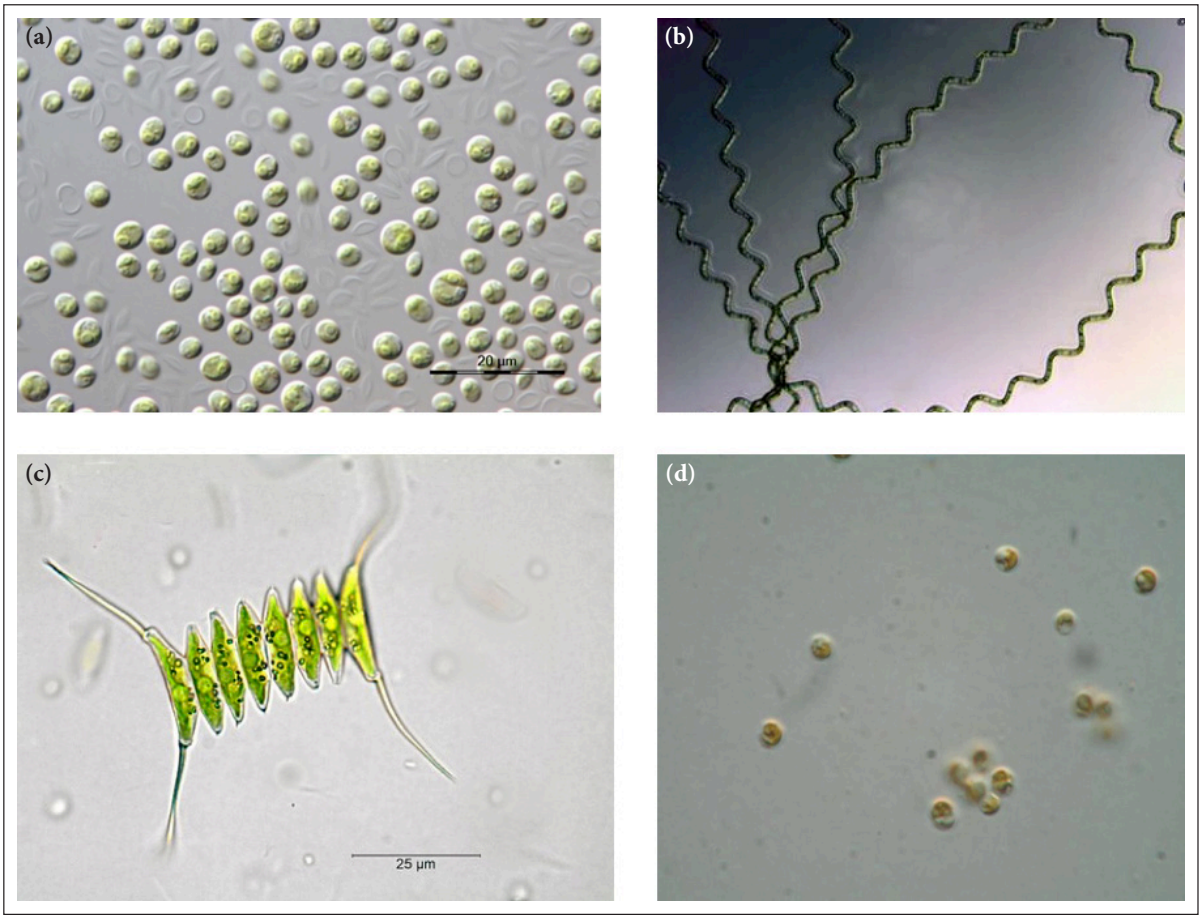

Figure 3. Some algae with high potential energy: **(a)** Chlorella sp. [44], **(b)** Spirulina sp. [45], **(c)** Scenedesmus sp. [44], **(d)** Nannochloropsis sp. [46]

must be ready to allow for algae growth. A character with suitable algae adhesion and development characteristics may be installed, or a suitable coating may be applied (Fig. 2b) [31]. In bioreactors, a few species of algae will probably be planted or seeded on the prepared façade surface. The algae will then utilize the available sunlight to expand and photosynthesize [32]. Algae growth requires water and vital nutrients. Bioreactors can incorporate a controlled fertilizer and water supply system depending on the type of algae being grown there and the surrounding environment [33]. Harvest Energy: As they develop and photosynthesize, algae create biomass, and high-energy chemicals can be gathered and transformed into usable energy by creating biogas or biofuel extraction [34].

Algae bioreactors integrated into building exteriors can be utilized for several things, including energy production and environmental sustainability [22]. Algae bioreactors are devices that use sunlight to grow algae and are capable of photosynthesis on the exterior surfaces of buildings [30]. Many algae species may be utilized depending on the bioreactor's demands and goals [37]. Chlorella sp. use in biofuel production can provide an energy-efficient source and aid in lowering greenhouse gas emissions. The oil extracted from Chlorella sp. can be used to make biodiesel. As a more environmentally friendly substitute for fossil fuels, biodiesel is a renewable fuel. From an environmental sustainability standpoint, producing Chlorella sp. is desirable (Fig. 3a). Because of their high oil content, Chlorella sp. species have the potential to be helpful in the manufacture of biofuel and bioplastic. Chlorella sp. is well known for having a high lipid content per cell, making these lipids an essential source for biofuel manufacture [38]. Spirulina sp. could be used to produce biofuels, which could replace fossil fuels with a more sustainable energy source. Spirulina sp. can use photosynthesis to harvest solar energy. In photosynthesis, oxygen is produced as a byproduct, while carbon dioxide and water are converted into organic compounds (such as glucose). The carbon cycle and energy generation depend on this mechanism [39]. Effective use of microalgae such as Spirulina sp. for energy and nutrition is becoming increasingly important due to biofuel production and the increasing demand for sustainable energy sources (Fig. 3b) [40]. Spirulina sp. is a nutrient-rich form of algae, and because of its high oil content, it has a significant chance of being used to produce biofuel. The oils extracted from spirulina can be transformed into various biofuels, including jet fuel and biodiesel [32]. Scenedesmus sp. uses photosynthesis to absorb carbon dioxide and produce energy. To combat glob-

al climate change, this method can help reduce the amount of greenhouse gases released into the environment. Scenedesmus sp has a significant amount of oil per cell, which can be used to make biodiesel. A more sustainable fuel with lower greenhouse gas emissions than fossil fuels is biodiesel, which can be used instead. Scenedesmus sp. and similar microalgae can be grown in special bioreactors under carefully regulated conditions. The manufacturing process can be optimized in these facilities and the surrounding environment (Fig. 3c) [41]. Using photosynthesis, Nannochloropsis sp. takes carbon dioxide (CO_2) from the air and creates oxygen. The amount of greenhouse gases linked to global warming can decrease and decrease the carbon footprint. It is an essential algae species for biofuel. Like other microalgae, Nannochloropsis sp. has much oil in each cell. These oils can be used to make biodiesel. With its ability to replace fossil fuels and cut greenhouse gas emissions, biodiesel is a sustainable fuel that is better for the environment. Nannochloropsis sp. is a helpful algae for energy production because of its quick reproduction rate and ability to quickly generate a significant quantity of biomass (Fig. 3d) [42, 43].

4. REAL-WORLD EXAMPLES OF ALGAE IN BUILDINGS

Algae have been increasingly utilized in various real-world applications within the built environment, showcasing their potential to contribute to sustainable architecture and construction practices [10]. For instance, in the architectural realm, the use of algae in façade systems has gained traction to integrate renewable energy generation and bioremediation into building design. One notable example is the BIQ House in Hamburg, Germany, which features a reactive façade of glass panels filled with microalgae [47]. These algae photosynthetically convert sunlight and CO_2 into biomass, generating renewable energy while shading the building interior and enhancing thermal insulation. Also, the algae help regulate indoor air quality by absorbing CO_2 and releasing oxygen, contributing to a healthier indoor environment. Another pioneering project is the Algae Dome, showcased at the Expo Milano 2015, which demonstrates the potential of algae cultivation in architectural settings. Designed as a self-sustaining ecosystem, the Algae Dome utilizes sunlight and wastewater to cultivate algae, which can be harvested for various applications, including biofuel production, food supplements, and wastewater treatment. The modular design of the Algae Dome allows for scalability and adaptability to different environmental conditions, making it a versatile solution for urban sustainability challenges [10]. In addition to façade systems, algae-based materials have been explored for interior finishes, insulation, and structural elements in building construction. For example, research initiatives such as the Algae Brick project aim to develop bio-based building materials using algae as a critical component, offering renewable alternatives to traditional construction materials. These real-world examples underscore algae's potential to revolutionize how we design, construct, and inhabit buildings, offering innovative solutions that integrate renewable energy generation, bioremediation, and biomimicry principles into architectural practice. However, further research and technological advancements are needed to overcome technical challenges and scale up algae-based building solutions for widespread adoption in the construction industry [10].

5. PHOTOBIOREACTORS: TOOL FOR SUSTAINABLE DESIGN

Integrating photobioreactors (PBRs) in buildings holds significant promise for sustainable design, offering a renewable source of biomass while simultaneously enhancing environmental performance [48]. To effectively incorporate PBRs into buildings, several technical requirements must be considered. Firstly, adequate space and access to sunlight are essential for successfully operating PBRs. Buildings must be designed or retrofitted with suitable rooftop or façade configurations to optimize sunlight exposure for algal cultivation. Additionally, orientation, shading, and nearby obstructions must be evaluated to maximize solar irradiance. Secondly, PBRs require a controlled environment to support optimal algae growth. This includes maintaining suitable temperature, pH levels, nutrient concentrations, and CO_2 supply within the reactor system. Building systems must incorporate temperature regulation, nutrient dosing, and CO_2 capture mechanisms to ensure favorable conditions for algal cultivation [48]. Furthermore, effective nutrient management is critical to sustain algae growth in PBRs. Nutrient sources like wastewater or organic effluents should be readily available and compatible with the cultivation system. Proper nutrient cycling and monitoring protocols must be established to prevent nutrient depletion or excess, which can adversely impact algae productivity and system stability. Moreover, the design of PBRs should prioritize operational efficiency and ease of maintenance. Accessible components, automated monitoring systems, and remote control capabilities can streamline operations and facilitate timely maintenance activities. Additionally, consideration should be given to selecting durable, corrosion-resistant materials suitable for long-term use in the building environment. In summary, successfully integrating PBRs into buildings requires careful consideration of technical requirements related to sunlight exposure, environmental control, nutrient management, and system reliability [48]. By addressing these aspects in the design and implementation phases, photobioreactors can emerge as a viable, sustainable building design tool, contributing to energy production and environmental stewardship [48]. These can use sunlight to convert carbon dioxide into biomass, oxygen, and essential bioactive chemicals. They allow for the production of bioenergy and carbon capture. In photobioreactors, photosynthetic microorganisms may take in carbon dioxide from the environment as they grow [34]. This procedure acts as a carbon capture and storage method, lowering greenhouse gas emissions. Additionally, the biomass produced can be transformed into bioenergy using a variety of processes, including the creation of biogas, bioethanol, or biodiesel. Various transparent and leak-proof

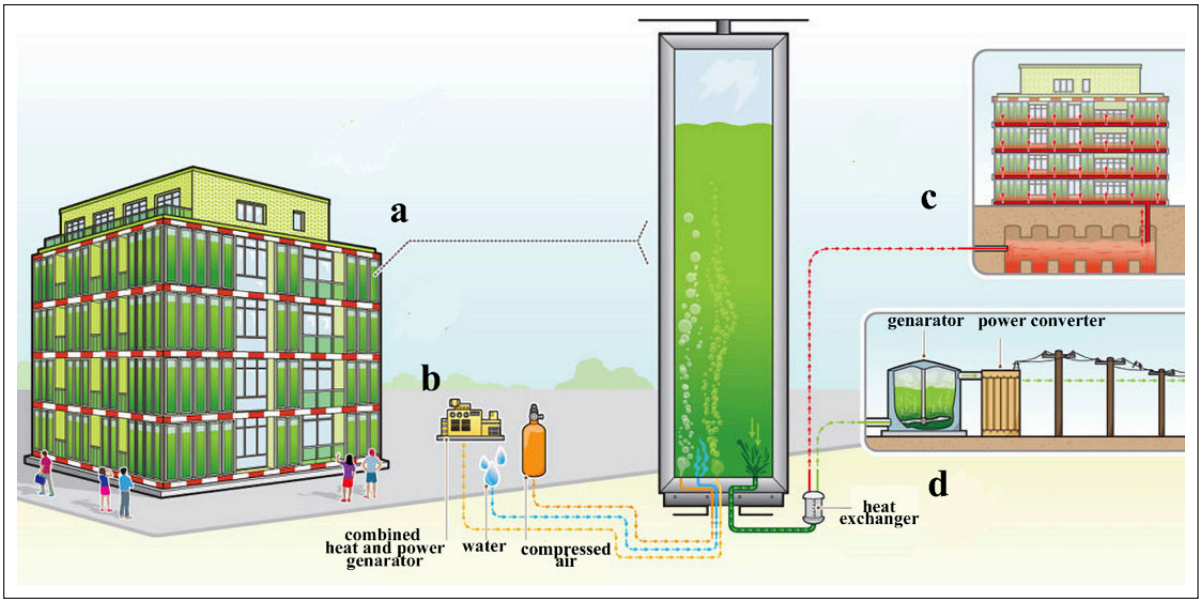

Figure 4. Bioreactor working principle [52].

containers are used in photobioreactors [30]. To efficiently harness solar energy for bioenergy production from algae, most photobioreactors have large surfaces exposed to sunlight (Fig. 4). The efficient facilitation of bioenergy generation should be a goal of photobioreactor design [49]. To accomplish this, they need a mixing system that guarantees adequate agitation of the algal culture and a high mass transfer rate. To maximize light exposure, it is essential to consider efficient light utilization and a suitable surface-to-volume ratio [50]. Thanks to the design, high CO_2 transfer rates should be possible, which should be with high-density algae cells. Solar energy should be maximized when it is deployed in outdoor settings. Furthermore, it's essential to ensure that accumulated O_2 is removed effectively [51].

Figure 4a represents that the bioreactors at BIQ are fastened to the south-facing walls of the structure and are made to function with a minimum of maintenance by humans. Between laminated safety glass panels, each bioreactor is around six gallons of water thick, more than eight feet high, and three inches wide [53]. Figure 4b represents that water, phosphorus, and nitrogen are pushed through the bioreactors by a sophisticated circulatory system that keeps the algae alive. Carbon dioxide, the food source, is produced by a generator on the first floor (In the future, the algae might consume CO_2 released from other structures.) While tiny beads scratch the glass and prevent the organisms from adhering to it, compressed air blasts keep the algae from becoming too thick [54]. Figure 4c represents that the water in the bioreactor can reach 100°F on a bright day because algae emit heat when they reproduce. To heat the rooms or to pre-heat the water used in the kitchen and showers, that water passes through an exchanger and heats a second supply of water that flows through pipes set into the floors. Eight boreholes under the structure that are more than 260 feet deep are used to store extra hot water. The algae from the bioreactors collectively generate enough energy to heat four apartments all year round [52]. Figure 4d represents that the algae are filtered from the water and trucked three kilometers to a university, where they are processed for methane and hydrogen. This procedure happens at least once a week. They might be burned to produce power, but this may be an expensive and unproductive solution to reduce carbon emissions [16].

6. CHALLENGES SETTING UP THIS SYSTEM

The façades of buildings can be used to generate energy by installing algae bioreactors, but this process is complex and may present several challenges. Algae can produce oxygen and biomass using photosynthesis in algae bioreactors, which are devices involved in energy production. These systems are very effective in terms of sustainability but in terms of challenges [55]. In bioreactors, technical elements, including an appropriate environment, water flow, light, and temperature, must be carefully controlled for algae to grow and produce energy effectively [34]. Potentially insufficient at this time are reliable data and technology that demonstrate the biological activity of algae in outdoor conditions [56]. Choosing the kinds of algae that are most suited for bioreactors and making them climate-change resistant might be challenging at the same time [56]. Erratic weather and environmental pollutants can negatively impact Algae's ability to function effectively [57].

6.1. Environmental Impacts and Benefits

The environmental crisis we face today necessitates innovative solutions that can address multiple challenges simultaneously [58]. Algal application technology, especially in the context of green buildings, presents multifaceted environmental advantages [10]. This section delves into the specific environmental impacts and benefits of this technology.

6.1.1. Carbon Sequestration Potential

One of the most promising attributes of algae is its ability to absorb and store carbon dioxide (CO_2) from the atmosphere, a process known as carbon sequestration. When deployed on building façades, the algae interact directly with ambient air, capturing CO_2 as they undergo photosynthesis. This not only helps mitigate urban air pollution but also actively reduces the carbon footprint of the building itself [59]. Algae's efficiency in capturing CO_2 surpasses many traditional terrestrial plants. For every kilogram of dried algae, there's an absorption of approximately 1.83 kilograms of CO_2 [40]. As urban areas grapple with high CO_2 concentrations, integrating algae application technology in construction could present a tangible solution for atmospheric carbon reduction [60].

6.1.2. Reduction in Greenhouse Gas Emissions

Beyond just CO_2, the construction and operation of buildings are responsible for various greenhouse gas emissions, including methane (CH4) and nitrous oxide (N2O). By transitioning to algal-based energy solutions for buildings, there's a potential to displace some fossil fuel usage, thus decreasing greenhouse gas emissions from energy consumption. Moreover, when used for heating or other building needs, the energy produced by algal biomass releases only the amount of CO_2 initially absorbed by the algae, creating a closed carbon loop. This ensures no net increase in atmospheric CO_2 levels [21].

6.1.3. Wastewater Treatment and Purification

Algal technology's lesser-known but equally vital advantage is its role in wastewater treatment [61]. Algae thrive in nutrient-rich environments, and when exposed to wastewater, they can effectively absorb pollutants, including nitrogen and phosphorus compounds [62]. This not only purifies the wastewater but also prevents the release of these compounds into natural water bodies, which could lead to problems like eutrophication [63].

6.2. Economic Implications and Considerations

Incorporating algal technology within the construction and architectural realm is not solely an environmental undertaking; it intertwines deeply with the economic fabric of the industry [10]. Understanding the economic implications is pivotal for decision-makers, investors, and other stakeholders in gauging the viability and scalability of this technology.

6.2.1. Cost-benefit Analysis

While the initial installation costs of algal application systems, including photobioreactors, might be higher than traditional building materials or systems, it's crucial to consider the long-term savings and benefits. Operational Savings: By generating bioenergy, buildings can offset some energy costs, leading to significant savings over the building's lifecycle [64]. The harvested algae can be processed to produce valuable by-products such as biofuel, organic fertilizers, and proteins, creating additional revenue streams. Algal systems can reduce wastewater treatment and purification costs, providing dual functionality. With growing emphasis on carbon trading and credits, buildings employing algal technology may qualify for credits or incentives, further improving the financial model [16]. Considering the cumulative savings and potential revenue streams, the return on investment over time can be considerably positive, making the technology economically attractive in the long run [65].

6.2.2. Market Potential and Growth Forecast

The global demand for sustainable and energy-efficient buildings is on the rise, driven by regulatory pressures and consumer demand. As awareness about the multifaceted benefits of algal technology spreads, its market potential is expected to witness an uptrend. With increasing urban population densities, there's a pressing need for solutions tackling air quality issues and carbon emissions. As countries commit to the Sustainable Development Goals, technologies that offer solutions for both energy and the environment will be in high demand [66]. As research continues and innovations in the algal application field evolve, the efficiency and applicability of the technology are likely to improve, driving market adoption.

6.2.3. Stakeholder and Industry Reception

The construction and architectural industry's reception of algal technology has been cautiously optimistic. While many laud the environmental and economic potential, others express concerns regarding maintenance, aesthetics, and long-term durability [53]. Several collaborations between biotechnologists and architects are emerging, pointing towards a growing interest in integrating biology with building design. As green technology investments gain traction, venture capitalists and green funds have shown notable interest in algal startups and initiatives [10]. Encouragingly, some governments and local municipalities offer incentives or grants for sustainable construction practices, boosting the adoption of such technologies [67].

6.2.4. By-products and their Utility

Algae, given their prolific growth and diverse composition, are not just valuable for their primary roles in carbon capture or bioenergy production. Their biomass offers myriad by-products, each with its utilities that promise for various sectors. Delving into the potential by-products and their applications showcases the multifaceted benefits of cultivating algae on building façades [68].

6.3. Algal Biomass as Organic Fertilizer

One of the significant advantages of harvested algal biomass is its potential use as an organic fertilizer [69]. Algae are known to be high in essential nutrients, such as nitrogen, phosphorus, and potassium, making them an excellent source of plant nourishment [70]. The organic matter present in the algal biomass can stimulate beneficial soil microbes, enhancing soil health. Using algal biomass reduces the need for chemically synthesized fertilizers, reducing the environmental damage these chemicals often inflict. By integrating this by-product into agriculture, we could witness increased crop yields, healthier soils, and reduced chemical pollutants infiltrating our natural ecosystems.

6.4. Production of Algal Oil and its Uses

Algal oil extraction has gained significant attention due to its myriad of applications. One of the most renowned applications of algal oil is its conversion into biodiesel. This biofuel is more sustainable than fossil fuels and emits fewer greenhouse gases upon combustion [71]. Algal oil contains omega-3 fatty acids, eicosatetraenoic acid, and docosahexaenoic acid [72]. These compounds benefit cardiovascular health, making algal oil a sought-after ingredient in dietary supplements. The unique composition of algal oil, loaded with antioxidants and fatty acids, finds its way into various cosmetic products, offering hydration and anti-aging benefits [73].

6.5. Protein Extraction and its Potential

Beyond oil, the algal biomass is a protein powerhouse, opening doors to several promising applications. The protein-rich algal biomass can be processed into poultry, fish, and livestock feed, providing a sustainable alternative to traditional feed sources. Some algae species have been explored for their potential as protein supplements in human diets. Given the global demand for alternative protein sources, algae offer an exciting potential. Specific algal proteins have bioactive properties, making them candidates for drug development and other medical applications [74]. To conclude, the range of by-products derivable from algal biomass underscores the versatility and potential of this organism. From fueling our vehicles with biodiesel to nourishing our soils and feeding our livestock, algae stand out as a promising pillar in the march towards a more sustainable and eco-friendly future.

7. CHALLENGES AND FUTURE DIRECTIONS

While algal application technology in green buildings is promising, adopting a balanced perspective is crucial to adopting both its potential and challenges. Understanding the existing solutions in the pipeline and anticipated future trends provides a comprehensive view of the road ahead for this innovative integration of biology and architecture. When integrated with buildings, pPhotobioreactorsequire regular maintenance. Ensuring the health of the alga when integrated with buildings, cleaning the systems, and managing potential contamination are concerns. Algal growth rates and productivity can be significantly affected by changing climatic conditions. Inconsistent sunlight, extreme temperatures, or unpredictable weather patterns can impact system efficiency. Algal systems can change in appearance over time. Concerns about the visual appeal of green-tinted façades and potential public perception can be barriers to broader adoption. The upfront investment required for integrating algal technology can be high, deterring some stakeholders.

7.1. Potential Solutions and Ongoing Research

Research is ongoing to develop self-cleaning and more durable photobioreactor systems, which can minimize maintenance demands. Biotechnologists optimize algae strains for specific climatic conditions, enhancing resilience and productivity. New business models and financial incentives are being explored to make the initial investment in algal systems more feasible for builders and property owners. Combining algal systems with technologies like solar panels or wind turbines can address some energy variability issues and enhance overall building efficiency [21].

7.2. Future Trends and Predictions

Beyond building façades, the future might see dedicated urban algal farms catering to dense urban populations' energy, food, and other by-product needs. As the world moves towards stricter climate targets, governments might offer more incentives or mandates for green construction practices, propelling the adoption of algal technologies. Research hints at the possibility of using algae directly in building materials, like bricks or panels, allowing for carbon sequestration and insulation benefits. With algal systems' potential in wastewater treatment, future buildings might adopt a more decentralized approach to waste management, enhancing sustainability. In summary, while the path of integrating algal technology into green building practices is riddled with challenges, the solutions on the horizon, combined with the potential future trends, paint an optimistic picture. As technology advances and the urgency for sustainable solutions increases, algal applications in architecture could become commonplace in tomorrow's cities.

8. CONCLUSION

In the contemporary epoch characterized by rapid urbanization juxtaposed with climatic vicissitudes, the synthesis of biological innovations, notably algal technology, within sustainable architectural methodologies emerges as a potential panacea. This discourse endeavors to encapsulate the salient attributes and inherent challenges of this avant-garde amalgamation. At the environmental forefront, algal applications underscore a multifaceted approach, adept not merely at diminishing carbon dioxide efflux but also instrumental in wastewater rectification, ambient purification, and sustainable energy genesis. Economically, transcending its environmental prowess, the algal paradigm augments the edification domain, offering fiscal efficacies, engendering innovative revenue avenues, and catalyzing sectoral growth. Moreover, the diverse array of by-products, spanning biofuels to organic enhancers and proteomic adjuncts, underlines the holistic benefits of this integrative venture. Yet, the journey to ubiquitous adoption is riddled with tangible constraints. However, the present scholarly landscape, marked by relentless research, technological evolutions, and strategic fiscal models, appears poised to surmount these hurdles. Regarding architectural and energy implications, the algal foray heralds a paradigmatic shift from conventional design philosophies towards ecologically synergistic modalities. The edification arena, invigorated by algal derivatives, presents a cornucopia of novel commercial prospects, alliances, and revenue trajectories. Concurrently, algal-equipped infrastructures epitomize the zenith of energy diversification, curbing traditional power reliance and accentuating resilience. The difficulties for

stakeholders encompass the necessities of academia-industry confluences, an intensification of public cognizance initiatives, regulatory incentivization, and robust financial endorsements of boundary-pushing endeavors within the algal architectural sphere. To conclude, integrating such pioneering modalities is no longer a discretionary endeavor but a cardinal collective mandate at the intersection of ecological imperatives and technological ascendancy. In light of this, further research should focus on elucidating optimal integration methodologies, refining cultivation techniques, and assessing long-term environmental and economic impacts to facilitate the seamless integration of algal technology into mainstream architectural practices.

ETHICS

There are no ethical issues with the publication of this manuscript.

DATA AVAILABILITY STATEMENT

The authors confirm that the data that supports the findings of this study are available within the article. Raw data that support the finding of this study are available from the corresponding author, upon reasonable request.

CONFLICT OF INTEREST

The authors declare that they have no conflict of interest.

FINANCIAL DISCLOSURE

The authors declared that this study has received no financial support.

USE OF AI FOR WRITING ASSISTANCE

Not declared.

PEER-REVIEW

Externally peer-reviewed.

REFERENCES

1. Çelekli, A., Yeşildağ, İ., Yaygır, S., & Zariç, Ö. E. (2023). Effects of urbanization on bioclimatic comfort conditions. *Acta Biol Turc, 36*(4), 1–10.
2. Dincer, I., & Rosen, M. A. (2001). Energy, environment and sustainable development. *Appl Energy, 64*(1–4), 427–429. [CrossRef]
3. Singer, S. F. (1985). Global environmental problems. *Eos Trans AGU, 66*(15), 164–165. [CrossRef]
4. Mudakkar, S. R., Zaman, K., Khan, M. M., & Ahmad, M. (2013). Energy for economic growth, industrialization, environment and natural resources: Living with just enough. *Renew Sustain Energy Rev, 25*, 580–595. [CrossRef]
5. World Health Organization. (2016). Ambient air pollution: a global assessment of exposure and burden of disease. *Clean Air J, 26*(2). [CrossRef]
6. Yu, X., Wu, Z., Zheng, H., Li, M., & Tan, T. (2020). How does urban agglomeration improve the emission efficiency? A spatial econometric analysis of the Yangtze River Delta urban agglomeration in China. *J Environ Manag, 260*, 110061. [CrossRef]
7. Say, C., & Wood, A. (2008). Sustainable rating systems around the world. *CTBUH J, 2008*(2), 18–29.
8. Li, K., & Lin, B. (2015). Impacts of urbanization and industrialization on energy consumption/CO_2 emissions: Does the level of development matter? *Renew Sustain Energy Rev, 52*, 1107–1122. [CrossRef]
9. Wang, Z., Zeng, J., & Chen, W. (2022). Impact of urban expansion on carbon storage under multi-scenario simulations in Wuhan, China. *Environ Sci Pollut Res, 29*(30), 45507–45526. [CrossRef]
10. Sedighi, M., Pourmoghaddam Qhazvini, P., & Amidpour, M. (2023). Algae-powered buildings: A review of an innovative, sustainable approach in the built environment. *Sustainability, 15*(4), 3729. [CrossRef]
11. Zariç, Ö. E., Yeşildağ, İ., Yaygır, S., & Çelekli, A. *Removal of harmful dyes using some algae*. 10.5281/zenodo.8190776.
12. Çelekli, A., & Zariç, Ö. E. (2024). Plasma-enhanced microalgal cultivation: A sustainable approach for biofuel and biomass production A. In Shahzad & M. He (Eds.), *Emerging Applications of Plasma Science in Allied Technologies* (pp. 243-263). IGI Global. [CrossRef]
13. Corliss, J. O. (2002). Biodiversity and biocomplexity of the protists and an overview of their significant roles in the maintenance of our biosphere. *Acta Protozool, 41*(3), 199–219.
14. Round, F. E. (1984). *The ecology of algae*. Cambridge University Press.
15. Çelekli, A., & Zariç, Ö. E. (11–13 October, 2023). *Assessing the environmental impact of functional foods. 6th International Eurasian Conference on Biological and Chemical Sciences*. Ankara, Türkiye.
16. Chew, K. W., Khoo, K. S., Foo, H. T., Chia, S. R., Walvekar, R., & Lim, S. S. (2021). Algae utilization and its role in the development of green cities. *Chemosphere, 268*, 129322. [CrossRef]
17. Benedetti, M., Vecchi, V., Barera, S., & Dall'Osto, L. (2018). Biomass from microalgae: The potential of domestication towards sustainable biofactories. *Microb Cell Fact, 17*(1), 173. [CrossRef]
18. Sepehri, F. (2016). Lighting and energy supply for heating in building using algae power. *J Fundam Appl Sci, 8*(3), 1021–1036 [CrossRef]
19. Bisen, P. S., Sanodiya, B. S., Thakur, G. S., Baghel, R. K., & Prasad, G. B. K. S. (2010). Biodiesel production with special emphasis on lipase-catalyzed transesterification. *Biotechnol Lett, 32*(8), 1019–1030. [CrossRef]
20. Hossain, N., & Mahlia, T. M. I. (2019). Progress in

physicochemical parameters of microalgae cultivation for biofuel production. *Crit Rev Biotechnol, 39*(6), 835–859.
21. Elrayies, G. M. (2018). Microalgae: Prospects for greener future buildings. *Renew Sustain Energy Rev, 81*, 1175–1191. [CrossRef]
22. Talaei, M., Mahdavinejad, M., & Azari, R. (2020). Thermal and energy performance of algae bioreactive façades: A review. *J Build Eng, 28*, 101011. [CrossRef]
23. Çelekli, A., & Zariç, Ö. E. (2023). From emissions to environmental impact: Understanding the carbon footprint. *Int J Environ Geoinf 10*(4), 146–156. [CrossRef]
24. Zariç, Ö. E., Çelekli, A., & Yaygır, S. (2024). Lakes of Turkey: Comprehensive review of Lake Çıldır. *Aquat Sci Eng, 39*(1), 54–63. 10.26650/ASE20241353730.
25. Çelekli, A., & Zariç, Ö. E. (2023). *Utilization of herbaria in ecological studies: Biodiversity and landscape monitoring*. Advance Online Publication. [CrossRef]
26. Çelekli, A., & Zariç, Ö. E. (2024). Breathing life into Mars: Terraforming and the pivotal role of algae in atmospheric genesis. *Life Sci Space Res, 41*, 181–190. [CrossRef]
27. Çelekli, A., & Zariç, Ö. E. (11–13 October, 2023). *Hydrobiology and ecology in the context of climate change: The future of aquatic ecosystems. 6th International Eurasian Conference on Biological and Chemical Sciences*. Ankara, Türkiye. https://doi.org/10.5281/zenodo.10021473
28. Murthy, G. S. (2011). Overview and assessment of algal biofuels production technologies. *In Biofuels*. Elsevier. [CrossRef]
29. Ramaraj, R., Tsai, D. D.W., & Chen, P. H. (2015). Carbon dioxide fixation of freshwater microalgae growth on natural water medium. *Ecol Eng, 75*, 86–92. [CrossRef]
30. Kükdamar, İ. (2018). Cephelerde fotobiyoreaktör kullanımının binaların sürdürülebilirliğine etkisi. *Tesis Mühen, 2018*(166), 34–48.
31. Tran, T. H., & Hoang, N. D. (2016). Predicting colonization growth of algae on mortar surface with artificial neural network. *J Comput Civ Eng, 30*(6), 4016030. [CrossRef]
32. Mata, T. M., Martins, A. A., & Caetano, N. S. (2010). Microalgae for biodiesel production and other applications: A review. *Renew Sustain. Energy Rev, 14*(1), 217–232. [CrossRef]
33. Parmar, A., Singh, N. K., Pandey, A., Gnansounou, E., & Madamwar, D. (2011). Cyanobacteria and microalgae: A positive prospect for biofuels. *Bioresour Technol, 102*(22), 10163–10172. [CrossRef]
34. Sarwer, A., Hamed, S. M., Osman, A. I., Jamil, F., Al-Muhtaseb, A. H., Alhajeri, N. S., & Rooney, D. W. (2022). Algal biomass valorization for biofuel production and carbon sequestration: A review. *Environ Chem Lett, 20*(5), 2797–2851. [CrossRef]
35. Buchheister, C. Bioenergy façade 2.0 presented at Glasstec. https://www.arup.com/news-and-events/bioenergy-facade-20-presented-at-glasstec
36. Loomans, T. (2013). *The world's first algae-powered building opens in Hamburg*. Inhabitat.
37. Walker, T. L., Purton, S., Becker, D. K., & Collet, C. (2005). Microalgae as bioreactors. *Plant Cell Rep, 24*(11), 629–641. [CrossRef]
38. Rai, M. P., Nigam, S., & Sharma, R. (2013). Response of growth and fatty acid compositions of Chlorella pyrenoidosa under mixotrophic cultivation with acetate and glycerol for bioenergy application. *Biomass Bioenergy, 58*, 251–257. [CrossRef]
39. Milano, J., Ong, H. C., Masjuki, H. H., Chong, W. T., Lam M. K., Loh, P. K., & Vellayan, V. (2016). Microalgae biofuels as an alternative to fossil fuel for power generation. *Renew Sustain Energy Rev, 58*, 180–197. [CrossRef]
40. Brennan, L., & Owende, P. (2010). Biofuels from microalgae—A review of technologies for production, processing, and extractions of biofuels and co-products. *Renew Sustain Energy Rev, 14*(2), 557–577. [CrossRef]
41. Farronan, B., Carrasco, R., Flores, J. W. V., Olivera, C. C., Lopez, J., & Alfaro, E. G. B. (2021). Microalgae scenedesmus sp as a clean technology in reducing greenhouse gas carbon dioxide. *Chem Eng Trans, 86*, 445–450.
42. Sarkar, A, "Algae-Based Carbon Capture System: Modelling Photosynthesis for Carbon Dioxide Reduction," Algae, 2020.
43. Tran, N. A. T., Seymour, J. R., Siboni, N., Evenhuis, C. R., & Tamburic, B. (2017). Photosynthetic carbon uptake induces autoflocculation of the marine microalga Nannochloropsis oculata. *Algal Res, 26*, 302–311. [CrossRef]
44. AlgaeBase. (2024). *Listing the world's algae*. http://algaebase.org/
45. UTEX. (2024). *UTEX culture collection of Algae at UT-Austin*. https://utex.org/
46. Nordic Microalgae. (2024). *Nannochloropsis granulata Karlson & Potter, 1996*. https://nordicmicroalgae.org/taxon/nannochloropsis-granulata/
47. Nowicka-Krawczyk, P., Komar, M., & Gutarowska, B. (2022). Towards understanding the link between the deterioration of building materials and the nature of aerophytic green algae. *Sci Total Environ, 802*, 149856. [CrossRef]
48. Chisti, Y. (2006). Microalgae as sustainable cell

factories. *Environ Eng Manag J, 5*(3), 261–274. [CrossRef]
49. Schenk, P. M., Thomas-Hall, S. R., Stephens, E., Marx, U. C., Mussgnung, J. H., Posten, Kruse, O., & Hankamer, B. (2008). Second generation biofuels: High-efficiency microalgae for biodiesel production. *BioEnergy Res, 1*(1), 20–43. [CrossRef]
50. Rezvani, F., & Rostami, K. (2023). Photobioreactors for utility-scale applications: Effect of gas–liquid mass transfer coefficient and other critical parameters. *Environ Sci Pollut Res, 30*(31), 76263–76282. [CrossRef]
51. Zittelli, G. C., Rodolfi, L., Bassi, N., Biondi, N., & Tredici, M. R. (2013). Photobioreactors for microalgal biofuel production. In Algae for biofuels and energy (pp. 115–131). *Springer*. [CrossRef]
52. Ferris, D. (2013). *Algae Haus*. https://www.sierraclub.org/sierra/2013-6-november-december/innovate/algae-haus.
53. Poerbo, H. W., Martokusumo, W., Koerniawan, M. D., Ardiani, N. A., & Krisanti, S. (2018). Algae facade as green building method: Application of algae as a method to meet the green building regulation. *IOP Conf Ser Earth Environ Sci, 99*(1), 012012. [CrossRef]
54. Kendrick, M. (2011). *Algal bioreactors for nutrient removal and biomass production during the tertiary treatment of domestic sewage* [Doctoral Thesis, Loughborough University].
55. Kunjapur, A. M., & Eldridge, R. B. (2010). Photobioreactor design for commercial biofuel production from microalgae. *Ind Eng Chem Res, 49*(8), 3516–3526. [CrossRef]
56. Peter, A. P., et al. (2022). Continuous cultivation of microalgae in photobioreactors as a source of renewable energy: Current status and future challenges. *Renew Sustain Energy Rev, 154*, 111852. [CrossRef]
57. Singh, R. N., & Sharma, S. (2012). Development of suitable photobioreactor for algae production–A review. *Renew Sustain Energy Rev, 16*(4), 2347–2353. [CrossRef]
58. Dincer, I. (2000). Renewable energy and sustainable development: A crucial review. *Renew Sustain Energy Rev, 4*(2), 157–175. [CrossRef]
59. Kumar, K., Dasgupta, C. N., Nayak, B., Lindblad, P., & Das, D. (2011). Development of suitable photobioreactors for CO2 sequestration addressing global warming using green algae and cyanobacteria. *Bioresour Technol, 102*(8), 4945–4953. [CrossRef]
60. Huseien, G. F., & Shah, K. W. (2021). Potential applications of 5g network technology for climate change control: A scoping review of Singapore. *Sustainability (Switzerland), 13*(17), 9720. [CrossRef]
61. Ahmad, A., Banat, F., Alsafar, H., & Hasan, S. W. (2022). Algae biotechnology for industrial wastewater treatment, bioenergy production, and high-value bioproducts. *Sci Total Environ, 806*, 150585. [CrossRef]
62. Gondi, R., Kavitha, S., Kannah Y. R., Karthikeyan, O. P., Kumar, G., Tyagi, K. V., Banu, J. R. (2022). Algal-based system for removal of emerging pollutants from wastewater: A review. *Bioresour Technol, 344*, 126245. [CrossRef]
63. Abdel-Raouf, N., Al-Homaidan, A. A., & Ibraheem, I. (2012). Microalgae and wastewater treatment. *Saudi J Biol Sci, 19*(3), 257–275. [CrossRef]
64. Wilkinson, S. J., & Stoller, P. (2018). Algae building technology energy efficient retrofit potential in Sydney housing. Proceedings of the 10th International Conference in Sustainability on Energy and Buildings. In Kaparaju, P., Howlett, R., Littlewood, J., Ekanyake, C., Vlacic, L. (eds) *Sustainability in Energy and Buildings*. Springer. [CrossRef]
65. Yulistyorini, A. (2017). A mini review on the integration of resource recovery from wastewater into sustainability of the green building through phycoremediation. *AIP Conf Proc, 1887*(1), 020048 [CrossRef]
66. Ahmad, I., Abdullah, N., Koji, I., Mohamad, S. E., Al-Dailami, A., Yuzir, A. (2022). Role of algae in built environment and green cities: A holistic approach towards sustainability. *Int J Built Environ Sustain, 9*(2–3), 69–80. [CrossRef]
67. Chan, A. P. C., Darko, A., & Ameyaw, E. E. (2017). Strategies for promoting green building technologies adoption in the construction industry-An international study. *Sustainability (Switzerland), 9*(6), 969. [CrossRef]
68. Talebi, A. F., Tabatabaei, M., Aghbashlo, M., Movahed, S., Hajjari, M., Golabchi, M. (2020). Algae-powered buildings: A strategy to mitigate climate change and move toward circular economy. In S. Patnaik, S. Sen, M. S. Mahmoud. (Eds.). *Smart village technology* (pp. 353–365). Springer. [CrossRef]
69. Khan, S. A., Sharma, G. K., Malla, F. A., Kumar, A., Rashmi, Gupta, N. (2019). Microalgae based biofertilizers: A biorefinery approach to phycoremediate wastewater and harvest biodiesel and manure. *J Cleaner Prod, 211*, 1412–1419. [CrossRef]
70. Ammar, E. E., Aioub, A. A. A., Elesawy, A. E., Karkour, A. M., Mouhamed, M. S., Amer, A. A., El-Shershaby, N. A. (2022). Algae as bio-fertilizers: Between current situation and future prospective. *Saudi J Biol Sci, 29*(5), 3083–3096. [CrossRef]
71. Adeniyi, O. M., Azimov, U., & Burluka, A. (2018). Algae biofuel: Current status and future applica-

tions. Renew. *Sustain Energy Rev, 90*, 316–335. [CrossRef]

72. Topuz, O. K. (2016). Algal oil: A novel source of omega-3 fatty acids for human nutrition. *Sci Bull Ser F Biotechnol, 20*, 178–183.
73. Çelekli, A., Özbal, B., & Bozkurt, H. (2024). Challenges in functional food products with the incorporation of some microalgae. *Foods, 13*(5), 725. [CrossRef]
74. Zhang, S., Qamar, S. A., Junaid, M., Munir, B., Badar, Q., & Bilal, M. (2022). Algal polysaccharides-based nanoparticles for targeted drug delivery applications. *Starch-Stärke, 74*(7–8), 2200014. [CrossRef]